Western Australia School of Mines
Department of Exploration Geophysics

Feasibility of Rock Characterization for Mineral Exploration Using Seismic Data

Christopher Bernard Harrison

This thesis is presented for the Degree of
Doctorate of Philosophy
Curtin University of Technology

July 2009

Declaration

This thesis contains no material which has been accepted for the award of any other degree or diploma in any university.

To the best of my knowledge and belief this thesis contains no material previously published by any other person except where due acknowledgment has been made.

Signature: _____

Date: _____

For my parents

Dr. Bernard and Lucille Harrison

Abstract

The use of seismic methods in hard rock environments in Western Australia for mineral exploration is a new and burgeoning technology. Traditionally, mineral exploration has relied upon potential field methods and surface prospecting to reveal shallow targets for economic exploitation. These methods have been and will continue to be effective but lack lateral and depth resolution needed to image deeper mineral deposits for targeted mining. With global need for minerals, and gold in particular, increasing in demand, and with shallower targets harder to find, new methods to uncover deeper mineral reserves are needed. Seismic reflection imaging, hard rock borehole data analysis, seismic inversion and seismic attribute analysis all give the spatial and volumetric exploration techniques the mineral industry can use to reveal high value deeper mineral targets.

In 2002, two high resolution seismic lines, the East Victory and Intrepid, were acquired along with sonic logging, to assess the feasibility of seismic imaging and rock characterisation at the St. Ives gold camp in Western Australia. An innovative research project was undertaken combining seismic processing, rock characterization, reflection calibration, seismic inversion and seismic attribute analysis to show that volumetric predictions of rock type and gold-content may be viable in hard rock environments. Accurate seismic imaging and reflection identification proved to be challenging but achievable task in the all-out hard rock environment of the Yilgarn craton. Accurate results were confounded by crocked seismic line acquisition, low signal-to-noise ratio, regolith distortions, small elastic property variations in the rock, and a limited volume of sonic logging. Each of these challenges, however, did have a systematic solution which allowed for accurate results to be achieved.

Seismic imaging was successfully completed on both the East Victory and Intrepid data sets revealing complex structures in the Earth as shallow as 100 metres to as deep as 3000 metres. The successful imaging required homogenization of the regolith to eliminate regolith travel-time distortions and accurate constant velocity analysis for reflection focusing using migration. Verification of the high amplitude reflections within each image was achieved through integration of surface geological

and underground mine data as well as calibration with log derived synthetic seismograms. The most accurate imaging results were ultimately achieved on the East Victory line which had good signal-to-noise ratio and close-to-straight data acquisition direction compared to the more crooked Intrepid seismic line.

The sonic logs from both the East Victory and Intrepid seismic lines were comprehensively analysed by re-sampling and separating the data based on rock type, structure type, alteration type, and Au assay. Cross plotting of the log data revealed statistically accurate separation between harder and softer rocks, as well as sheared and un-sheared rock, were possible based solely on compressional-wave, shear-wave, density, acoustic and elastic impedance. These results were used successfully to derive empirical relationships between seismic attributes and geology. Calibrations of the logs and seismic data provided proof that reflections, especially high-amplitude reflections, correlated well with certain rock properties as expected from the sonic data, including high gold content sheared zones. The correlation value, however, varied with signal-to-noise ratio and crookedness of the seismic line. Subsequent numerical modelling confirmed that separating soft from hard rocks can be based on both general reflectivity pattern and impedance contrasts.

Indeed impedance inversions on the calibrated seismic and sonic data produced reliable volumetric separations between harder rocks (basalt and dolerite) and softer rock (intermediate intrusive, mafic, and volcaniclastic). Acoustic impedance inversions produced the most statistically valid volumetric predictions with the simultaneous use of acoustic and elastic inversions producing stable separation of softer and harder rocks zones. Similarly, Lambda-Mu-Rho inversions showed good separations between softer and harder rock zones. With high gold content rock associated more with “softer” hard rocks and sheared zones, these volumetric inversion provide valuable information for targeted mining. The geostatistical method applied to attribute analysis, however, was highly ambiguous due to low correlations and thus produced overly generalized predictions. Overall reliability of the seismic inversion results were based on quality and quantity of sonic data leaving the East Victory data set, again with superior results as compared to the Intrepid data set.

In general, detailed processing and analysis of the 2D seismic data and the study of the relationship between the recorded wave-field and rock properties measured from borehole logs, core samples and open cut mining, revealed that positive correlations can be developed between the two. The results of rigorous research show that rock characterization using seismic methodology will greatly benefit the mineral industry.

Acknowledgements

First and foremost I would like to thank my parents, Dr. Bernard and Lucille Harrison, who have guided me through the past 34 years. Their emotional, physical and let's not forget financial support, through university degree's, rock star attempts, and adventures overseas has been invaluable. Without them I would not be the man I am today.

I would like to thank my supervisor, Dr. Milovan Urosevic who has been instrumental in guiding me towards the completion of this thesis. I am grateful for his continual advice, motivation and knowledge which has provide the momentum for me to push through the hard times during my PhD research. I would like to thank Dr. Ned Stolz (originally with Gold Fields, now with Geoscience Australia) for his invaluable research contributions to this work. I would also like to thank Prof. Brian Evans for his support and guidance throughout this project. I would also like to thank Prof. Boris Gurevich for providing theoretical and technical input, as well as Prof. Bruce Hartley for technical editing. Thanks also goes out to Dominic Howman for allowing me to aid him in teaching several first and second year lab classes over the past 4 years.

I would also like to thank the sponsors of this project, Gold Fields Limited, Barrick Gold Corporation, and Santa Barbara for their financial support. A big thank you goes out to the ASEG (Australia society of Exploration Geophysics) for the grants that have been generously donated to the project. A further acknowledgement goes out to the Centre of Excellence for High Definition Geophysics at the Department of Exploration Geophysics, Curtin University of Technology, whose support was invaluable. I would also like to thank the Department of Exploration Geophysics Curtin University of Technology for their years of support, servers for the hours of processing, software licenses, desk facilities, stationary, and pens.

A special thanks to my partner, Kristie Dennerley, for putting up with me for the past two years.

Table of Contents

Table of Figures

Table of Tables

1 Introduction

"A pessimist sees the difficulty in every opportunity; an optimist sees the opportunity in every difficulty."

- Anonymous

1.1 Using Seismic Technologies to Delineate Complex Mineral Bodies in Hard Rock Environments.

The mineral industry is an integral part of economic development in Western Australia. Sustainable growth within this industry is based on discovery of new mining prospects, or expanding the viability of present mining operations. Mineral prospecting has been traditionally conducted using potential field geophysics, borehole drilling, and surface prospecting to reveal mineral deposits for development. These exploration techniques have been historically successful for discovering surface or shallow laying prospects. However, these methods suffer from low spatial resolution, especially over a substantial regolith over-burden, limiting the subsurface image to "blurry" shallow insights of the subsurface rock formations. With low lying shallow prospects in Western Australia more difficult to discover, new techniques for uncovering deeper targets are needed. Seismic exploration is proposed as the next step to enhance mineral exploration in Western Australia and hard rock environments throughout the world.

Seismic exploration provides higher resolution images in comparison to traditional mineral exploration techniques. Properly acquired seismic data can not only image reflections on the meter scale, but also be calibrated to predict structure, lithology, oil, gas and water content as evidenced by over 50 years of hydrocarbon exploration. However, the application of seismic exploration in hard rock environments, such as that observed in Western Australia has, to date, been fraught with difficulties in mapping detail. High structural complexity in Western Australia include low-order shear zones, reverse and relaxation faults, and altered and fractured zones which surround granite intrusions important for Archaean mesothermal gold mineralization. The regolith, a 20-100 meter

thick layer of reworked, altered and weathered material, wreaks havoc on seismic imaging by distorting, absorbing and deflecting seismic energy. With exploration being usually centred around active mine sites, constant equipment movement, and restricted areas cause both random noise and crooked data acquisition to occur. The random noise reduces signal-to-noise ratio (S/N) and affects imaging quality. Crooked seismic acquisition leads to line direction not being aligned with dominant structural dip in the area causing an increase in presence of out-of-plane events which have hamper 2D seismic imaging. All these difficulties added to complex geology make formation of seismic images in hard rock environments challenging.

The incomplete understanding of the sonic properties of hard rocks and how these properties will be represented on a seismic image add to imaging difficulties. Sonic properties come from *in-situ* measurements using full waveform sonic logging tool to acquired hard rock compressional (P) wave, shear (S) wave velocities, and densities. Full waveform sonic (FWS) logs provide valuable information for statistical analysis of the rock properties in relation to rock type, structure type, and alteration type. FWS also enables computation of synthetic seismograms which are essential for calibration of seismic data and further geological analysis. While borehole drilling is common practice in mineral exploration, acquiring FWS logs to depths of significance to seismic imaging is typically not a consideration in hard rock environments. When these logs are available however, calibration of their sonic data to the seismic data provides an invaluable base to verify seismic reflection information. Subsequent analysis could then include seismic inversion, which makes impedance predictions through sonic log calibrations, and attribute analysis which makes log properties predictions based on waveform calibrations. These are untested techniques in hard rock environments requiring a multi-disciplinary approach to assess viable results.

The first step to understanding requires that the hard rock seismic data reveal complex structure at both shallow (200 meters or less) and deep (over 2.0 km) depths. The imaging has to both identify mesothermal fluid conduits and traps, while revealing shallower faulting and shear zones where mineralization can take place. Proper reflection focusing requires processing algorithms such as dip moveout (DMO) and migration to image complex structure. However, these algorithms do not necessarily retain original reflections phase, frequency or amplitude information, needed for seismic inversion and attribute analysis. Further, the physical purpose and location of any reflections seen on the

seismic image remain ambiguous without calibration with other data sets. This calibration can be done through surface geology interpretations, and mine interpretations. For the first time however, sonic logging is available to this research to bridge the gap between reflection imaging and statistical analysis.

An understanding of sonic properties analysis in relation to various rock properties within hard rock environments is needed. A comprehensive study of the FWS logs could relate impedance changes to changes in rock type, structural changes or perhaps even alteration type. Synthetic seismograms generated from log data using a wavelet extracted from the seismic data would provide essential for rock type characterization and synthetic to seismic calibration in hard rock environments. The critical goals of this research are the elimination of distortions (or at the very least minimizing them), in both the seismic and sonic data sets. Techniques used in hydrocarbon exploration will be drawn upon to aid in solving these difficulties.

1.2 Previous Ground Breaking Work in Hard Rock Seismic Exploration

"Whether you can observe a thing or not depends on the theory which you use. It is the theory which decides what can be observed."

- **Abdus Salam (Conversation between Einstein and Heisenberg (1926) regarding quantum mechanics, 1990)**

The lack of published research shows that the applications of reflection seismic techniques in hard rock environments are a relatively new technology. However, pioneering researchers from around the world have not completely ignored hard rock seismic exploration. The majority of published work comes out of Canada, South Africa, and Australia with a smaller amount of work coming from Europe. It was first suggested by Nelson (1984) in South Australia that hard rock density and velocity differences would allow for unique seismic reflections. Indeed his early models and test cases proved that reflections were resolvable using course seismic techniques. However, it would take years before this pioneering work was followed up in Australia.

In 1999, several two dimensional (2D) regional seismic lines were recorded over gold bearing structures on the Yilgarn craton to asses seismic methods in Western Australia (Drummond, 2000)(Drummond, 2000). This survey proved that deep structures important for gold mineralization (> 2 km) and useful for mesothermal fluid flow could be imaged well with coarse acquisition parameters. The survey however, was inadequate to resolve shallower more complex structure of interest for mineral exploration. Similar low resolution surveys have been conducted around the world to image large mineral deposits or zones of interest prior to more precise acquisition techniques. In Canada a large survey was complete to confirm massive sulphides through the Manitouwadge Greenstone Belt in 1995 and 1996 (Roberts, 2003). In Sweden, Juhlin (2003) showed reflections associated with sub-horizontal fracture zones, and dolerite / granite interfaces at depths below 2 kilometres. Salisbury (1997) dealt with sulphide imaging of hard rocks using both 2D seismic and vertical seismic profiling (VSP) to image horizontal reflectors. The earliest demonstration of 2D seismic profiling in a hard rock setting was completed in South Africa in 1983 when large volumes of 2D vibroseis data were acquired across the Kaapvaal craton by major South African mining companies. These previous studies showed that seismic reflection method in hard rock environments can resolved deep regional scale events, but typically were unable to image shallow or structural complex targets.

In 2002 follow up high resolution surveys were completed in Western Australia to address the lack of complex structural and shallow imaging missing from the original 2D regional surveys. Preliminary results indicated that strong reflections associated with complex stratigraphy compared well with detailed geological sections constructed from drilling and mining data (Urosevic, 2005). Salisbury (1997) researched P-wave and density relationships of massive sulphides in Canada showing that impedance differences exists which means that massive sulphide deposits could be imaged by seismic reflection methods. The Canadian work was based on alteration type within the rock and demonstrated that stronger alteration could display higher impedance contrasts. Greenhalgh (1997) used cross plotting techniques to observe P-wave relationships with density in rock samples from Kambalda in Australia revealing marginal statistical groupings. Proper conditioning of sonic data set shown by Harrison et al. (2007) revealed that seismic to sonic calibration are achievable in hard rock environments in Western Australia.

Pretorius (1997) researched 3D images made of the Ventersdorp Contact 'Reef' gold ore body in South Africa. The survey was able to show the approximate location of the

mineral deposits, but was unable to pinpoint structural events within the data set for underground mining. A low-fold 3D survey in 1997 in the Witwatersrand basin was able to match reflections on the seismic image to known faults in the mining operation to within three meters (Stuart, 1999). This survey also used seismic attributes (perhaps for the first time in mineral exploration) to enhance faults imaged in the seismic data. The South African studies had the good fortune of gold mineralization taking place mainly in sedimentary conglomerates with good impedance contrasts to host rocks. Larroque (2002), showed how 3D seismic surveys were able to directly detect sub-metric layered platinum mineral deposits at a shallow depth of 800 m. Canada has also seen its share of 3D seismic surveys for mineral exploration. Milkereit (2000) has extensive research on 3D methods used for imaging nickel-copper deposits on the Sudbury Igneous Complex. In 2000 a large blind massive sulphide was imaged at the Halfmile Lake Area of the Bathurst Mining camp in Canada (Adam et al., 2000) and is fully reprocessed and reported by Malehmir and Bellefleur (2008). Australia saw the advent of 3D seismic surveys in mining coal (Hatherly, 1994; Urosevic, 1992a; Urosevic, 1992b) with several recent 3D hard rock seismic surveys acquired in 2007 and 2008.

Small scale cross-hole and vertical seismic profiling (VSP) were used by Greenhalgh (2000) at the Hunt mine in Kambalda, Western Australia. The results indicated that hard rock layering could be imaged, but there was still a lack of understanding of sonic properties. Surface and borehole seismic have also been tested for near vertical kimberlite pipe detection in semi hard rock environments in Australia (Urosevic, 2000). Further vertical seismic profiling studies have been used to image thin shallow dipping kimberlites in Venezuela (Hearst, 1998) and Canada (Hammer et al., 2004). While there is a lack of overall published research available, seismic methods in hard rock environments are poised to play a major role in mineral exploration around the world.

When new technologies are employed in the place of older time tested techniques, lack of understanding and resistance follow. Seismic surveying will not eliminate traditional methods for mineral exploration but will enhance interpretation of results, reveal more feasible mineral sources sources, and have a smaller environment impact. The full development and integration of these techniques however, will take a bit more time while the mineral exploration industry absorbs the potential value seismic acquisition brings to the table.

1.3 New Technologies for Hard Rock Seismic Imaging

"If you're not failing every now and again, it's a sign you're not doing anything very innovative."

- Anonymous

Successful seismic exploration in Western Australia needs to address several key aspects: imaging of complex shallow lying structures (above 100-1000 metres) while revealing deeper (below 2000 meters) lying structures important for mesothermal fluid flow, analysis of sonic properties to verify why and where reflections are coming from in hard rock environments, reflection identification through sonic-seismic calibration, predicting sonic properties of rocks through the seismic data based on those calibrations, and analysis of seismic attributes as a prediction base. Seismic techniques as applied in sedimentary rock environments have yielded valuable information in hydrocarbon exploration through reservoir characterization, hydrocarbon detection, rock type and porosity predictions. Innovations in these techniques for hard rock seismic exploration will result in similar advances for the mineral industry.

Gassmann (1951) was the first to show that bulk modulus and shear modulus change with saturation fluid type in sedimentary rock units. Castagna (1985) showed that a systematic relationship between compression (P-wave) and shear (S-wave) exist in clastic rocks. Potter and Stewart (1998) examined the empirical relationship of S-wave and density for hydrocarbon exploration. Although these studies were conducted with sedimentary rocks for hydrocarbon exploration, hard rock exploration parallels can be made. Salisbury and Snyder (2004) have conducted research in Canada that indicates that alteration changes will have an effect on acoustic impedance in hard rock environments. Structural changes in hard rock environments such as shearing and mylonite can be seen as analogous to porosity (minus the pore fluid) changes in clastic environments. Sheared rock is weak, cracked and brittle as compared to the host rock allowing mineralization and deposition causing impedance changes within the localized rock properties. Impedance changes then translate into reflectivity changes giving rise to reflection imaging. The challenge is to extract as much reliable information from the sparse amount of borehole sonic data and then relate it to two dimensional (2D) seismic images.

Reliable seismic interpretation requires seismic reflectors from sonic data be tied with geological units to provide "ground truth" to the seismic data (Box, 2003). The calibrated synthetic and seismic data will reveal precise depth and verify reflectors in seismic data. A comprehensive analysis of offset reflectivity from the full waveform sonic data (FWS) will be conducted for amplitude versus offset analysis (AVO). Parallels as illustrated by Hilterman (1990), Castagna (1993), Connolly (1999), Goodway (1997), and Cambois (1998) will be used to investigate AVO. A thorough understanding of the why and how of reflections in this hard rock environment will give a basis for reconstruction of geophysical measurements through calibrated sonic and seismic data via seismic inversion techniques (Treitel & Lines, 2001). Precise processing of the seismic data is a necessary prerequisite for further analysis towards rock type characterization.

Proper processing requires feasible solutions for the ever present problems of low signal-to-noise ratio and the focusing of complex structure in a hard rock environment. Single and multi-channel filtering of the seismic data to enhance signal and attenuate noise is a necessity to retain proper reflection information. Coherent and random noise can be attenuated through spread parameters, stacking of shots, common midpoint stacks, and band-pass filtering (Evans, 1997). Solutions to random noise attenuation while enhancing low signal are documented by Canales (1984) with other possible solutions including Surface Consistent Deconvolution (Levin, 1989; Wang, 1995), and F-X deconvolution (Gulunay, 1986). While some of these techniques are quite "harsh" on the seismic data, they work well under the low signal-to-noise ratio ever-present in hard rock environments. Improvement of the S/N ratio is crucial for reflection focusing, statistical analysis and eventually quantitative interpretation.

Interpretable depth of the image is another critical concern for the mineral exploration industry. Shallow targets, 100-500 metres in depth, are ideal to image for economical mining access. However, deeper structures of over one kilometre in depth are also of interest with respect to crustal-scale mesothermal lode gold transportation conduits and trapping mechanisms (Cox, 2004).

Complex statics and reflection correction are also needed to ensure regolith distortions are minimized. To form accurate complex seismic images in hard rock environments, the effectiveness of both post-stack migrations and pre-stack migrations need to be investigated. Post-stack migrations are considered less computationally costly with an overwhelming number of studies to draw upon as a knowledge base for its

application. Al-Yahya (1989), Lafond and Levander (1993), and Pasasa et al (1998) have shown that pre-stack depth migrations (PSDM) give far more accurate shallow earth images. However, PSDM requires accurate velocity analysis through *a priori* velocity information as well as velocity analysis as discussed by Al-Yahya (1989), and Urosevic (2005) in Australian hard rock environments. Preservation of phase, frequency or amplitude of the original seismic signal is clearly difficult in hard rock environments due to low S/N ratio.

Due to their complexity in hard rock environments, reflection images need to be verified using surface geology, mine data, and sonic data to provide a base for inversion and attribute analysis. Sonic to seismic calibrations will be reported for the first time in hard rock environments through this research. For that purpose synthetic to seismic tying will be conducted as suggested by e.g. Lindseth (1979), Treitel and Lines (1982, 2001), and Latimer (2000). The limited amount of borehole data and lack of check shots for time-to-depth conversions require multiple iterations of log stretching and wavelet extraction to ensure a good statistical fit between the sonic and seismic data. While the lack of data is not ideal, statistical rigour will be employed to ensure best calibrations possible to allow for the further processes of inversion and attribute analysis.

Inversion is the process by which known impedances from *in-situ* or laboratory rock measurements are used to convert seismic traces into pseudo-reflection-coefficient time series (Becquey et al., 1979). The resulting pseudo-reflection-coefficient time series or pseudo-logs are roughly equivalent to logs recorded in wells drilled at every seismic trace location (Watson and Lines, 2000). Seismic attribute analysis, which uses the same calibrations as inversions will also be attempted for the first time in this hard rock environment. Attribute analysis uses seismic waveform information to predict the distribution of physical properties (e.g. porosity, lithology, and bed thickness) of the strata being imaged seismically (Hart, 2002). These seismic attributes are specific measures of geometric, kinematic, dynamic, and statistical features derived from seismic data (Marfurt, 2006). Both seismic inversion and attribute analysis requires minimal phase, frequency or amplitude distortions in the original seismic reflections. Attribute analysis, however, requires higher number of borehole sonic logs for reliable predictions than seismic inversions (Hampson-Russell, 2007). Careful pre-conditioning of the sonic data sets, and proper processing of the seismic image is required for successful inversion and attribute analysis. Both inversions in combination with attribute analysis have never been reported before in hard rock environments.

To achieve successful results this study will first investigate effectiveness of processing techniques such as post and pre-stack migration to image both shallow complex structures and deeper structures, while minimizing the inherent frequency distortions these techniques produce. The second task is the systematic analysis of rock characteristics from borehole interpretations and FWS logs based on rock type, structure, alteration, and stratigraphy. The third task will be to utilize the preconditioned seismic images, and the borehole impedance data to generate lithological, structural, or alteration predictions via seismic inversion. The fifth task will involve using seismic attributes from the preconditioned seismic images for possible lithological, structural, or alteration predictions. The last task will be to assess whether these techniques have proven useful through statistical analysis. While ideal results are years away, this research should pave the way for the inevitable future work that will arise when hard rock seismic imaging is accepted as a standard in mineral exploration.

1.4 Thesis Configuration

The structure of this thesis is designed to follow the chronological development of my research. The first chapter summarizes the state of the current knowledge of the application of seismic methods for hard rock exploration. Chapter 2 provides the concepts for possible characterization of hard rocks by seismic methods. The chapter provides a discussion of the physical rock properties which will be studied. A extensive library of elastic rock properties and a good understanding of wave propagation in solids presents a fundamental basis for hard rock characterization. Chapter 2 ends off emphasizing the potential uses of acoustic inversion, elastic inversion and multi-attribute inversions for hard rock characterization. Chapter 3 gives an overview of the St. Ives gold camp and the geological requirements of gold mineralization of the area. This chapter provides the reader with the understanding that seismic methods and rock characterization in a hard rock environment such as that in Western Australia, is not an easy task.

Chapter 4 shows the inversion methodologies for the East Victory seismic data. Various difficulties in hard rock environments discussed. Chapter 5 shows a second attempt at inversion methodologies on the highly crooked Intrepid seismic line. Various difficulties in hard rock environments are discussed. The final conclusions and recommendations of my research are outlined in Chapter 6. A full list of cite references followed by appendices completes this thesis.

2 Hard Rock Seismic Exploration

"There is a theory which states that if ever for any reason anyone discovers what exactly the Universe is for and why it is here it will instantly disappear and be replaced by something even more bizarre and inexplicable. There is another that states that this has already happened."

- **Douglas Adams (The Book, Hitchhikers Guide to the Galaxy, 1979)**

2.1 Introduction to the Methodology for Hard Rock Seismic

With seismic exploration being a relatively new technology in hard rock environments, a comprehensive understanding of the process affecting results has to be explored. Two types of data sets with differing resolutions were available to this study: Seismic data, which resolves layers at tens of metres scale, and borehole data which resolves layers on the centimetres scale (Figure 2-1). Bridging the resolution gap in these two data sets in the hard rock mining environment is difficult and is the main focus of this research. Many of these seismic process methodologies and their applications have a long and successful history in hydrocarbon exploration. Modifications through research of these techniques will inevitably benefit mineral exploration.

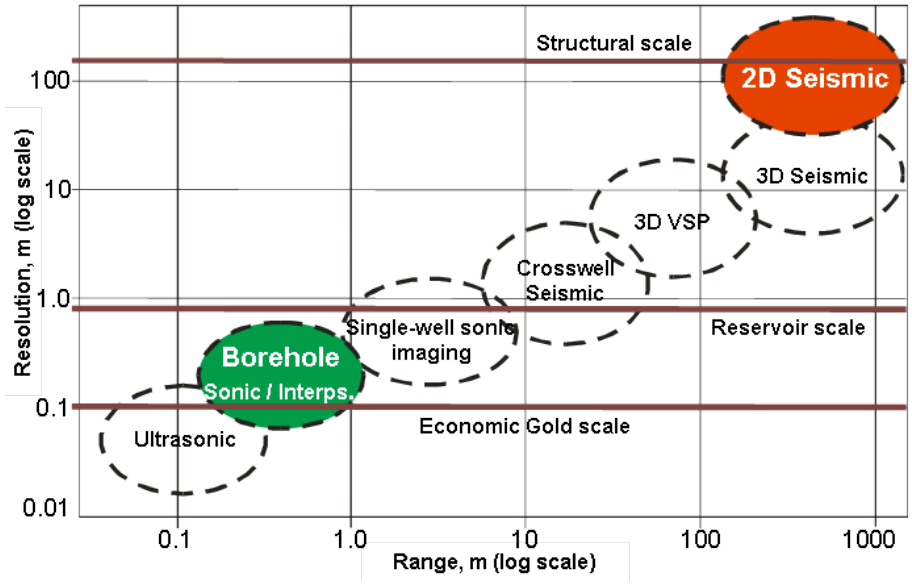

Figure 2-1. Scale difference between borehole sonic and 2D seismic data (After Chabot et al., 2002).

2.2 Vertical and Horizontal Resolution of Seismic Data

The spatial resolution of seismic data is extremely important for hard rock environments where low signal-to-noise ratio and complex structure make seismic imaging difficult. The minimum separation of two bodies before their individual identities is lost on the resultant map or cross-section (Sheriff, 2004) defines the resolution of the data. Horizontal resolution is a direct function of the received signal bandwidth. Wave theory states that a seismic source produces a spherical wavefront that will reflect from areas of boundaries, not single points, which are known as the Fresnel zone. Figure 2-2 shows the Fresnel zone that defines the limit of horizontal resolution with the geometrical reflection point at the centre. The first Fresnel zone is the area on a reflector from which reflected energy can reach a seismic receiver within one-half wavelength of the first reflected energy. Any reflections between A and A' will interact constructively with each other and be indistinguishable at receiver locations.

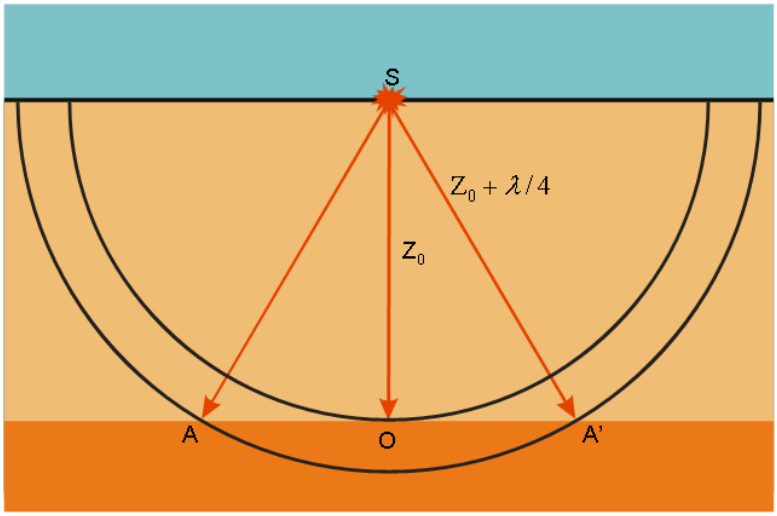

Figure 2-2. The Fresnel zone (after Yilmaz, 2001).

The radius of the Fresnel zone is dependent on depth and the dominant wavelength (Yilmaz 2001), where z is the depth, λ is the reflection wavelength and r is the Fresnel radius and give by:

$$r = \sqrt{\frac{z\lambda}{2}} \tag{2.1}$$

Or in terms of reflection frequency:

$$r = \frac{v}{2}\sqrt{\frac{t}{f}}, \tag{2.2}$$

where *t* is the two-way travel time of the seismic reflecting energy.

Vertical resolution is defined on the dominant wavelength of the seismic data and given by:

$$\lambda = \frac{V}{f}. \tag{2.3}$$

where f is the dominant frequency and *V* is the average medium velocity (Yilmaz, 2001). The limits of vertical resolution depend on both the wavelength of the seismic wave as well as the thickness of the target. Figure 2-3 illustrates defined limits in seismic vertical resolution. Thin beds are not resolved if the thickness of the bed is smaller than the zero crossings of the wavelet. Typical velocities and frequencies in hard rock environments are 5000 m/s and 50 Hz. This results in an initial resolving power of only 100 metres. With Ricker's resolution criteria being ¼ of the wavelength, we can expect approximately 25 metres for two dimensional (2D) resolution in using these velocity and frequency values for mineral exploration. For an ideal S/N ratio of over 50 calibration of the seismic data with full waveform sonic data can increase the resolving limit as will be shown later. At un-calibrated resolutions, hard rock 2D seismic will resolve generalized mineral bearing features including mineralization zones, shear zones, and large alteration halos.

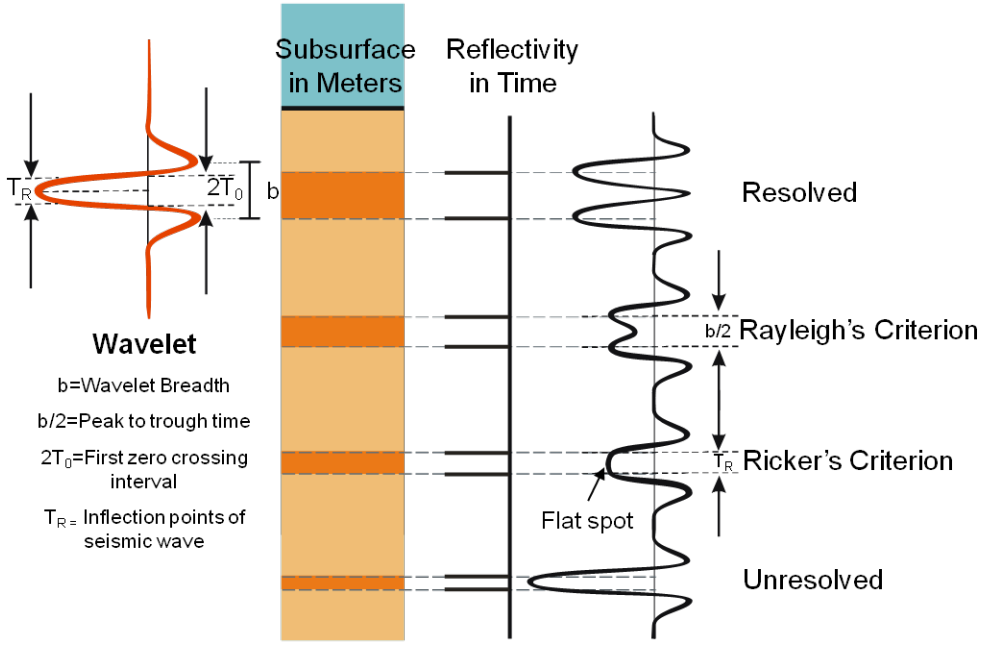

Figure 2-3. The limits of vertical resolution are compared using a sample Earth model, the positive reflectivity as calculated from that Earth model, and the resulting seismic signal (after Kallweit and Wood, 1982).

Figure 2-4 displays a wedge model (Lines and Newrick, 2004) of the Earth with associated reflection coefficients with the same sign showing interfering wavelets. Where the reflectivity is sufficiently separated, the bed is resolved. However as the separation of the reflectivity decreases or the layer thickness decreases, the wavelets merge into one spike. Beyond the temporal resolution point, no more detail can be resolved from the layering. This model is typical for flat laying and slightly dipping reflectors as seen in hydrocarbon exploration. Hard rock mineral exploration, on the other hand, has far more subtle thin rock changes and steep dips which make vertical and horizontal detail more difficult to resolve.

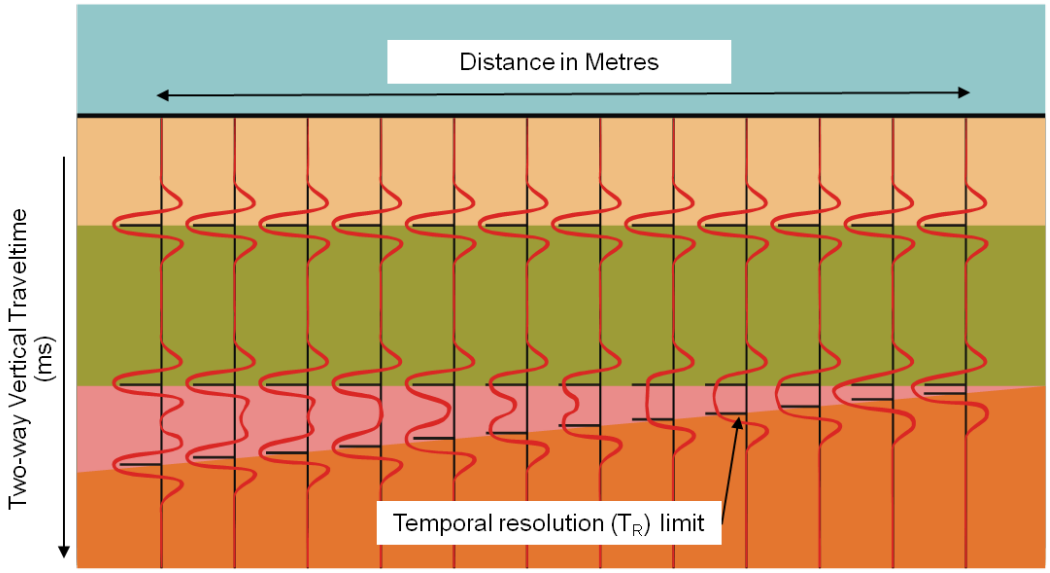

Figure 2-4. Vertical resolution in a wedge model. After the temporal resolution limit no detail can be ascertained due to layering thickness being smaller then λ/4 (after Sheriff, 2004) where λ is the wavelength of the wavelet .

2.3 Seismic Reflectivity

Seismic reflectivity in the Earth arises from changes in seismic velocity, rock density, or both in combination. A seismic wave travelling through the Earth encounters these changes and depending on the proportion of the difference, the seismic energy will be partitioned at each boundary. Reflection coefficients of seismic energy normal to an interface are given by:

$$R = \frac{\rho_2 V_2 - \rho_1 V_1}{\rho_2 V_2 + \rho_1 V_1} = \frac{Z_2 - Z_1}{Z_2 + Z_1}, \tag{2.4}$$

where *Z* is the acoustic impedance of a layer, *ρ* is density of individual layers and *V* is velocity of individual layers. However, reflectivity is also based on angle of incidence of a wave arriving at an interface. Moreover incident P-wave energy is partitioned into reflected and transmitted P- and S-wave energy (Figure 2-5).

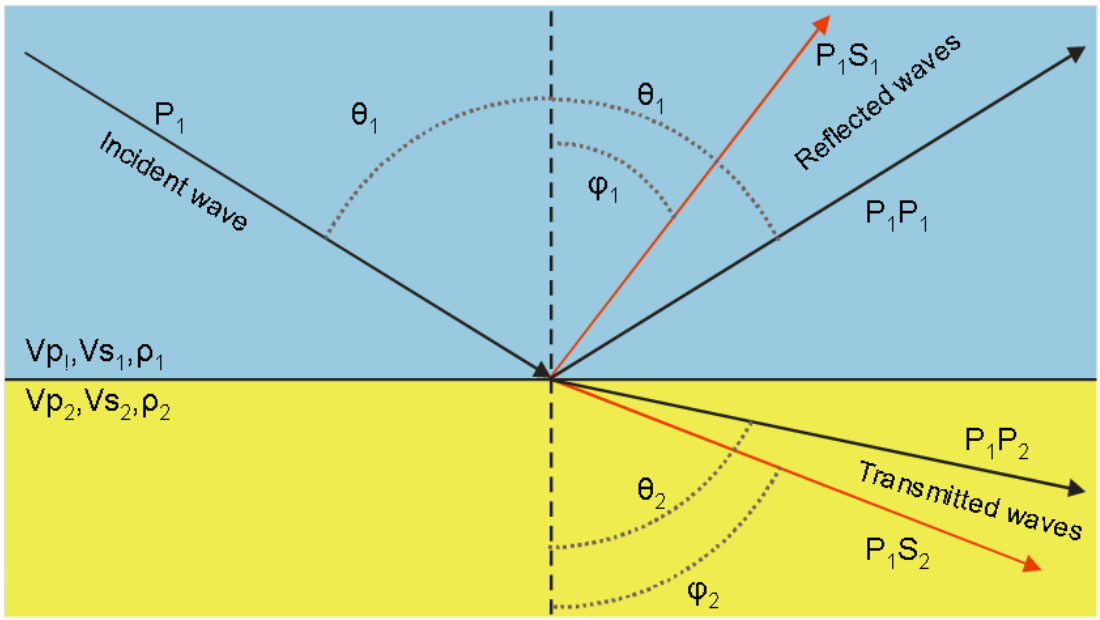

Figure 2-5. A P-wave incident at an interface with resulting in both shear wave reflection and transmission data (after Yilmaz, 2001).

Using Snell's law, the reflection angles and transmission angles of each wave can be calculated as follows:

$$p = \frac{\sin\theta_1}{V_{p1}} = \frac{\sin\theta_2}{V_{p2}} = \frac{\sin\varphi_1}{V_{s1}} = \frac{\sin\varphi_2}{V_{s2}}, \tag{2.5}$$

where θ_1 is the angle of incidence greater then 0^o as well as the reflected P-wave, θ_2 is the angle of transmitted P-wave, ϕ_1 is the reflected S-wave, and ϕ_2 is the transmitted S-wave. V_{P1} and V_{P2} are the P-wave velocities in the upper and lower half spaces respectively while V_{S1} and V_{S2} are the S velocities in the upper and lower half spaces respectively.

Zoeppritz (1919) calculated the displacement and stress potentials at the reflecting interface as boundary conditions to solve for the reflection and transmission coefficients as functions of incident angle and the elastic properties of the media (densities, bulk, and shear moduli). The form of the Zoeppritz calculation is as shown by Yilmaz (2001):

$$\begin{pmatrix} \sin\theta_1 & \cos\phi_1 & -\sin\theta_2 & \cos\phi_2 \\ -\cos\theta_1 & \sin\phi_1 & -\cos\theta_2 & -\sin\phi_2 \\ \sin 2\theta_1 & \frac{\alpha_1}{\beta_1}\cos 2\phi_1 & \frac{\rho_2\beta_2^2\alpha_1}{\rho_1\beta_1^2\alpha_2}\sin 2\theta_2 & -\frac{\rho_2\beta_2\alpha_1}{\rho_1\beta_1^2}\cos 2\phi_2 \\ \cos 2\phi_1 & -\frac{\beta_1}{\alpha_1}\sin 2\phi_1 & -\frac{\rho_2\alpha_2}{\rho_1\alpha_1}\cos 2\phi_2 & -\frac{\rho_2\beta_2}{\rho_1\alpha_1}\sin 2\phi_2 \end{pmatrix} \begin{pmatrix} A_1 \\ B_1 \\ A_2 \\ B_2 \end{pmatrix} = \begin{pmatrix} -\sin\theta_1 \\ -\cos\theta_1 \\ \sin 2\theta_1 \\ -\cos 2\phi_1 \end{pmatrix} \quad (2.6)$$

where α_1 is P-velocity in the upper half space, α_2 is the P-velocity in the lower half space, β_1 is the S-velocity in the upper half space, and β_2 is the S-velocity in the lower half space. A_1 is the reflected P-wave, B_1 is the reflected S-wave, A_2 is the transmitted P-wave and B_2 is the transmitted S-wave. This equation is quite complex but is simplified by Aki Richards (1980) with several assumptions which are relevant to seismic acquisition: (1) property changes are significantly small, (2) second-order terms can be neglected and (3) the incident angle does not approach the critical angle. These assumptions allow for elastic angle dependant reflectivity measurements and calculations for seismic data. Further implications to these equations for hard rock seismic exploration are discussed in the elastic impedance section (2.7.2 Elastic Impedance).

2.4 Quality Factor of Rocks

The quality factor or (Q) is defined as the ratio of the peak energy to the energy dissipated in a wave's energy through a cycle of material. The Q-factor is related to absorption '*a*' as follows:

$$\frac{1}{Q} = \frac{aV}{nf} = \frac{a\lambda}{n} = \frac{hT}{n}, \quad (2.7)$$

where *V* is velocity, *f is* frequency, λ is wavelength, and *T* is period (Sheriff and Geldart, 1995). A low Q value indicates a larger dissipation of energy from the seismic wave through the Earth. The damping factor (*h*) is related to the decrease in amplitude with time.

In hard rock seismic exploration in Western Australia, energy loss and dispersion is relatively high through the regolith zone. The rock quality is low in this area due to the rock having been reworked and weathered. Rock quality is generally high beneath the regolith (Stolz, 2004) promising good transmission for the generation of reflections.

2.5 Rock Characterization

Core sample tests, gold asseys, and full waveform sonic logs (FWS) were available to this research. These sets of data are essential for understandings of *in-situ* statistical rock properties and corresponding synthetic seismogram information. Lithology, structural, and alteration changes along with velocity, density and susceptibility are interpreted from borehole studies. Comparative analysis of these data sets is necessary for understanding elastic rock properties and geological information.

2.5.1 Borehole Interpretations

Interpretations of the borehole core are conducted by trained geologists who quantify grain size, colour, mineral content, rock type, alteration (style, intensity, and minerals), vein (type and intensity), structure (type and intensity), statigraphy (specific rock formation), and gold assessment. These detailed studies have shown that gold mineralization occurs in shear zones, relaxation faults and "softer" hard rocks (intermediate intrusive, sheared dolerite, and sheared basalt) where fluid flow was allowed to move from a deep source to the deposition point (Groves et al., 1992). Groves et al. (1992) and Libby et al. (1991) describe sheared and fractures zones as major areas of gold mineralization in Western Australia. Both the shearing and the faulting allow for mineralization in quartz veins in host basalts and dolerites (Vearncombe, 1998). Figure 2-6 displays a typical shear zone as seen in a mine site wall.

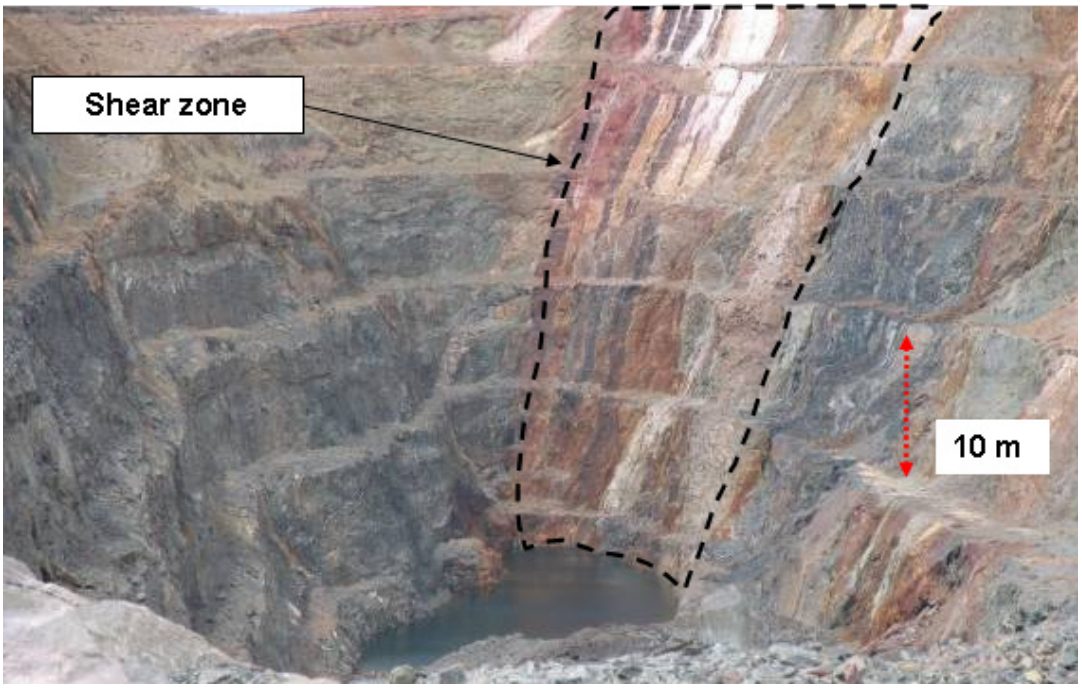

Figure 2-6. The wall of an abandoned mine with a shear zone through the south wall. Each tier or "bench" is approximately 10 metres in height.

Alterations of rocks are also taken into consideration for possible gold indicators as described by Bruhn et al. (1994), Salisbury and Snyder (2004) and Vearncombe (1998). Halos of alteration zones which occur around fractured and shear zones have a prospective reflectivity difference compared with the surrounding host rocks (Salisbury and Snyder, 2004). Alteration changes specifically in the case of Western Australia hydrothermal alteration haloes (Cassidy and Hagemann, 2001) may give a good seismic reflection response. However, these haloes can range from a few metres in size, which are interpretable on borehole sonic logs, to one to two kilometres in width. Two major alteration types are of interest in regards to their potential for being detected in the seismic data as put forward by Neumayr et al. (2004). Namely magnetite halo around gold-bearing structures, interpreted as oxidized hydrothermal fluid, and gold associated, zoned cholorite-biotite-feldspar-carbonate-pyrite quartz alterations.

Full waveform sonic logs (FWS) record two important rock properties in boreholes: direct P- and S-wave velocities. Recording of sonic logs is done on the centimetre scale with Figure 2-7 showing the layout of a typical FWS logging tool illustrating several receivers at different offsets along the body of the tool. The rock formations surrounding the borehole are sampled repeatedly while the well-logging tool is moved up-hole. Bed boundaries are captured on the order of centimetres using FWS logging techniques. For zero-offset, or full stack, we are only interested in P-wave and density and for AVO, elastic impedance we are

interested in P-wave, S-wave and density. The scale difference between FWS logs and seismic data is addressed in the inversion section (2.7 Seismic Inversion).

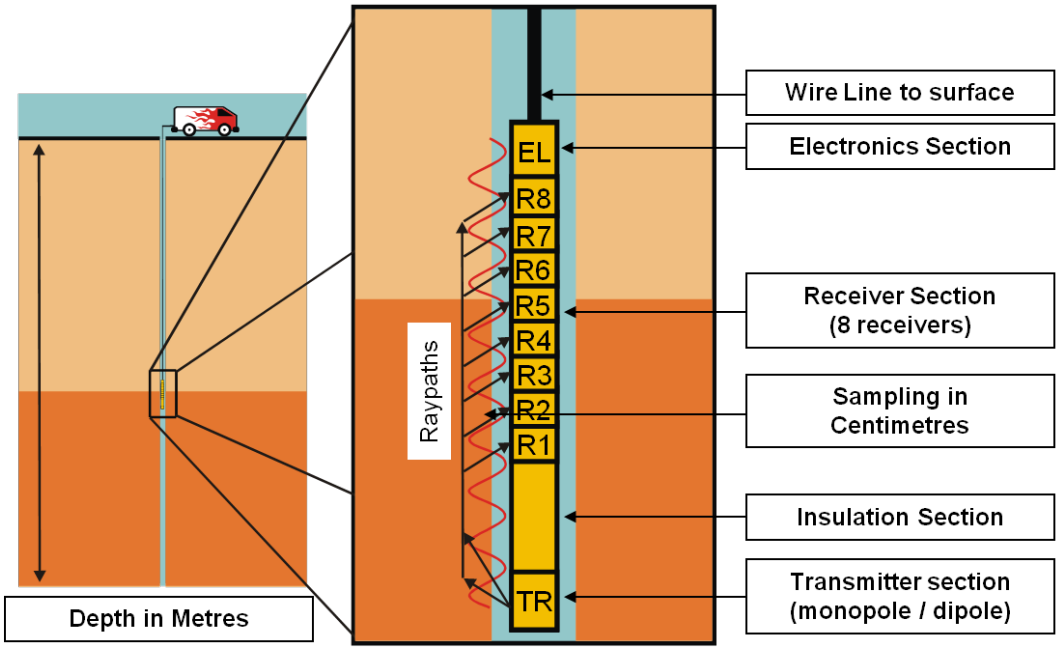

Figure 2-7. The schematic of a typical well-logging tool (after Schlumberger, 2007)

For soft rocks, Gardner et al. (1974) showed that velocity and density can be related by the following equation:

$$\rho = aVp^{b}, \tag{2.8}$$

where ρ is density, V_p is velocity in m/s and a and b are dependent on the type of rock being investigated. The derivation of this relation comes from the plotting of log(ρ) against log(Vp). The above equations can be written in a log-log form in a linear equation where log(a) is an intercept and b is the slope of the least squares trend line gives the following equation:

$$\log(\rho) = b * \log(V) + \log(a). \tag{2.9}$$

Potter and Stewart (1998) extended this empirical P-wave relationship to S-wave and density. The results of plotting and analysing the equations have revealed trends in both Vp and Vs velocities with respect to densities. Knowing that these trends allows for a predictive foundation for reflection coefficients which are based on Vp, Vs, and density information. Castagna et al. (1985) extended these investigations and showed that a simple systematic relationship between P and S-wave exists in clastic rocks. The research was conducted to investigate porosity and saturation for hydrocarbon exploration and

lithological identification. It was shown that the ratio of Vp/Vs reveals definite trends for wet and saturated sandstones, and mudstones. Compressional and shear velocities along with density provide sufficient information to determine the elastic parameters of isotropic media. The statistical relationship that Castagna et al. (1985) defined between Vs and Vp is called the mud rock line and is described as follows:

$$V_p = 1.16V_s + 1360\,. \tag{2.10}$$

The results of equation (2.10) are extensively quoted by many authors in hydrocarbon exploration.

The analogous hard rock conditions for using the above relationships are: structural change, such as shear zones and faulting, alteration changes, with regards to mineralization, and rock type differences, between harder and softer rocks. Salisbury and Snyder (2004) detailed and plotted properties of hard rock types with respect to density and compressional velocity for sonic data acquired in Canada.

Sheared rock is typically weakened as compared to the surrounding host rock allowing for mineralization and deposition to occur. Cox and Ruming (2004) show that mesothermal gold mineralization takes place in relaxation faults and shear zones, revealing a possible gold content indicator. However, reliable results in hard rock characterization are only possible through extensive statistical analysis of the FWS logs crucial for such a study.

2.5.2 Elastic Parameters

The calculation of elastic parameters (Poisson's ratio, bulk modulus, rigidity modulus, Lame's constant and Young's modulus) of rock formations require the use of sonic Vp, Vs and density (ρ) logs. Velocities are related to these elastic parameters as follows:

$$Vp = \sqrt{\frac{\kappa + \frac{4}{3}\mu}{\rho}} = \sqrt{\frac{\lambda + 2\mu}{\rho}}\,, \tag{2.11}$$

$$Vs = \sqrt{\frac{\mu}{\rho}}\,, \tag{2.12}$$

where μ is the shear modulus or rigidity, κ is the bulk modulus, λ is the incompressibility, ρ is density and:

$$\mu = Vs^2\rho \tag{2.13}$$

$$\kappa = Vp^2\rho - \frac{4}{3}Vs^2\rho \;\; \kappa = Vp^2\rho - \frac{4}{3}Vs^2\rho \tag{2.14}$$

$$\lambda = Vp^2\rho - 2\mu = Vp^2\rho - 2Vs^2\rho\,. \tag{2.15}$$

Poisson's ratio (σ), which is closely tied to V_p/V_s, would also be a consideration for hard rock environments based on how this parameter relates transverse and longitudinal deformations (shear zones). Sheared rocks in a hard rock environment should have distinctive rigidity changes. Differing pressure changes through the rock should also appears in bulk modulus variations. Incompressibility, while typically associated with fluid content, should be effected in hard rock environments by showing the difference between weaker and stronger rock. Recovery of elastic parameters from seismic data is not easy, especially in hard rock environments due to inherently low S/N ratio. Hence, precise data processing of the raw data in hard rock environments is a critical step towards successful rock characterization.

2.6 Seismic Data Processing in Hard Rock Environments

A common assumption is a layer cake geology that is consisting of stacked horizontal, homogenous layers with constant velocity and density. However, hard rock environments generally have extreme structural and lithological changes over short distances, with a low signal-to-noise ratio, regolith distortions, seismic lines not laid out with respect to dominant geological structures, and latent mine site noise making seismic exploration difficult. With the final stages of seismic inversion and attribute analysis in mind, a balance has to be struck between what imaging techniques are useful to satisfy both reflection positioning and statistical analysis. Consequently processing of seismic data in hard rock environments is typically a lengthy exercise that needs to be repeated multiple times until the most likely geological model is recovered.

Poor Earth coupling of geophones and sources, seismic energy dispersion and loss through the regolith, and mine site noise from heavy machinery all contribute to an already low signal-to-noise ratio readily seen in hard rock environments in Western Australia. Signal-to-noise ratio is enhanced using NMO, DMO, or migration algorithms. These processes, however, "smear" and "stretch" reflections to properly place reflections in time or depth. This "smearing" or "stretching" causes frequency distortions particularly for

shallow events and at large offsets (Yilmaz, 2001). Muting removes the far offset stretch distortions but may adversely lead to remove wide-angle reflections. A reasonable muting scheme can be selected by checking the images against a synthetic seismogram based on the known velocity distribution (Buchholtz, 1972). Monitoring of the seismic frequency content is necessary to ensure minimal reflection distortion.

Filtering of the seismic data is needed to eliminate both coherent noise and random noise prevalent on seismic data acquired in hard rock environments. Coherent noise is undesirable seismic energy that shows consistent phase from trace to trace, such as ground roll and multiples. Although these coherent noises occur in hard-rock environments, they are sometimes less sever than sedimentary environments, especially multiples. Mine equipment, and vehicle movement on mine sites add large amounts of random noise on seismic data acquired in hard rock environments. The excessive noise needs to be treated with care as robust methods can often alter steeply dipping events which are often very important primaries in hard rock environments.

2.6.1 Regolith Statics Corrections

In hard rock environments such as that seen in Western Australia, the near-surface layer or the regolith tends to distort seismic signals. Five effects occur due to the presence of the low velocity layer on seismic waves:

- High absorption of seismic energy,
- Travel-times affected by the low velocity and rapid velocity gradient change,
- Shorter wavelengths, smaller features produce significant scattering to increase heterogeneous material,
- Marked changes in velocity at the base of the low velocity layer results in wave propagation being nearly vertical regardless of its travel direction beneath the low velocity layer,
- The high impedance contrast at the base of the low velocity layer makes it an excellent reflector and can produce multiple reflections and mode conversions.

High resolution seismic acquisition requires statics corrections for proper imaging and positioning of reflection information. Removing these effects is immensely important for

hard rock environments where shallow seismic imaging is important for economic targets. Complete details for static corrections can be found in Cox (1999) with methods for hard rock seismic data shown by Hatherly et al. (1994), with special identification of the method by Urosevic et al. (2005).

2.6.2 Dynamic Corrections

The normal moveout (NMO) equation is as follows:

$$t_x^2 = t_0^2 + \frac{x^2}{V^2}, \tag{2.16}$$

This equation is derived for a layer cake model. Hard rock environments such as those seen in Western Australia, have far more steep and irregular structure than NMO can resolve. Consequently, additional techniques are required such as dip moveout (DMO), common reflection surface stacking (CRS), multi-focusing, and prestack depth migration. However, these methods have their limitations in hard rock environments. Dip moveout is a partial migration technique to enhance the dipping reflectors directly under the seismic line. Figure 2-8 shows the geometry of a dipping reflector.

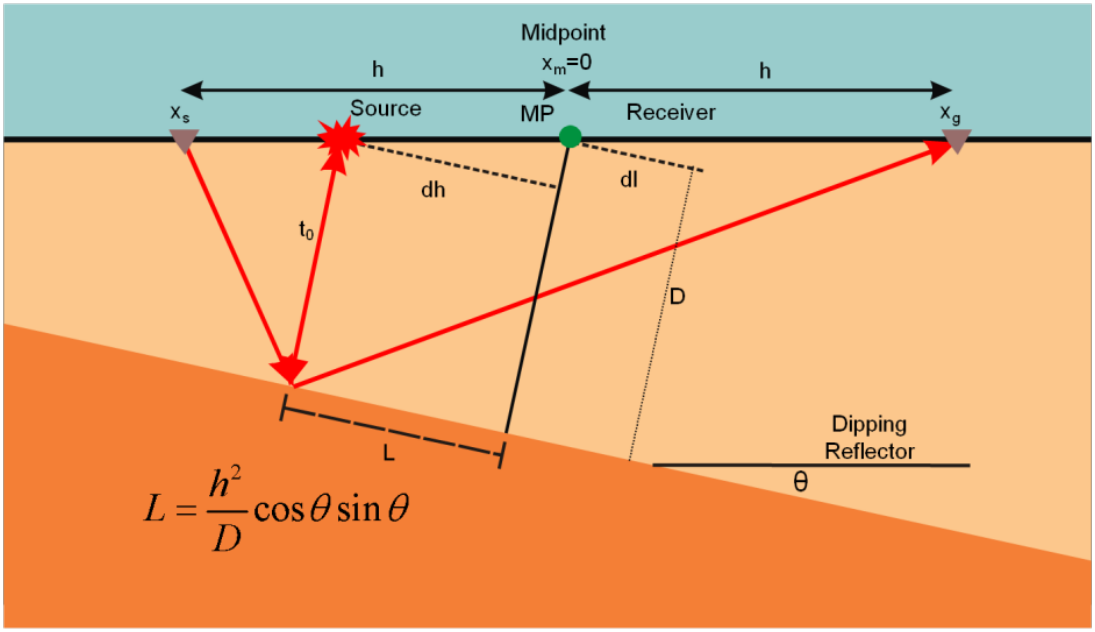

Figure 2-8. A dipping layer. Midpoint (MP) moves up-dip for amount L. The maximum possible movement is large and equals to ½ of the reflector midpoint depth (after Shang, 1990).

The up-dip movement L of the true reflection point changes with source-receiver offset along the same reflector. This results in a "smear" effect of the reflection over a large area. The solution to the dipping layer case is as follows:

$$T^2 = \frac{4d^2}{V^2} + \frac{h^2}{V^2} - 4dh\cos(90-\theta), \tag{2.17}$$

where T is the travel time, h is the midpoint, d is the true depth to the reflector, V is the velocity of the top space, and ϑ is the dip of the layer. These corrections were first derived by Shang et al. (1990) and known as dip moveout (DMO) corrections. The complete derivation can be found in Hale (1995).

Liner (1999) compiled from multiple sources useful aspects of DMO that also have particular importance for hard rock environment:

- Reflection point dispersal is reduced,
- Conflicting dips are stacked with comparable velocities,
- Post-DMO velocity analysis brings stacking velocities closer to the real geological velocities and enables preservation of steeply dipping events and
- Steep dips are imaged better and enable improved post-stack migration algorithm performance.

The constant velocity formulation (Deregowski, 1982) is best suited for hard rock environments, particularly for a depth range of 0-1000 m, which is of the greatest interest for mining exploration. Migration techniques preceding DMO corrected stacked data successfully reposition steeply dipping events in their true spatial and temporal location. However, Liner (1999) outlined that:

- DMO cannot handle significant velocity variations.
- While DMO aids migration techniques in reflection position, post-stack migration techniques can "smear" small discontinuities and have problems in collapsing numerous intersecting events of different amplitude as well as restoring very steep dips.

Because of the complexity in structure and high variation in velocities seen in hard rock environments, DMO is also not a complete solution for hard rock seismic imaging, but is an important velocity analytic tool in hard rock environments. Cross-dip moveout (CDMO) as

suggested by Nedimovic and West (2003) is a partial solution to focusing reflection energy in a complex environments. This however, is a 2.5 dimensional solution to a 2D seismic line in a 3D environment. Care must be taken when using these methods for imaging in hard rock environments.

2.6.3 Migration

Migration has the ability to handle variable velocities, complex structure, shallow structure, and low signal-to-noise ratios (post stacking) readily seen in hard rock environments. Migration techniques collapse diffraction events on unmigrated seismic data to localized points successfully moving reflection events to their proper locations and creating a true image of the Earth. Migration processing can be conducted both pre-stack and post-stack as well as in time and in depth. Time migrations have been used historically due to computational limitations and because sonic logs synthetics, and attribute techniques work in time and frequency domain. Depth migration is known to be more accurate (Pasasa et al., 1998), more intuitive for interpretation, but is far more sensitive to velocity variations and require conversion (which could be inaccurate) to be of use for inversions. The focusing of the reflections used in migration technique depends heavily on a specific Earth (velocity) model requiring rigorous velocity analysis in hard rock environments.

Post-stack migrations have in the past been the migrations of choice based on their efficiency and straight forward imaging conditions (exploding reflector). These methods are less sensitive to velocity but overall performance of the technique is better if velocity analysis is correct. Historically pre-stack migrations have been more computationally and financially expensive to perform over their cheaper and faster post-stack migration counter parts. The “costliness” of the pre-stack migration, however, has been reduced with the advent of faster computers and more efficient algorithms. Pre-stack time migrations utilize interval velocities as derived from RMS or *a priori* geological models for best imaging. These migrations are considered the most accurate seismic solution for imaging Earth structures based on their ability to focus and position reflections in the context of strong lateral velocity variations (Guo and Fagin, 2002). Pre-stack migration also creates common reflection points for summing which no longer smears the amplitudes as seen in post-stack migrations. While pre-stack depth migration methods have been predominantly used in

deep hydrocarbon exploration, it has been suggested by several sources (Bradford et al. 2006; Pasasa et al. 1998) as a better solution to resolve shallow reflectors. The improved shallow image comes from the use of highly detailed velocity models to suppress steeply dipping coherent noise, while stacking out migration effects on the final image (Bradford et al., 2006). The velocity model is required to be as close to the *a priori* geological model as possible. However, with limited borehole data available in hard rock environments, pre-stack depth migrations require a self-extracting velocity model with references to log data for increased accuracy. This type of analysis requires all pre-stack traces contributing a scatterer to be horizontal for the velocity to be correct (Faye and Jeannot, 1986; Al-Yahya, 1989). In a hard rock environment, this type of analysis is hard to pursue due to the low S/N ratio. An alternative approach is to "populate" the depth image provided by post-stack migration with the "best" velocities. These velocities are typically constructed by combining logs data, RMS velocities and local geological knowledge.

After the "best" time-depth image has been generated the main task is to attempt to recover an impedance section which corresponds as accurately as possible to the actual geology.

2.7 Seismic Inversion

Inversion is the process of deriving a consistent Earth model from calibrated seismic and borehole impedance measurements. Acoustic impedance inversion was developed in the hydrocarbon industry in the 1970s by Lindseth (1979) and has since been used extensively, and successfully, for reservoir characterization, lithology prediction, and hydrocarbon prediction. In hard rock environments, seismic inversion could have many prospective uses such as: lithology prediction, mineralization zones prediction, sheared rock detection, or alteration halos in host rocks may be identified through hard rock seismic inversion. For example, shear zones have a particular seismic signature (Urosevic, 2005) but unknown inversion properties.

Proper seismic inversion requires calibration of good quality seismic data and sonic logs drilled on the seismic recording line for reliable results. Special considerations must be be taken during processing to preserve true relative amplitudes. This preservation is hard to achieve in a hard rock environment due to low signal-to-noise ratio. Seismic data is also inherently band-limited with lower frequencies missing and the high frequencies being distorted by noise. Some of the lost frequency information can be derived from well

control and geostatistical analysis (Latimer, 2000) but original signal bandwidth is difficult to retain.

The process of inversion is essentially the opposite of forward modelling (Bancroft, 2002) with Figure 2-9 illustrating graphically both forward modelling and inversion. An exact impedance prediction in inversion is more difficult to attain due to the unknown wavelet, noise in the data, and band-width limitations in the seismic data. With inversions already being highly ambiguous, these difficulties make inversion in hard rock environments even more challenging. Figure 2-10 illustrates a typical seismic inversion process that is frequently utilized in the oil industry.

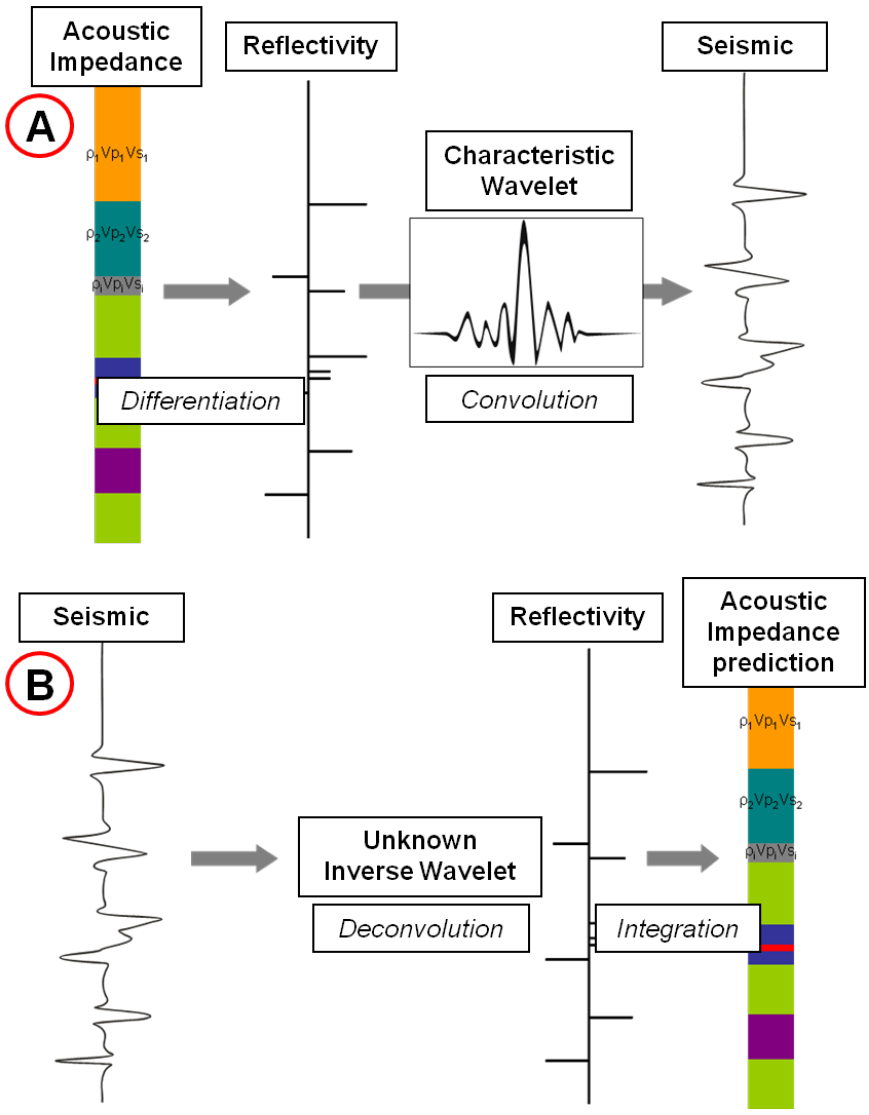

Figure 2-9. (A) illustrates the forward modelling process, and (B) illustrates the reverse of forward modeling, or inversion (after Bancroft, 2002).

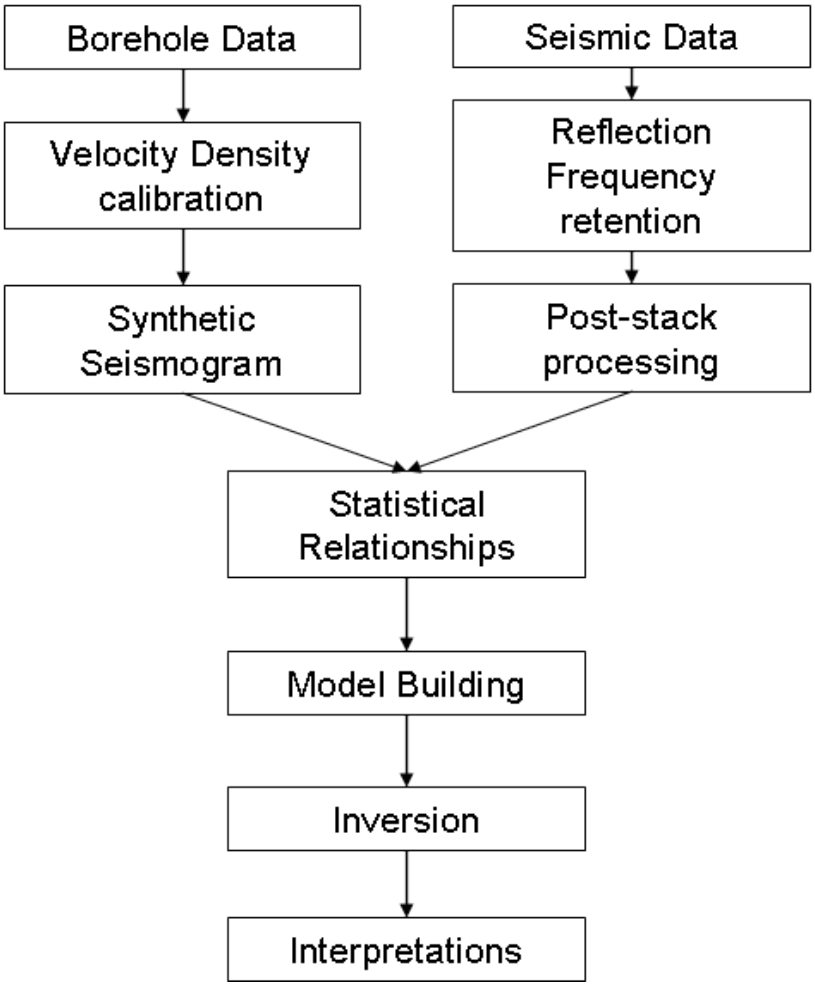

Figure 2-10. The inversion process (after Hampson-Russell, 2007)

2.7.1 Acoustic Impedance

The inversion process takes the seismic traces and converts them into a pseudo reflection coefficient time series (Becquey et al., 1979). The acoustic impedance that results from the pseudo reflection coefficient is as follows:

$$Z_{i+1} = Z_i \frac{1+k_i}{1-k_i} = \rho_i V_i \frac{1+r_i}{1-r_i} = \rho_{i+1} V_{i+1}\,. \tag{2.18}$$

This equation represents a simple two layer system where Z_i is the acoustic impedance in the *i*th layer and k_i is the pressure amplitude reflection coefficient at the *i*th interface. The acoustic impedance of the Z_i in the first layer is assumed to be known. With the first layer known, equation (2.18) is used iteratively to calculate subsequent layers. The resulting pseudo reflection coefficient time series, or pseudo logs are roughly equivalent to logs

recorded in wells drilled at every seismic trace location and is referred to as 'trace based' data (Watson and Lines, 2000).

A major challenge of inversions is the limited frequency bandwidth from which seismic recordings suffer (Lindseth, 1979). Trends that are found within an impedance model created from seismic inversion do not come from the seismic amplitudes but from the low frequency model (Francis, 1997). Specifically, a lack of low frequency and decay curve (DC) affects the seismic data thus limiting the inversion results. Converting the seismic reflection amplitudes to impedance profiles as near to the subsurface as possible requires the removal of the band-pass filter or wavelet used in seismic acquisition and processing. Well control through full waveform sonic logs is used to calibrate the wavelet and also restore low frequency information to the seismic data. Proper calibration results in accurate impedance predictions throughout the seismic data. However, as pointed out by Francis (1997), since the same well log values are used for both the seismic amplitude inversion and the low frequency model, the strong apparent correlation between seismic acoustic impedance estimates and rock parameters is not surprising. An increased number of borehole sonic logs will improve the inversion results, but large quantities of good sonic data are not always available in hard rock environments.

A broader bandwidth of the impedance data through conditioning of the seismic and sonic log data not only maximizes vertical resolution, but also minimizes tuning effects (Savic et al., 2000). Sometimes tuning effects, if positive, enable us to "see" clearly small geological features that otherwise would be difficult to detect such as shear zones. Inversion in hard rock environments is undoubtedly a difficult yet potentially rewarding method for mineral exploration.

2.7.2 Elastic Impedance

Unlike acoustic impedance, elastic impedance has angle dependence which can be seen on amplitude-versus-offset (AVO) plots. Elastic impedance inversions and analysis must be used with offset stacks or gathers, either distance or angle, where AVO results can be calibrated and observed. As was the case with acoustic impedance inversions, elastic impedance is band-limited and suffers from non-unique results. Unlike acoustic impedance, however, elastic impedance takes into consideration not only P-wave and density, but also S-wave. This results in a far more complicated method in comparison to

acoustic impedance which utilizes vertical incidence angles. For elastic impedance seismic rays are now allowed to strike boundaries at non-zero incidence angles giving four possible curves: reflected P-wave amplitude, transmitted P-wave amplitude, reflected S-wave amplitude and transmitted S-wave amplitude (Figure 2-5).

The calculation of amplitude variation with offset involves Poisson's ratio which is related to P-wave and S-wave velocity in the following equation:

$$\sigma = \frac{\left(\frac{V_P}{V_S}\right)^2 - 2}{2\left(\left(\frac{V_P}{V_S}\right)^2 - 1\right)}, \tag{2.19}$$

in which the theoretical bounds are between 0 and 0.5 for isotropic rocks.

Amplitudes of near-offset reflections and impedance predictions can be tied to well logs using synthetics based on acoustic impedance or inverted, to some extent, back to acoustic impedance using post-stack inversion algorithms (Connolly, 1999). Connolly (1999) derives the elastic impedance and arrives at the convenient formula:

$$EI(\theta) = V_P^{(1+\tan^2\theta)} V_S^{(-8K\sin^2\theta)} \rho^{(1-4K\sin^2\theta)}, \tag{2.20}$$

and

$$K = \frac{V_S^2}{V_P^2}, \tag{2.21}$$

Full derivations of these equations are prepared in Appendix A. Elastic impedance inversion analysis is necessary in hard rock environments due to the extreme structural complexity.

2.7.3 Convolutional / Deconvolution Model for Geophysical Inversion

Seismic data can be considered as the convolution of a wavelet with reflectivity. In the one dimensional sense, the convolutional model appears as reflectivity r and wavelet w(t) convolved as follows.

$$s(t) = r * w(t) + n(t), \tag{2.22}$$

where *n(t)* represents the additive noise. To simplify this function, additive noise can be considered zero. While this assumption is not correct, the resulting equations are less cumbersome. In the case of the Earth's response in equation (2.22), the reflectivity *r* is unknown. A simplified prediction is presented in Appendix B:

$$b_t * x_t = b_1 * k_t * f_t = s_t * f_t = \widehat{f}_t . \tag{2.23}$$

The final derivations show that the more information we can gather about the mapping kernel (source wavelet) and the model term will still only give us estimation of what our observation (seismic) truly is.

2.7.4 Optimal Conditions for Inversion

The mathematical understanding of inversion has shown that quantifiable results are readily obtained from properly calibrated data. Knowing the characteristic wavelet of noise free seismic data with a good Earth model will produce an inversion that represents the area directly under the seismic line. However, acquiring the characteristic wavelet and having noise free seismic data is all but impossible to achieve in practice. Inversion has been described as "interpretation of inaccurate, in sufficient and inconsistent data" (Jackson, 1972). While this quote shows the potential bleak outlook for inversion processes, many studies have shown that with proper constraints and calibrations, inversion does have a place in geophysical interpretation.

Rigourously processing the seismic data so that original reflection phase, frequency, and amplitude is retained is essential for inversion. Check shots, while very important are practically never available in hard rock environments. To work around the lack of check shots, it is necessary to arrive at the "most likely" well tie away from conventional calibration approach. Local geological knowledge and core samples may be necessary to compensate for missing check shot measurements.

Constraining of the seismic data to sonic data can be handled in two ways: "hard", such as density and velocity known between a given upper and lower limit and "soft" which are multidimensional probabilities dependant on parameters in a given model (Treitel and Lines, 2001). However, the seismic data has inherent limitations that inversion simply cannot resolve. "Blind spots" where the seismic data is not able to reveal geological form due to bed thicknesses or a large Fresnel zone cannot be reconstructed by inversions. As

shown by Wapenaar (1996), fine layering issues that arise from bed thickness can essentially be ignored in inversion and migration as long as both inversion and migration are based on the same "extended macro model". This "extend macro model" is based on the known geology from the borehole interpretations and full waveform sonic logs to position the reflections properly on the seismic image.

It is critical in the case of hard rock environments that the boreholes be located and drilled on-line due to the extreme structural complexity, rapid lateral variations in velocity and reflectivity, and unconformable dips (White and Hu, 1998). With low signal-to-noise ratio in the seismic data, and no check shot for time-to-depth information, inversion results require careful analysis.

2.7.5 Wavelet Extraction

The synthetic seismogram is created by the convolution of an appropriate wavelet with the primary reflectivity series from the sonic log.

$$d_k = p_k * r_k , \tag{2.24}$$

where d_k is the resultant synthetic seismogram, p_k is the known pulse or wavelet and r_k is the impedance as created from the FWS. The results of d_k (synthetic seismogram) are dependent on both the wavelength of p_k and the sample rate of r_k.

Wavelet estimates are taken only from the seismic data and described as follows:

- Compute the desired phase (zero, constant, minimum),
- Calculate the autocorrelation over a chosen window,
- Calculate the amplitude spectrum of autocorrelation under the assumption of a white reflectivity spectrum,
- Take the square root of the autocorrelation spectrum which approximates the amplitude spectrum of the wavelet, and
- Take the inverse FFT to produce the wavelet (Todorov 1998).

When matching has been completed through all synthetic and seismic data, extending of those known contacts through a seismic image can take place. This process is known as "horizon" picking referring to reflections which have occurred at impedance

changes between different rock types in hydrocarbon exploration. In hard rock environments most prominent reflections have been known to come from shear zones (Urosevic personal communication, 2005) limiting our use of the word "horizon". "Rock contact" will presently be used in place of "horizon" in this hard rock environment due to rock characterization showing most reflections occurring at rock contacts. Rock contact picking is not a trivial process in a complex environment such as that seen in Western Australia. All data sets available are included in the picking process to ensure that proper contacts are interpreted through the seismic data. Harrison et al. (2007) showed that the seismic attribute of instantaneous phase can be used to help delineate rock contacts in areas where low signal-to-noise ratio blurs reflections for contact picking. Ultimately however, the low signal-to-noise ratio and limited bandwidth of the seismic data make some rock contacts unresolvable. Final model creation takes place when seismic reflections have been matched with sonic data.

2.7.6 Types of Inversion

Inversion generally has non-unique solutions to finding the reflection coefficient series of seismic data (Latimer and Van Reil, 2000). Moreover, both the bandwidth limitation of the seismic data and the limitations of the sonic data increase ambiguity of inversion solutions. The choice of an inversion is based on the type of data available, the quality of data available, the turn-over around the project, known (or believed) relationships between rock properties and acoustic impedance in the area, and the desired thickness and depth of targets. The inversions that were considered for hard rock environments are all robust processes that work well on post-stack data. An extensive analysis of each type of inversion can be found in "Introduction to Seismic Inversion Methods" by Russell (2006). Several key inversions are covered qualitatively below.

2.7.6.1 Model Inversion

The model inversion is a generalized linear inversion (GLI) algorithm which attempts to modify a model until the resulting derived synthetic matches the seismic trace within some acceptable bounds (Russell, 2006). The model comes from the *a priori* matched geological information and the seismic data and used to create synthetic seismograms at each trace

and then compared with seismic data. The correlation of the two data sets depends on which type of model inversion is utilized.

The "Hard" constraint uses more the statistical constraints within the borehole sonic logs for its prediction base through the seismic data. "Soft" constraint inversions use more probabilistic correlation between the borehole impedance and the seismic data for inversion.

2.7.6.2 Band Limited

This algorithm uses a classical recursive inversion which ignores the effects of the seismic wavelet and treats the trace as if it were a reflection coefficient (Hampson-Russell, 2007b). One of the key problems with recursive inversion is the loss of low-frequencies within the seismic data. This is due to the seismic trace being assumed to be a series of reflection coefficients filtered by a zero-phase wavelet. Frequency content is restored by using smoothed model constraints.

2.7.6.3 Coloured Inversion

The algorithm used for coloured inversion approximates an unconstrained sparse-spike inversion by deriving an inversion operator that matches the amplitude spectrum of the seismic to that of the impedance (Connolly, 1999). Coloured inversion only uses a single operator applied to the seismic trace to transform it directly.

$$I = O * S\,, \tag{2.25}$$

where the operator *O* is in the frequency domain and has a phase of -90 degrees. Borehole data are used to generate an amplitude spectrum with a straight line indicating the desired output impedance. A seismic spectrum is generated in a neighbourhood of traces around boreholes. The combination of these two spectra and a -90 degree phase shift produces the coloured inversion. The resulting impedance is relative impedance (Coloured) with only positive or negative values. Frequencies can be added back for comparison purposes.

2.7.6.4 Sparse Spike

A sparse spike operation approximates a time series by a few sizeable impulses, for example, approximating a reflectivity function by a small number of reflecting interfaces. The algorithm creates a sparse reflection that produces the best match between the derived synthetic and the seismic trace subject to the constraint that the number of spikes be a minimum (Hampson-Russell, 2007b). By minimizing the error between the model trace and the seismic trace, sparse reflectivity is recovered from the impedance model. The maximum likelihood algorithm uses the model to perturb a reflectivity series estimate from the seismic data. An optimal sparse reflectivity series is found by adding reflection coefficients and increasing the number of iterations and tolerance levels.

2.7.6.5 Neural Network

This algorithm applies a probabilistic neural network to the seismic trace to produce the impedance (Hampson-Russell, 2007b). It is similar to a neural network function discussed later in the attribute analysis section.

2.7.7 Inversion Error

Error analysis in inversions can be achieved in several ways. One method, which will be used in this study, uses “hidden” boreholes which are not included in the inversion process and revealed afterwards to observe how accurate the inversion is with respect to those holes. These “hidden” boreholes are originally tied with the seismic data and corrected for borehole affects prior to being hidden (Latimer and Van Riel, 2000). After an inversion is complete, hidden wells are made “visible” once again and their true impedances checked against the prediction results. For this type of testing many boreholes are needed for highly accurate results, however multiple boreholes with sonic logs are not always available in hard rock environments.

2.8 Seismic Attributes

Seismic attributes are specific measures of geometric, kinematic, dynamic and statistical features derived from seismic data (Marfurt, 2006). The study of attribute analysis attempts to use derived attributes from seismic data to predict the distribution of physical properties (e.g. P-wave, impedance, porosity, lithology, and bed thickness) of the strata being imaged seismically (Hart, 2002). While inversion utilizes known acoustic and elastic impedances with matched horizons for predictions throughout the seismic section, attribute analysis uses suspected ties between rock properties from the log and wave field attributes for predictions throughout the seismic section. Seismic attributes can be classified as the following types of 2D attributes (Russell et al., 1997):

1. Instantaneous attributes, derived from a combination of input seismic trace and Hilbert transform of the trace.
2. Window frequency attributes which is the amplitude spectrum of the seismic trace over a window.
3. Recursive attributes which are found by applying a recursive operator along the trace.
4. Bandpass attributes which are narrowband filter slices of the seismic traces.

Simple attribute analysis has shown predictive abilities for sonic velocity (Todorov et al., 1997), predictions of faulting and fractures (Neves et al., 2004), lithology mapping (Walker et al., 2005), and specifically in the case of mining in South Africa, lithological variations in gold bearing conglomerates (Stuart et al., 2000). Time derived attributes can explain structure while amplitude derived attributes as well as frequency derived attributes address problems of stratigraphy and reservoir properties. Brown (2000) listed the plethora of known attributes (Figure 2-11) and suggested three criteria for evaluation of attributes for possible statistical analysis: 1) Seismic attributes have to be unique, 2) seismic attributes have to have a clear and useful meaning (do not use attributes if you don't know what they are doing), and 3) seismic attributes should not vary greatly in response to small data changes. Staying clear of weighted attributes has also been suggested by Brown (2000) due to the weight only acting as a gain possibly distorting the results. While seismic attribute utilization is considered a mature technology in the hydrocarbon industry (Eastwood, 2002), almost no reported research is available for

attribute use in hard rock environments. Therefore, the first attributes that are considered must be the most basic as derived from the complex analysis of the analytical signal. Proper conditioning and calibration of both seismic and sonic data for successful attribute analysis is done the same way as seismic inversions. Fundamental attributes are discussed in Appendix C.

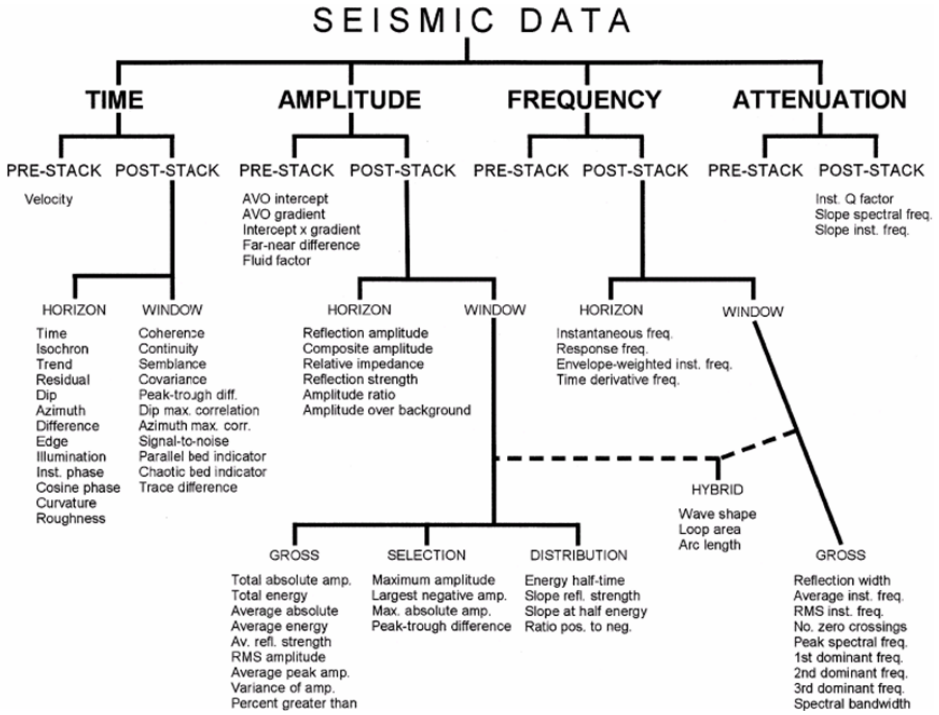

Figure 2-11. A list of seismic attributes (after Brown, 2000)

2.8.1 Logs and Seismic Attributes

As described by Todorov et al., (1997) the relationship between the log property and seismic attributes can be written as follows:

$$P(x,y,t) = F[A_1(x,y,t), A_2(x,y,t), \ldots A_n(x,y,t)], \tag{2.26}$$

where *P(x,y,t)* is a log property, *F[…]* is a functional relationship and A_i are the seismic attributes. Equation 1.3 can be placed in a linear convolution model as follows:

$$P_N = W_1 * A_1 + W_2 * A_2 + \ldots W_M * A_M + W_{M+1}, \tag{2.27}$$

where W_i are convolutional operators and W_{M+1} is a constant. Knowing if there is a linear relationship between the log properties and the attributes will allow better predictions of the property throughout the seismic section. Figure 2-12 A) illustrates the combination of several attributes at single points for log predictions. Figure 2-12 B) illustrates how a

neighbourhood of attribute values can be used to predict potential log values. However, while we do know that seismic signals are caused directly by rock physics properties, the relationship between the properties and the more obscure seismic attributes are not obvious (Shultz et al., 1994). Neural networks are used as prediction tools for nonlinear optimization of attributes and for log calibrations.

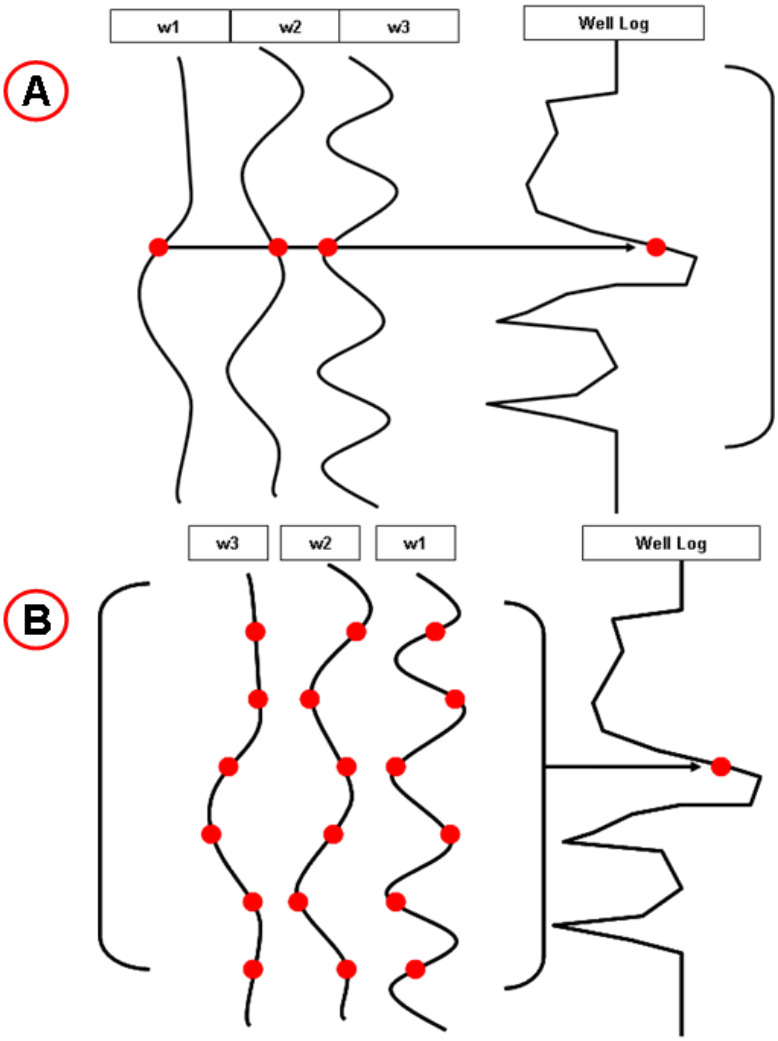

Figure 2-12. This figure represents the linear combination of several seismic attributes to a targeted log. A) shows the use of only one single point from a set of attributes for prediction of one point on the log while B) displays the weighted sum of attributes for prediction (after Hampson-Russell, 2007b).

Finding a potential relationship between seismic attributes and log properties sometimes required searching for trends within both sets of data which are non-linear, non-unique, and non-trivial. Neural networks use mathematical algorithms that are trainable to solve the statistical links between seismic attributes and log properties. Neural network applications can either do classification problems, which use input classes such as

sand, shale etc, or regression which requires a specific value such as P-velocity, impedance, gamma ray, etc.. As described by Todorov et al. (1997), neural output can be described mathematically as follows:

$$\text{Neuron's output } = f\left(\sum_{i=0}^{n-1} x_i w_i + w_n\right), \tag{2.28}$$

where:

w_i – connections weights (w_n is a constant called bias)

x_i – neuron inputs

f = activation function, usually the sigmoid function.

Figure 2-13 illustrates graphically how the neural network operates.

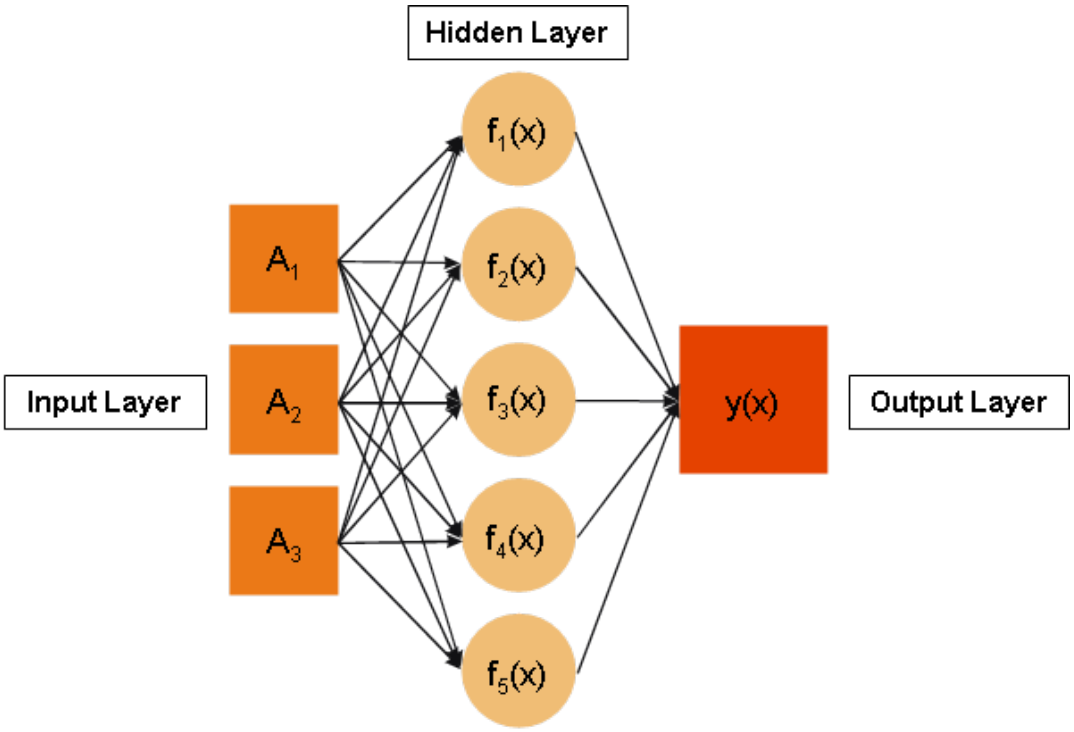

Figure 2-13. Representation of a neural network where there are three inputs, five hidden nodes, all generating one output layer. Each connection between the layers represent a weight, however excess weighting can be removed by normalizing the variables prior to input (Shultz et al., 1994).

The objective is to fit a non-linear function to the sample data set that best matches the output layer. The more input layer and hidden layer information that is available, the more statistically probable the output layer prediction. A smooth, but not

necessarily linear function that links all layers is desired because if the relationship exists between input (attributes) and output (property), it will have to originate from some rock physics basis (Shultz et al., 1994). The process of weighting the data is known as quadrature training which increases in accuracy through multiple iterations.

2.8.2 Validation of Multi-Attribute Analysis

Verification of prediction results for attribute analysis is not trivial. Validation of results consists of dividing the entire data set into two subsets: the training data set and the validation data set. The training data set is used to derive the transform, while the validation data set is used to measure its final prediction (Hampson et al., 2001). Accuracy of prediction results depend on quality and quantity of borehole data. However, borehole sonic data is not always available in the quality, nor quantity desired for valid results in hard rock environments.

2.9 Inversion Summary

Seismic data reveals information on the 10s of metres scale detailing structure, and trends over a large rock volume. Borehole data and sonic logs reveal information on the centimetre scale allowing precise measurements, but limited volume resolution. Bringing the two data sets together through statistical analysis is a major desire of this research. Mutual calibrations of the two data sets provide the basis for reliable seismic imaging as well as providing a statistical basis for seismic inversion and attribute analysis. Seismic inversion allows for log properties of acoustic and elastic impedance to be predicted throughout the seismic image, while attribute analysis aims to use suspected links between seismic attributes and log properties for predictions. Proper processing of the seismic image and precise conditioning of the sonic data is vital for successful seismic inversion and attribute analysis. The following chapters will apply these principles to study the seismic and borehole sonic data sets from two distinct locations at the St. Ives gold camp in Western Australia

3 Geological Setting of the St. Ives Gold Camp

"There is nothing more difficult to take in hand, more perilous to conduct or more uncertain in its success than to take the lead in the introduction of a new order of things."

- **Niccolo Machiavelli (The Prince, 1532)**

With the world demand for gold almost equivalent to the demand for petroleum, (Denham, 2008), and gold increasingly hard to find, there is a need for mankind to find new and innovative techniques to explore for this precious resource. Generally, mineral exploration in hard rock environments is difficult due to the regolith and fresh rock complexities. Potential field geophysical methods have traditionally been used to detect structures and aid in pin-pointing possible mineral and gold targets. These methods have relatively low spatial resolution and are typically limited to shallow targets, especially in the presence of a thick regolith cover. To address the need for new exploration techniques in an industry where new prospects are difficult to find with present technologies, seismic imaging can offer a major new tool to the mining industry. Seismic methods have the ability to increase spatial resolution with their superior target imaging at depth. Mineral and lithological predictions through seismic, based on rock impedance and wave attribute analysis, are more than possible with the proper sonic logging and processed seismic data. Seismic methods offer the quantum leap in mineral exploration but do require a thorough investigation to reveal possibilities and limitations of this new technology for hard rock environments.

The focus of this study is rock characterisation utilizing seismic reflection methods and sonic log data to image gold bearing ore in the St. Ives gold field located near Kambalda, 60 kilometres south of Kalgoorlie in the Eastern Goldfields Province, Western Australia (Figure 3.1). Gold mining began in this area at the turn of the 19th century but ceased during the 1930s (Webb, 1993). In the 1980s new reserves of gold were discovered at the Victory mine with several other deposits being found at the Revenge, Junction, and Argo mines in the St. Ives gold camp. The camp at present produces 500,000 oz of gold per year from open pit and underground mines (Stolz et al, 2004). The St. Ives camp is 40

kilometres long and 10 kilometres wide trending south-southeast from Kambalda. It is located on the southern tip of the Norsemen-Wiluna greenstone belt of the Yilgarn craton.

The Yilgarn craton accounted for almost 80% of cumulative Western Australian gold production up to 2001 (Cassidy and Hegemann, 2001). The craton is an Archaean mafic sequence made up of basalts, ultra-mafics and interflow sediments. These formations are found primarily in a southerly plunging anticline, overlain with unknown crusts of felsic composition and intruded by dolerites and felsic porphyries (Drummond et al., 2000). The Boulder-Lefroy fault zone, which is of interest to this research, is trending north-northwest to the east and the Merougil fault zone to the west. Intermediate and felsic porphyry dykes are of particular abundance where gold mineralization has a high probability. Massive shear zones abounding in the areas around greenstone belts are also abundant sources of gold and nickel mineralization. These areas are commonly 0.5 to 3 km wide and characterized by foliated schists, mylonite and gneiss (Vearncombe, 1998).

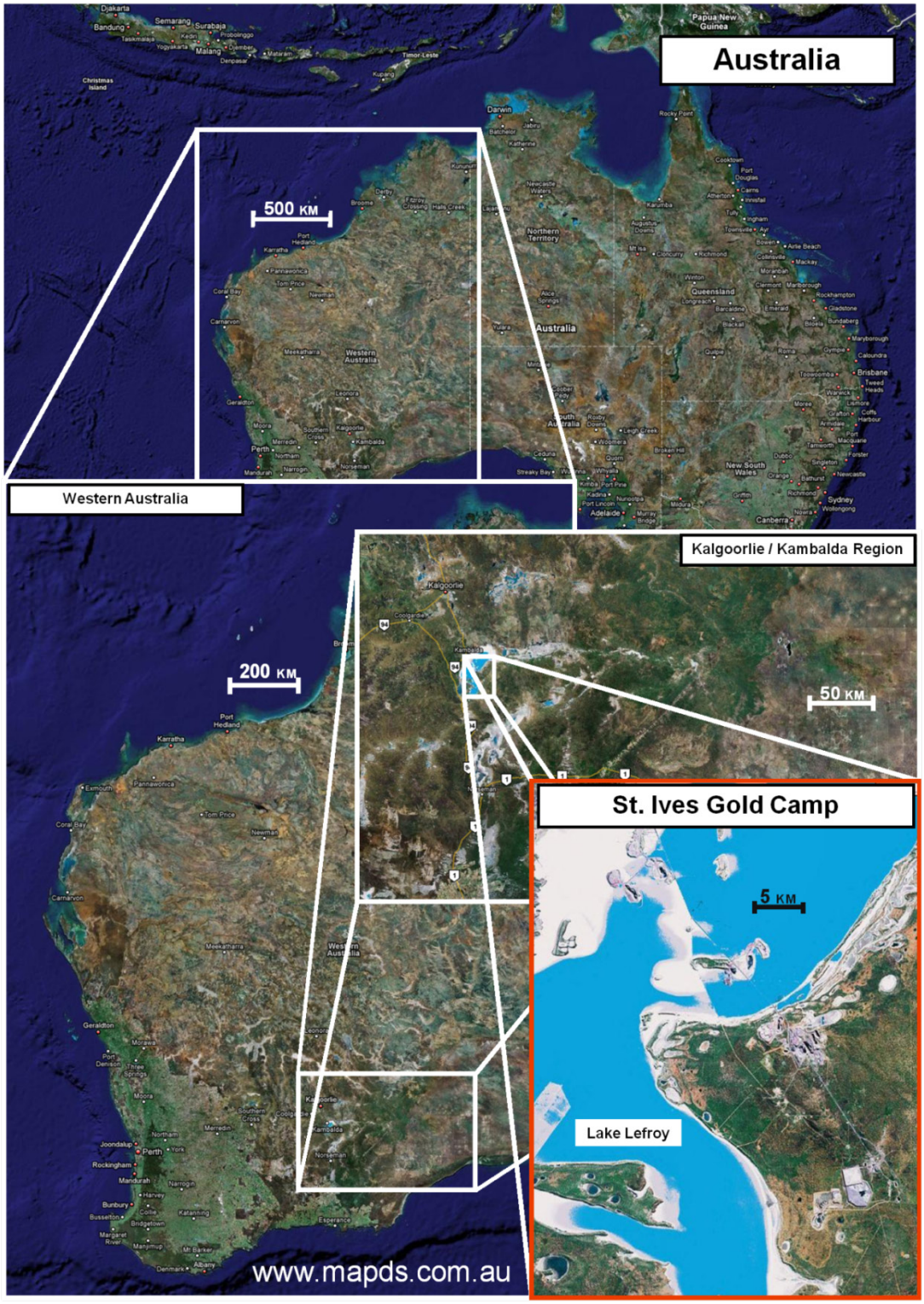

Figure 3-1. The St. Ives gold camp is located in Western Australia 60 kilometres south of Kalgoorlie. (from www.mapds.com.au.)

As pointed out by Neumayer et al. (2004), despite the large database on, and the myriad of genetic models for, Achaean orogenic gold deposits, the predictive capability of delineating high-grade (>5 g/t Au) gold deposits and/or ore shoots (>10 g/t) within a gold camp is limited. The Boulder-Lefroy shear zone which dominates the St Ives gold camp has the following important features associated with gold mineralization (Weinberg et al., 2004):

- Crustal scale shear zones,
- It is near an abundance of faults and shear zones both parallel and oblique to crustal scale major shear zones over low straining host sequences,
- Close to hinge of regional-scale anticlines, particularly double plunging folds,
- Complex lithostratigraphic sequences of varied orientation,
- It has a presence of small ridged granitic intrusions,
- Host rock with high total Fe or high Fe/(Fe +Mg) ratios to induce sulfidation and gold precipitation , and
- Preferential formation depths of 5-100 km at temperatures between 300 and 4000^{0}C.

A diverse range of depositional site characteristics (host lithologies, structural setting, and mineralization styles) at both the camp and the deposit-scale contribute to the overall complexity of mineral exploration. Cassidy and Hagemann (2001) break deposit characteristics of the world-class gold camps into identification of the following identifiable parameters:

- Host lithologies
    - mafic-ultramafic extrusive and intrusive rocks, felsic-intermediate volcaniclastics
- Style of mineralization
    - Reactivation of shear zones / thrust systems
    - Brittle-ductile shear zones with quartz vein systems
- Hydrothermal alteration system
    - Host rock rheology
    - Stress configuration at the ore-shoot to regional scale
    - Fluid pressure variations

- Various aspects of fluid and core chemistry (oxidation state, gold fineness)
    - Salinity
    - mixed aqueous-carbonic hydrothermal fluids

Most of these characteristic mechanisms for gold mineralization are of keen interest around faults, thrusts and shear structures which can act as pluming systems for mesothermal fluid. An increase in conductivity of the host rock is expected at these structures due to the increase of mineralized fluid and rock alteration. Figure 3-2 shows an aeromagnetic survey of the St. Ives gold camp (Meyers et al, 2001) which illustrates the susceptibility contrasts across the region. The St. Ives anticline appears as the dominant magnetic high with smaller folds and faulting across the flanks of the structure. A regional gravity surveys (Figure 3-3) also imaged major structural information of the gold camp. Again the St. Ives anticline is quite prevalent on the gravity survey revealing a prime location for major thrusts, faults and shear zones.

Higher resolution gravity and magnetic studies were completed at the camp by Whitford et al. (2004, 2005). Depth of the regolith was confirmed, but the correlations results were dependant on depth and width of the weathered zones within the regolith. The observational plane of gravity and magnetic surveys are well above the fresh rock with resolutions decreasing $1/r^2$ and $1/r^3$ respectively (Stolz, 2003). The gravity and magnetic surveys were unable to resolve complexity of the fresh rock to accurately identify gold mineralization zones. The increased porosity of the weathered regolith at the camp scale further allows for groundwater ten times more saline than seawater to saturate the rock (Stolz, 2003). This salinity content forms a highly conductive layer through the regolith and distorts the already low horizontal and vertical resolution of magnetic surveys.

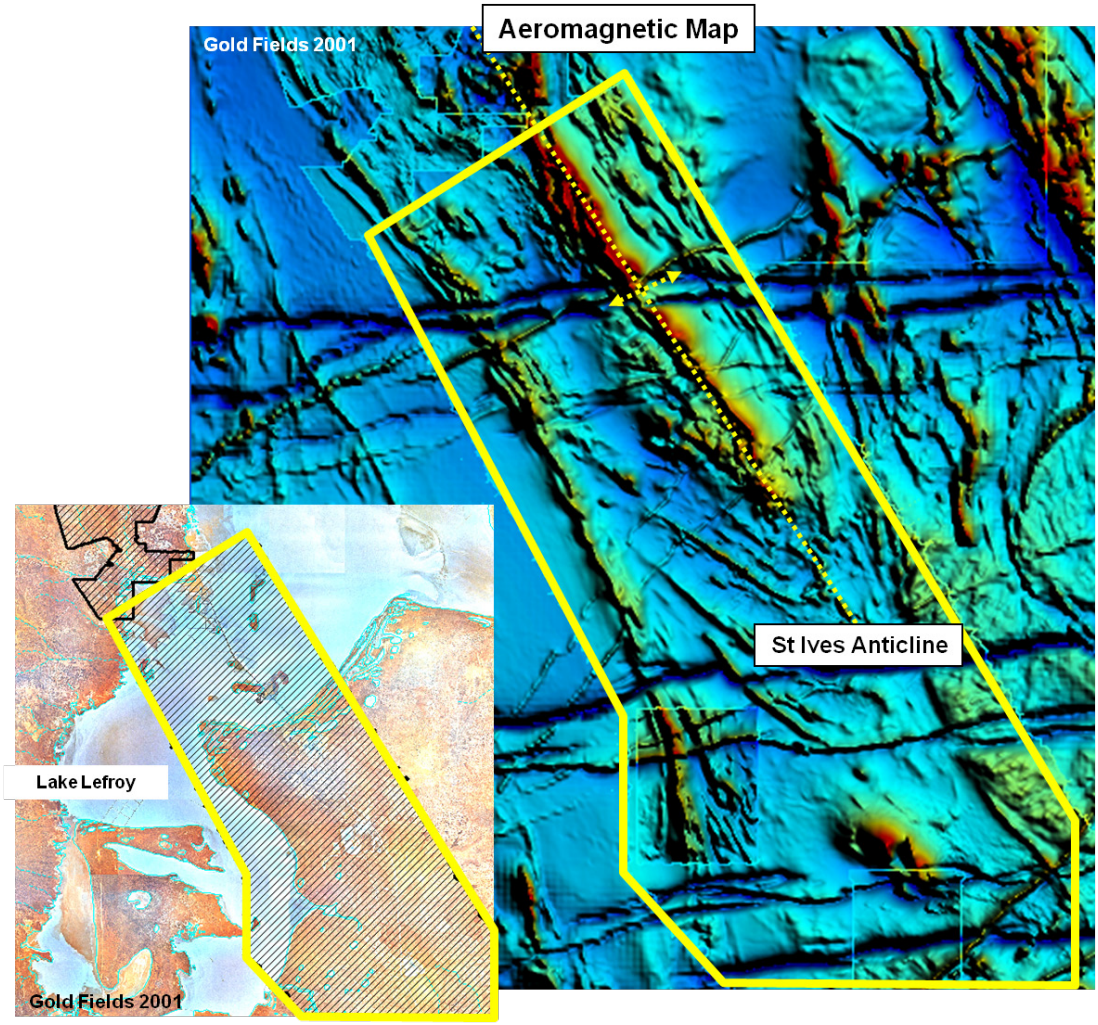

Figure 3-2. Aeromagnetic survey of the St. Ives gold camp. Inset image shows the aerial map location.

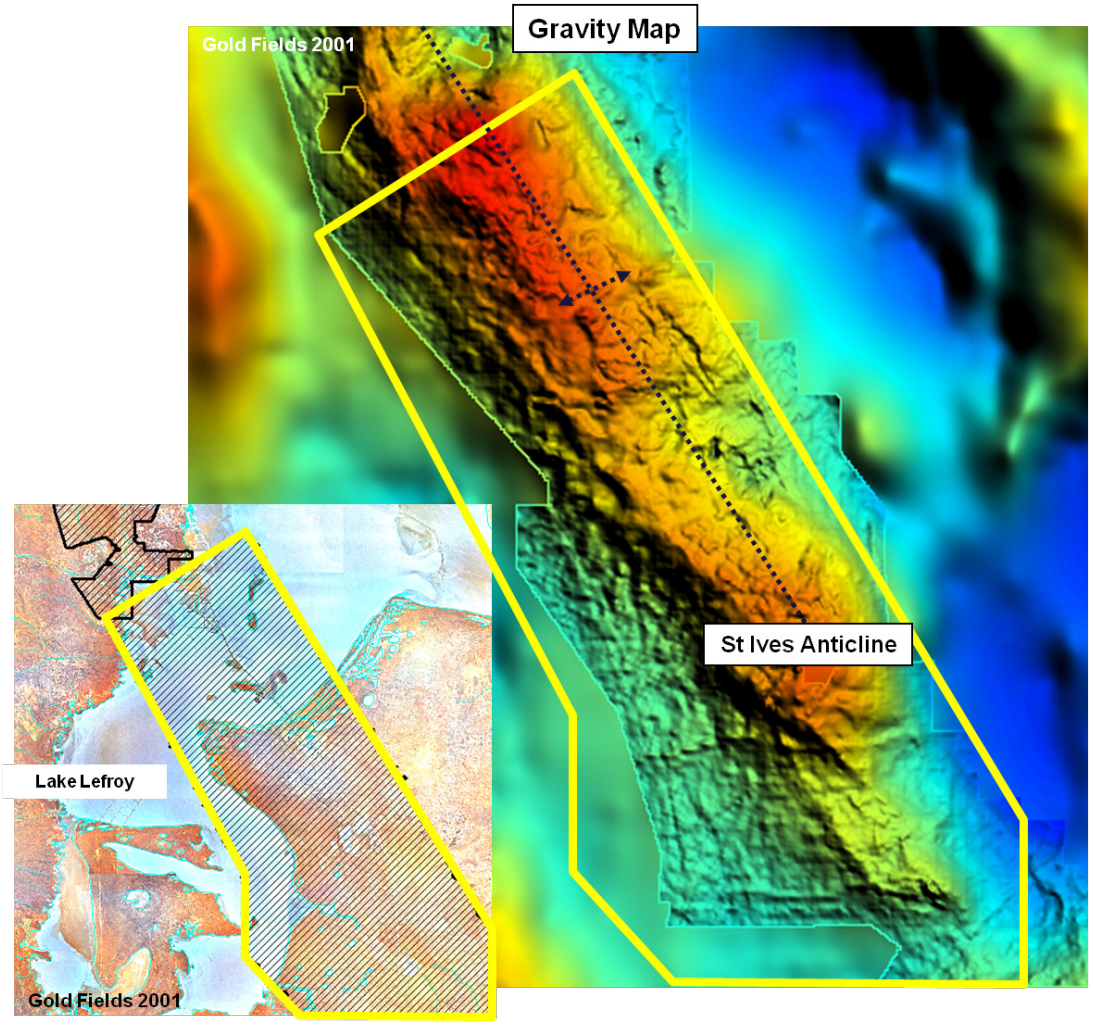

Figure 3-3. Gravity survey of the St. Ives gold camp. Inset image shows the aerial map location.

Direct drilling provides a far more precise means to pinpoint mineralization. Complexity in rock type, structure type, alteration type and stratigraphic interpretations are shown for borehole interpretations for CD10662 on Figure 3-4 and LD42105 on Figure 3-5. These precise interpretations show the rapid changes in structural complexity that is typical for the St. Ives gold camp. These changes are also seen as velocity and density contrasts on the full waveform sonic data for each borehole (details discussed in Chapters 4 and 5). While extremely accurate, a single borehole does not provide a large enough volumetric "window" and large scale drilling and sonic logging are un-economical for targeted mining. Sonic logging does, however, provide the unique ability through synthetic seismograms, to correlate small scale mineralization interpretations with larger scale reflection data.

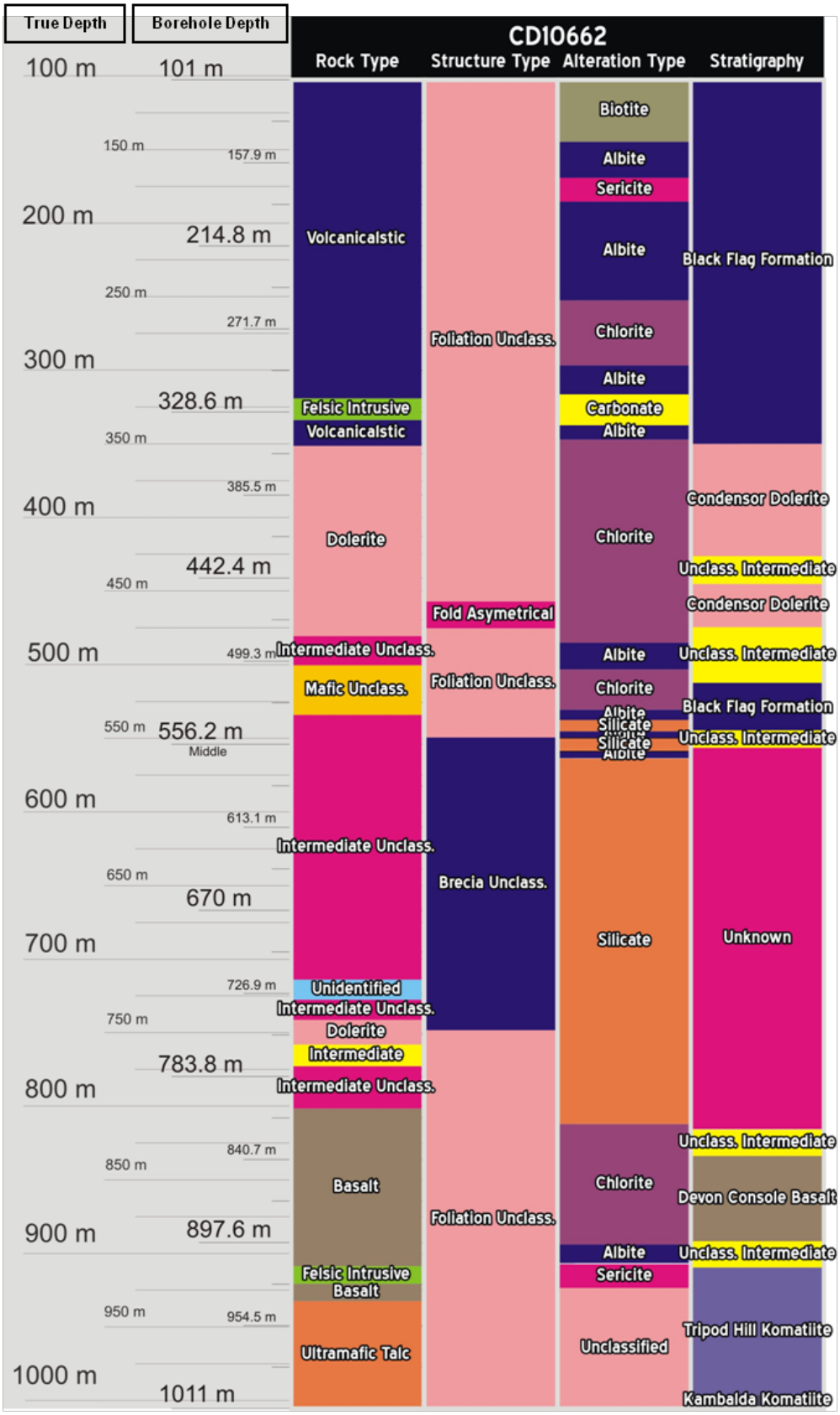

Figure 3-4. Rock type, structure type, alteration type and stratigraphy for borehole CD10662

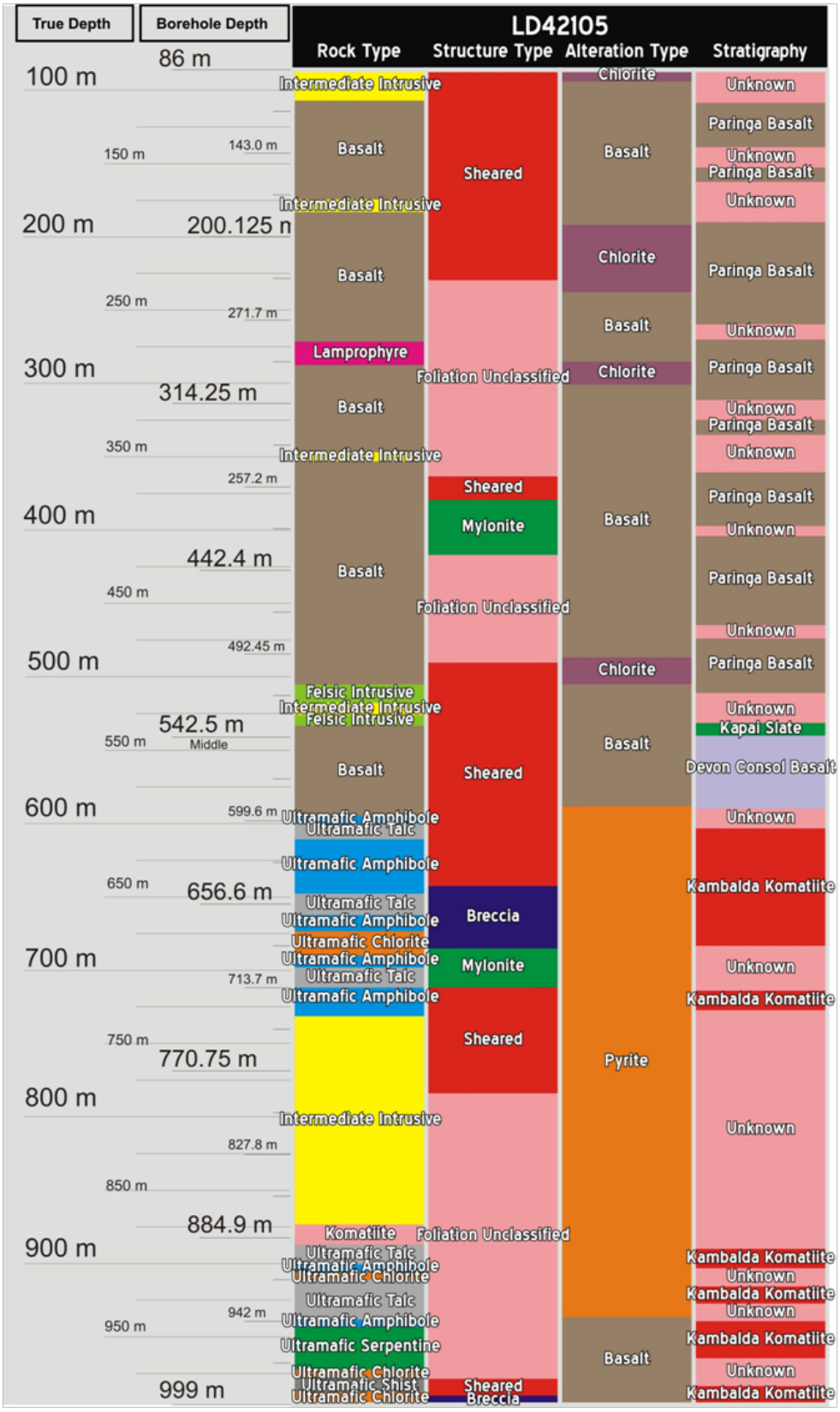

Figure 3-5. Rock type, structure type, alteration type and stratigraphy for borehole LD42105.

Ultimately, exploration for gold deposits is particularly difficult since gold presently has no known geophysical signature. Consequently, imaging favourable structures which could contain conduits for fluid and hence enable precipitation of gold is one of the main aims of the seismic method. Drilling and potential field methods are unable to identify these structures due to their depth and lateral extensions. With gold bearing structures being typically complex, potential field methods and wildcat drilling to deeper deposits become uneconomical. Seismic methods have the ability to provide information from the surface or near-surface down to tens of kilometres revealing themselves to have high potential in mineral exploration in mature fields such as the St. Ives Gold camp. The lithological and possible mineral predictive ability of seismic inversion and attribute analysis are further key features unavailable to other exploration techniques.

With world gold mining reaching its peak in 2001 (Denham, 2008) and most easy-to-find deposits already discovered, the challenge now is to develop new and innovative techniques to both locate new resources and extend the life of present mining operations. Seismic techniques have shown themselves to be extremely useful in hydrocarbon exploration, but acceptances and implementation of seismic technologies depend on the following.

- Price of gold,
- Ability of technology to explore desired areas,
- Capital investment in exploration.

In an already marginal industry, the challenge of research is to show the economic viability of seismic methods for hard rock exploration.

4 Field Data – East Victory Seismic Processing and Sonic Data Analysis

Hard rock seismic interpretation is typically hindered by low signal-to-noise ratio, complex structure and the lack of deep boreholes logs and interpretations for calibration of seismic data to geology. However, the East Victory seismic line is unique in the high quality of data available for analysis. This data set not only includes a high resolution seismic line but also five sets of boreholes drilled online with interpretations and sonic logs available for reflection calibration. Because of the high quality of data available in the area, proper reflection imaging and statistical analysis of seismic inversion and attribute analysis had a high likelihood of success.

The East Victory seismic line data was acquired over known gold deposits at the St. Ives gold camp in Western Australia. The data was part of a high-resolution seismic test program for Gold Fields Limited and Placer-Dome Asia Pacific in 2004. The regional seismic survey had shown that large-scale hard rock reflection-imaging was possible for deeper targets, but did not produce useable images of shallow targets under 1000 meters. Subsequently a high-resolution survey was undertaken to assess the viability of seismic methods for mineral exploration within accessible geological formations at the gold camp.

Figure 4-1 provides the seismic line location and regional geology of the study area. The geological map shows the main structural features including the Boulder-Lefroy Fault, the Foster Thrust, and the St. Ives anticline. The seismic test line was designed to image these mine-scale features as well as: the base of a known mafic package, felsic mineral deposits beneath the Victory mine, listric structures, and flat lying stratigraphy at the prospect scale, shallower than 500 metres (Stolz et al., 2004).

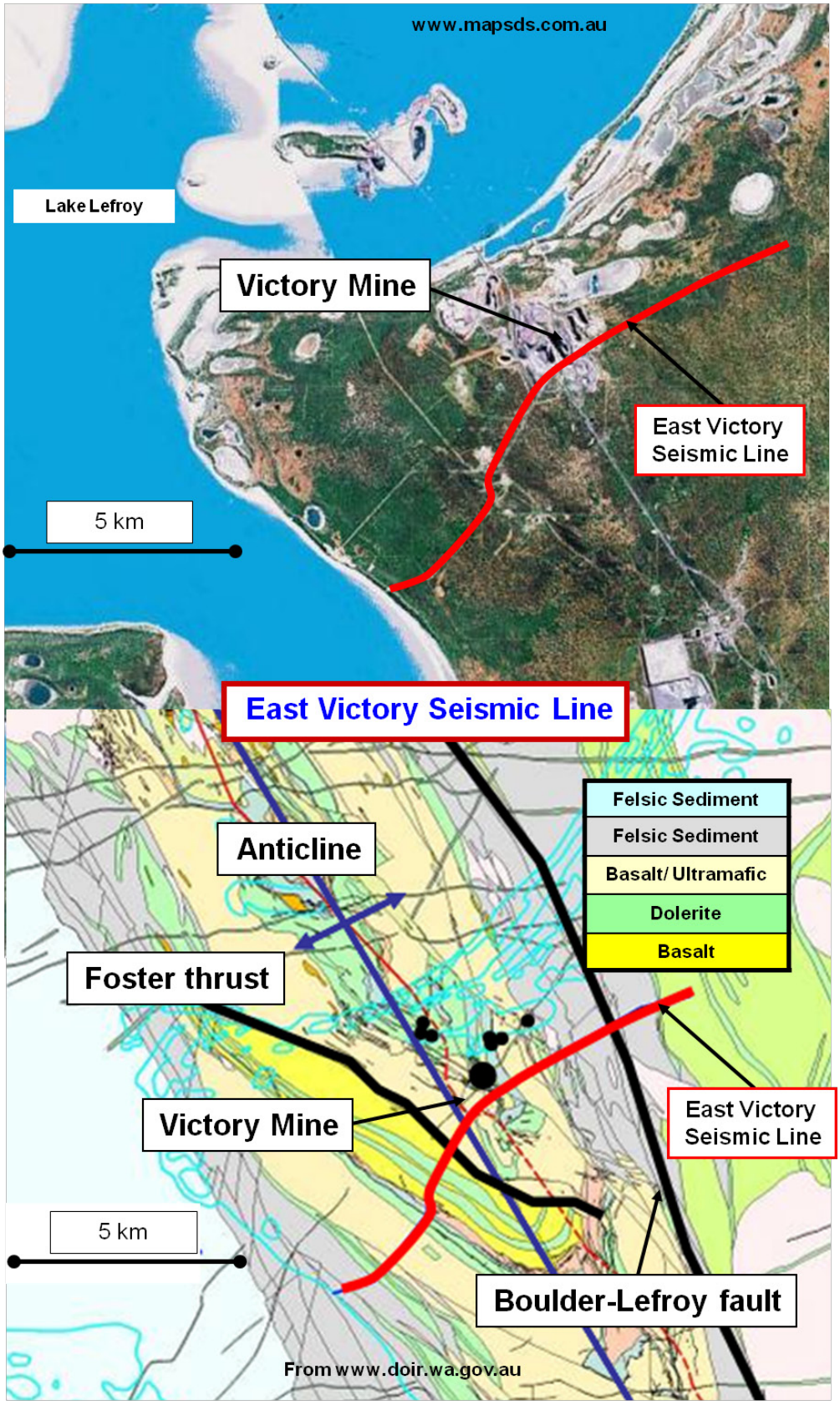

Figure 4-1, The East Victory seismic line located at the St. Ives gold camp in Western Australia. The aerial photo (top) and the geological map (bottom) reveal topographical and geological of the area (from www.mpsds.com.au and www.doir.wa.gove.au).

A total of 10.34 kilometres of seismic data were collected utilizing 2 Hemi60 Vibroseis' and a 10 metre geophone spacing. Acquisition parameters for the East Victory seismic line are listed in Table 4.1 Sparser source separation was initially tested with shot points every 20 metres resulting in a lower fold of 60. Closing the shot spacing to 10 metres and hence doubling the fold from 60 to 120 as well as using a 20-120 Hz sweep resulted in improved images.

Instrument	ARAM24 NT Recording System
Sample Rate	1millisecond
Record Length	4000 milliseconds
Recording Filters	Low cut 3Hz, High Cut 246Hz
Source Type	2 x Hemi60
VP Interval	20m & 10m
Sweep Type	Linear, 2 x 12s/SP
Sweeps	12-100Hz, 20-120Hz
Receiver Array	12 geophones in-line
Receiver Interval	10m
Spread	240 groups per shot record
Near & Far Trace	5m & 1195m
Coverage	60 & 120 fold

Table 4-1 Survey parameters for the East Victory seismic line.

Figure 4-2 shows typical raw shots as well as those same shot records with refraction statics, residual statics, muting, bandpass filtering, amplitude corrections, and Normal moveout (NMO) applied. Trace editing can also be seen on the central shot-record. While data from the entire depth will be analysed, only the top 500 ms will be of direct focus for much of this research.

Clearly raw or pre-processed shot records have not displayed high signal to noise ratio at early times which would be highly desirable for the task attempted – inversion to acoustic impedance. Consequently processing of the seismic data became very important as the objective was not only to enhance the useful signal but also to preserve relative amplitudes which are exceptionally difficult task for hard rock seismic data.

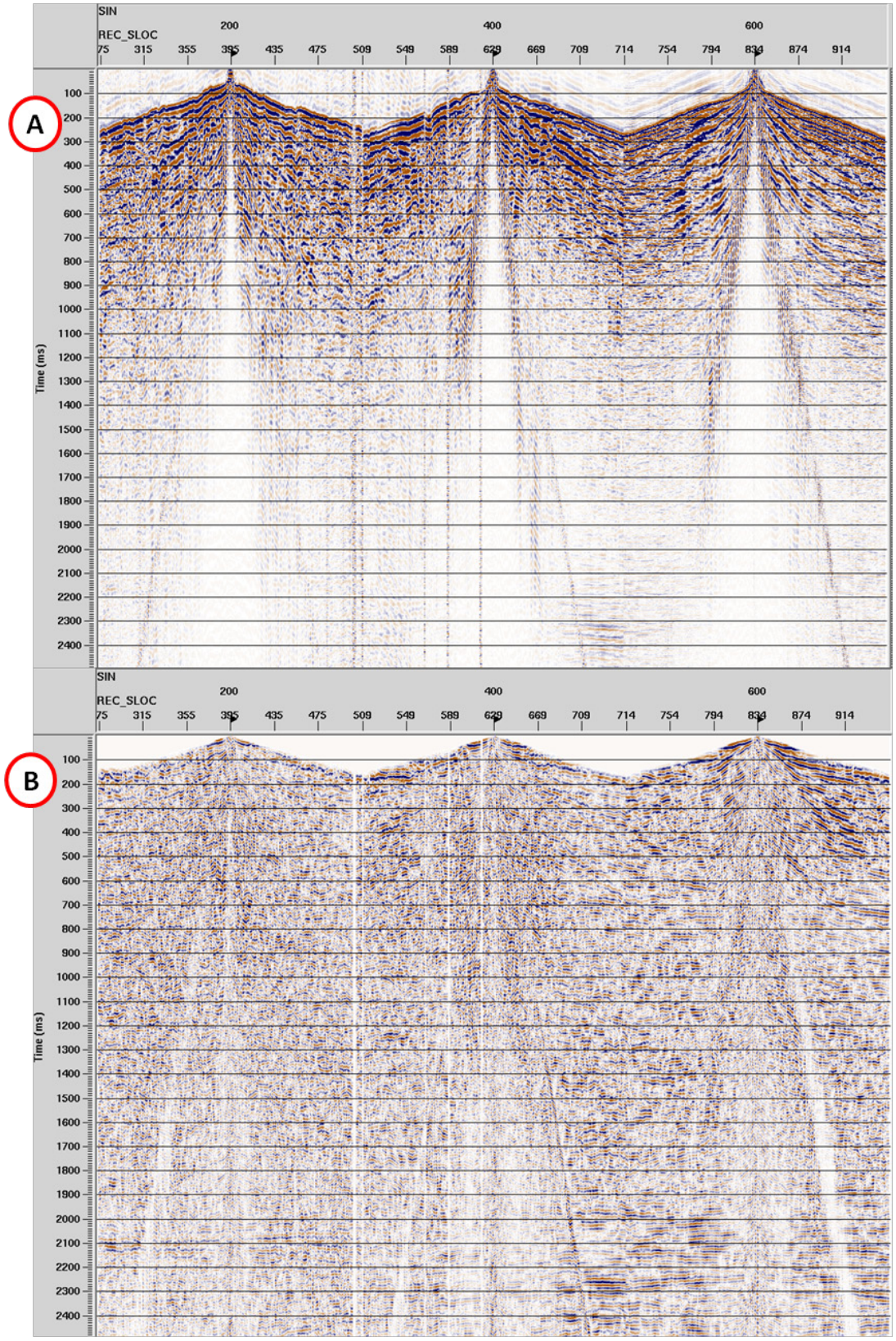

Figure 4-2 Raw (A) and pre-processed (B) shots from the East Victory seismic line. Each shot is approximately 2.4 kilometres long and 12 kilometres deep.

4.1 Processing of the East Victory Seismic line

Processing of the East Victory seismic data aimed to focus the complex reflections within the Earth while retaining as much of the original reflections amplitude, phase and frequency content as possible. However, the low signal-to-noise ratio and highly variable data quality as typical for hard rock environment in Australia makes it necessary to find a trade off between image quality and statistical reliability. Several key processing steps were required to address these challenges:

- Exceptional accuracy of static correction computation was essential to address regolith heterogeneities and accordingly large variations in travel times through this layer, necessary for preservation of reflection continuity and frequency content of the primaries.
- Careful application of single and multi-channel filtering required for removal of coherent and random noise while retaining primaries and their original bandwidth.
- Multi-phase velocity analysis was necessary to converge to a plausible model representing main geological features in this area.
- Inverse modelling or migration incorporated partial pre-stack migration (DMO) and full post-stack time and depth migration. Full pre-stack migration had limited success starting with low signal strength.

Figure 4-3 shows the seismic processing flow for the East Victory seismic line. Final seismic images were compared against current geological model, drilling information and finally calibrated with synthetic seismograms derived from the logging data. All seismic processing was complete in the Promax software package.

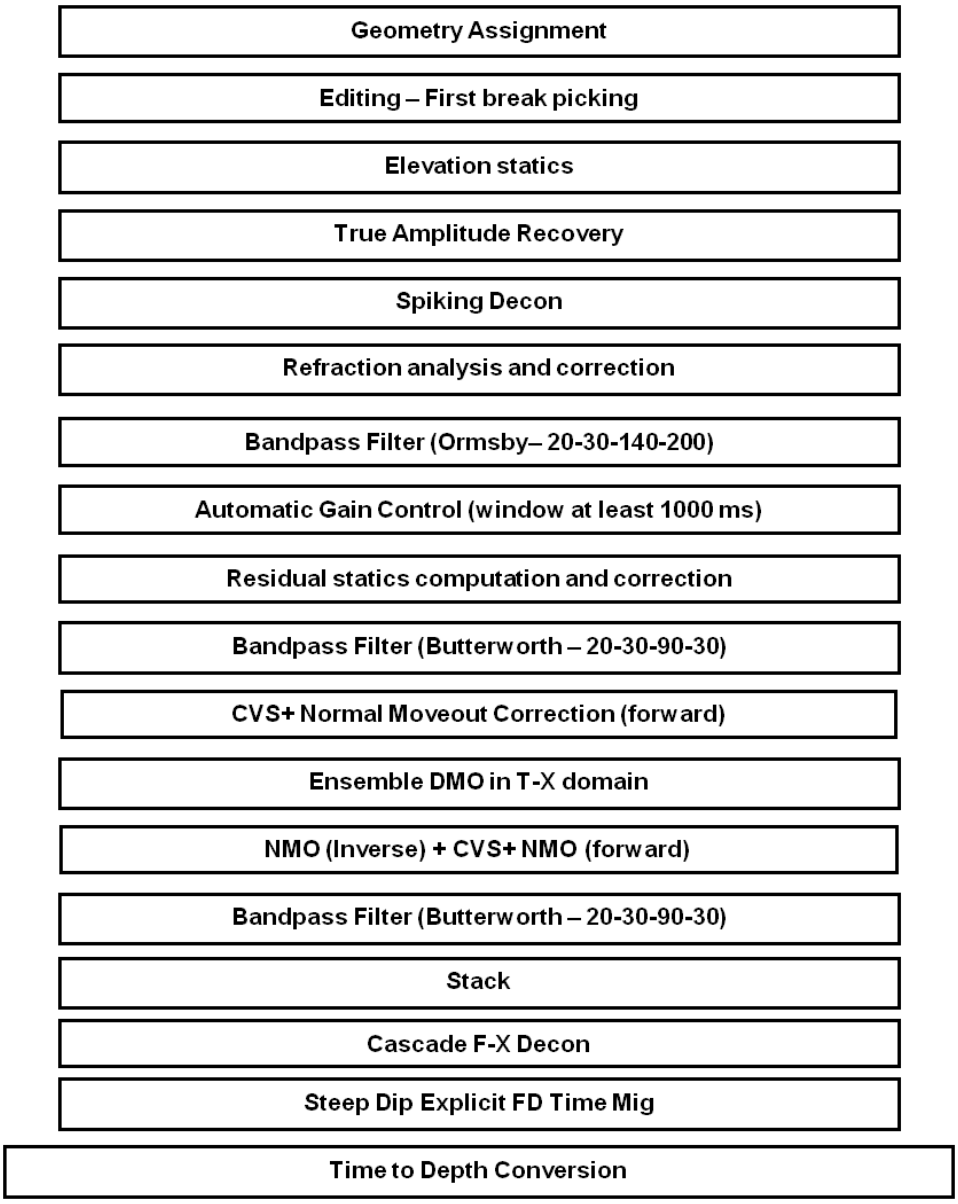

Figure 4-3. The processing flow for the East Victory seismic line.

The regolith, or top 20-100 meters, wreaks havoc with seismic signals. The shallowest part of the regolith typically displays velocities of 500-800 m/s which are followed by clay dominated sequence which often displays a velocity gradient with 2.0 to 3.0 km/s before rapidly increasing to over 6.0 km/s. Figure 4-4 shows a two layer model which was successful in accounting for delay times through the regolith that otherwise had the velocity gradient in the lower section varying from 2.0 to 3.0 km/s. Figure 4-4 illustrates short period variations in regolith depth which translates into highly variable delay times. If not accounted for these travel time variation can completely distort seismic images.

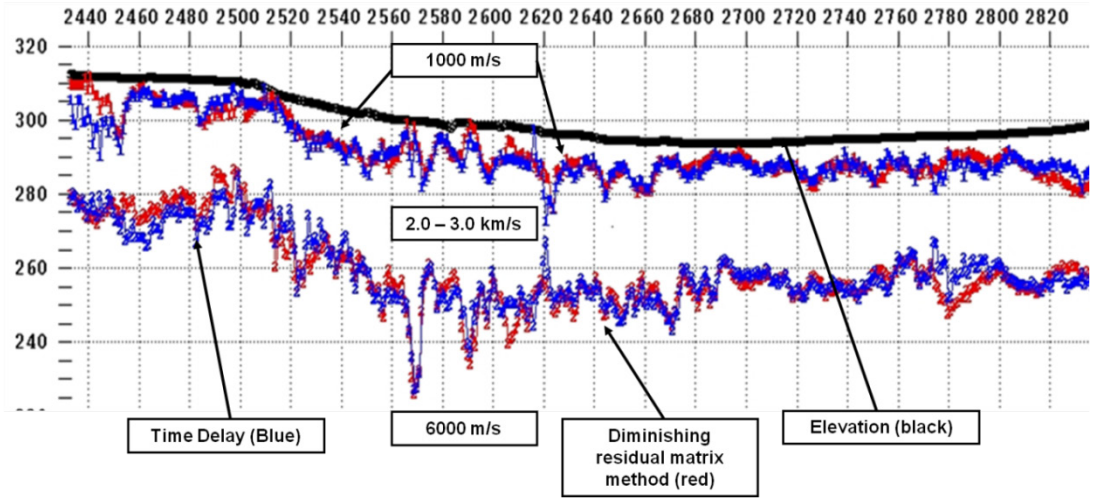

Figure 4-4. Velocity and depth estimation through the regolith. Diminishing residual matrix (DRM) (Gulunay, 1985) is in red and time delay (TD) is in blue.

Significant effort was put into delay time computation in order to "homogenise" otherwise very heterogeneous regolith layer. First, the head waves were corrected for linear move-out (LMO) using constant velocity of typically 6000 m/s. This approximately flattens head wave arrivals. The waves were then enhanced by adaptive deconvolution and band-pass filters. Representative shots were then used to train a neural network for first break picking. The automatic picks were then saved to a data base and inspected and corrected on a shot by shot basis. The picks were then transferred to trace headers, linear move-out removed and picks were then saved back to the data base. The final step was the computation of refraction statics using diminishing residual matrix and time delay.

Spectral analysis prior to processing revealed the peak frequencies of the seismic data to be between 25 and 100 Hz with a dominant frequency near 50 Hz. Surface wave coherent noise appears between 10 and 45 Hz (direct wave) with random noise from mine site vehicle movement appears as frequency higher than 80 Hz. With the large overlap in the reflection and noise spectrum, single trace signal enhancement techniques were less effective. Multi channel filtering such as F-K, τ-P, 2-D media filters in time and frequency are generally avoided in processing of hard rock data as they can alternate or even eliminate steep dips. It found that most effective S/N enhancement can be achieved by the simple stacking process, hence the need for high fold recording in hard rock environments. A cascaded F-X was chosen to enhance the reflection signal while further attenuating

random noise. The cascade F-X decon over smooth spectra causing adjacent traces to look alike, but it is of value when dealing with a low S/N ratio such as that seen in this hard rock environment.

With the regolith "homogenized" through computation and application of refraction and residual reflection statics, and signal enhance through simple filtering, velocity analysis is needed for proper reflection focusing. Velocity analysis is not a trivial process in hard rock seismic exploration. Constant velocity stacks, sometimes considered "primitive" by hydrocarbon standards, turned out to be the most useful velocity estimation tool for hard rocks enabling the following simple rules to be established:

- Steeply dipping events appearing with low stacking velocities originate from out-of-plane structures (typically from shallow structures or discontinuities within the regolith),
- Steeply dipping events expressed on very high velocities (higher than 7.5 km/s) may be difficult to fully preserve in the final stack, despite DMO corrections, and constant velocity stack (CVS) panels should be saved for the final interpretation, and
- Events expressed over very small velocity range commonly originate from the projections of the deeper structures which are unfavourably oriented with respect to the line direction.

The final pre-DMO velocity profile determined from CVS was eventually saved in raw and smoothed versions for further processing. While efforts were made to generate the "best" velocity model the reality is that the model is only a 2D representation of a 3D earth. Hence the full complexity of hard rock environments cannot be fully resolved by 2D seismic methods.

4.1.1 Post Stack Imaging

Figure 4-5 shows the seismic data fully processed without DMO showing limited steep dip reflections. Applying DMO improves the ability to stack conflicting dips, reduce reflection point dispersal, and is used in conjunction with post-stack migration techniques for proper reflection imaging (Liner, 1999). Constant velocity stacks are necessary after DMO for better velocity analysis. The stacked image (Figure 4-6) shows that steep dips are

better preserved than brute stacking by applying DMO corrections to the seismic data. The flanks of the imaged "dome" are better defined and reveal the known St. Ives anticline. The inset images, A, B and C, show strong reflections appear more focused than in the pre DMO brute stack (Figure 4-5).

Steep Dip Explicit Finite Difference Time Migration was chosen to better focus the complex structure due to the algorithms ability to handle lateral variations in the velocity field. Figure 4-7 shows well focused reflections after migration. Enlarged sections of this show that complex structure can be comprehended and interpreted. Migrated reflections conformed well to known geological features in this area. The projection of the Condenser dolerite, the projection of the Repulse fault from mine interpretations, and the surface projection of the Foster Thrust onto the seismic image have been confirmed by Gold Fields geoscientists. The regional green-stone package is interpreted below the anticline by Stolz et al. (2004) of Gold Fields. For correlation, the geological map view of the East Victory seismic line has been inset on Figure 4-8.

The total depth of the seismic image was over 5000 metres revealing deeper structures which allow for understanding of regional mesothermal gold mineralization. Crustal scale shear zone represented in the greenstone package on Figure 4-8 can be seen as potential contributor to mesothermal gold mineralization in the area. The structures suggest that deep sources of mesothermal fluid have followed the contours of the anticline upwards through the green-stone package. Possible alteration plumes through shear zones on the flanks of the anticline, weak zones at rock-types in contact associated with gold mineralization (basalt, dolerite and intrusive), and the lateral and vertical extent of these features are of high interest for mining. Relaxation faults near the bottom of the regolith between 200-800 meters are of high interest for gold mineralization as well. Complete geological and geochemical requirements for deep-imaging are covered extensively in papers by Cox and Ruming (2004), Neumayr et al. (2004), Weinberg et al. (2004) and Cassidy and Hegemann (2001).

Post-stack migration images (Figure 4-8) have shown good structural results pointing toward possible locations of gold mineralization potential. "Direct" indictors of lithology and gold mineralization however, require further analysis. Borehole logs and core data need to be used to calibrate seismic and analyse properties of reflected events. Cross-plot of all the logs are then used to attempt to relate lithologies to seismic attributes such

as acoustic impedance or instantaneous attributes. The red box on Figure 4-8 shows where seismic inversion and seismic attribute analysis was focused.

As can be seen from results to this point, 2D processing of the East Victory seismic line shows good imaging along the entire line. CVS, DMO and migration analysis showed no significant presence of out of plane events. Hence conditions for 2D inversion of the seismic data were met.

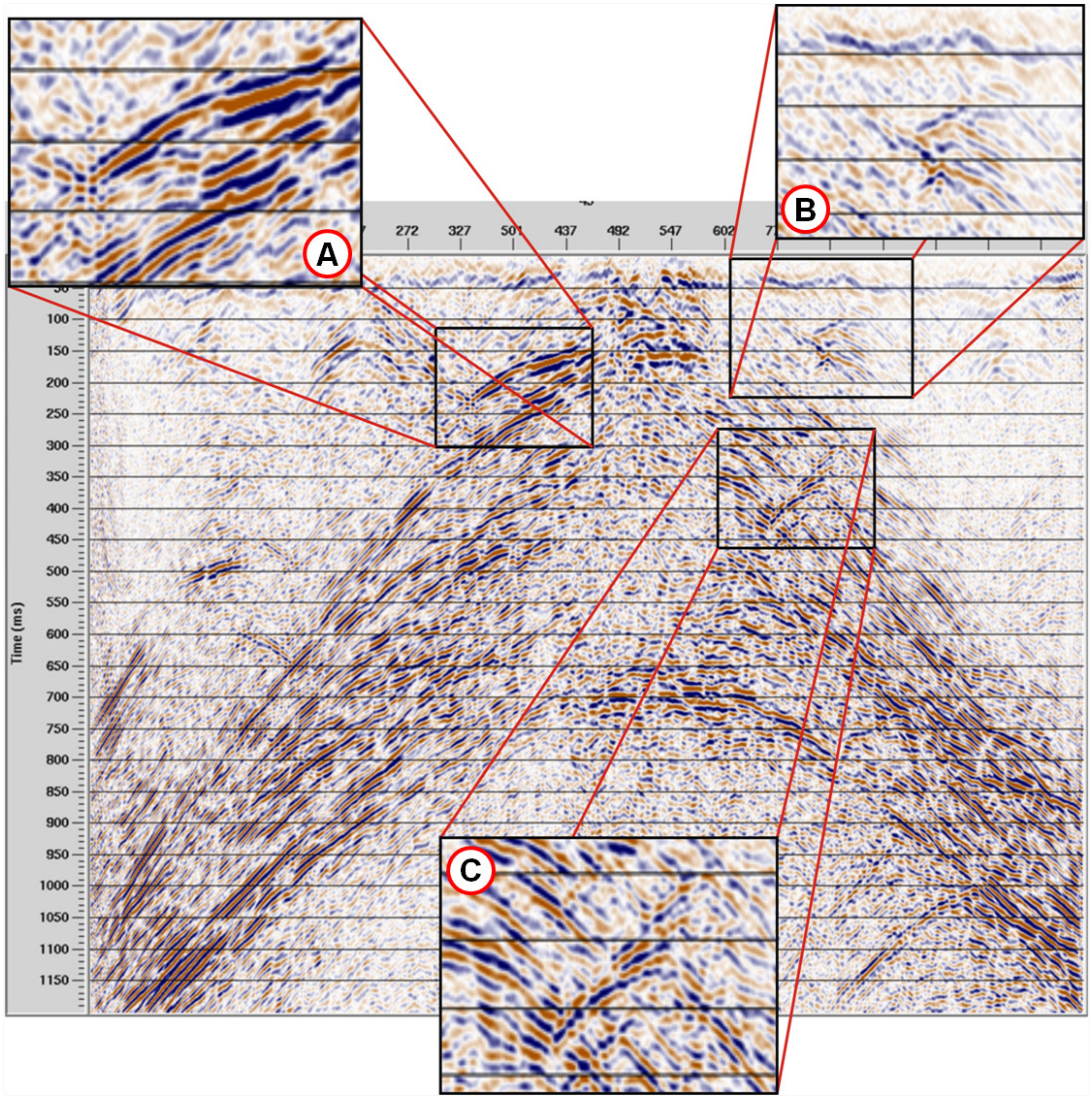

Figure 4-5. Full stack without DMO.

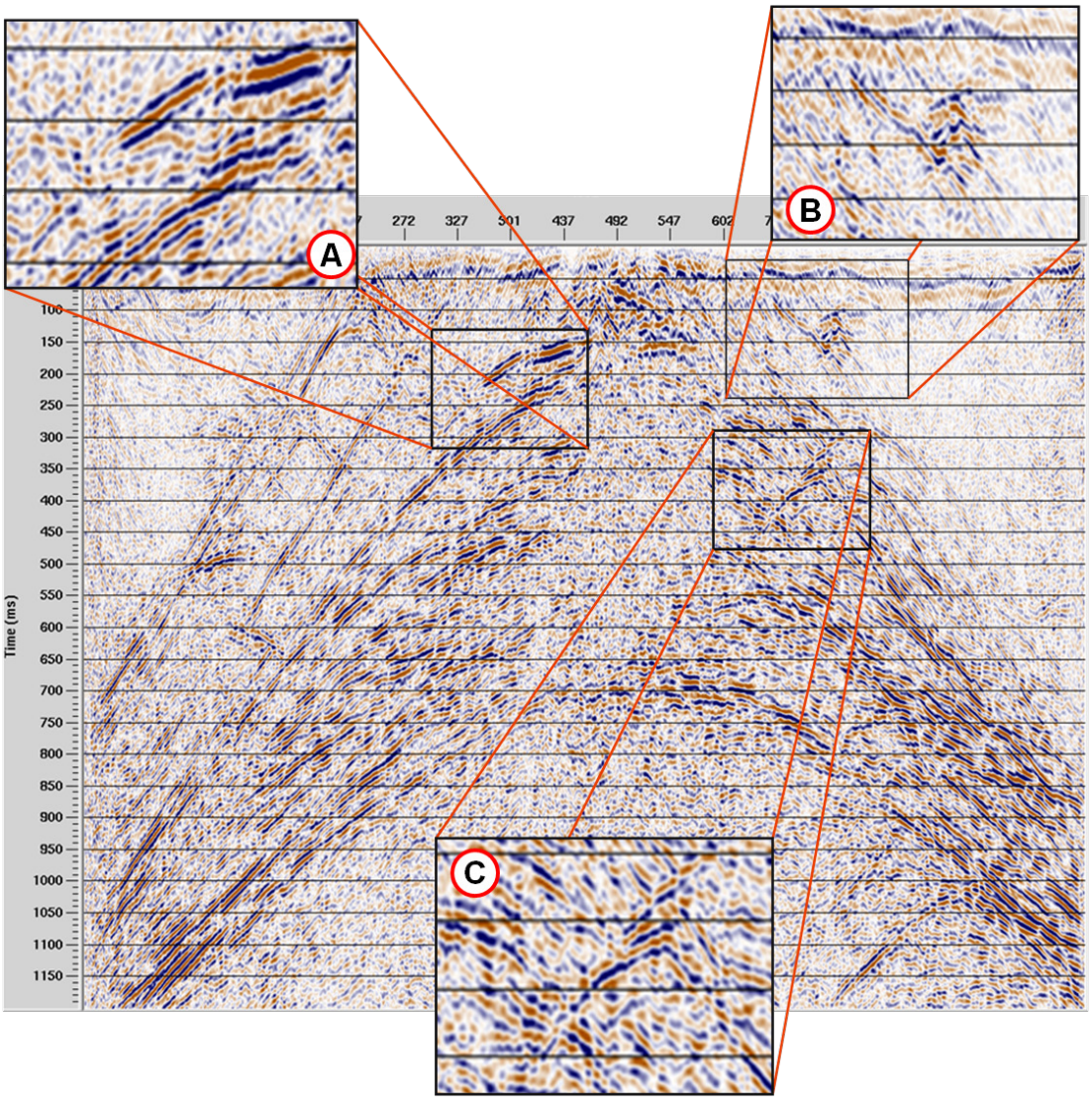

Figure 4-6. DMO corrected and stacked East Victory seismic line.

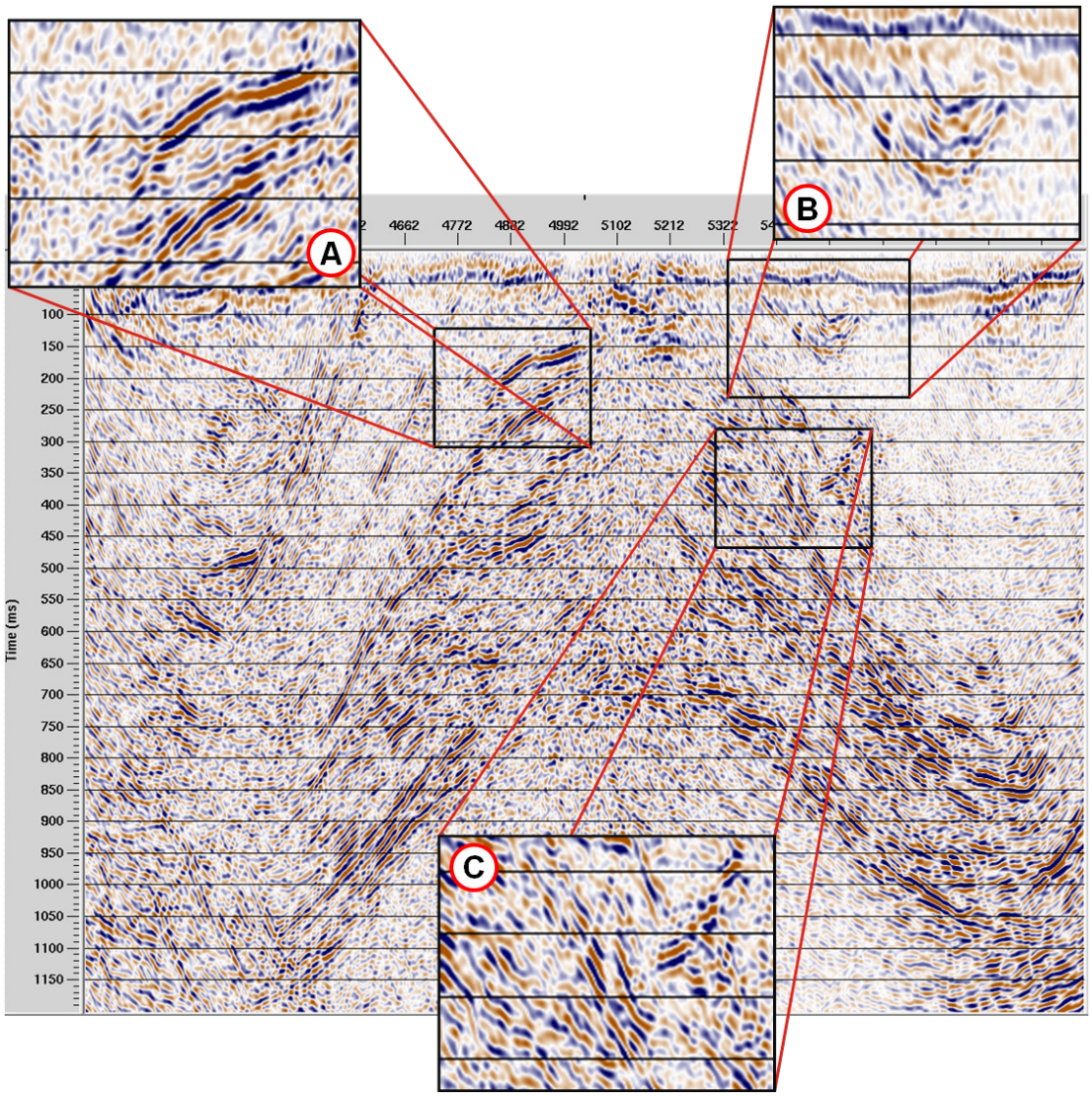

Figure 4-7. The Steep Dip FD Time Migration of the East Victory seismic line.

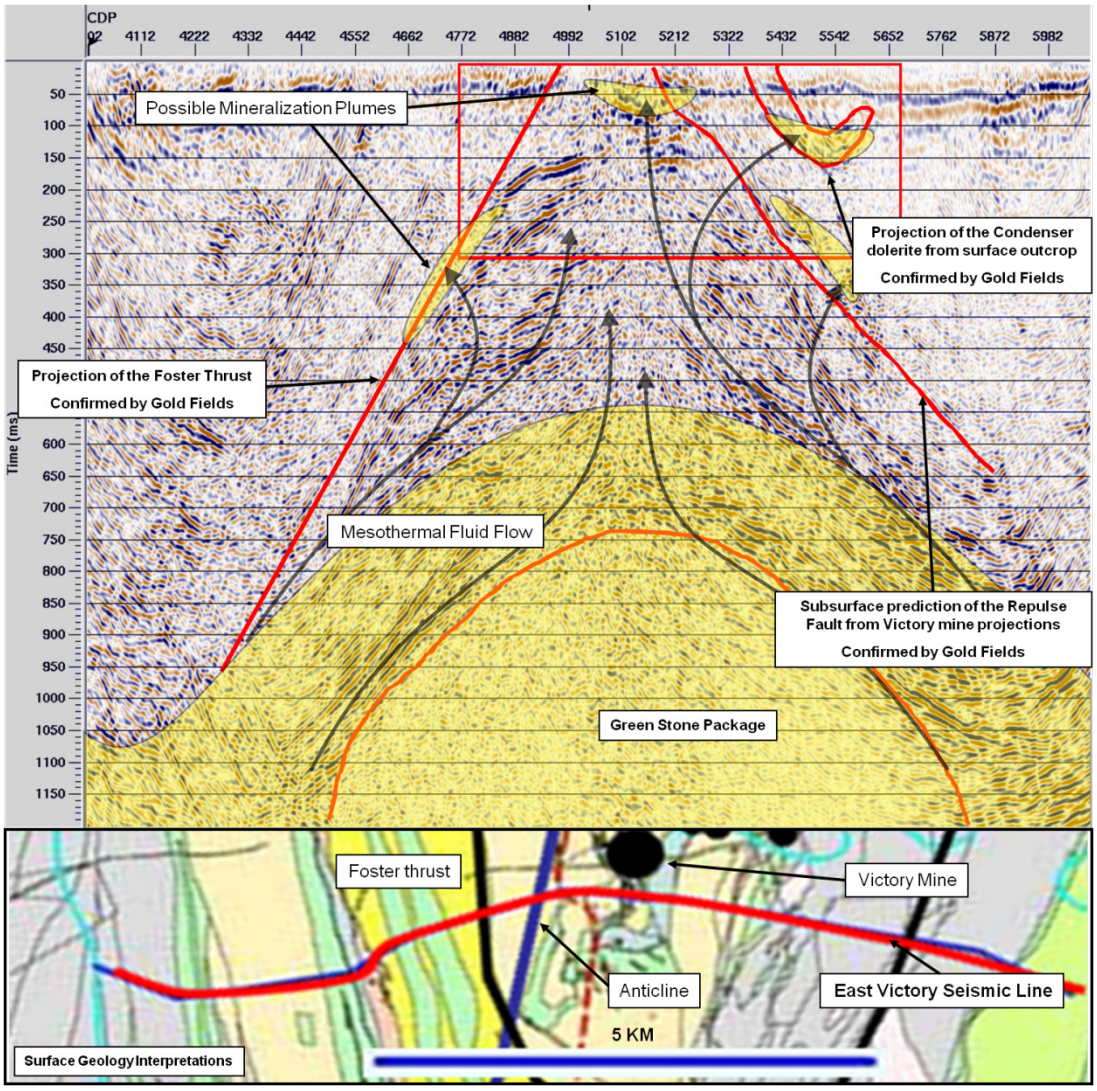

Figure 4-8. The Steep Dip Explicit FD Time Migration of the East Victory line. The surface geology interpretation is inserted at bottom of this figure.

4.2 Statistical Sonic Evaluation

Rock property analysis is a powerful tool used for lithological predictions, reservoir characterization, and fluid content predictions in hydrocarbon exploration. Statistical analysis of hard rock sonic data is attempted for the first time in this research and should provide a basis for lithological predictions, mineralization identification, and possible direct gold content indictors.

Data from five boreholes with full waveform sonic logs (FWS) and interpreted rock units were available along the East Victory seismic line. The sonic data, considered a rarity in hard rock seismic geophysics, provided conditions for seismic inversion intended for direct characterization of rocks units in hard rock environments. Inversion is only

meaningful when seismic data are calibrated to logs that have synthetic seismic derived from log data. Borehole locations used for inversion are shown in Figure 4-9 together with the East Victory seismic line traverse. Table 4.2 contains specific detail of each borehole with respect to depth, deviations, sonic and interpretation / analysis of data. Each borehole had rock type, structure type, alteration type and stratigraphic interpretations as shown by borehole CD10662 in Figure 3-4. This figure shows the complexity typical in hard rock areas.

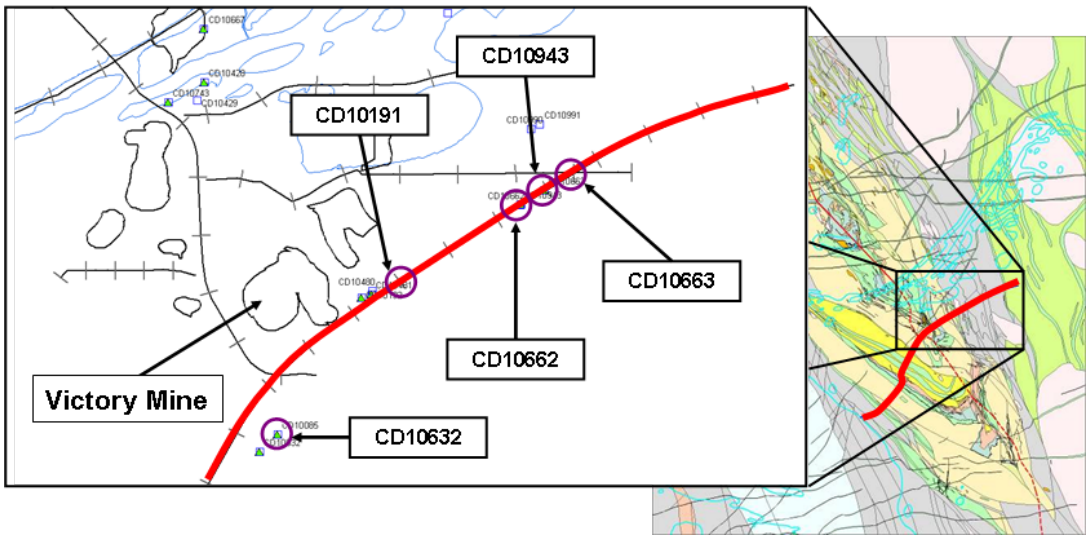

Figure 4-9 Borehole locations of the full waveform sonic (FWS) logs on and near the East Victory seismic line (red).

Borehole	Easting	Northing	Depth for sonic	Deviated	Sonic Data				Interpretations / Analysis						
					ρ	Vp	Vs	G	MS	R	RT	SR	AL	SA	Au
CD10191	383711.1	6533499	47 m – 260 m	No	✓	✓	✓	✓		✓	✓	✓	✓	✓	✓
CD10632	383043.9	6532251.5	131 m – 585 m	No	✓	✓	✓	✓	✓	✓	✓	✓	✓	✓	✓
CD10662	385045.75	6534355	107 m – 1012 m	Yes	✓	✓	✓	✓	✓	✓	✓	✓	✓	✓	✓
CD10663	385250.6	6534480.5	68 m – 613 m	Yes	✓	✓	✓	✓	✓	✓	✓	✓	✓	✓	✓
CD10943	385046.4	6534361.2	142 m – 548 m	Yes	✓	✓	✓				✓	✓	✓	✓	✓

ρ – Density Vp – P- wave, Compression Vs – S-wave, Shear
G – Gamma Log MS – Magnetic Susceptibility R – Resistivity RT – Rock Type
SR – Structure AL – Alteration SA – Stratigraphy Au – Gold Assessment

Table 4-2. Generalized information for borehole data on the East Victory seismic line.

4.2.1 Zero Offset Synthetic Seismograms

Zero-offset synthetic seismograms were created along each borehole to observe where prospective seismic responses were most likely to be located. Filtering or "blocking" the log data to 10 metre intervals was necessary to approximate an optimistic bandwidth of the seismic data to limit synthetic seismogram distortion. P-impedance calculated from each set of sonic data was convolved with a characteristic wavelet extracted from the seismic data to generate each synthetic seismogram.

Borehole	Depth	Visual Response	Rock		Structure		Alteration		Gold (ppb)
CD10192	200	Weak	Unclassified	✓	Unclassified		Pyrite	✓	0
			Ultramafic Talc				Chlorite		
	230	Strong	Shist	✓	Breccia		Undifferentiated	✓	> 6000
			Unclassified		Unclassified		Biotite		
CD10632	280 - 300	Weak	Basalt	✓	Sheared		Carbonate	✓	0
			Schist				Biote		
	310-320	Weak	Basalt	✓	Sheared		Chlorite		0
			Schist						
	375 - 400	Weak	Dolerite	✓	Sheared		Biotite		0
			Basalt						
	480 - 510	Strong	Mafic	✓	Sheared		Biotite		< 300
			Dolerite						
CD10662	250 - 300	Strong	Volcaniclastic	✓	Unclassified		Undifferentiated		< 100
			Dolerite						
	410-470	Strong	Dolerite	✓	Unclassified	✓	Serucite	✓	> 400
			Intermediate		Fold Asymmetrical		Chlorite		
	800 - 850	Strong	Intermediate	✓	Unclassified		Silica	✓	> 400
			Basalt				Sericite		
CD10943	275 - 300	Strong	Dolerite		Unclassified		Biotite	✓	< 400
							Albite		
	500 - 525	Strong	Dolerite	✓	Unclassified		Silica	✓	0
			Siltstone				Haematite		
CD10663	275 - 300	Strong	Volcaniclastic	✓	Unclassified		Albiite		0
			Dolerite						
	475 - 500	Strong	Intermediate	✓	Mylonite		Albite		0
			Dolerite						

Table 4-3. Synthetic reflection location based on rock type, structure type, and alteration.

Synthetic seismograms were created in the absence of regolith distortions, signal attenuation and had no coherent or random noise to lower the signal-to-noise ratio. These

synthetic reflection results can be considered ideal responses for real rock types associated with this hard rock environment. Table 4.3 shows the compiled results for synthetic reflection analysis and indicate that most distinct synthetic seismic reflections occurred at rock-type changes with one third of the reflection responses also coinciding with alteration changes. Further statistical verification of rock-type, structure and alteration were necessary to narrow the possible causes of reflections on the synthetic seismograms.

4.2.2 Log Data Analysis

All five borehole sonic datasets (density, P- and S-wave velocities) were separated and compiled into rock-type and further subcategorized into structure and alteration for statistical analysis. Cross-plots of log density versus log P-wave velocities were generated to observe statistical relationships similar to Gardner et al. (1974) investigation in clastic environments. Cross-plotting and linear regression analysis of all sonic data indicated that statistically valid results were only extractable from rock-type and structure-type. Figure 4-10 shows two examples of cross-plots and regression line results for dolerite and sheared dolerite (top) along with basalt and shear basalt (bottom). Zero-offset synthetic models indicated reflection possibilities at alteration changes (Table 4.3), but with 12 different types of alteration no unique rock characteristics were found. Only rock and structural change were consistent through most rock-types giving unique cross-plot and linear regression analysis trend.

Table 4.4 contains the Gardner relationship for density versus Vp, the Potter-Stewart (1998) relationship for density and S-wave velocity and the mean calculations for average P- and S-wave values. These variances in the final rock characterizations from the East Victory sonic logs show how sensitivity hard rocks are to differences in densities and velocities.

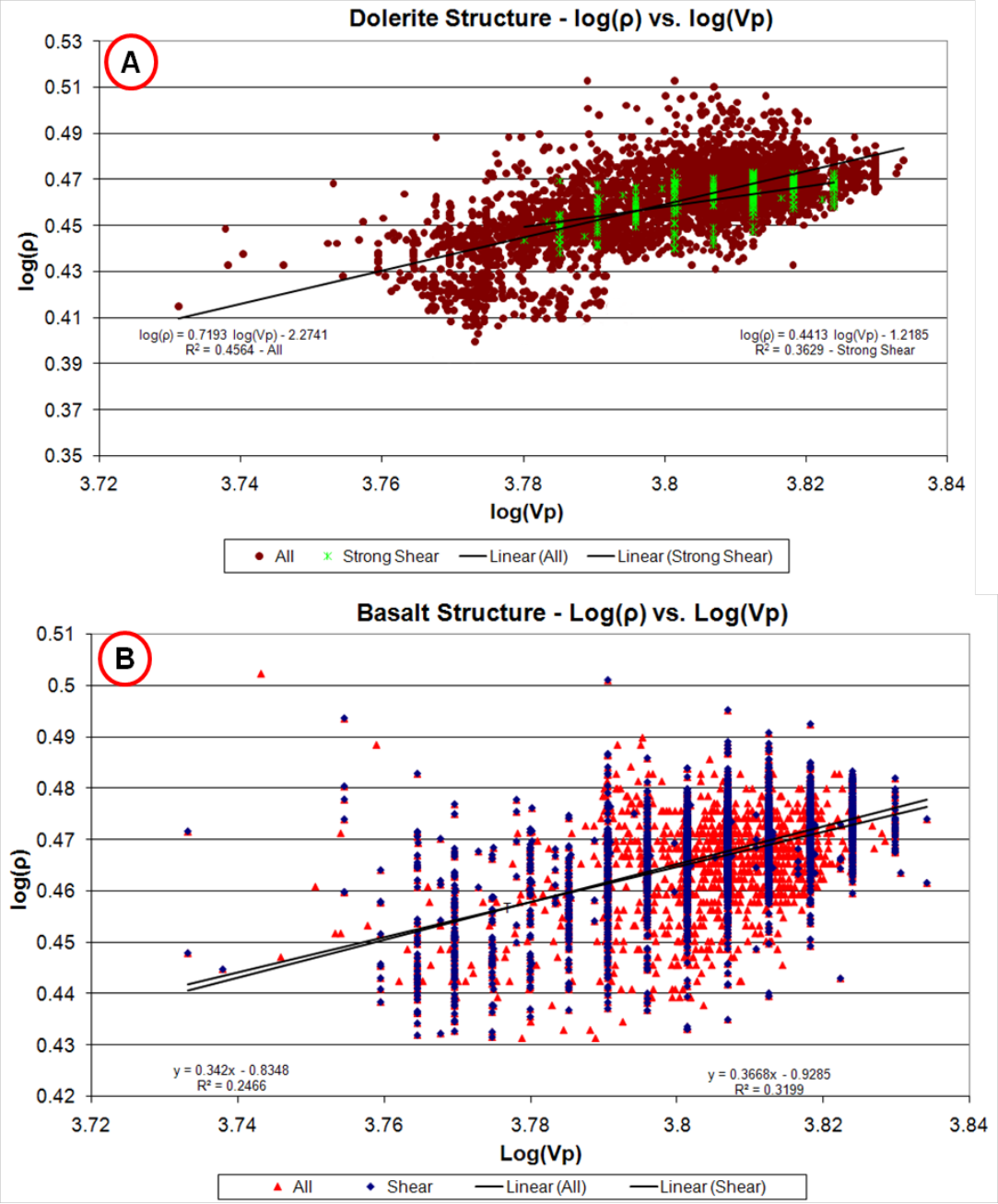

Figure 4-10. Log(ρ) versus log(Vp) cross-plots of (A) for dolerite (dark red) and sheared dolerite (green). (B) basalt (red) and sheared basalt (blue).

Rock	Structure	Density (g/cc)	P Wave Measured (m/s)	P Wave Predicted (m/s)	S Wave Measured (m/s)	S Wave Predicted (m/s)
Dolerite		2.89 (0.055)	6348	6248	3700	3474
Dolerite	Sheared	2.87 (0.085)	6248	6937	3679	4165
Basalt		2.93 (0.065)	6377	6488	3751	3867
Basalt	Sheared	2.93 (0.065)	6428	6372	3744	3772
Volcanicalstic		2.64 (0.07)	5918	5999	3551	3239
Mafic		2.775 (0.115)	5990	6179	3493	3592
Intermediate		2.6 (0.07)	5814	5894	3704	3475

Table 4-4. Rock characterization for major rock units from all boreholes.

4.2.3 Vp/Vs and Acoustic Impedance Analysis

Substantial research in clastic environments is available that illustrates correlations exist between the Vp, Vs and acoustic impedance, for lithological and hydrocarbon identification (Domenico, 1984; Tatham, 1982; Landro, 2004; Guliyev, 2006; Ikwuakor, 2006). In hard rock environments P- and S-wave velocities and their ratio can be turned into Poisson's ratio (σ) which relates to rock strength which can be used for lithological and gold bearing rock predictions and are important for planning future underground mining operations. Figure 4-11 illustrates the Vp/Vs versus acoustic impedance cross-plot for all rock-types from borehole interpretations along the East Victory seismic line. The cross-plots reveal that, depending on impedances and depth, softer rocks (intermediate, mafic and volcaniclastic) can be distinguished from harder rocks (basalt and dolerite). However, the cross-plot also shows ambiguous results from all rock-types at mean values of both Vp/Vs and acoustic impedance. Proper calibration of both the sonic and seismic data will be required to show subtle differences in rock type predictions.

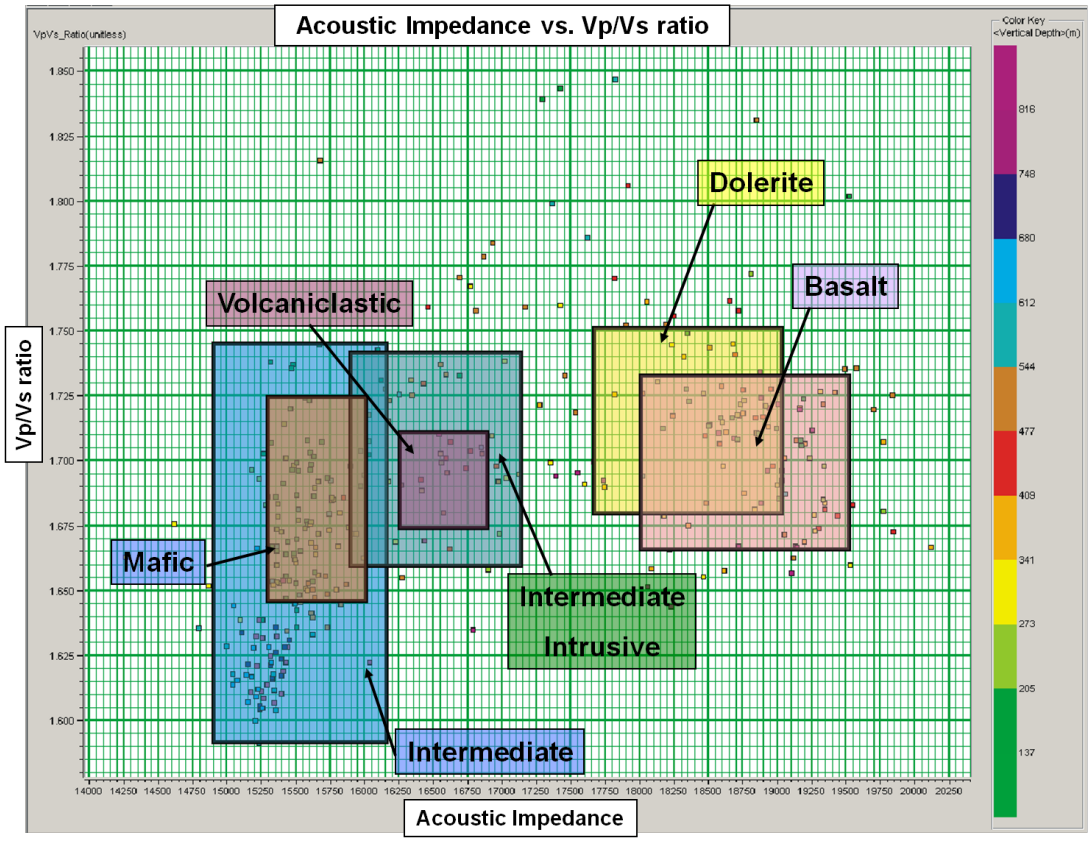

Figure 4-11. Vp/Vs ratio versus acoustic impedance plot for different rock-types from borehole interpretations on the East Victory line.

Each borehole sonic log was examined separately using Vp/Vs and acoustic impedance cross-plots. Figure 4-12 shows the Vp/Vs versus acoustic impedance for CD10662 with blocked zones to observe gold separation. Zoning on all borehole data indicated that the high gold content rock appear to have a narrowed Vp/Vs ratio with broad P-impedance values. Vp/Vs and acoustic impedance values for high gold content ore zones from all borehole data are shown on Table 4.5 and graphed on Figure 4-13 and Figure 4-14 respectively. Table 4.5 specifies the depth in time and meters, rock type, structure, alteration, gold content, Vp/Vs and P-impedance at high gold content sections of each borehole. Figure 4-13 and Figure 4-14 illustrate Table 4.5 by showing maximum and minimum (light grey), standard deviation values (dark) grey of Vp/Vs and AI of rock at high gold content (orange) of each borehole.

The resulting Vp/Vs and acoustic impedance characterization of the borehole data so far indicate, at the very least, a way that softer and harder rocks can be distinguished from each other. With gold content being associated more with softer intermediate intrusive, a possible volumetric basis for gold content estimation appears to be possible.

However, with a 20-25 metre vertical resolution limit in the seismic data several of the gold-bearing zones seen on the borehole logs may be un-resolvable but quite detectable as the ratios of the seismic wavefront to zone thickness is such that constructive interference or tuning effect is produced. Modelling was required to see if these layers were resolved.

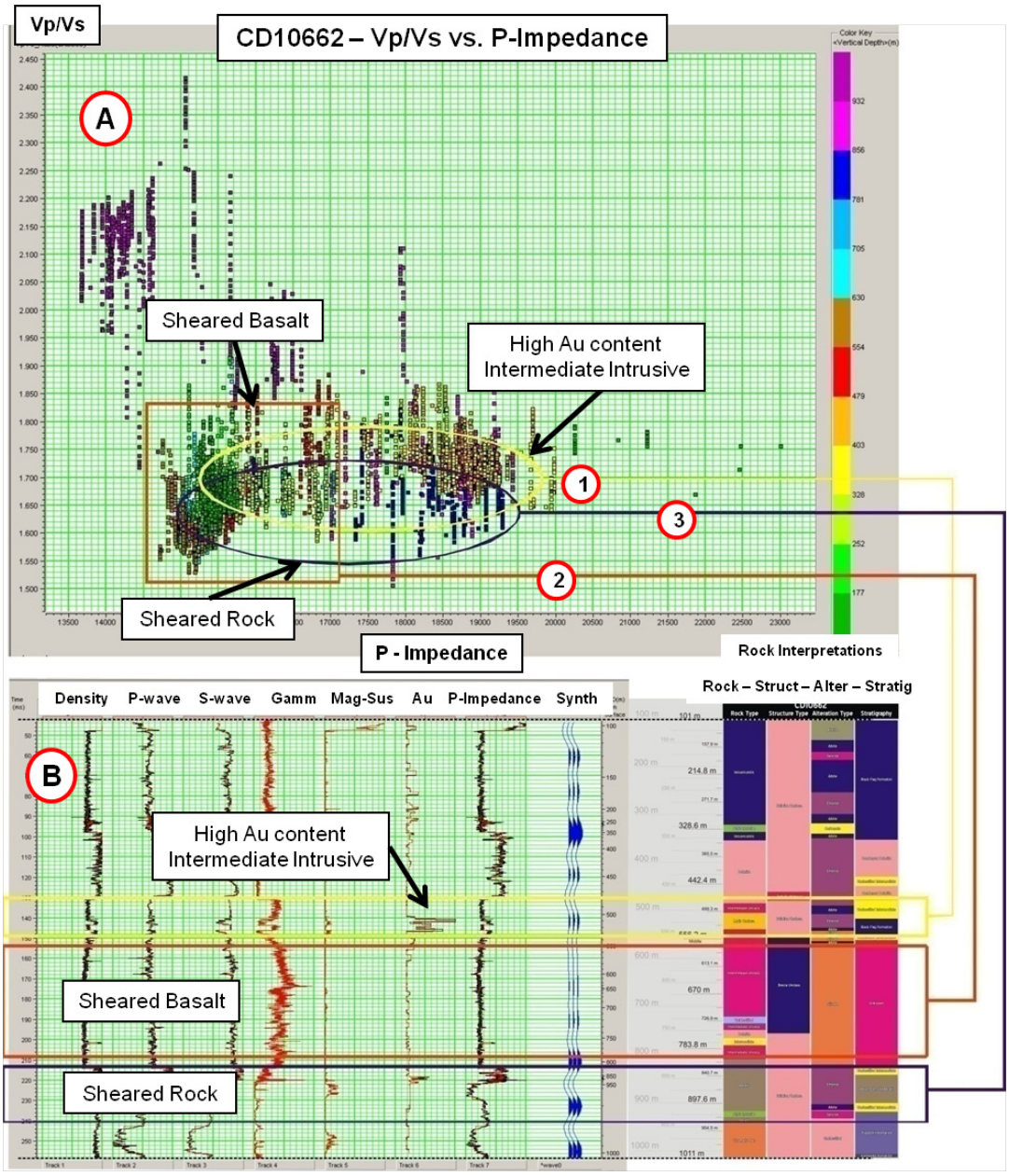

Figure 4-12. Vp/Vs versus P-impedance for CD10662. (1) is a high gold content zone, (2) is a sheared basalt zone and (3) is associated with an unknown sheared rock unit.

	Depth (m)	Depth (ms)	Rock	Structure	Alteration	Gold	Vp/Vs	P-Impedance
CD10191	206 – 210	58 - 60	Ultrmafic Talc	Unclassified	Chlorite	2000	1.50 – 1.9	13500 - 16500
	228 - 258	66 - 77	Intermediate	Unclassified	Biotote	10000	1.60 – 1.7	14000 - 23000
CD10632	334 - 355	144 - 154	Paringa B - DD	Sheared	Cholorite	500 +	1.60 - 1.95	15500 - 18250
	440 - 490	175 - 200	Mafic	Sheared	Biotote	500 +	1.45 – 1.75	15200 - 16800
CD10662	500 - 586	145 - 168	Dolerite-Intermedi	Unclassified	Chlorite	400 +	1.60 - 1.75	15250 - 19500
	854 - 938	234 - 250	Basalt	Unclassified	Chlorite	200	1.50 - 1.825	14500 - 17100
CD10943	281 – 320	77 - 89	Dolerite	Sheared	Biotote	1000 +	1.70 – 1.85	13500 - 17000
CD10663	250 – 310	103 - 126	Volcaniclastic - Intermediate	Unclassified	Albite	1000 +	1.625 - 1.725	14500 - 16500

Table 4-5. Vp/Vs, P-impedance and interpretations for gold bearing zones on all boreholes.

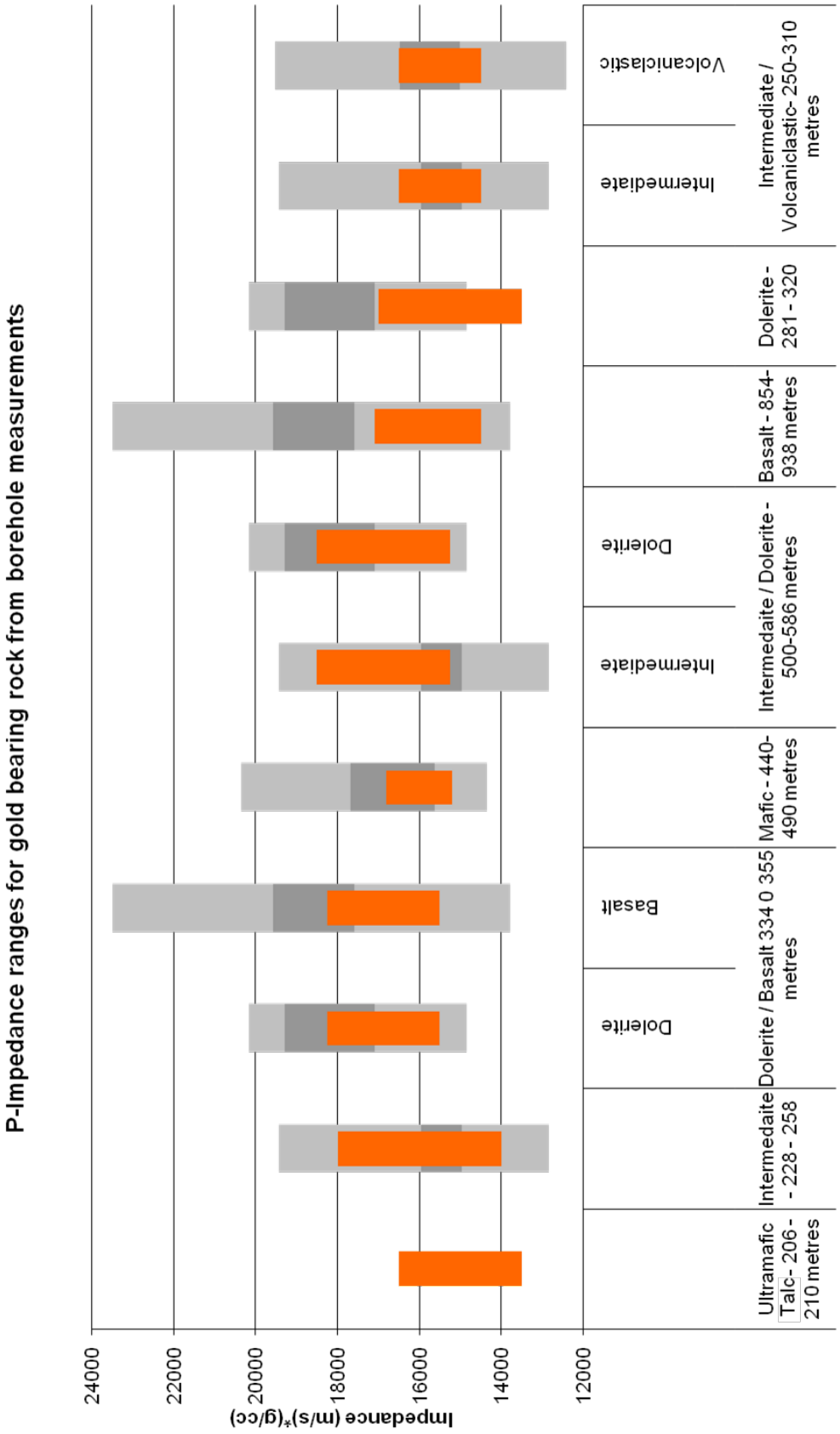

Figure 4-13. Acoustic impedance for high gold content from Table 4.5. Light gray show minimum and maximum values of impedance, dark grey is the standard deviation, and orange are gold impedances at respective locations.

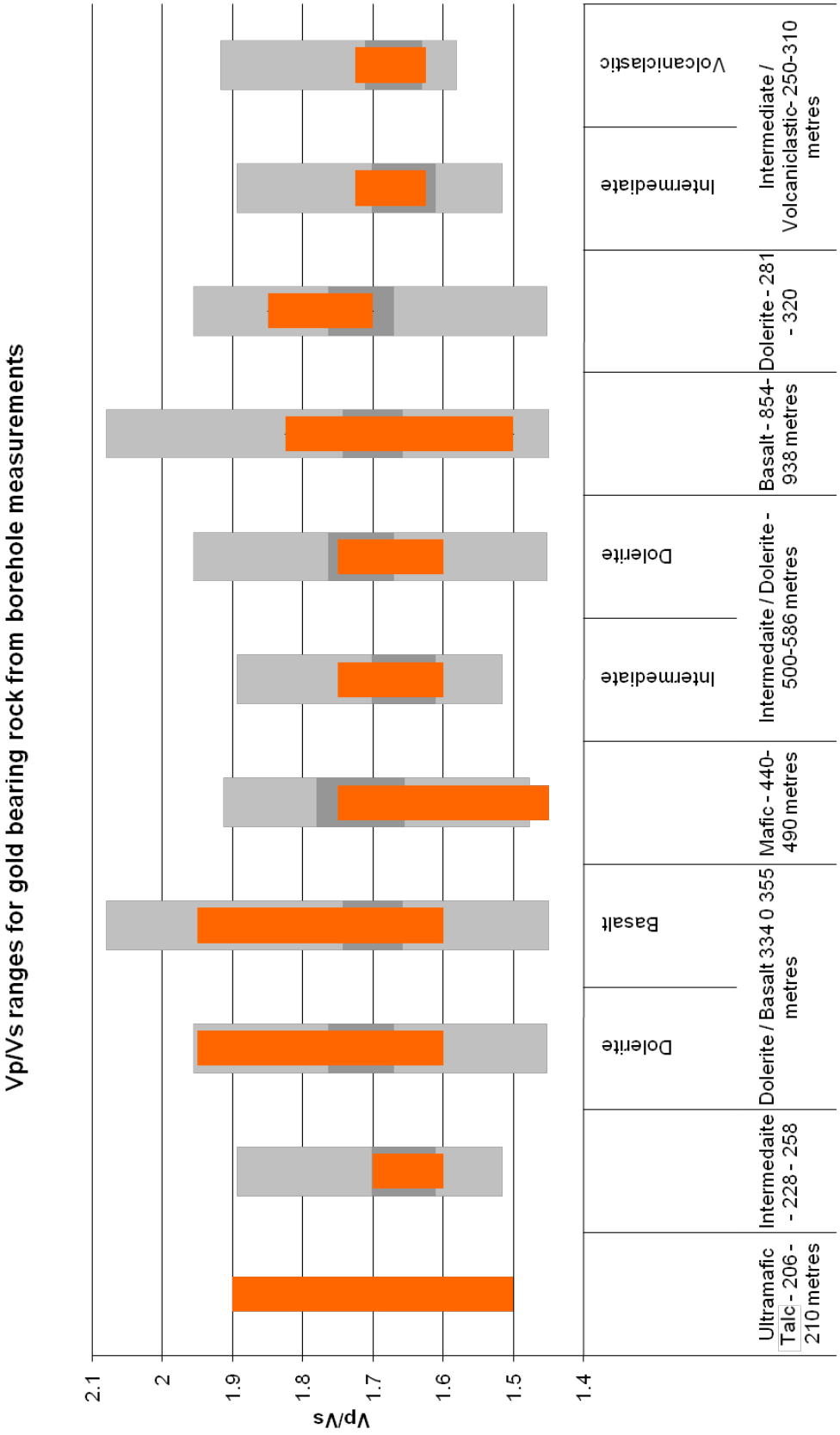

Figure 4-14. Vp/Vs for high gold content from Table 4.5. Light gray show minimum and maximum values of Vp/Vs, dark grey is the standard deviation, and orange are gold Vp/Vs at respective locations.

4.2.4 Elastic Versus Acoustic Impedance

Transforming and analysing elastic impedance and relating it to lithological analysis in hard rock environments is an approach that has not been attempted before in hard rock environments. Elastic impedance calculations from log data are dependent on Vp, Vs, and density for a select range of incidence angles. To facilitate a large spectrum of elastic impedance, both near-offset and far-offset angles were calculated from section 4.3.5 (Amplitude versus offset). The constant angles of 30^0 for near-offset and 50^0 for far-offset and K value of 0.36 were used to calculate the respective elastic impedance data for all sonic data and rock characterization from Table 4.4. Cross-plotting was again utilized for rock characterization using elastic impedance.

Figure 4-15 illustrates the cross-plots of near-offset and far-offset elastic impedance versus acoustic impedance for separate rock-types from Table 4.4. Poor separations are seen between the intermediate and volcaniclastic, with unique separations in impedance between "softer" (volcaniclastic, intermediate, mafic) and "harder" rock-types (basalt, dolerite). Borehole sonic logs were separately cross-plotted to observe zoned gold bearing rock differences in elastic and acoustic impedances. Analysis of all borehole plots indicated that gold-bearing zones have the similar acoustic impedance range as softer intermediate formations. The elastic impedance values of gold-bearing from each borehole are graphed on Figure 4-16.

Results indicate that cross plots of acoustic and elastic impedance for lithological prediction will give a good discrimination between softer and harder rocks in this hard rock environment. With sonic logs calibrated to seismic data, volumetric predictions based on softer and harder elastic rock properties with inversions will be possible. Since high gold content is associated more with softer intermediate rocks and sheared zones, these volumetric predictions can easily aid in targeted mining. However, once again, resolution limits in the seismic data, and low signal-to-noise ratio will factor in the precision of such predictions.

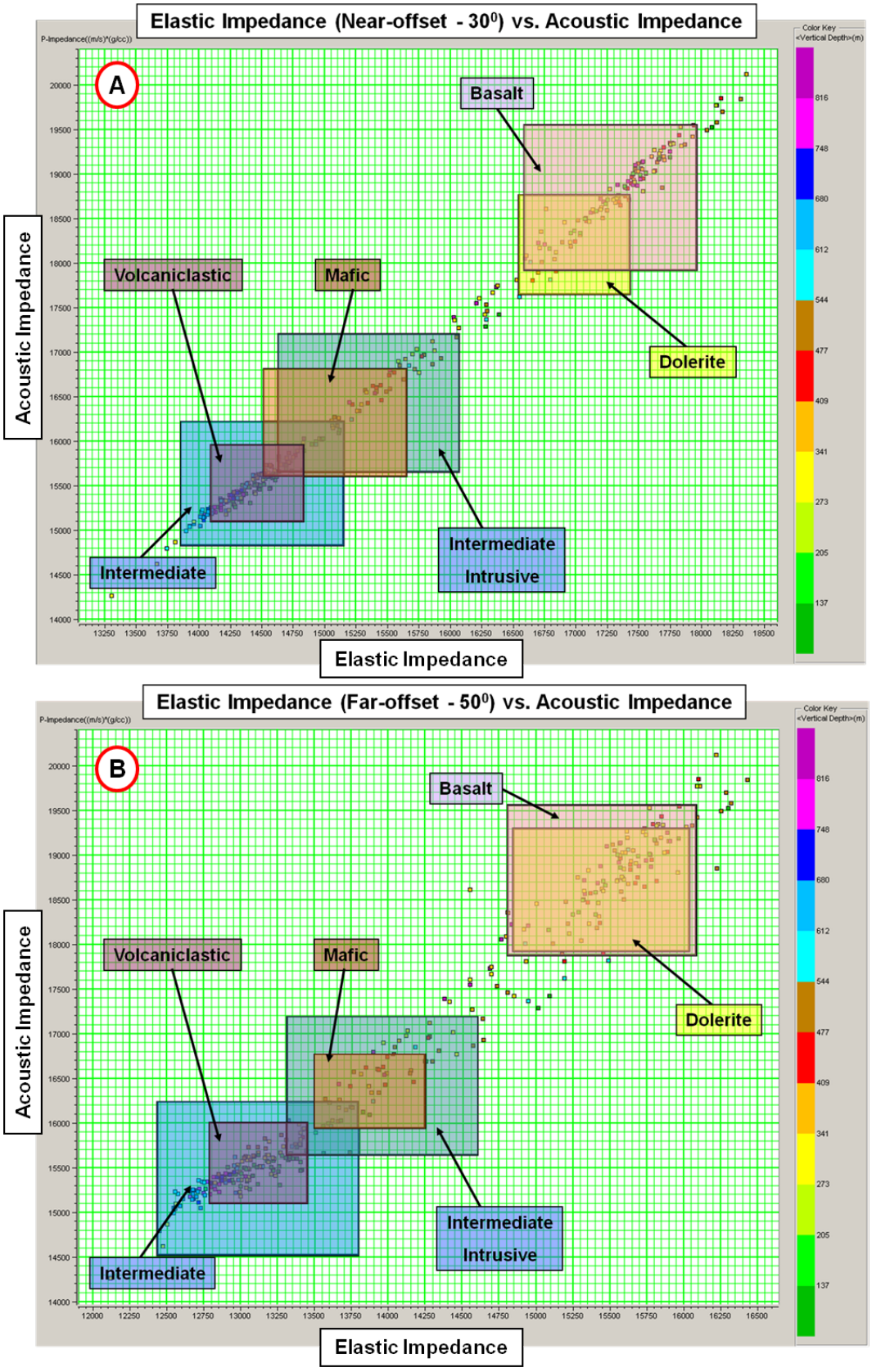

Figure 4-15. Cross-plot of elastic impedance versus acoustic impedance for near-offset (A) and far-offset (B) for all rock-types characterized on the East Victory seismic line.

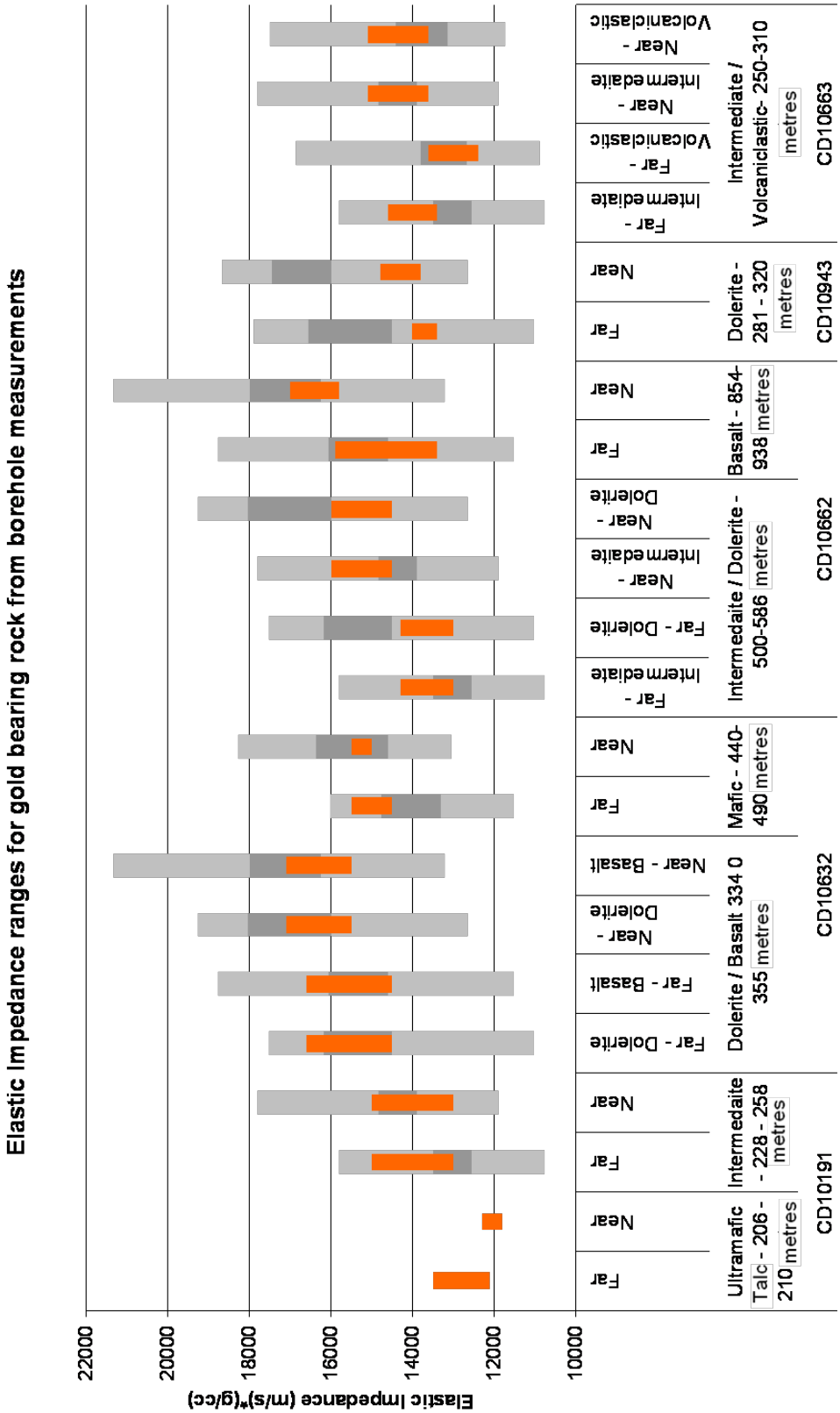

Figure 4-16. Near-offset and far-offst elastic impedances for high gold content rock from each borehole log. Light gray show minimum and maximum values of elastic impedances, dark grey is the standard deviation, and orange are gold elastic impedances at respective locations.

4.2.5 Amplitude Versus Offset Analysis

Amplitude versus offset (AVO) calculations have been used extensively in hydrocarbon exploration in search of anomalous seismic amplitude responses related to use classification of fluid type and content in pore space. Since this is a new technology for hard rock environments, analogous hard rock responses can be expected from lithology changes, structural change and possibly gold mineralization. Rutherford and Williams (1989) classified AVO anomalies as: Class 1 – Dim out, Class 2 – phase reversal and Class 3 – bright spot (Figure 4-17). Rock characterization from Table 4.4 and the Zoeppritz explorers located at the CREWES website (www.crewes.org) were used to observe the AVO response from typical rocks in contact on the East Victory borehole data (Figure 4-18). Both P-wave (red) and S-wave (green) reflection coefficients are shown. The compiled reflection responses in Table 4.4 indicate that rocks in this hard rock environment will be class two for small angles.

The AVO results from Table 4.4 show that reflection coefficients are generally below 0.1 with larger (0.2) reflectivity changes at larger angles ($>50^{o}$). There were almost no observable polarity changes with offset on the P-P reflections for any rocks in contact. Some polarity changes were seen on the P-S reflection coefficients when the angle approached critical. Analysis of contacts at high gold content ore zones shows that the magnitude of the reflection amplitude increases with small angles of incidence. In most cases reflection coefficients stay unchanged until large angles. This shows that reflection data in hard rock environments must be acquired with very large offsets to benefit from an increased reflection changes with increased angle of incidence. Luckily steep dips are common in hard rock environments so that these conditions are occasionally met even for short offsets.

Near-offset and far-offset were respectively considered to be at angles, 30^{0} and 50^{0}. These angles are of importance for elastic impedance calculations on sonic data as covered in section 4.3.4 (Simultaneous use of Elastic and Acoustic impedance).

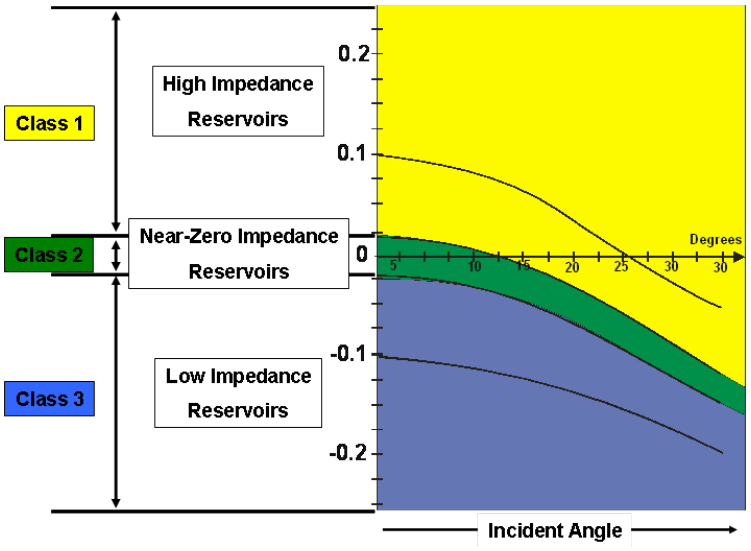

Figure 4-17. Classification of AVO responses (after Rutherford and Williams, 1989).

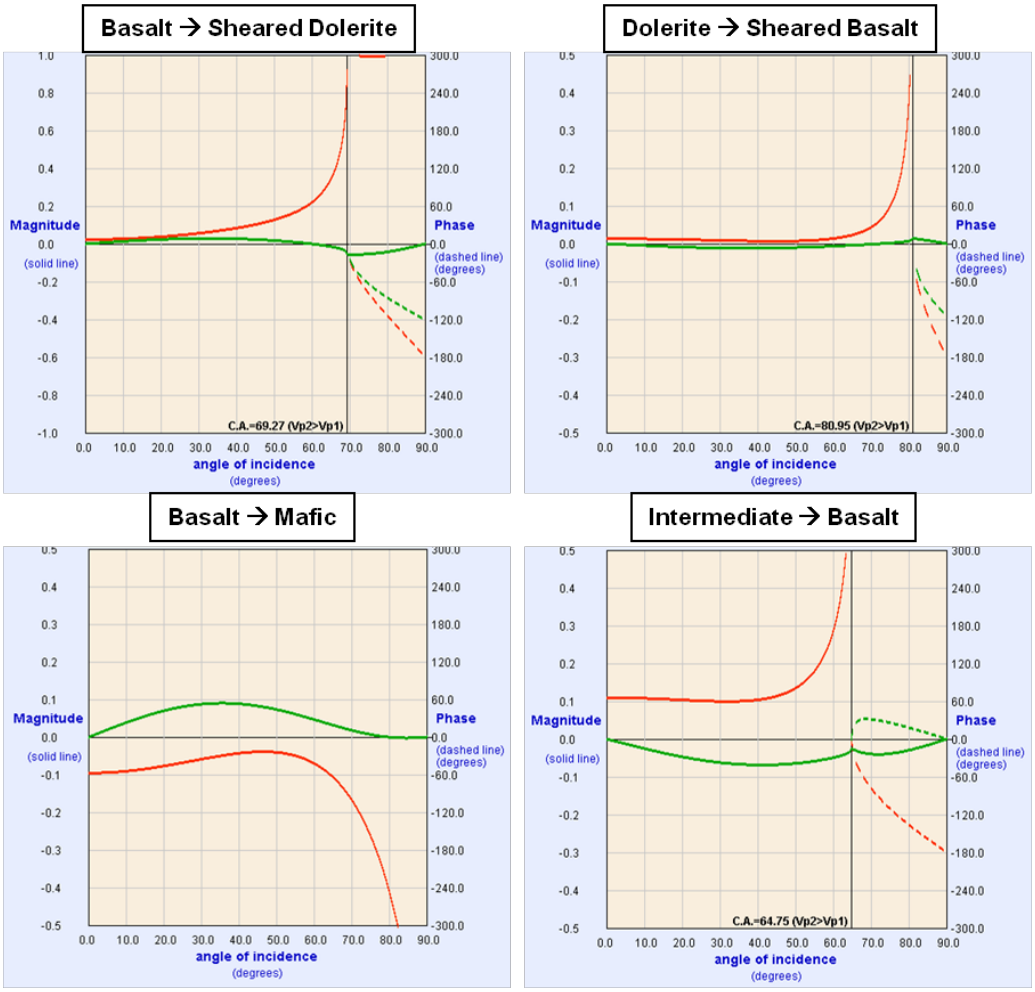

Figure 4-18. AVO response for common rocks in contact on the East Victory seismic line. Red lines indicate P-P wave reflection coefficients and green lines indicate P-S wave reflection coefficients.

Top Rock	Bottom Rock	Rpp	Polarity Change	Rps	Polarity Change	Critical
Dolerite	Sheared Dolerite	0.04 – 0.01	×	0 – -0.04	✓ - 67°	68
	Basalt	0.02 – 0.02	×	0 – 0	✓ - 75°	79
	Sheared Basalt	0.01 – 0.005	×	0 – -0.01	✓ - 75°	82
	Volcaniclastic	-0.08 – -0.04	×	0 – 0.05	×	> 90
	Mafic	-0.05 – -0.02	×	0 – 0.04	✓ - 78°	> 90
	Intermediate	-0.09 – -0.12	×	0 – 0.05	×	> 90
Basalt	Sheared Dolerite	0.03 – 0.01	×	0 – -0.04	✓ - 52°	68
	Sheared Basalt	0.01 – 0.04	×	0	×	82
	Volcaniclasitc	-0.08 – -0.04	×	0 – 0.08	×	> 90
	Mafic	-0.08 – -0.04	×	0 – 0.06	✓ - 78°	> 90
	Intermediate	-0.10 – -0.09	×	0 – 0.07	×	> 90
Mafic	Sheared Dolerite	0.09 – 0.03	×	0 – -0.09	✓ - 55°	60
	Sheared Basalt	0.07 – 0.03	×	0 – -0.05	✓ - 65°	68
	Volcaniclastic	-0.03 – -0.03	×	0 – 0.02	×	> 90
	Intermediate	-0.05 – -0.08	×	0 – 0.04	×	> 90
Intermediate	Sheared Dolerite	0.14 – 0.10	×	0 – -0.10	×	58
	Sheared Basalt	0.11 – 0.10	×	0 – -0.07	×	65
	Volcaniclastic	0.01 – 0.08	×	0 – 0.01	✓ - 50°	80

Table 4-6. Table of reflectivity in PP and PS, as well as critical angle from amplitude versus offset plots for hard rock.

Full Zoeppritz equation in the Hampson-Russell software package was chosen to create elastic offset seismograms at each borehole to observe synthetic reflectivity changes through the sonic data. The solution to Zoeppritz equations were not exact seismic responses due to Zoeppritz modelling plane waves, while seismic waves are spherical (Lines and Newrick, 2004). Regolith distortions, coherent noise and random noise are also absent from the synthetic offset seismogram calculations. Nevertheless Zoeprritz is easier to interpret and hence relate to synthetic to seismic.

Figure 4-19 shows the logs (left), the 0-1000 metre offset synthetic calculations (centre), and the respective location of the deviated borehole on the seismic data (right) for boreholes CD10662 and CD10663. The highlighted areas on both synthetic and seismic images indicate areas of high gold content. Both synthetic offset plots show an increase in amplitude with increased offset at high gold content zones. The magnitude of the amplitude changes in the synthetic elastic model, however, appears non-unique. As can be

seen on Figure 4-19 comparison between the flat laying synthetic and the complex seismic image is also non-trivial.

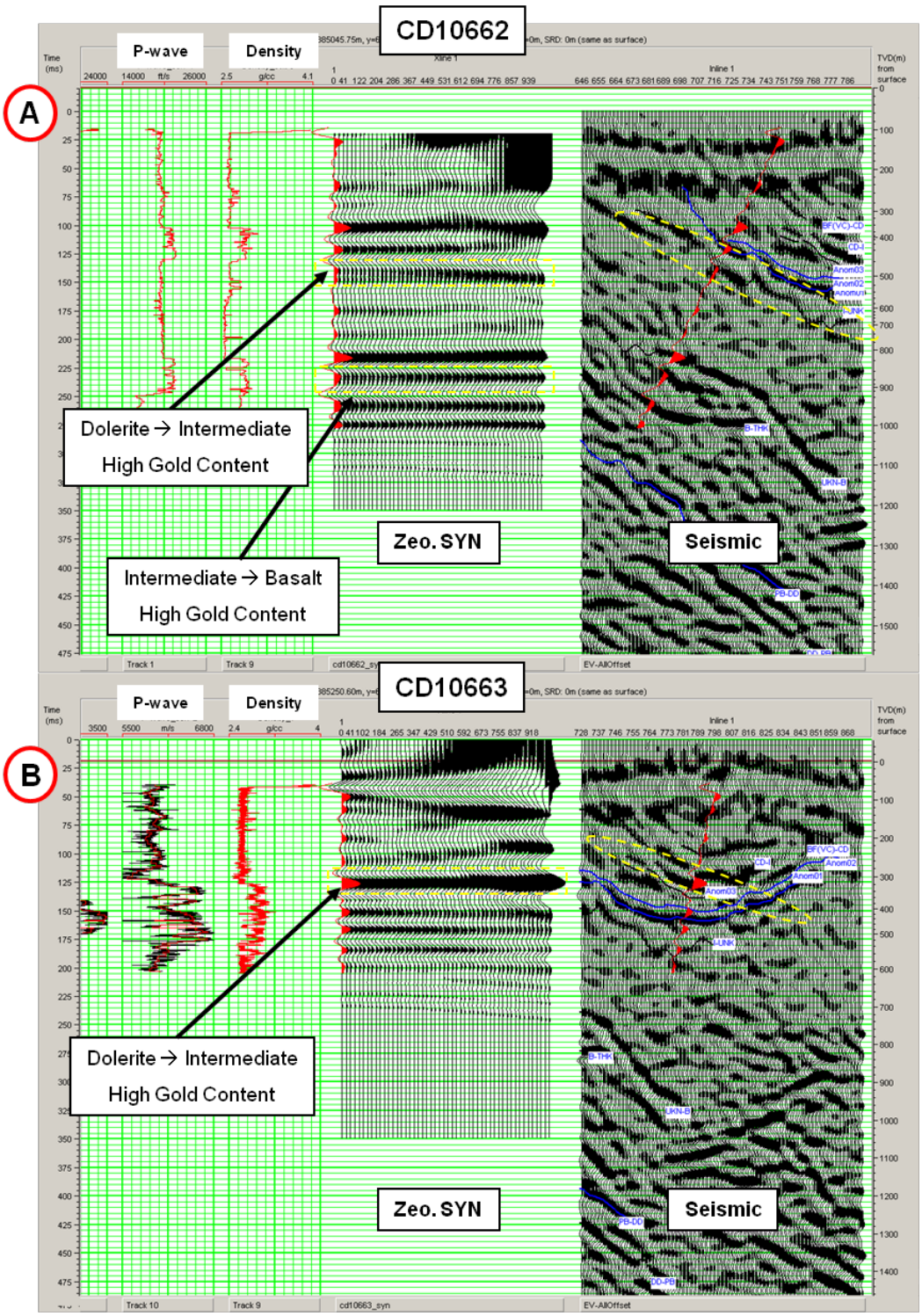

Figure 4-19. Logs (left), Zoeppritz synthetic (centre) and seismic data (right) for boreholes CD10662 (A) and CD10663 (B). AVO response for high gold content zones are indicated on each borehole Zoeppritz synthetic seismogram.

4.2.6 Lambda-Mu-Rho

Due to remaining ambiguity in acoustic and elastic impedance analysis, further investigations were necessary to observe other possible elastic consistencies in hard rock data. The use of Lambda-Mu-Rho (LMR) elastic parameters is a technique that inverts seismic amplitudes to Lame's parameters (λρ and μρ) scaled by density. Lambda (λ) is known as the fluid incompressibility and is sensitive to fluid content while Mu (μ) does not respond to fluid saturation with μρ being considered the "matrix indicator". The rock-types are different, and fluid content ultimately not in consideration, but parallels in lithology and gold content prediction are attempted here.

Figure 4-20 shows the Lambda-Rho versus Mu-Rho cross-plot of the compiled rock-type data for the East Victory line. The results indicate that volcaniclastic, intermediate intrusive, intermediate, and mafic rocks were difficult to distinguish from each other using LRM analysis. However, the data also suggests that, in general, the lower values of λρ and μρ show a way to discriminate between softer rock and harder basalts and dolerites. The values of λρ and μρ are also depth dependant making LMR analysis in hard rock environment most useful at shallow depths (above 800 metre). Lambda-Mu-Rho cross-plotting was carried out on all boreholes to observe possible correlations with gold content. Figure 4-21 displays the cross-plots Lambda-Rho versus Mu-Rho for boreholes CD10662. High gold content zones coincided with softer rocks revealing LMR inversion may allow for volumetric predictions of gold content.

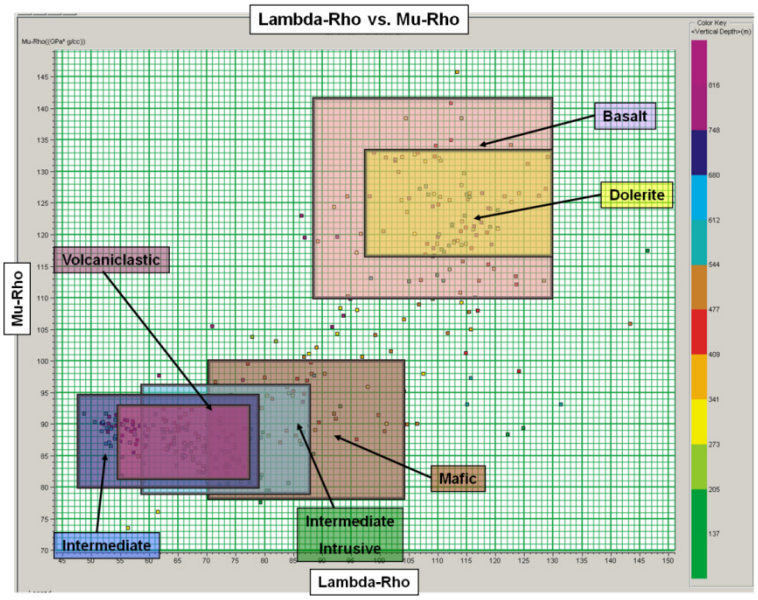

Figure 4-20. Lambda-Rho versus Mu-Rho cross-plot for all rock major rock-types from the East Victory line.

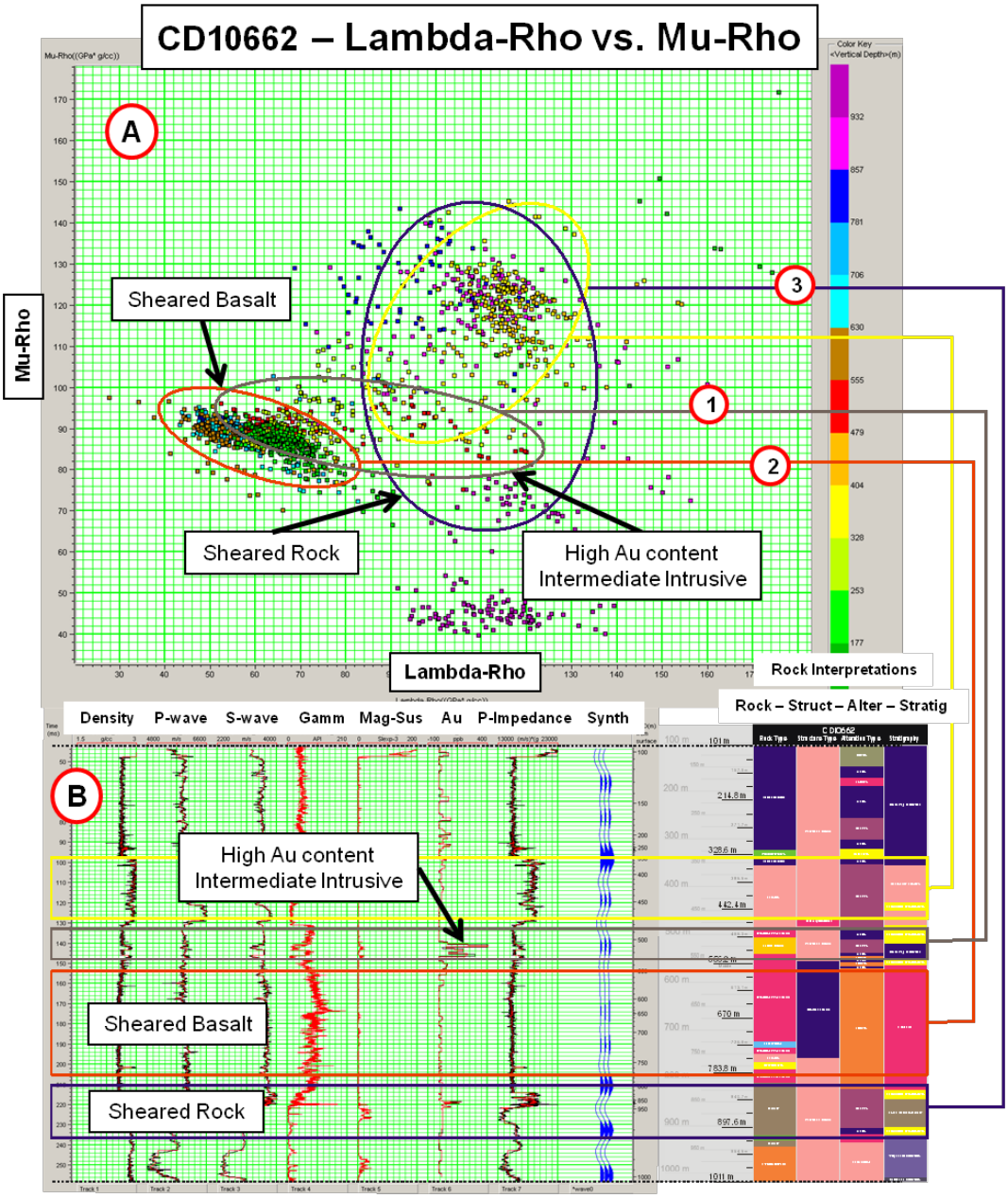

Figure 4-21. Lambda-Rho versus Mu-Rho for borehole CD10662. (A) is the cross plot and (B) is the sonic data with rock interpretations. (1) represents a high gold content zone, (2) is a sheared basalt zone and (3) is associated with an unknown sheared rock unit.

4.2.7 Rock Characterization Summary

Differentiating between specific rock types using sonic data was not as definite as was the ability to distinguish between softer and harder hard rocks. The softer rocks (intermediate, mafic and volcaniclastic) and harder rock (dolerite and basalt) zones were shown to have distinct acoustic impedances, elastic impedances, AVO effects and LRM

properties. Log derived synthetic seismic responses occurred at unique rock type and structural changes along the borehole sonic data. These synthetic reflections showed that seismic reflections on the East Victory hard rock seismic image are most likely due to similar types of rock contacts. These consistencies in the synthetic reflection and the statistical rock characterization show that good connections exist between physical rock properties and wave field rock properties. With seismic reflections analogous to borehole synthetic reflections, calibration of the sonic data to seismic images should provide a basis for data inversion. However the reflection information from synthetic seismograms are calculated in the absence of regolith distortions, coherent noise, random noise, and signal loss. The sonic data is also acquired with much higher frequencies than seismic data requiring both sets of data to be conditioned properly to ensure calibrations are valid. Under ideal circumstances, data inversion and rock identification through seismic data will be possible.

5 Rock Identification from Seismic Data

Processing of the East Victory seismic line has revealed reflections from economically viable depths of 300-800 meters down to mesothermal fluid flow at 4000 metres (Figure 4-7 and Figure 4-8. Borehole sonic logs and their respective synthetic seismograms have shown that reflections are identifiable at rock interfaces, and structural changes. Correlating the log data and seismic data for statistical predictions of lithology and possible mineral content is a necessary for seismic inversion. While seismic inversion is a mature technology for hydrocarbon exploration, it is new territory for exploration in hard rock environments.

The reliability of seismic inversion is dependent on quality, quantity, and location of sonic data, and dependent on the accuracy of the correlation between the synthetic and seismic reflection sets. To limit ambiguity in inversion results, only the top 500 ms of the East Victory seismic, which represents the deepest penetration of borehole data, was considered in this research. Figure 5-1illustrates the area of focus for inversion on the East Victory seismic line. Borehole acoustic impedance logs are inset on the image. Acoustic inversions were first tested since the original East Victory seismic image was stacked with all offsets. The inversion process requires the following steps be completed before full inversions could be considered reliable:

- Seismic data has to be zero-phased to enhance interpretation,
- characteristic wavelet extracted with frequency spectrum of the seismic data,
- borehole sonic data correlated with the seismic image via synthetic seismograms,
- Careful rock contact picking to enable creation of acoustic impedance sections,
- Inversion,
- Error analysis, and
- “Hidden” sonic log error analysis.

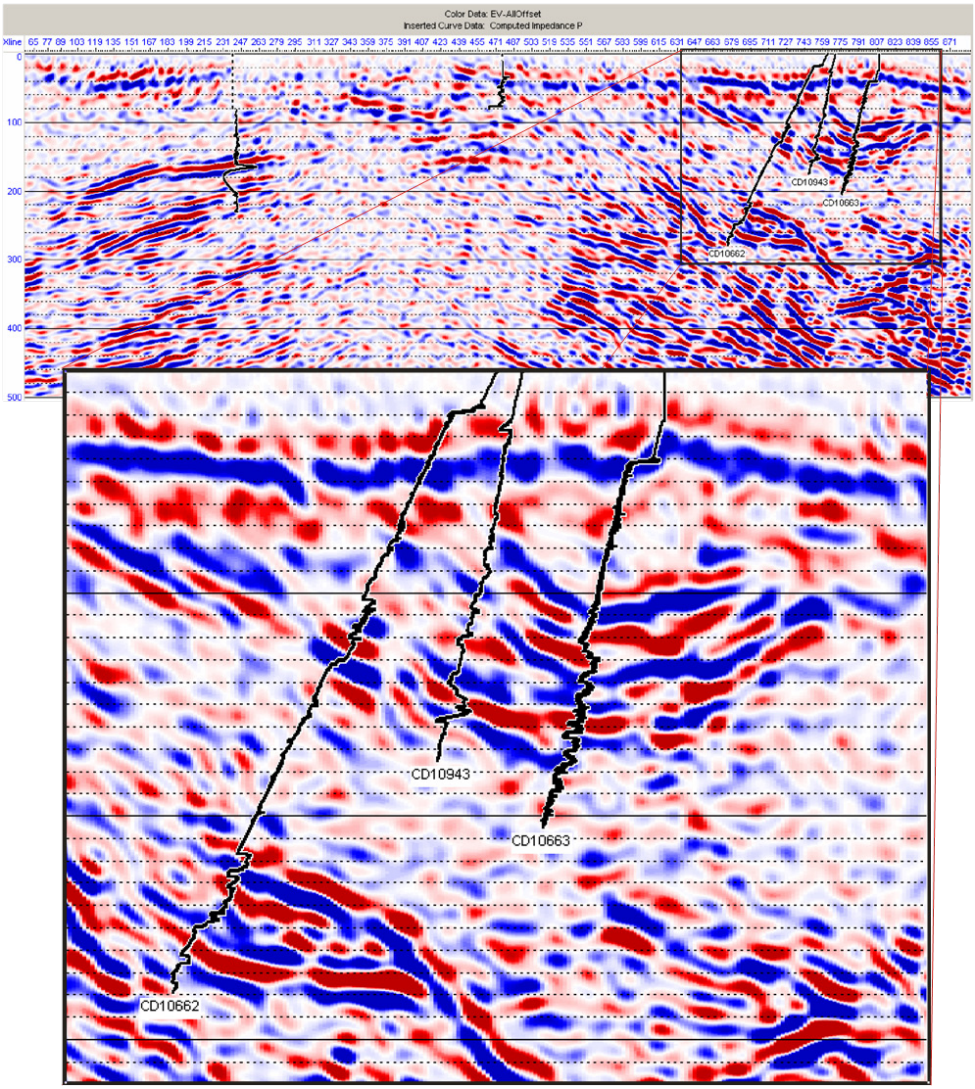

Figure 5-1. The top 500 ms (top) of the East Victory. Inset image of CD10662, CD10943 and CD10663. Acoustic impedances logs are shown for each borehole.

Correlating borehole sonic data to seismic data is a non-trivial process. Check-shots are typically used to give time-depth relationship to validate matching of sonic to seismic data. As is the case in this study, check shots are very rarely available for hard rock environments. Without a check-shot matching of seismic and synthetic reflections requires additional effort and may lead to ambiguous correlations.

A 67 degree phase rotation was found to be necessary to zero phase the seismic data using the wavelet as a reference. Wavelet extraction was only conducted at the cluster of boreholes (CD10662, CD10943, and CD10663) on the eastern side of the seismic line were error analysis using "hidden" logs was possible. Figure 5-2 shows the final statistical wavelet used for correlating all borehole sonic logs to the seismic data. The wavelet

extracted has to have the same spectrum and dominant frequency of seismic data to ensure that synthetic seismograms were representative of the seismic image. The final wavelet parameters were:

- Wavelet length: 150 ms
- Taper Length: 20 ms
- Sample Rate: 1 ms

Figure 5-3 shows each synthetic seismogram matched with the seismic data. The inset image illustrates the area around boreholes CD10662, CD10943 and CD10663. Cross-correlation windows between synthetic and seismic data were limited to major reflections and did not encompass the entire length of any sonic log.

There was a high level of ambiguity when borehole synthetic seismograms CD10632 and CD10191 were matched with seismic data. CD10632 was off line by 470 meters with only two synthetic reflections matching the seismic data. CD10191 was short and it too had very few synthetic reflections to match with seismic data. Ultimately, to ensure inversion results were reliable, these two boreholes were only used as reference for the remainder of this study.

CD10662, CD10943 and CD10663 correlations results, while low (<0.71), were realistic with respect to known rock-types in the area. Cross-correlations were not higher for several possible reasons:

- Signal distortions through the regolith,
- Noise not completely attenuated, or signal over attenuated during processing,
- Out-of-plane reflections still in the data,
- Improper datum due to lack of check-shots,
- Deviated borehole trajectories resulting in mismatched reflection correlations,
- Poor or variable quality in logs (which is often the case).

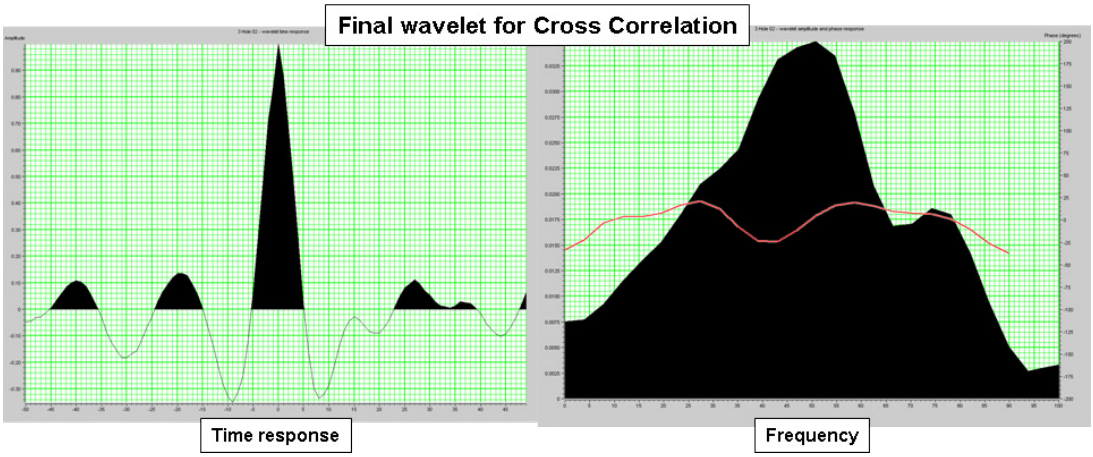

Figure 5-2. Wavelet used for cross correlations of sonic logs with seismic data. The red line is the phase angle of the frequency

The term "horizon" is used very loosely in hard rock seismic interpretations. Reflections seen in mineral exploration have come from rock alterations in rock type variations as well as shear zones, and structure changes. The term "Rock contacts" will be used in place of "horizons" since most matched synthetic reflections with seismic reflections were located at impedance changes between rock types. Figure 5-3 shows the rock-contact extensions that were interpreted throughout the East Victory seismic data. Instantaneous phase (Figure 5-4) was used to help delineate the rock-contacts where weak amplitudes blurred reflection continuity. Nine main rock-contacts were interpreted on the seismic data:

- Paringa basalt into the Deviance dolerite on borehole CD10632,
- Defiance dolerite into the Paringa basalt on borehole CD10632,
- Devon Consol basalt on top of the Kambalda komatiite on CD10191,
- Back Flag banded iron formation near the Codensor dolerite,
- A high gold content contact between an intermediate intrusion through the condenser dolerite,
- dolerite / intermediate intrusion into an shear zone on CD10662, CD10663 and CD10943,
- and an unknown basalt unit at the bottom of CD10662.

Three smaller rock contacts on the eastern section denoted Anom01, Anom02 and Anom03 were picked to help delineate the Condenser dolerite.

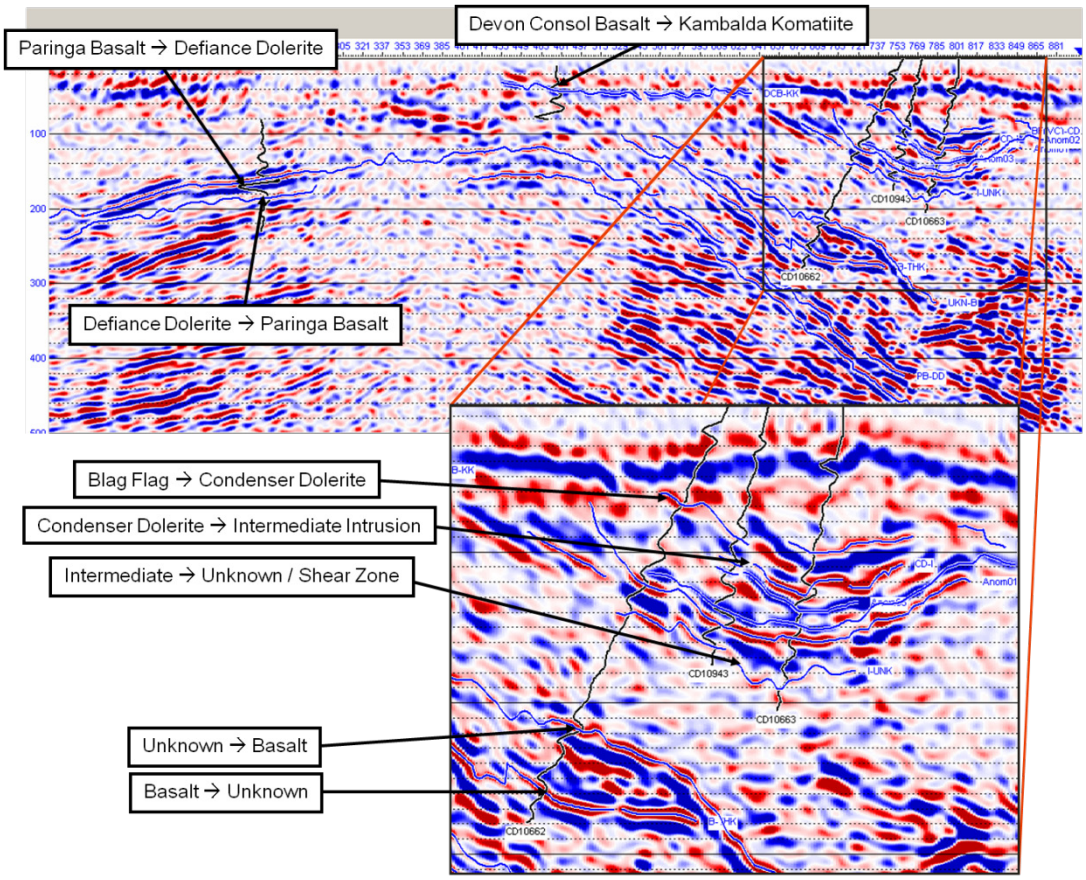

Figure 5-3. The rock contact picks and extensions on the East Victory seismic line.

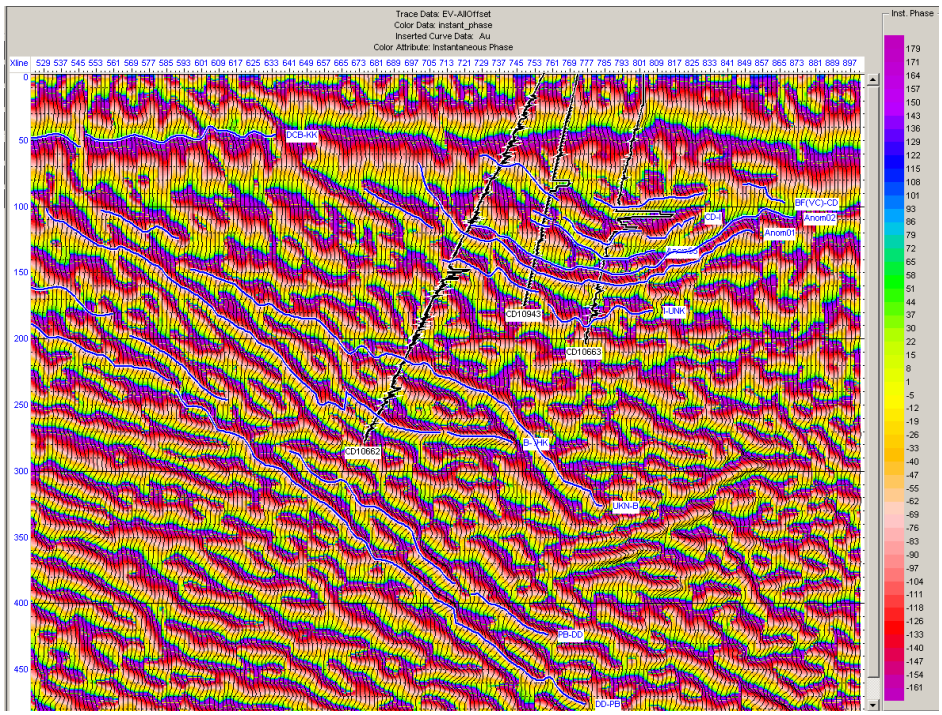

Figure 5-4. Instantaneous phase used to aid in rock contact picking on the East Victory seismic line.

5.1.1 Results and Analysis of Acoustic Inversion

Figure 5-5 shows the acoustic impedance model for the East Victory seismic line. The inset image on this figure shows detail of the eastern section of the seismic line where CD10662, CD10943 and CD10663 are located. P-impedance values used for modelling were generated from the blocked, stretched, and normalized impedance logs from each borehole.

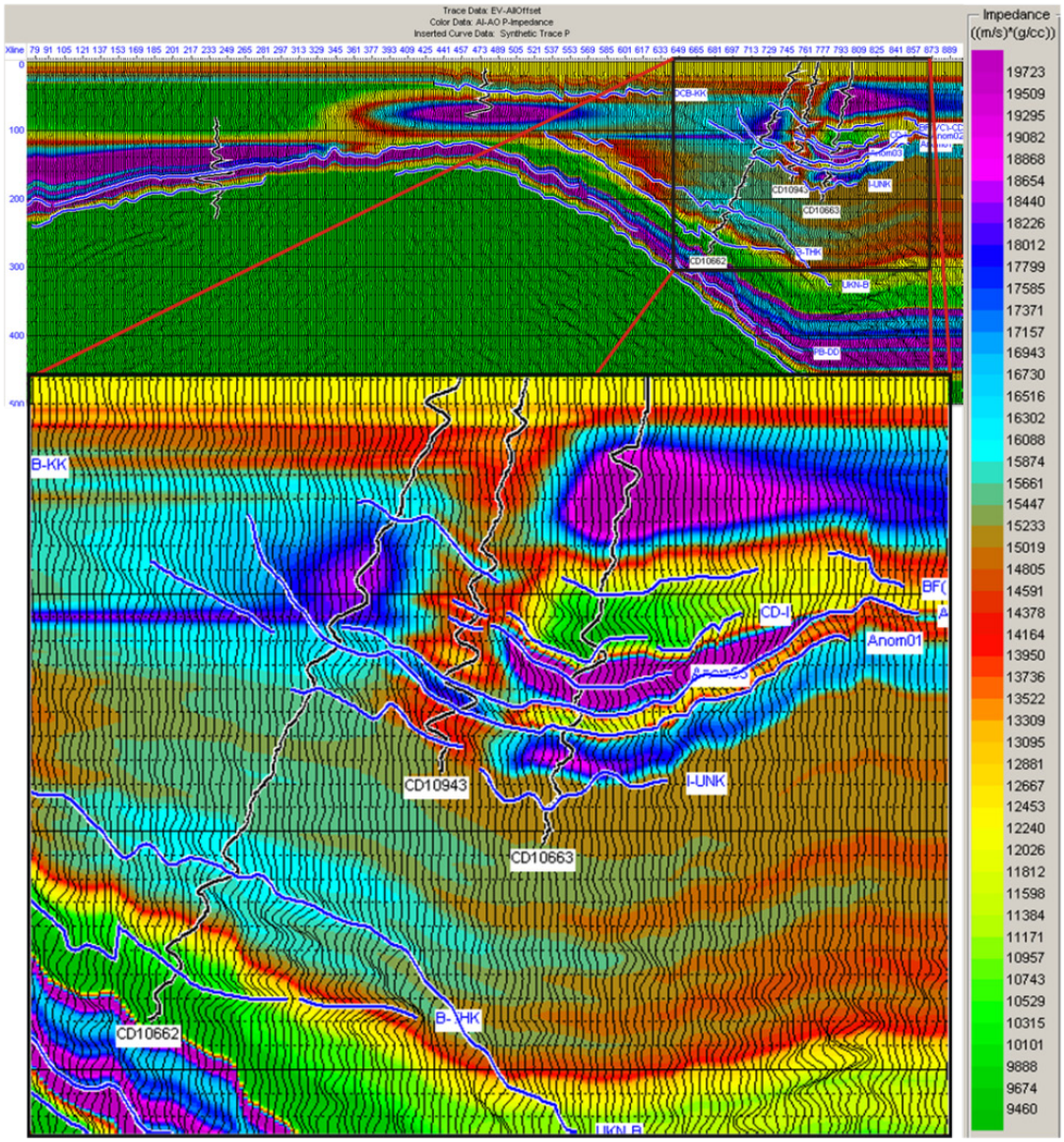

Figure 5-5. The acoustic impedance model of the East Victory seismic line. The inset image illustrates the CD10662, CD10943 and CD10663 area of interest.

The following is a list of all inversions computed for the zero-offset acoustic model of the East Victory seismic line:

- Model Based
    - Hard Constraint biased
    - Soft Constraint biased
- Band-limited
- Coloured Inversion
- Linear Programming Sparse-Spike
- Maximum Likelihood Sparse-Spike.

Figure 5-6 shows the results of three inversions: modelled hard constraint, frequency recovered coloured inversion, and maximum likelihood sparse-spike. The differences between these selected inversions are illustrated in Figure 5-7. Coloured inversion analysis shows high level of error below all sonic logs. All inversion results show a prediction base for lithological separation, but also appear to have inherently, and sometimes widely varying, prediction results. Further statistical analysis was necessary to verify which inversion best represents the data available.

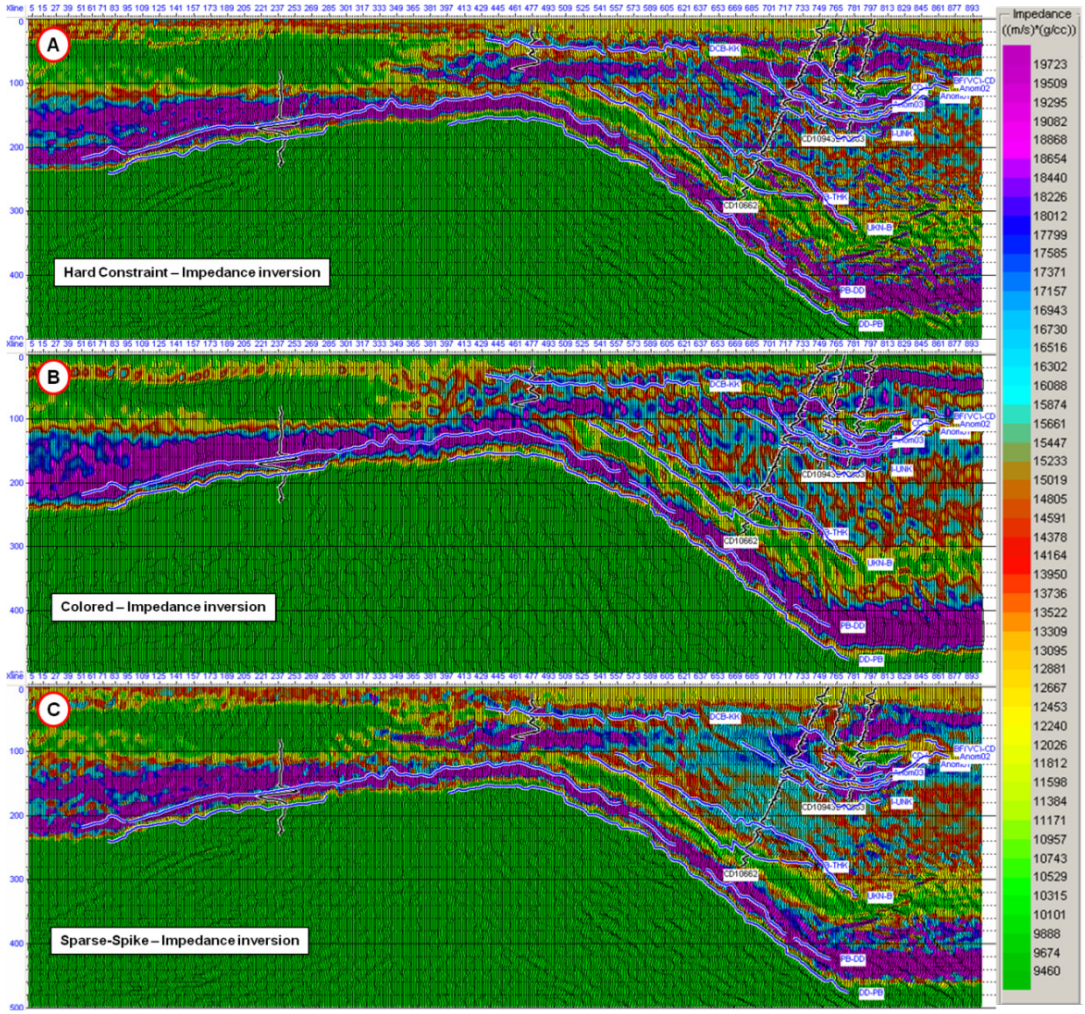

Figure 5-6. Acoustic impedance inversions: Model inversion hard constraint (A), frequency recovered Coloured (B), and maximum likelihood sparse-spike (C).

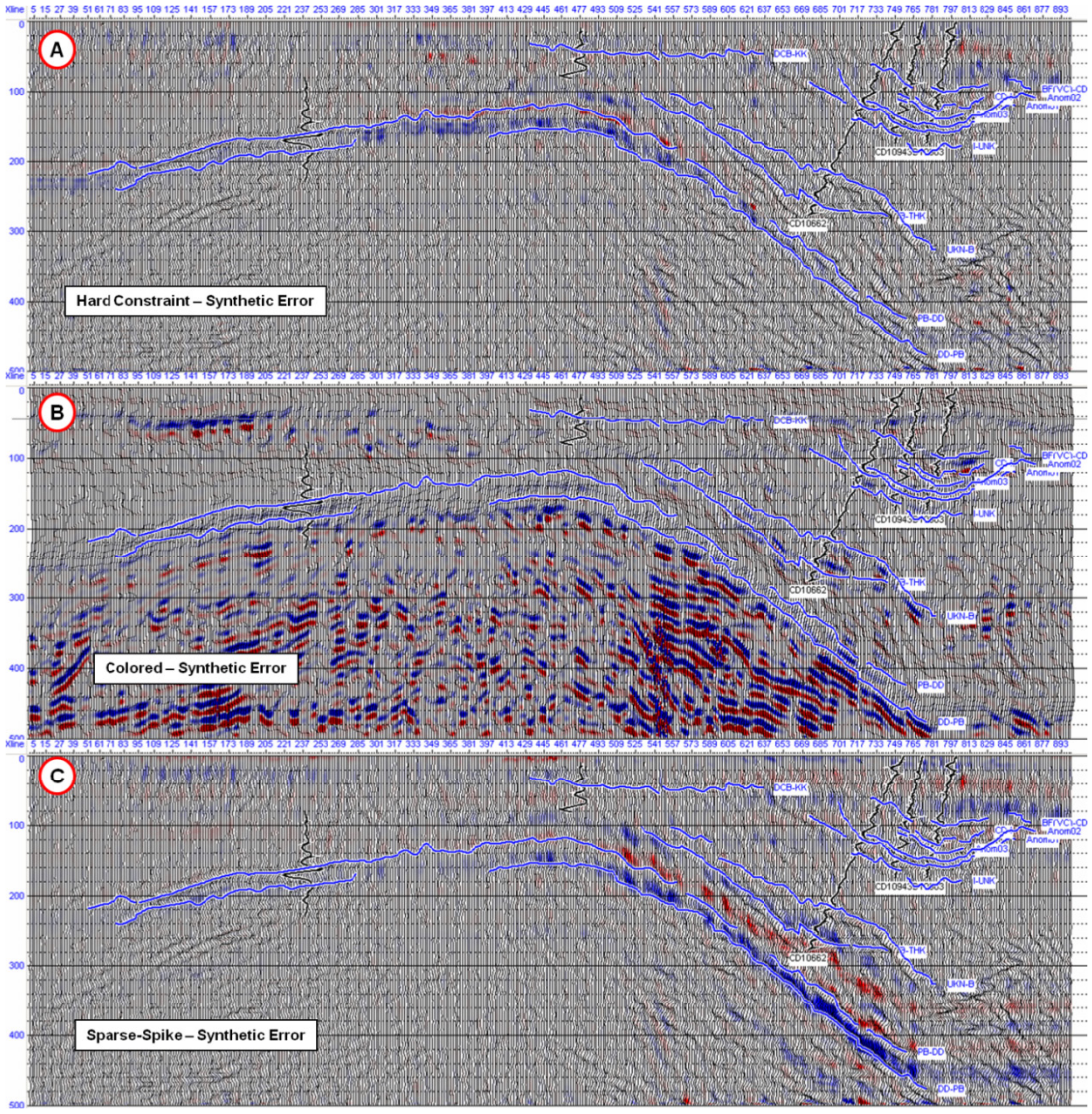

Figure 5-7. Difference between the inversion predictions and the East Victory seismic image for model inversion (A), frequency recovered coloured (B) and maximum likelihood sparse-spike inversions (C).

The universal quality check of the inversion results is to compare inverted impedance estimates to log data not used in the inversion (Latimer, 2000). The only area on the East Victory seismic image that was conducive to log "hiding" for error analysis was the eastern section associated with boreholes CD10662, CD10943 and CD10663. Three additional acoustic models were generated, each excluding one of the three boreholes for "hidden" borehole error analysis. Six inversions were generated on each of the four models for a total of 24 inversions. Figure 5-8 shows results of cross-correlation of the borehole data with the synthetic seismogram generated by the inversions.

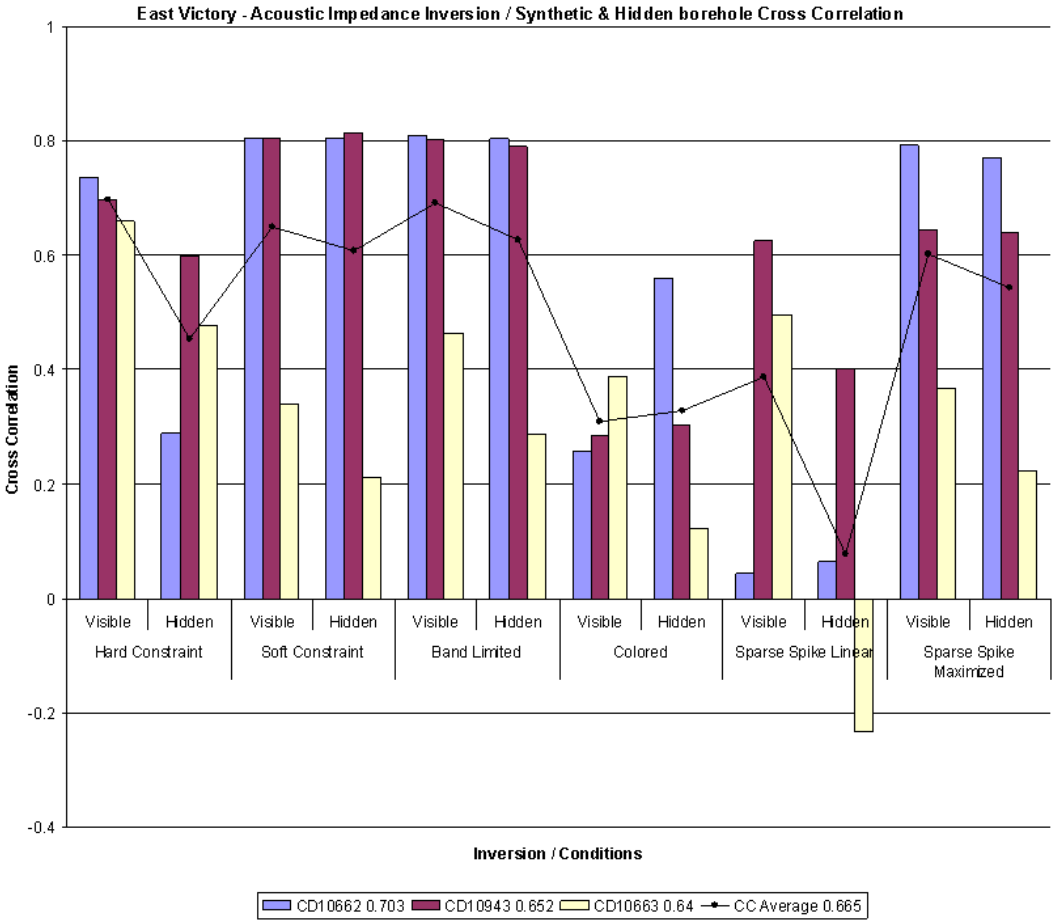

Figure 5-8. Graphed cross-correlation results for inversion verification. The black line connector indicates the average correlation between sets of inversions.

Model inversion, band-limited, and maximized sparse spike inversions had the best "hidden" log error results. The soft constraint biased model based inversion (Figure 5-9) clearly predicts a shear zone of alternating high and low impedance through most of the eastern side of the seismic line. This area is associated with the massive shear zone interpreted on the eastern flank of the St. Ives anticline. The outline of the Condenser dolerite is imaged quite well, along with a low impedance volcaniclastic and intermediate zone on CD10663, a sheared dolerite on CD10943, and an intermediate intrusive sandwiched between basalt layers at the bottom of CD10662. Inset logs are the gold assessment for each borehole. High gold content areas on borehole data are highlighted.

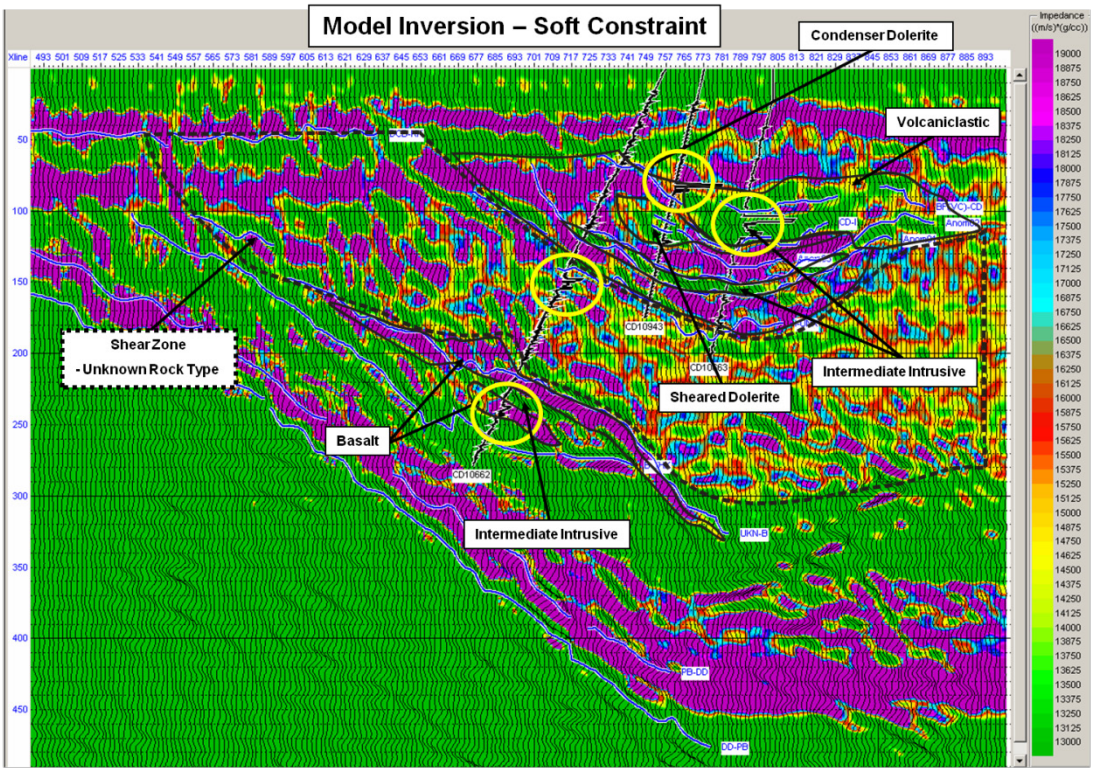

Figure 5-9. The soft constraint model based inversion of the seismic data to P-impedance.

The Band-limited, or recursive inversion, limited to 10-100 Hz is shown on Figure 5-10. The shear-zone on the flank of the St. Ives anticline appears more uniform and produces higher impedance values than the model inversion (Figure 5-9). The prediction of Condenser dolerite, while the same shape as the model inversion, has lower impedance over all. The intermediate and volcaniclastic package on top of the Condenser dolerite which coincides with high gold content interpretations from the CD10663 is imaged quite well. The results of inversion analysis (Figure 5-8) show that this inversion represents the highest correlation with the data-sets.

The Sparse-Spike inversion based on a Maximum-Likelihood deconvolution algorithm is illustrated in Figure 5-11. Sparse-Spike inversion, Maximum Likelihood for the East Victory seismic line.. The seismic inversions results are a high-frequency inversion which looks, fittingly enough, spiky. The results do not appear “natural”, but do produce similar delineations of features including those of the large shear-zone, the Condenser dolerite, the high gold content intermediate intrusive above the Condenser dolerite. The prediction also provides good separation of the intermediate intrusive sandwiched between dolerite at the bottom of CD10662. All inversions show a possible way to attempt volumetric gold predictions.

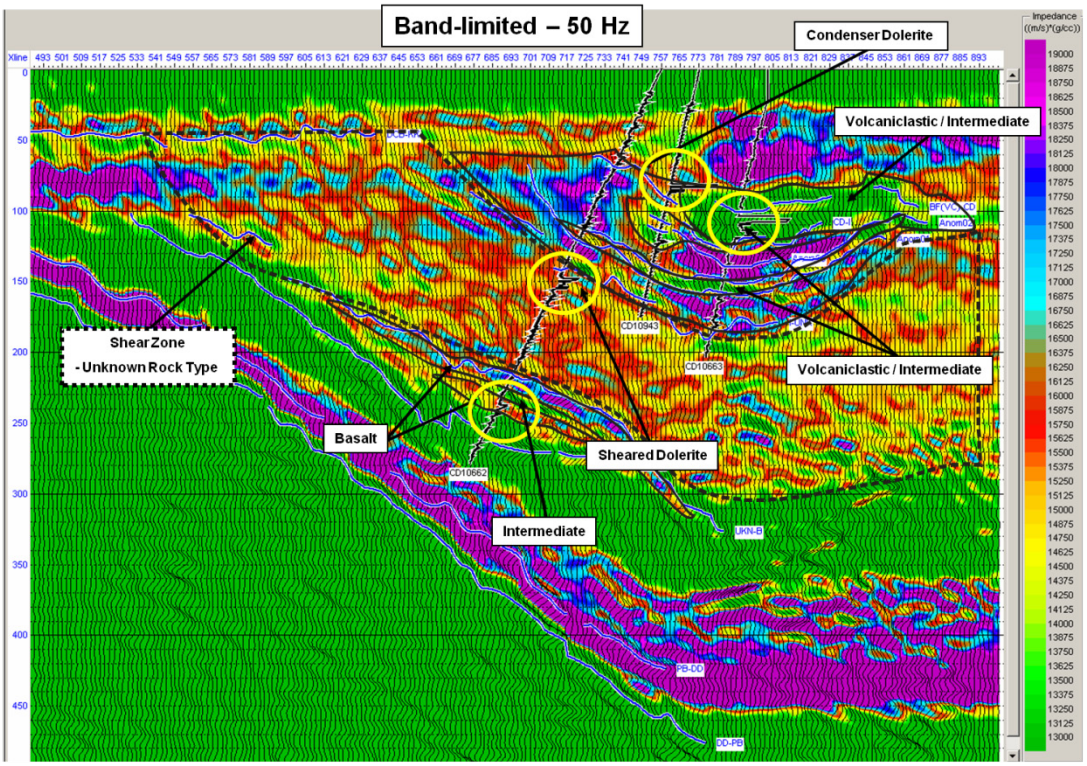

Figure 5-10. The Band-limited inversion for the East Victory seismic line.

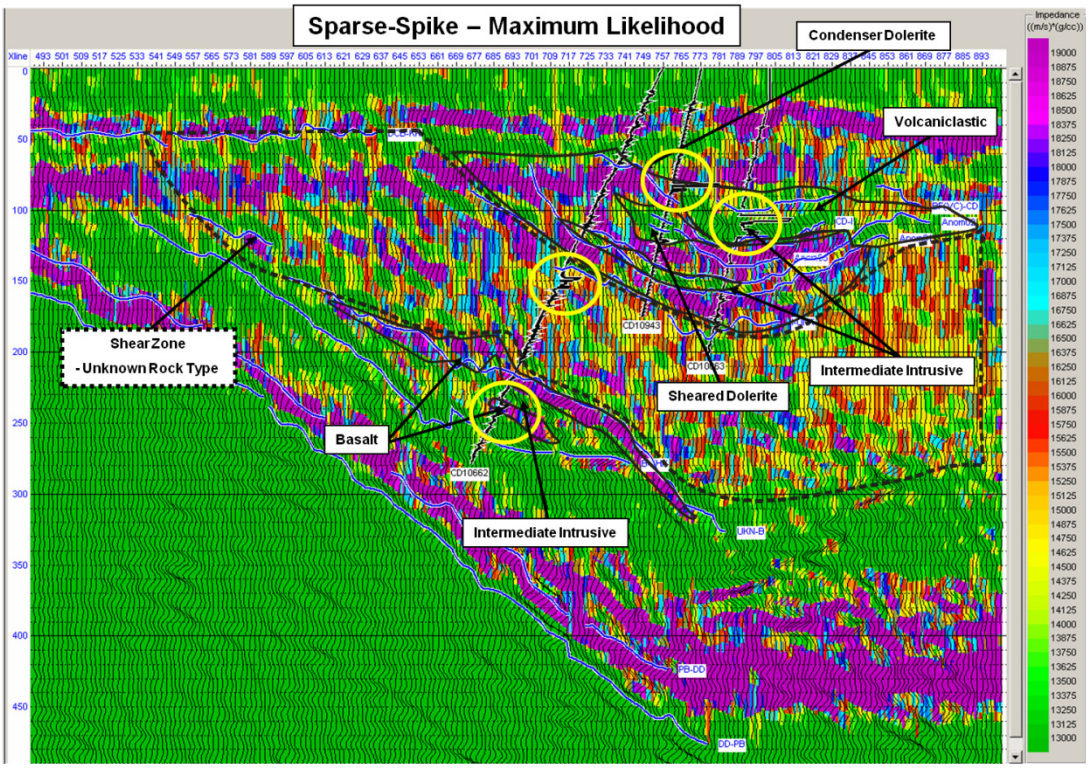

Figure 5-11. Sparse-Spike inversion, Maximum Likelihood for the East Victory seismic line.

Impedance differences between the inversions vary up to 400 - 600 (m/s)*(g/cc) in places with limited borehole control (i.e. below the Condenser dolerite, and shear zone on the flank of the St. Ives anticline) which are good results for hard rock environments. Physical size prediction also varies from 10 to 20 metres between inversions within the Codensor dolerite. The largest gold content located in the Condenser dolerite is on borehole CD10663 and CD10662 corresponding to a low impedance volcaniclastic and intermediate ore zone. On all inversions, this low impedance area is approximately 100 metres wide, ±10 metres depending on interpretation, and 50 ms deep (~5500m/s*0.05s = 250 metres), ±2 ms (25 metres). Mismatches between the inversion predictions could be from:

- Band-limited nature of the seismic data,
- Noise still present after processing in seismic data, and
- Errors in wavelet estimation.

5.1.2 Acoustic Inversion Summary

Calibration of the East Victory seismic data with sonic logs was not a trivial process. The seismic data had to both retain original phase, frequency and amplitude content of the reflections under the line while revealing the complex structure of the Earth. The sonic data revealed that statistically relevant information could be extracted from impedance information and synthetic reflections from sonic data. Tying of the seismic data and sonic data from the East Victory line allowed inversions to be conducted on hard rock seismic data for the first time.

Mismatches exist between all statistically valid inversions but the resulting ore-zone predictions give definitive estimates for depth and breadth of known rock units, such as the Condenser dolerite, and high gold content ore zones. These prediction shows that gold-bearing ore zones can be characterized from the calibration of borehole analysis and seismic data. Estimates on ore zones using the inversions from Figure 5-9, Figure 5-10 and Figure 5-11 give a maximum horizontal gold zone of 60-100 metres and a depth of 250 metres. Definitive gold content, however, still remain ambiguous since there is no known direct gold indicator that can be extracted from the seismic data. Verification of these ore zone predictions requires further drilling and sonic logging to assess whether lithology and gold-bearing ore has been predicted by the acoustic inversions.

5.2 Elastic Inversion

Conventional multi-channel seismic data records oblique reflections influenced by concurrent mode conversion from compressional to shear waves (Savic et al., 2000) and incurred amplitude changes due to angle dependencies. AVO results from Figure 4-18, Figure 4-19, and Table 4.6 show amplitude differences with increased offset in borehole synthetic seismograms. Failure to attempt to calibrate offset seismic and offset impedances and negate these offset changes could result in significant miss-ties between borehole, seismic data, and inaccurate impedance predictions.

To facilitate elastic impedance inversion the East Victory seismic data was separately restacked based on near-offset, 0-600 meters and far-offset, 600-1200 meters. Figure 5-12 shows the final zero-offset (full stack), near-offset, and far-offset seismic images for comparison. Figure 5-13 shows the difference between the full stack and near-offset, full stack and far-offset, and near and far-offset. Results indicate that near-offset stacked migration sections closely resemble the shallow locations (above 200 ms) of the full stack migrated sections. The far-offset section appears to be similar to deeper sections (below 200 ms) of the full stack image with reflections appearing thicker. Amplitude differences between the far and near-offset reflections are highlighted as A – E on Figure 5-12 and Figure 5-13.

A 4 – 10 ms apparent increase in time is seen on far-offset reflections when compared to the near-offset reflections at the same locations. From AVO analysis of the sonic data, a larger amplitude increase in reflections was anticipated on far-offsets. The reflections at A, B and E, represent typical areas where rock type changes from softer rocks (mafics, intermediates) to harder rocks (dolerite and basalt). Sonic log AVO analysis showed an increase in amplitude changes between these rock types at far-offset. In some locations, the lateral differences in reflection position between near-offset and far-offset vary between 20 to 100 metres.

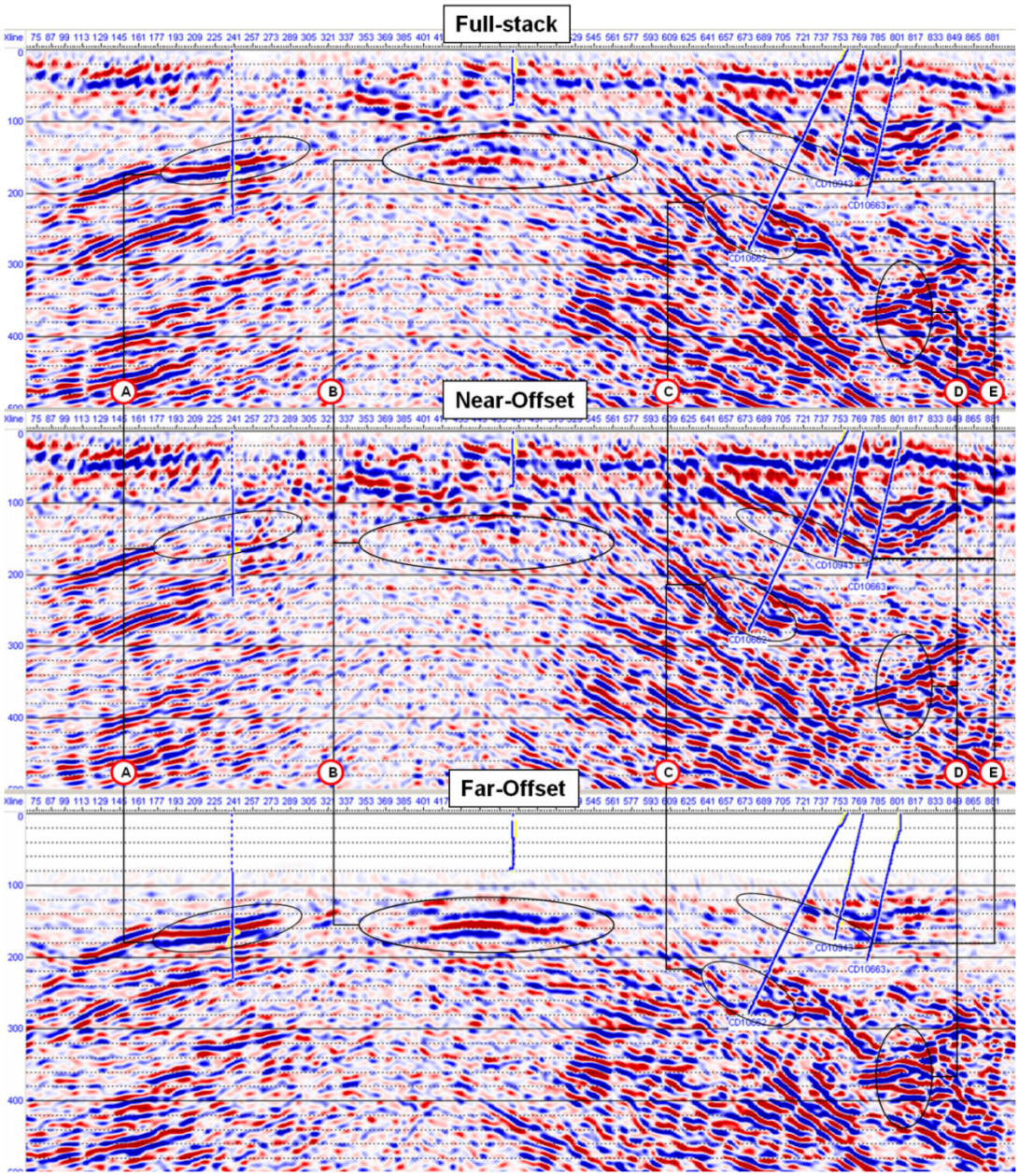

Figure 5-12. Full stack (top), near-offset (middle) and far-offset (bottom) East Victory seismic images.

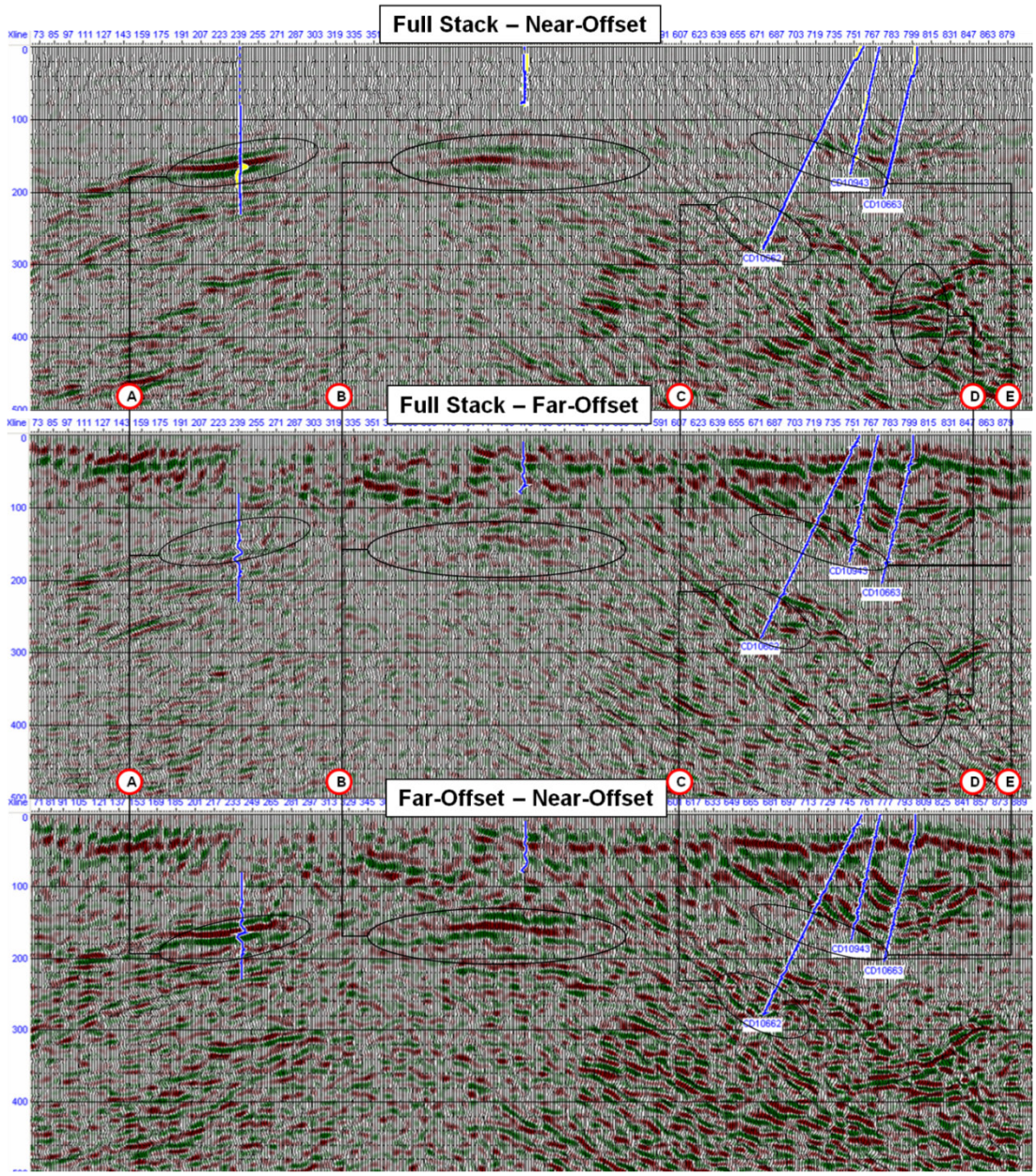

Figure 5-13. Differences between full-stack and near-offset (top), full-stack and far-offset (middle), and far-offset and near-offset (bottom).

Frequency analysis showed that the near-offset seismic image had a dominant frequency of 50 Hz while far-offset had a dominant frequency of 45 Hz. The frequency loss is evident in the reduction of reflection resolution on the far-offset seismic data. Again this shows the need for better velocities.

Figure 5-14 illustrates the two wavelets extracted along the three boreholes (CD10662, CD10943, and CD10663) on the eastern section of the seismic line. To maintain

consistent results, the parameters for the wavelets were kept similar to the wavelet used in the acoustic inversion (Figure 5-2).

Matching of synthetic reflection from boreholes with both near-offset and far-offset seismic reflections for elastic impedance inversion was carried out in the same manner as acoustic impedance. Figure 5-15 shows a sample of the matching from CD10662 on near-offset, far-offset, and full-stack seismic images. Matched rock contact interpretations had to be adjusted slightly to produce each model. In each case, instantaneous phase was used to aid in delineating the rock contacts in areas where signal-to-noise ratio was low. Figure 5-16 illustrates the near-offset and far-offset elastic impedance models respectively.

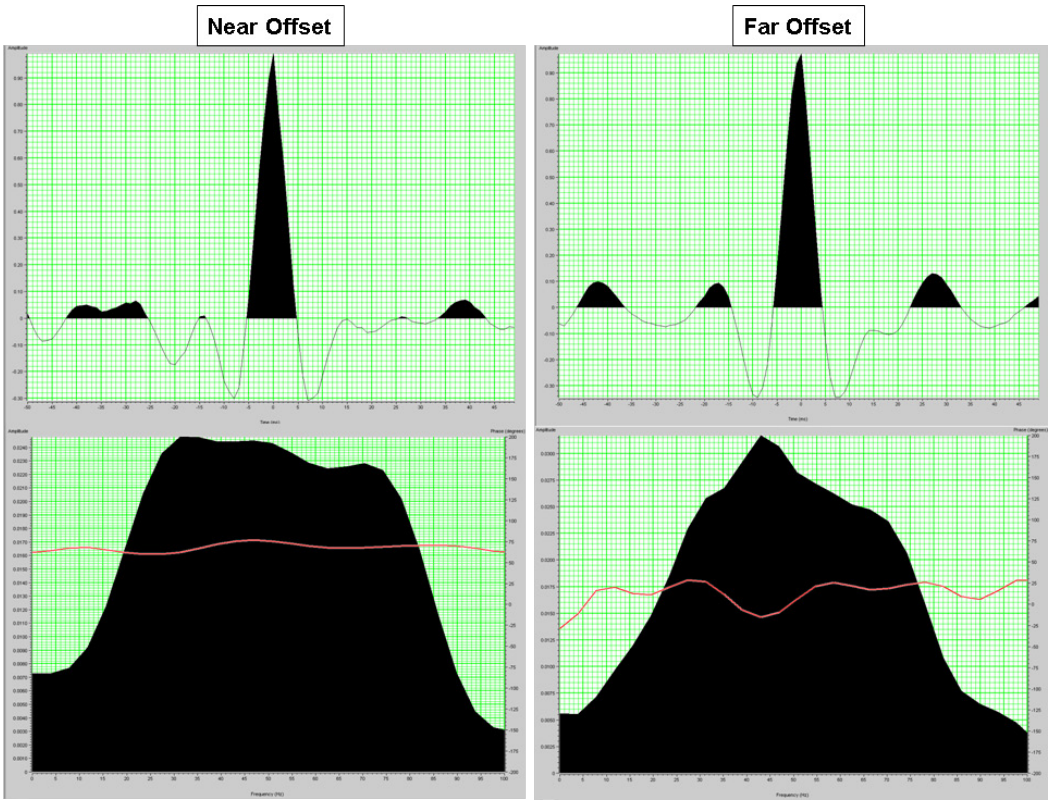

Figure 5-14. Wavelet extract (top) and the frequency spectrum (bottom) from the near-offset (left) and far-offset (right) seismic data. The red line is the phase spectrum.

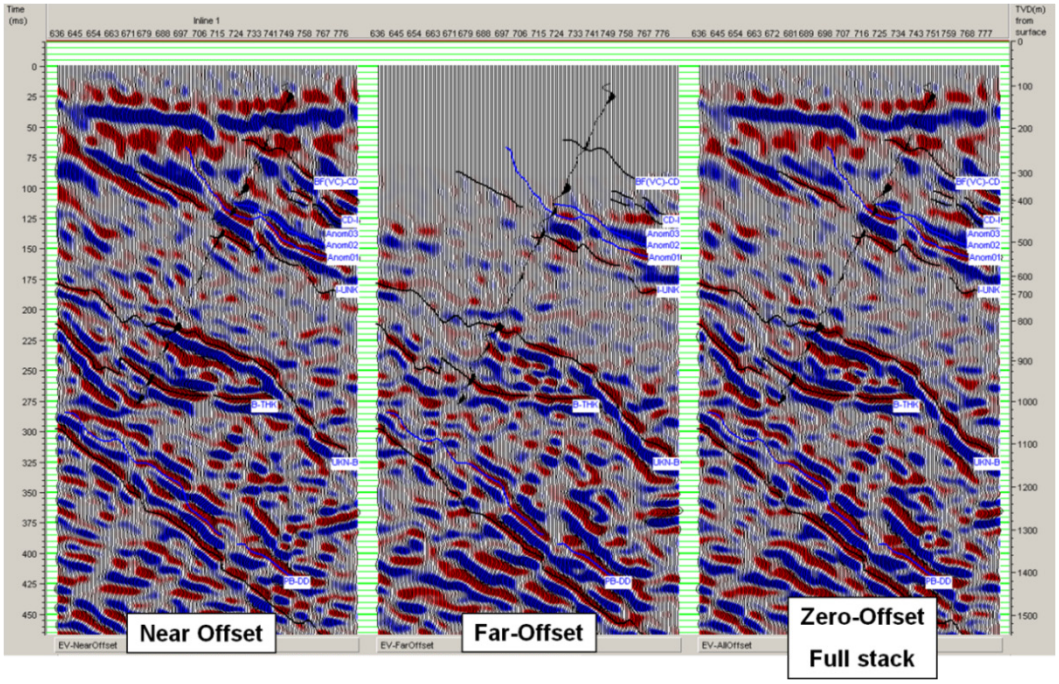

Figure 5-15. CD10662 matched on the near-offset (left), far-offset (middle) and full-stack (right) seismic image.

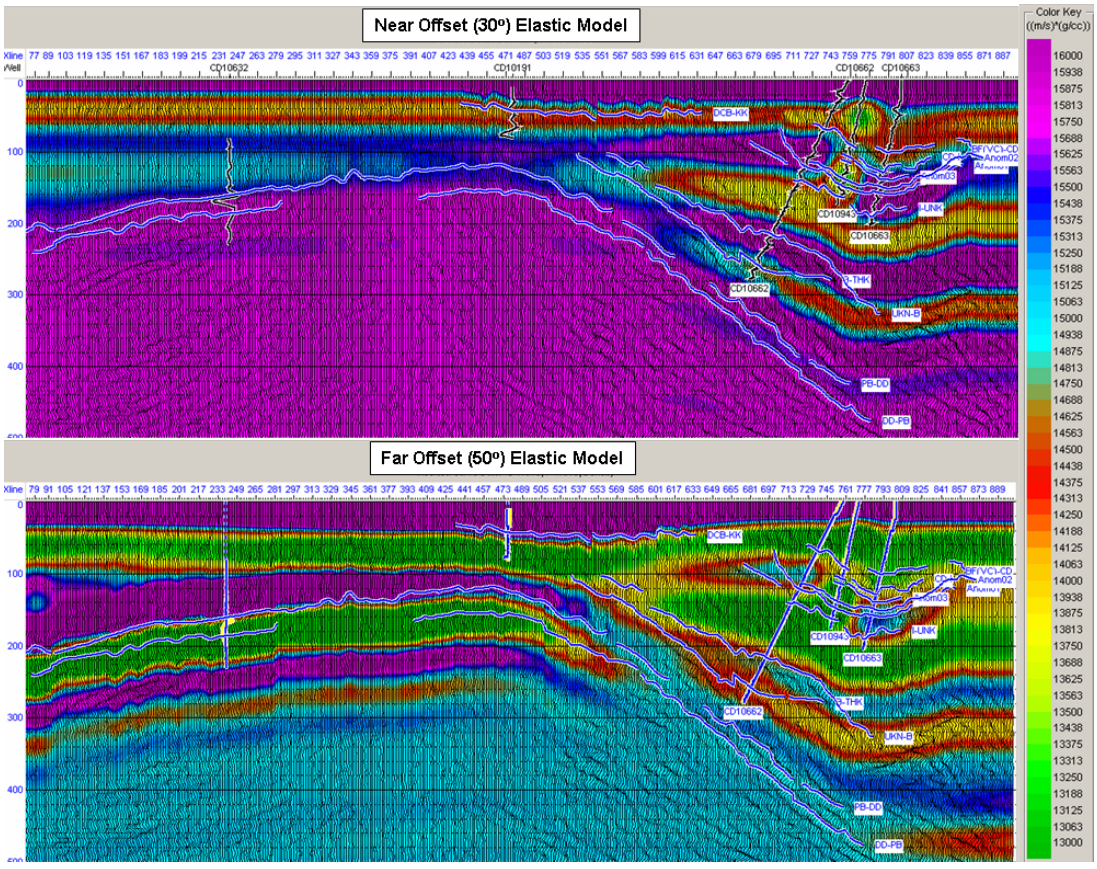

Figure 5-16. Elastic impedance model for the near-offset (top) and far-offset (bottom) seismic data.

5.2.1 Results and Analysis of Elastic Inversion

Only the eastern section of the East Victory seismic line was of interest for elastic inversion due to the number of boreholes available for error analysis. 18 inversions were calculated to asses which performed the best for the elastic seismic data. Figure 5-17 shows the correlations between borehole elastic impedances and inversion derived elastic impedances. The results indicate that the soft constraint biased model inversion, band-limited inversion, and sparse-spike maximum likelihood inversion gave the best overall cross-correlation between inversion and elastic log impedance. Borehole CD10191 consistently under perform on far-offsets due to its shallow depth.

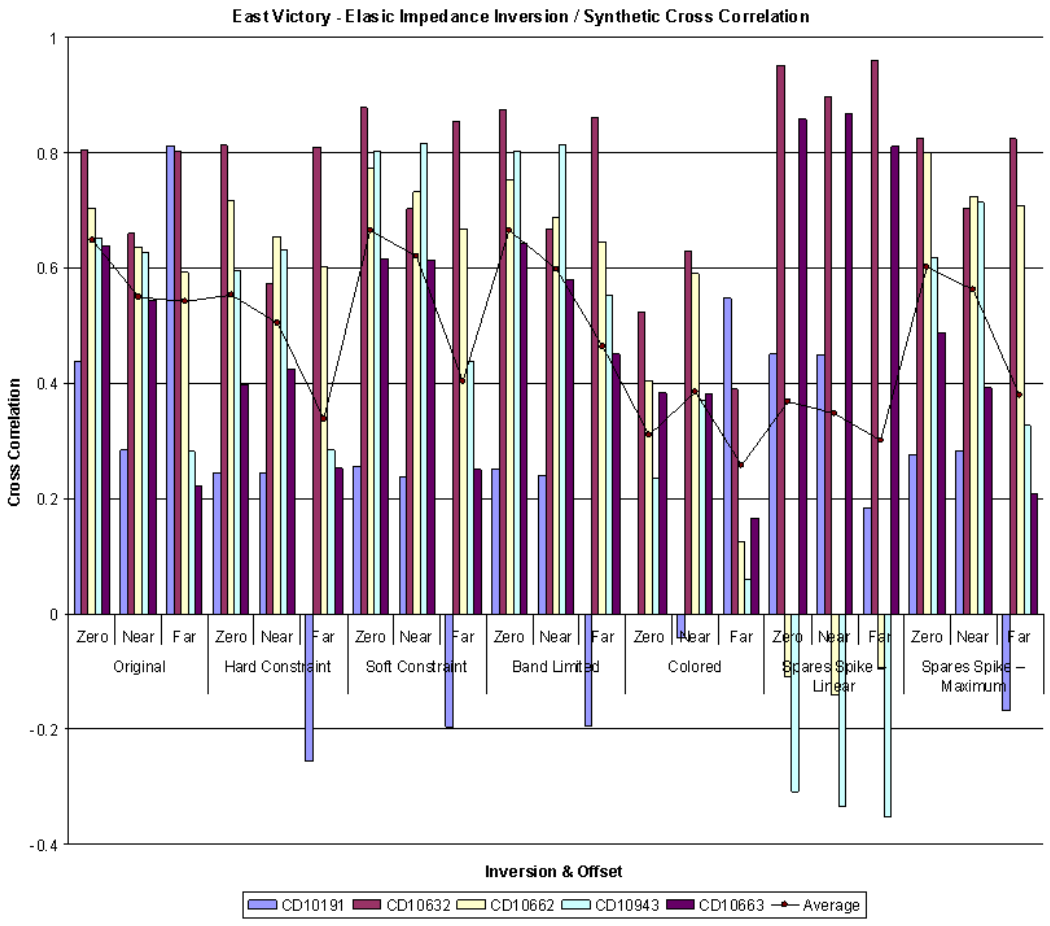

Figure 5-17. Graphed cross-correlation results for offset inversion verification. The black line connector indicates the average correlation between sets of inversions.

Figure 5-18 shows the results of each top performing inversion (Model (soft), Band-limited, and Sparse-spike) around boreholes CD10662, CD10663 and CD10943. A further seven elastic impedance models were generated utilizing hidden boreholes for further error analysis. 18 inversions were calculated with results of borehole hiding for inversion testing plotted in Figure 5-19. Results indicate that soft constraint biased model inversion and band-limited inversion have the overall best cross-correlation results and predictive ability for these data sets. Figure 5-20 and Figure 5-21 show the eastern end of these inversions.

Both the model based elastic inversion and the band-limited elastic inversion yield very good borehole tie results, however their impedance predictions differ greatly. Both near-offset and far-offset model inversions predict low impedance zones within the intermediate and volcaniclastic package on top the Condenser dolerite. These low impedance zone are not seen on either of the band-limited inversions. The appearance of band-limited inversion is considerably smoother than its model counterpart. This smoothing generalizes the larger volume of volcaniclastic and intermediate intrusive through the Condenser dolerite, but has eliminated almost any details in the Condenser dolerite itself.

High gold content zones are circled on each borehole on all inversion results. The abrupt impedance difference in the volcaniclastic package with intermediate intrusive in the Condenser dolerite are seen on all impedance predictions. These areas are associated with high gold content and potentially show a large body of gold-bearing ore. Due to no borehole control results below CD10662 are suspect.

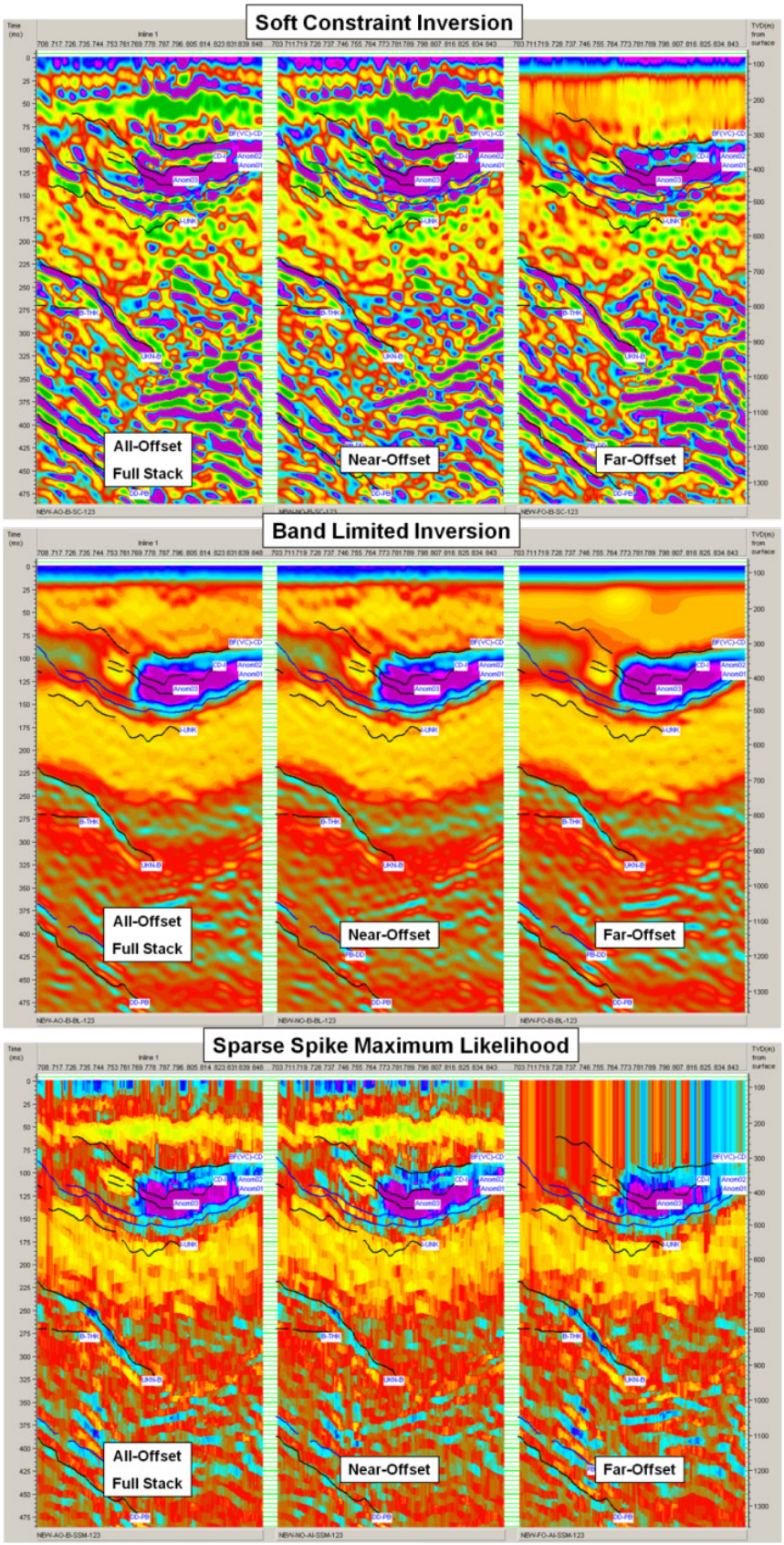

Figure 5-18. The soft constraint model inversion (top), band-limited inversion (middle) and sparse-spike maximum likelihood (bottom) for offset seismic on the East Victory line. All inversions are at the same scale.

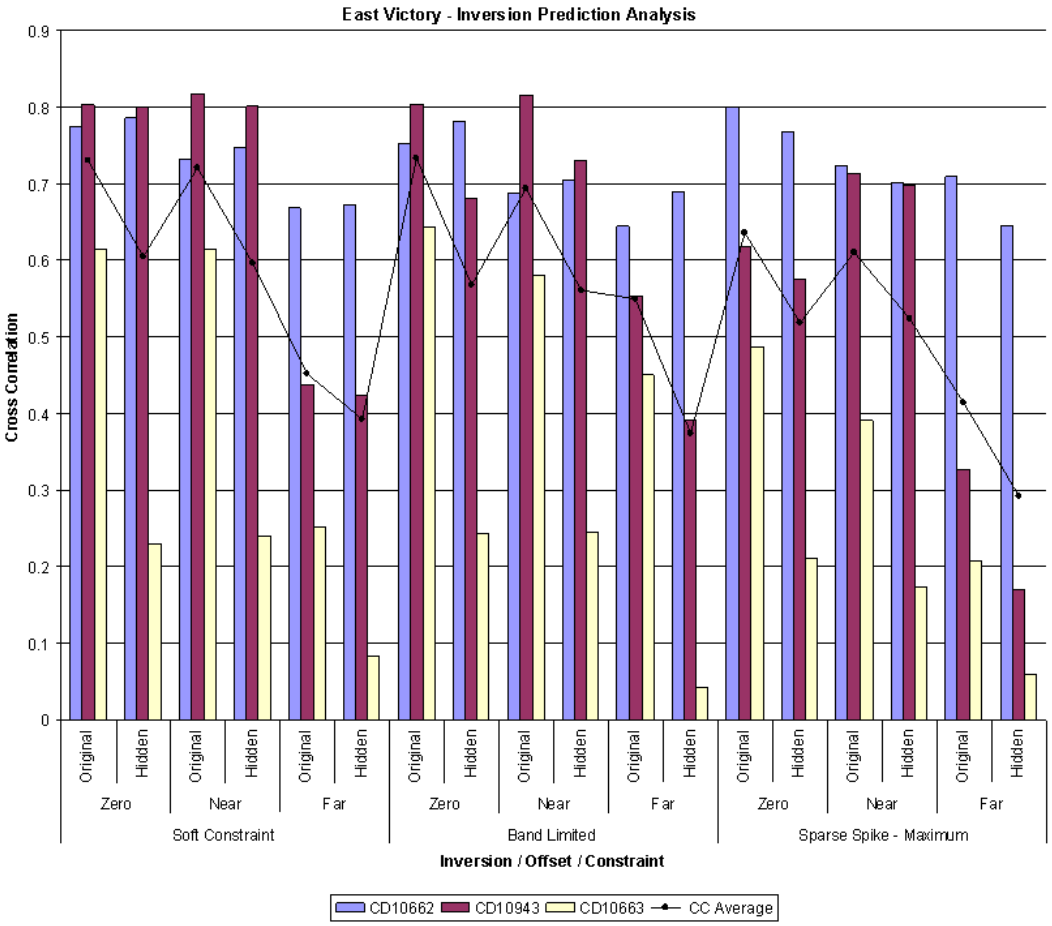

Figure 5-19. Graphed cross-correlation results for offset inversions and hidden borehole logs. The black line connector indicates the average correlation between sets of inversions.

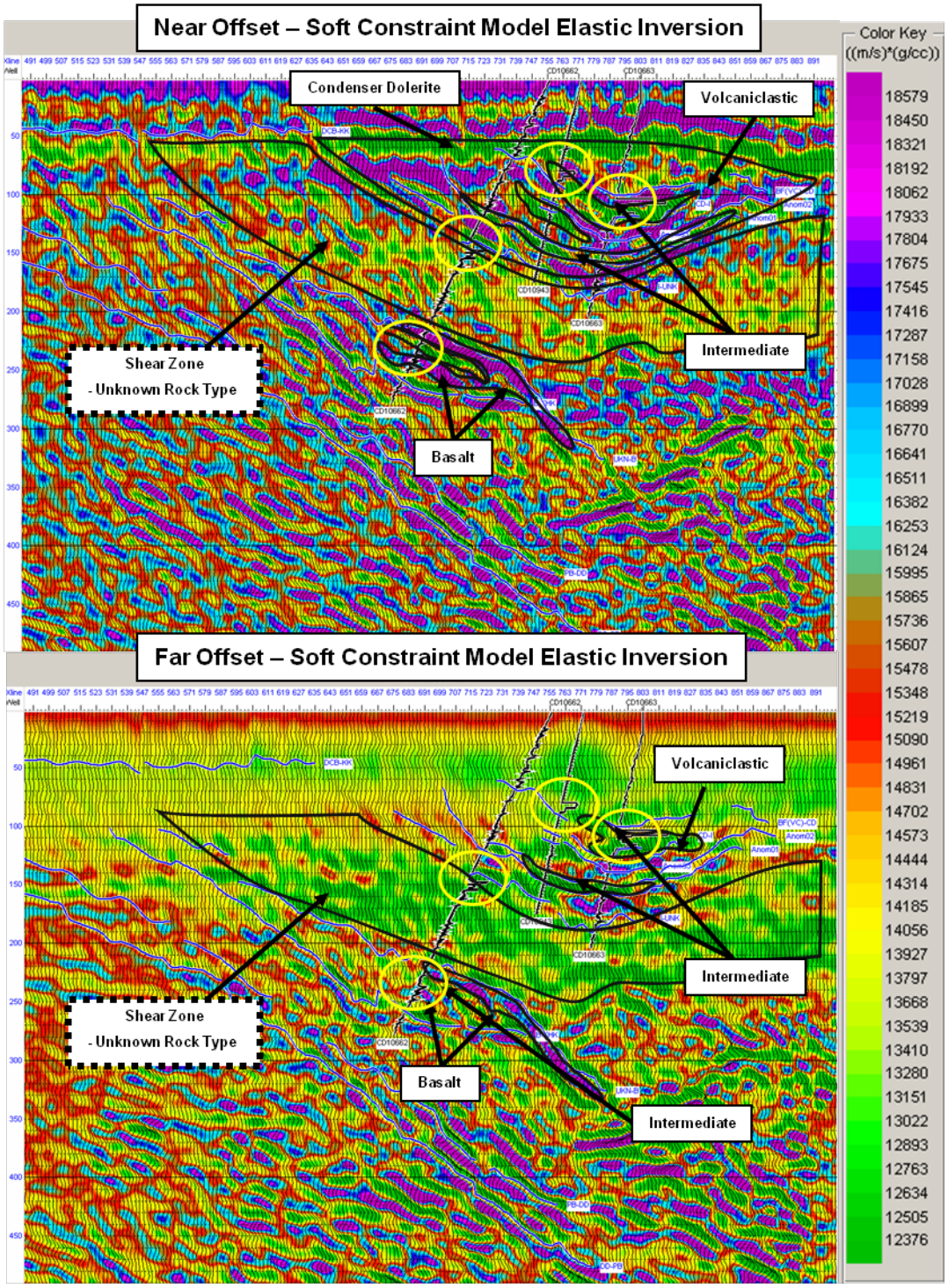

Figure 5-20. The soft constraint model inversion of both the near-offset (top) and far-offset (bottom) stacked and migrated seismic image. The yellow circles indicate where the high gold content is located.

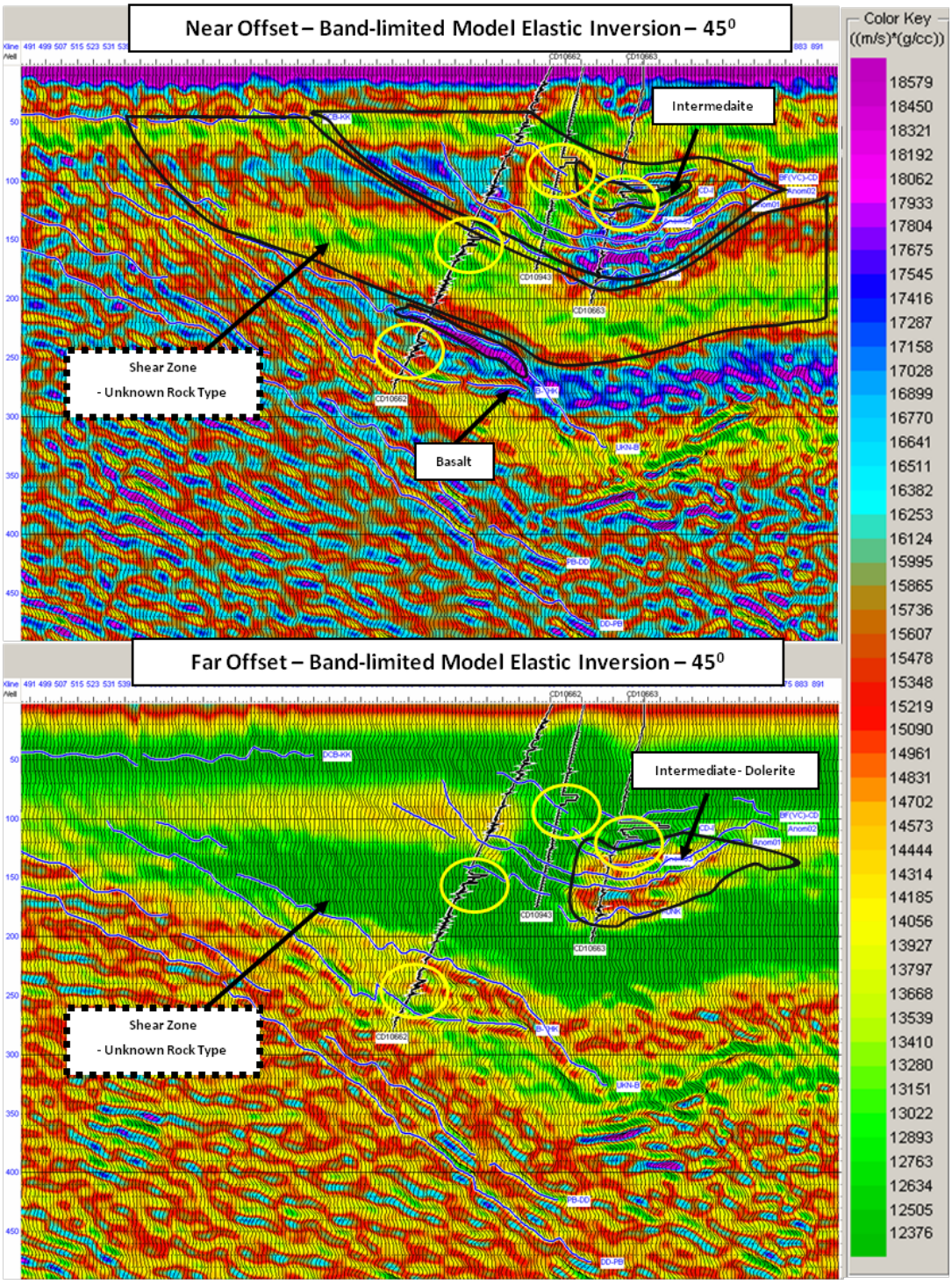

Figure 5-21. The band-limited inversion of both the near-offset (top) and far-offset (bottom) stacked and migrated seismic image. The yellow circles indicate where the high gold content is located.

Cross-plots were generated for both near and far-offset acoustic and elastic impedances from values extracted around each gold bearing zone. Blocking zones (Figure 5-22) were created based on acoustic impedance and elastic impedance of known gold ore zones found from Figure 4-14 and Figure 4-16. Band-limited near-offset and far-offset acoustic and elastic impedance as well as model inversion near-offset and far-offset acoustic and elastic impedance were used for cross plotting. Five zones were generated on each inversion image: Acoustic impedance range of known gold targets (orange), elastic range of known gold targets (red), the shared impedances zones of both acoustic and elastic ranges (yellow), lower impedance (light grey) and upper impedance (dark grey) zone. These high gold content zones were plotted on the seismic data in Figure 5-22.

Both model and band-limited offset impedance zoning indicate that acoustic impedance (orange) and areas with similar acoustic and elastic impedance (yellow) dominate the near-offset seismic image. Far-offset on both model and band-limited impedance zoning is dominated by elastic impedance (red). High impedance zones associated with basalt and dolerite (dark grey) helped delineate the Condenser dolerite and a high gold content intermediate intrusive. The cross-over point between acoustic and elastic impedance, which statistically represent the impedances values of high gold content rock, appears as yellow on both seismic images on Figure 5-23. These gold-bearing prediction results can be considered ambiguous except around boreholes where gold content can be referenced.

This simultaneous use of acoustic and elastic impedance shows a possible rock prediction capability than the separate acoustic or elastic impedance predictions by themselves. However, without further field tests and borehole sonic logs, results remain ambiguous.

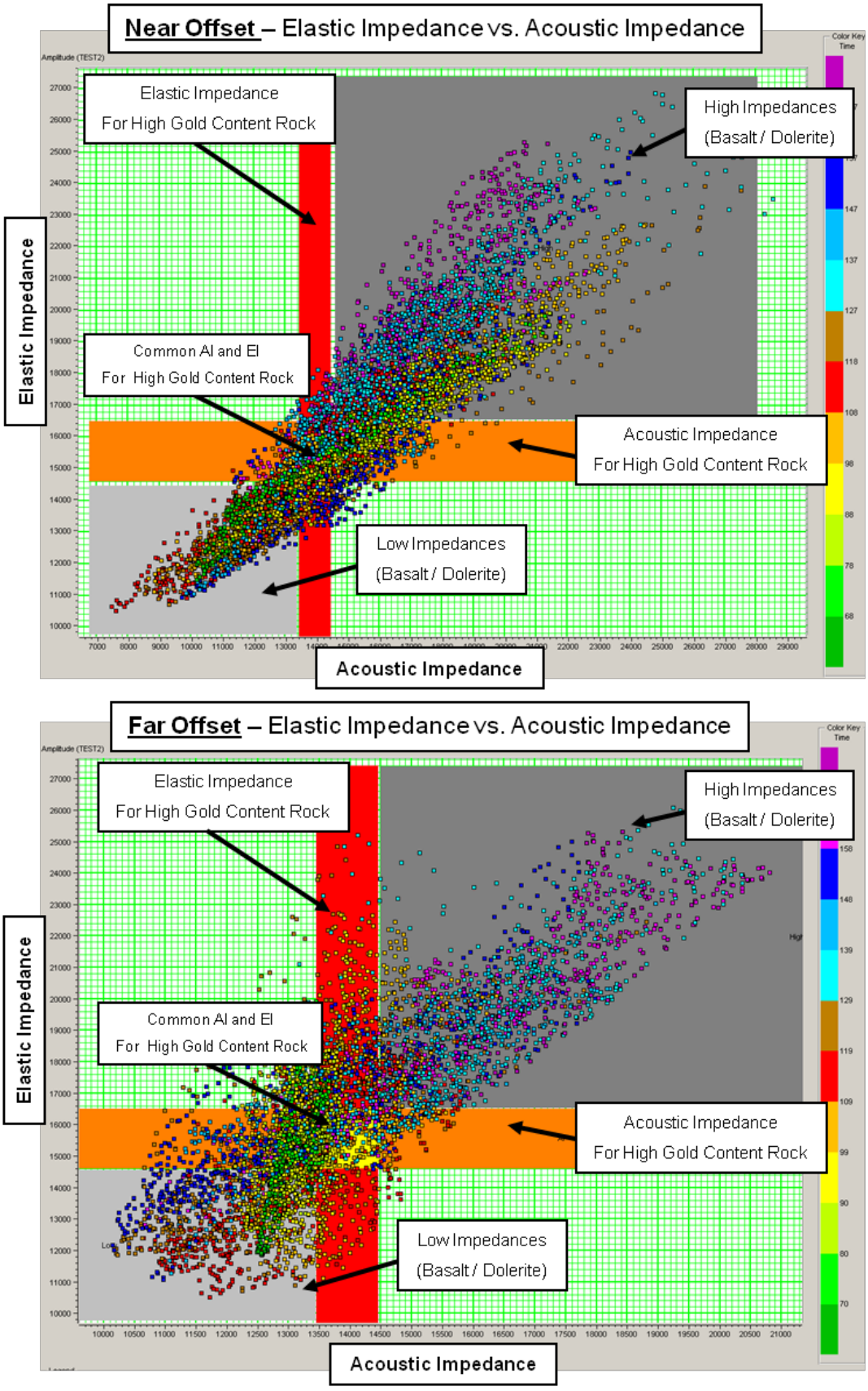

Figure 5-22. Cross-plotting and zoning of elastic versus acoustic impedance values for near-offset (top) and far-offset (bottom) band-limited inversions.

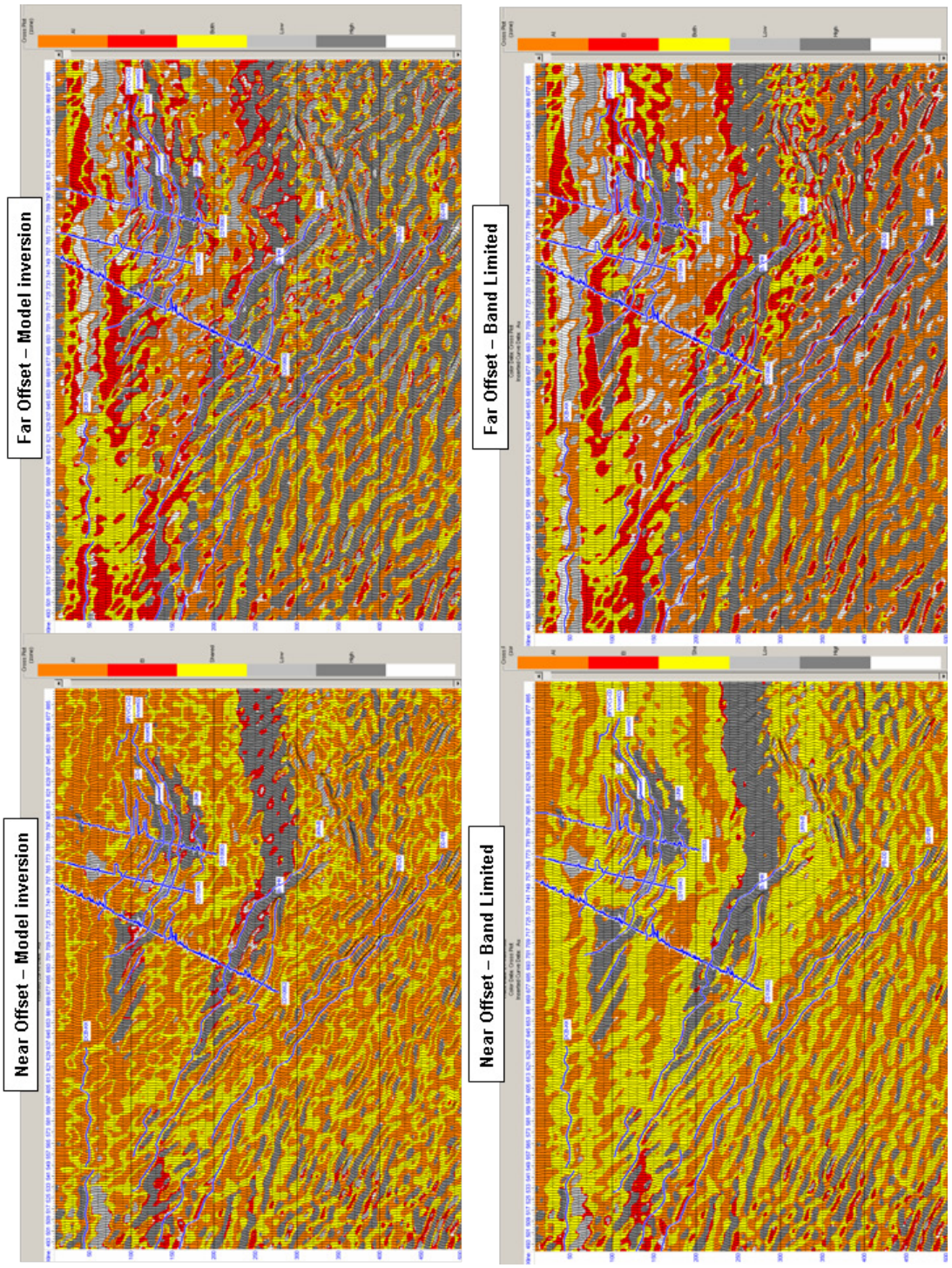

Figure 5-23. Plotting zoned cross-plot data for near and far-offset elastic and acoustic impedance prediction. Colours are based on cross plots seen in Figure 5-22. The red represents the elastic impedance dominated rock, orange represents the acoustic impedance dominated rock, light grey is low impedance dominated rock and dark grey is the high impedance dominated rock.

5.2.2 Lambda-Mu-Rho

Sonic log analysis showed that softer and harder rocks could be distinguished from each other using LMR elastic parameters. Converting the seismic data for LMR requires both P-wave and S-wave reflectivity for estimations. With no true S-wave seismic available, near-offset P-wave seismic data was substituted for LMR conversions. Figure 5-24 illustrates the Mu-Rho and the Lambda-Rho predictions for the East Victory seismic line. The Mu-Rho plot shows a vague outline of the Condenser dolerite, along with the volcaniclastic package, intermediate intrusive zones and basalt extensions. The Lambda-Rho plot does not resolve the Condenser dolerite, but images the softer high gold-content volcaniclastic and intermediate intrusive rock through borehole CD10663.

Cross-plotting and zoning of the volcaniclastic / intermediate gold-bearing rock and dolerite / basalt rock was conducted as seen on Figure 5-25. The lower incompressibility and lower rigidity of the volcaniclastics and intermediate intrusive, and the higher incompressibility and higher rigidity of the basalts were zoned on the cross plot. The zone values were plotted on the East Victory seismic line to observe predicted LMR values (Figure 5-25). The sparse borehole data and the fact that P-wave offset data was substituted for S-wave data limits any further investigation to give qualitative analysis for suggested drilling sites. Combined with other inversion techniques, LMR could find a place in hard rock exploration

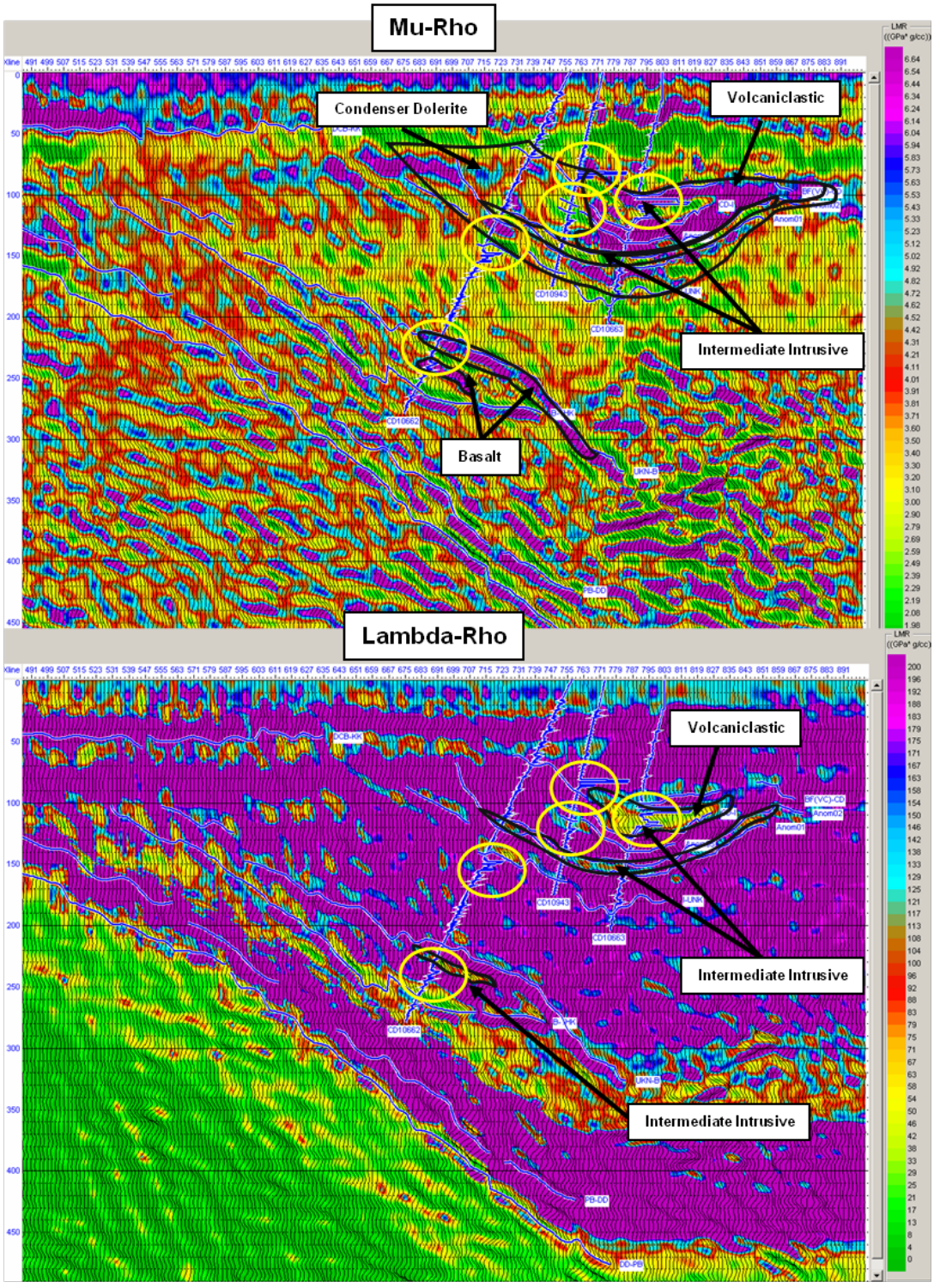

Figure 5-24. The Mu-Rho (top) and Lambda-Rho (bottom) predictions through the East Victory seismic data.

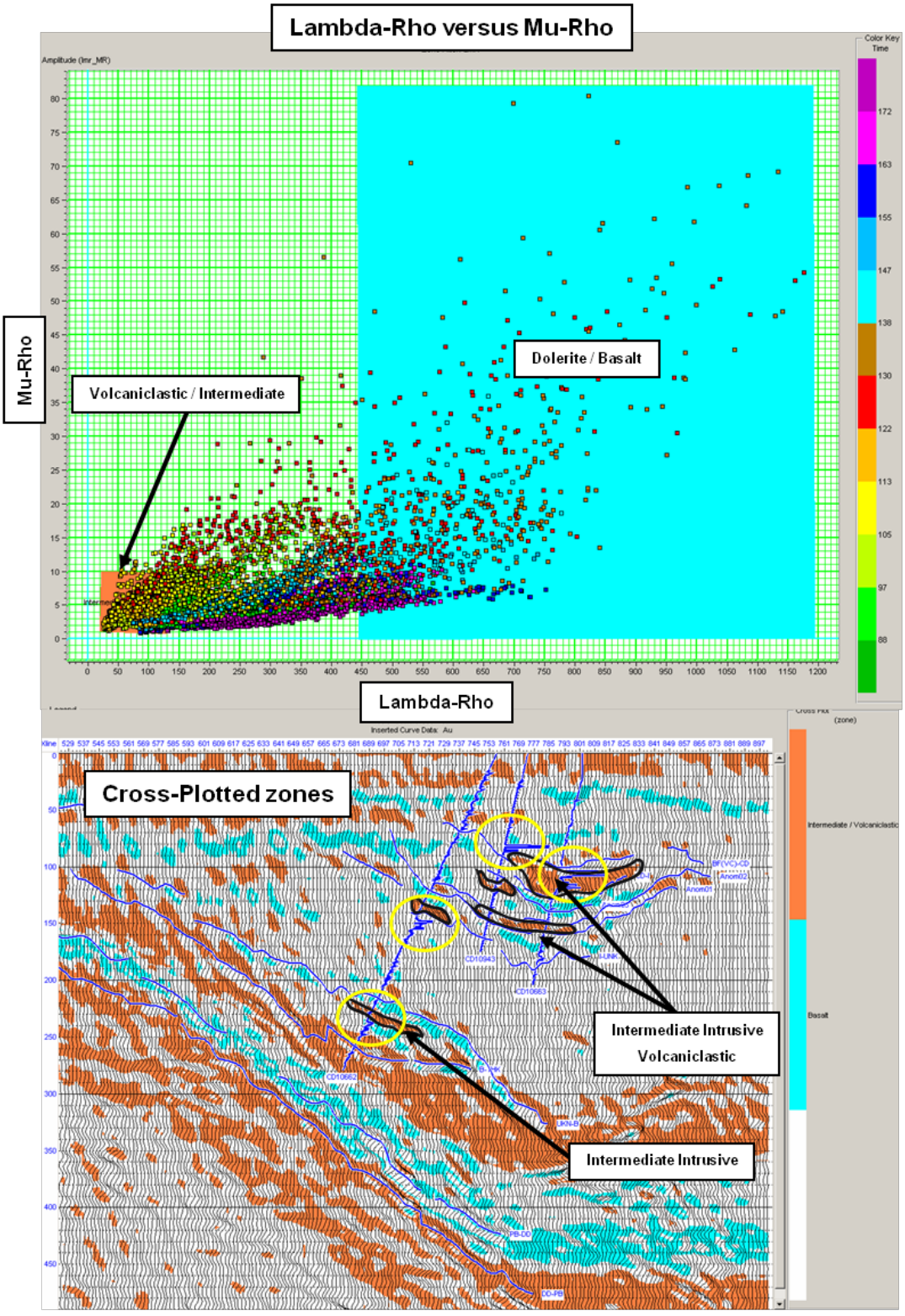

Figure 5-25. The cross plot of Lambda-Rho versus Mu-Rho of the gold bearing volcaniclastic intermediate package.

5.2.3 Elastic Inversion Summary

Near-offset and far-offset stacked seismic images have revealed differing reflections on the East Victory seismic line. Comparison of results have indicated that near-offset seismic images show more detail on shallow reflection while far-offset reveal deeper less complex reflection detail. Sonic data showed definitive separation between softer and harder rocks based both on statistical rock characteristics and offset reflection calculations. Calibration of the elastic sonic data to the seismic data provided a basis for inversion predictions. Inversion prediction results have been quite promising showing softer and harder rock differentiation based on near-offset and far-offset data sets. Near-offset stacked images and inversions revealed more detailed predictions at shallower target zones which would be of economic interest for mineral exploration. Far-offset data had an overall loss of frequency content reducing the reliability of far-offset data to image thin beds. LRM both from sonic data and calibrated seismic data showed interesting promise for future investigation, but inconclusive for reliable ore zone separation.

Overall, these techniques are new to hard rock environment and have shown themselves to have significant potential. Volumetric prediction for ore zone targeting, mineral content predictions and prospect mineral analysis can easily be completed with more data sets for analysis.

5.3 Multiattribute Inversion

Hydrocarbon exploration has utilized statistical connections between physical rock properties and seismic attributes to help predict lithology and conduct reservoir characterization. Analogous uses or attribute analysis in hard rock environments would include lithological predictions, structure identification, and possible prediction of gold content. Quantifying a geostatistical relationship(s) between hard rock properties and hard rock seismic data is difficult due to the inherent low signal-to-noise ratio, and poor reflection alignment of the seismic data. Rigorous analysis of the data sets was required to assess the validity of attribute analysis in this hard rock environment.

Harrison et al. (2007) used instantaneous phase as a rock type contact indicator in hard rock environments. As shown in sections 5.1.1 (Results and Analysis of Acoustic Inversion) above, instantaneous phase was used to delineate rock contacts in areas where

low signal-to-noise ratio make rock contact picking difficult. Amplitude envelope and instantaneous frequency were generated for the East Victory seismic data, but did not at the outset prove to be visually or statistically useful by themselves. Specific software was required to take advantage of the possibilities geostatistical analysis as for hard rock seismic and sonic data. Even then, it has been suggested by Russell (1999) that attribute analysis require twice as many sonic logs than inversion for a prediction base. The lack of sonic data for calibration, low signal-to-noise ratio, and complex structure within the East Victory seismic data set makes attribute analysis in this hard rock environment extremely challenging.

5.3.1 P-wave Predictions

Due to consistent sonic velocities through all rocks in Table 4.4, P-wave velocity was chosen as the first log property for attribute analysis testing. Similarly to inversions, attribute analysis was limited to the area surrounding CD10662, CD10633 and CD10943 on the eastern section of the seismic line to allow for successful borehole "hiding" for error analysis. Both user-chosen attributes and software-defined attributes were generated to compare results. User-defined attributes were based on Brown's (2006) criteria for attribute selection:

- Attributes have to be unique yet simple,
- Attributes have to have clear and useful meanings, and
- Attributes must not vary greatly in response to small data changes.

With seismic attribute analysis being new to hard rock environments, amplitude envelope and instantaneous frequency were initially considered for the user-defined analysis. Non linear transforms were used to maximize analysis results for these attributes. Figure 5-26 shows the results of attribute analysis for amplitude envelope, instantaneous frequency and the two combined. Correlations results were fairly low (>0.24) on all user attributes analysed.

Validation error results are acquired through "hidden" borehole logs cross-correlated against non-hidden logs shown on Figure 5-27. Increase in validation error and lower cross-correlation suggest that only amplitude envelope is useful for researcher defined attribute analysis. Software determined attribute analysis, however, returned much better statistical results as shown below.

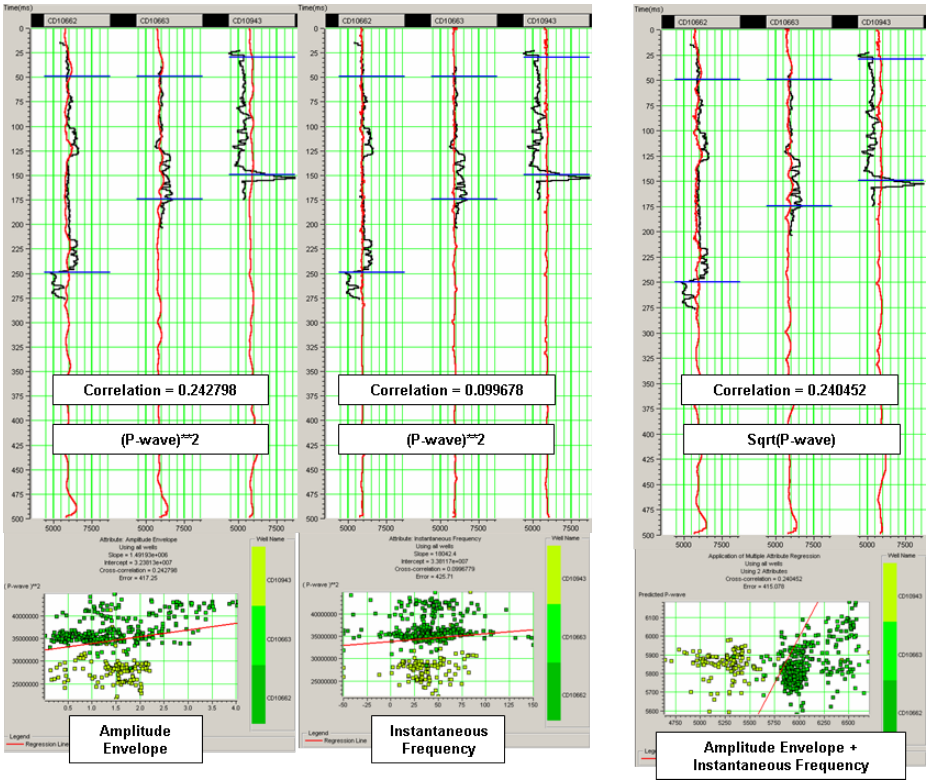

Figure 5-26. Single (left and middle) and multi attribute analysis (right) for user chosen amplitude envelope and instantaneous frequency. Black lines are log values, and red line are predicted values.

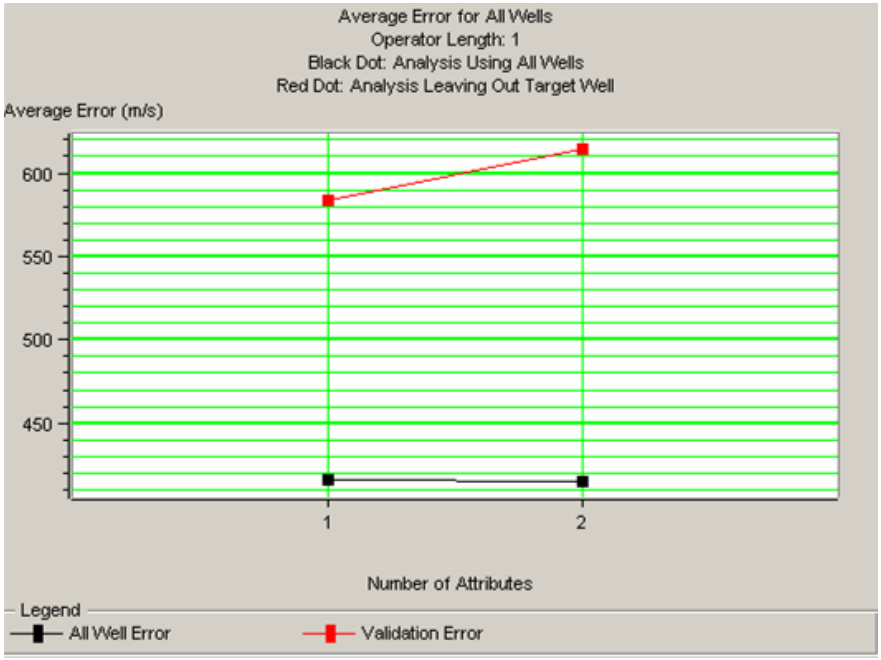

Figure 5-27. The validation error plot for two attribute user defined analysis of amplitude envelope and instantaneous frequency.

A maximum of seven random attributes with the highest correlations from a list of 24, were input for the software attribute analysis. Table 5-1 shows the resulting attributes calculated for best cross correlation while Figure 5-28 shows the validation error plot for the best number of attributes to use. Figure 5-29 provides a visual representation of what each of the chosen attributes appears like next to the P-wave and seismic data where it can be seen how closely attributes resemble the P-wave log. Figure 5-30 shows the multi-attribute prediction for 6 attributes resulting in a correlation of 0.64 and 7 attributes resulting in a correlation of 0.65. While the correlation is higher in the 7 attribute case, the validation error indicates that a maximum number of 6 attributes will result in the best possible correlation for the three borehole logs.

	Target	Final Attribute	Training Error	Validation Error
1	Sqrt(P-wave)	Average Frequency	406.284066	816.483955
2	Sqrt(P-wave)	Integrated Absolute Amplitude	352.400148	727.420430
3	Sqrt(P-wave)	Quadrature Trace	341.914098	724.846916
4	Sqrt(P-wave)	Apparent Polarity	333.824005	697.907481
5	Sqrt(P-wave)	Dominant Frequency	328.566696	692.797914
6	Sqrt(P-wave)	Amplitude Weighted Frequency	326.456707	676.119213
7	Sqrt(P-wave)	Amplitude Envelope	322.847482	695.225374

Table 5-1. Software calculated attributes (red box) for multi-attribute analysis of P-wave prediction.

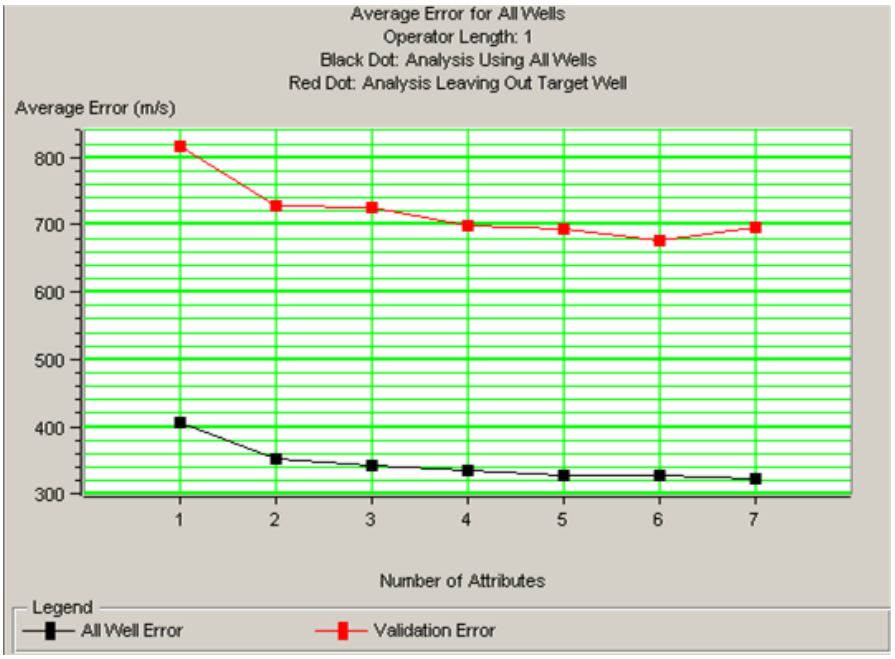

Figure 5-28. Validation error for software calculated results for multi-attribute analysis of P-wave prediction.

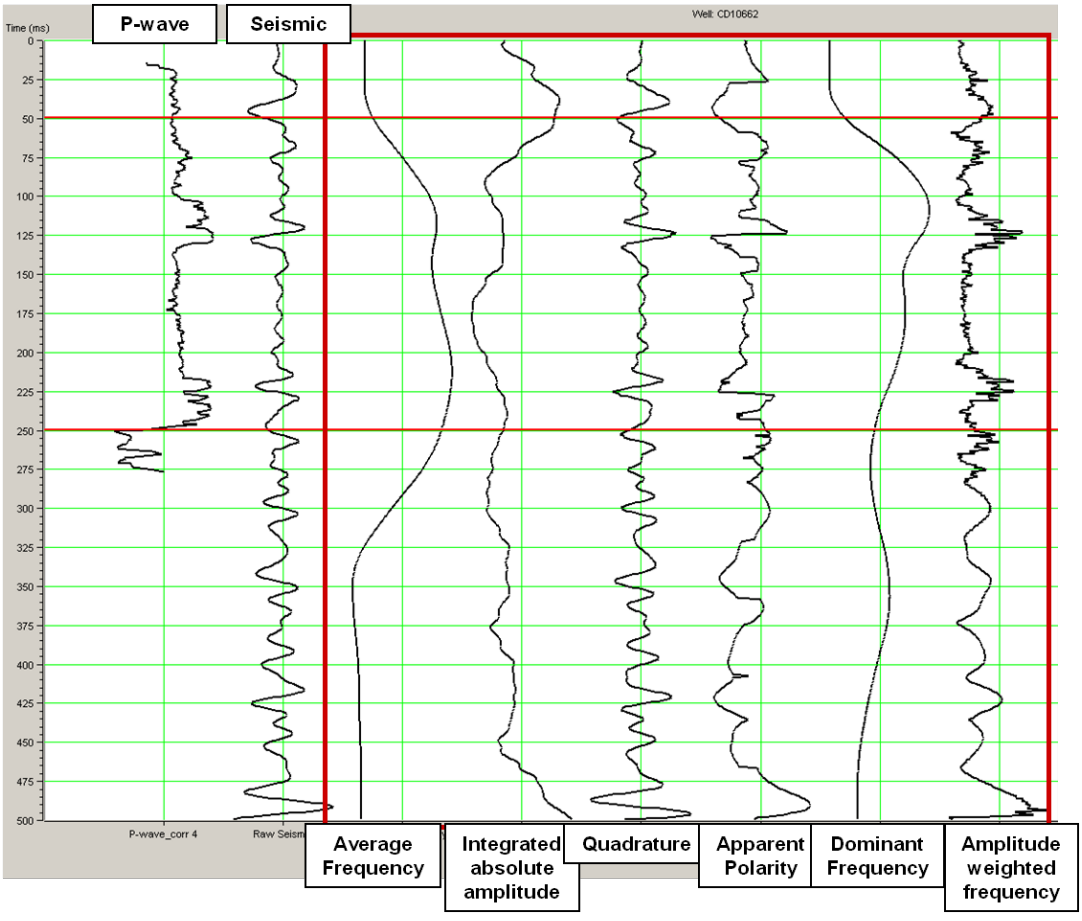

Figure 5-29. P-wave log (far left) and seismic (second from left) for CD10662, all attributes listed in Table 4.8 The red box indicates which attributes were used for the prediction.

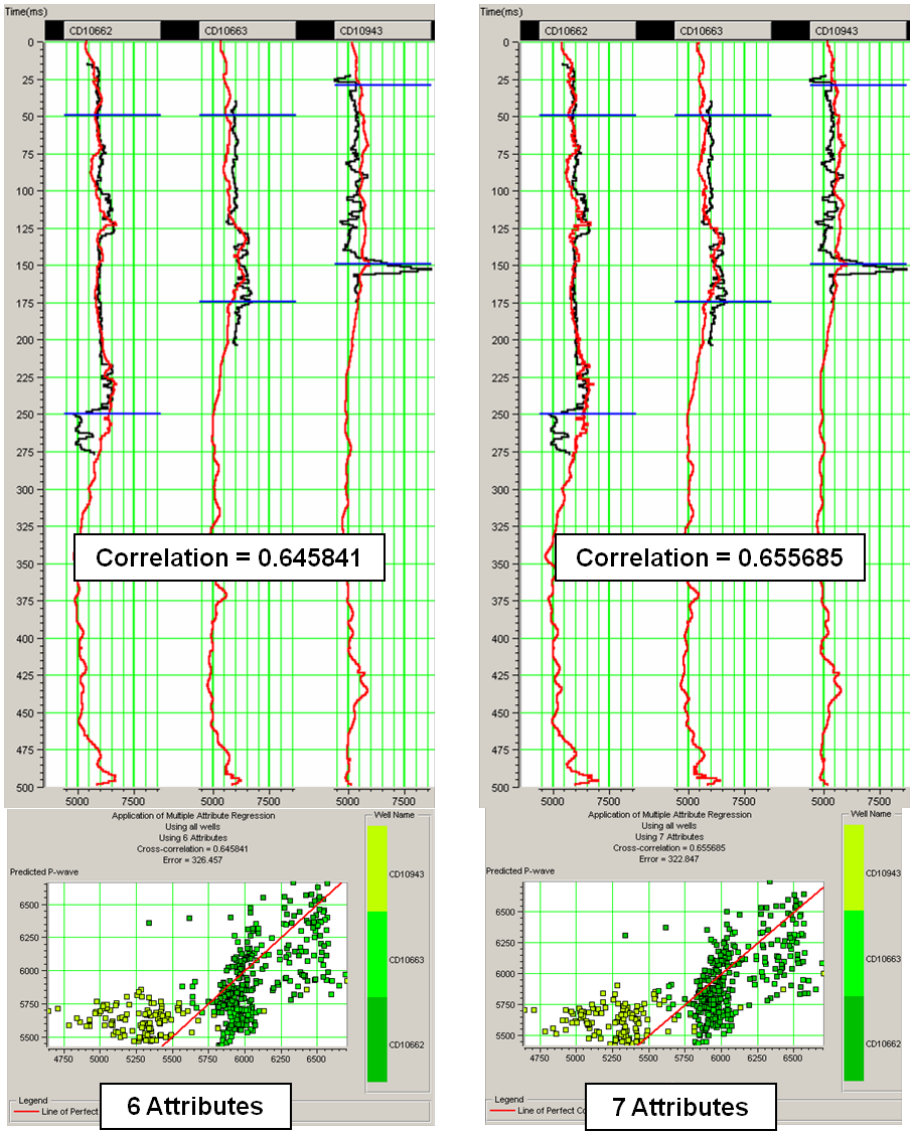

Figure 5-30. Multi-attribute analysis using software defined 6 and 7 attributes. Black lines are log values, red lines are predicted P-wave values.

Both user-defined and software optimized selection of attributes were used to train separate neural networks to generate P-wave predictions throughout the seismic data (Figure 5-31). Both approaches delineate the Condenser dolerite as a high velocity zone, and the major shear zone on the flanks of the St. Ives anticline as a lower velocity. The velocity predictions for the user-defined attribute case are roughly at proper magnitude between 5500 and 6000 m/s. The software-prediction of 6 attribute case's velocity values, however, are 500 m/s less than desired. This lower velocity prediction is most likely due to over-training and over- smoothing of the correlated data. The volcaniclastic/intermediate package seen on the zero-offset inversions (Figure 5-9, Figure 5-10, Figure 5-11, Figure 5-18, and Figure 5-20) related to high gold content is barely observable on both user

defined and software defined attribute predictions (Figure 5-31). Without foreknowledge from previous seismic inversions, the volcaniclastic/intermediate package could not be differentiated from the Condenser dolerite. However the shear zone that flanks the St. Ives anticline has been predicted well as middle to low velocity zones on both plots on Figure 5-31.

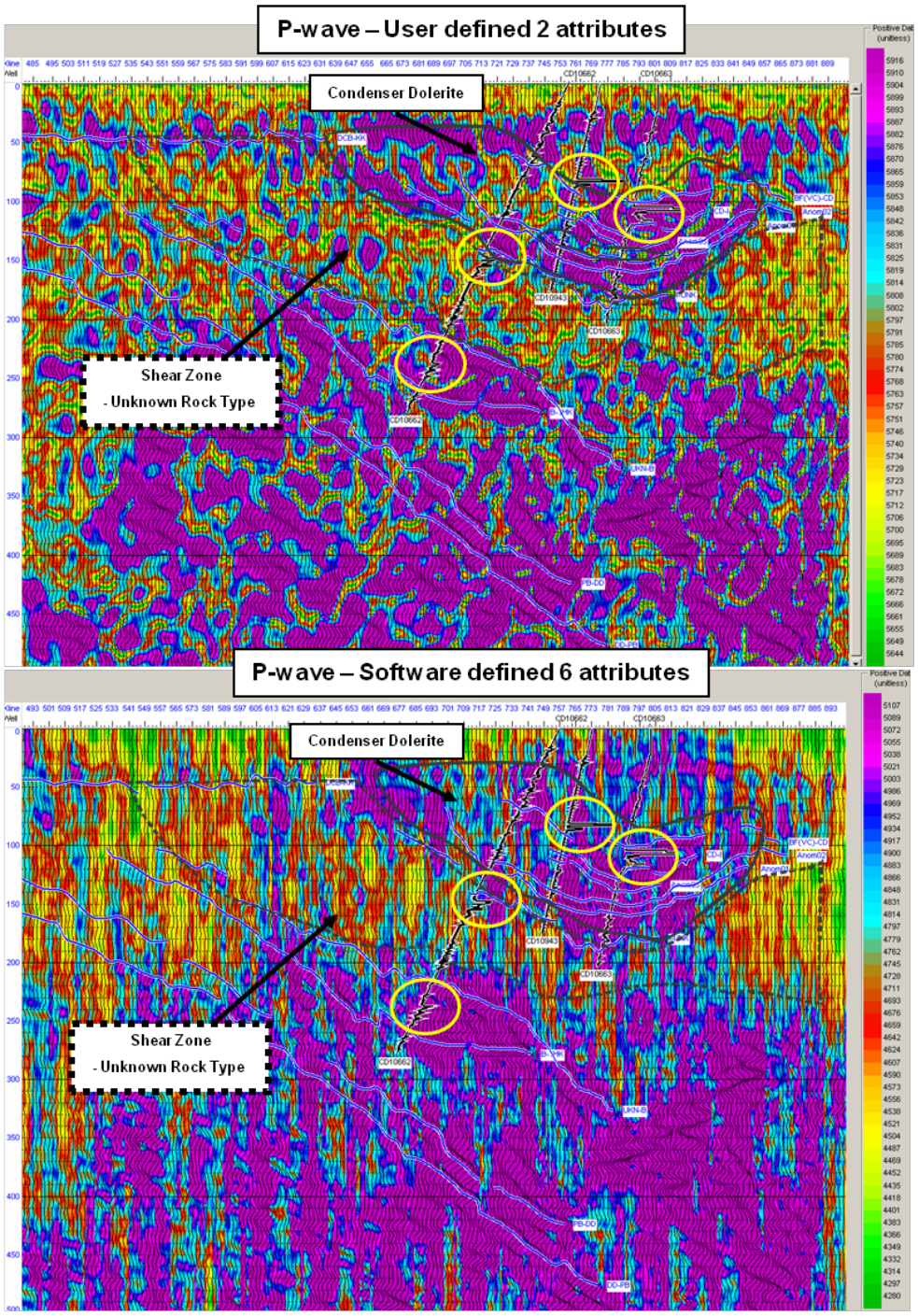

Figure 5-31. P-wave predictions using 2 attributes defined by the user (top) and 6 attributes computed by the software (bottom). High gold zones on the boreholes are indicated by yellow circles.

5.3.2 P-wave Seismic Attribute Predictions with Partial Offset Stacks

Both near-offset and far-offset East Victory seismic images were used for a second round of attribute analysis to investigate possible offset dependence. Results of multi-attribute regression using offset values are shown on Figure 5-32 for near-offset and Figure 5-33 for far-offset. In both near-offset and far-offset cases validation error showed two attributes with resulting correlations of 0.563708 for near-offset and 0.409743 for far-offset. P-wave predictions for both near-offset and far-offset images are shown on Figure 5-34. The Condenser dolerite and the shear zone on the flanks of the St. Ives anticline are imaged well on both P-wave predictions. Near-offset results show the low velocity volcaniclastic / intermediate intrusive located above the high velocity Condenser dolerite. This volcaniclastic / intermediate intrusive package is predicted on several seismic inversions and is associated with a high gold rock contact on CD10663. This high gold content zone, however, is not predicted very well on the far-offset image. As was the case with far-offset seismic inversions, shallow reflections were not focused well, if at all, making near-offset images more useful for shallow lithology predictions. More borehole data were needed for further refinement of the results.

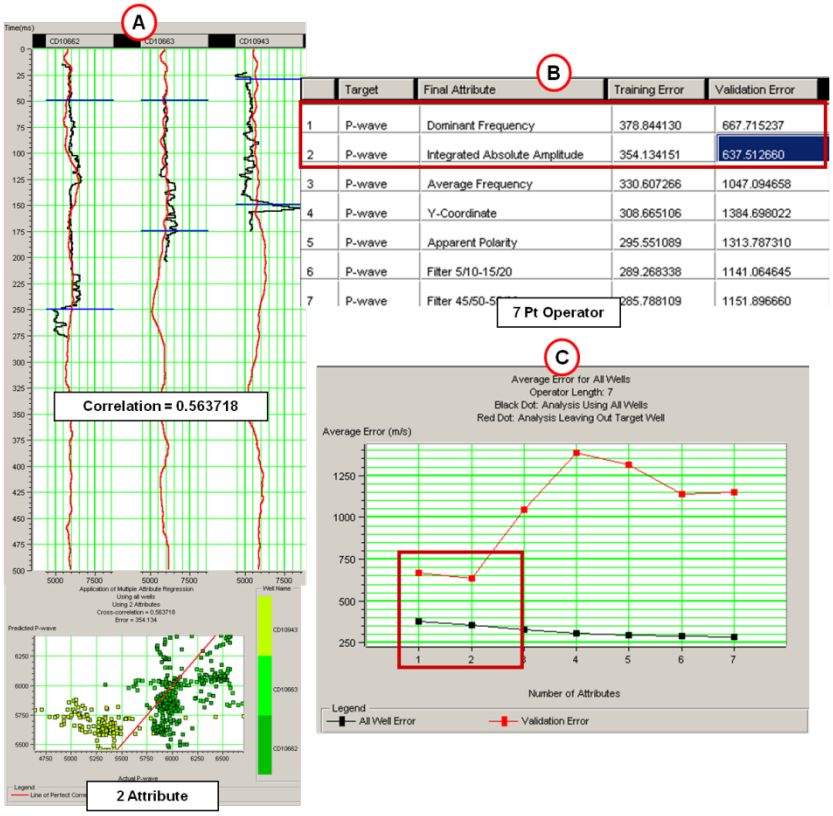

Figure 5-32 Near-offset multi-attribute analysis of P-wave prediction utilizing near-offset seismic. Correlation values (A), attributes utilized (B) and validation error (C) are shown.

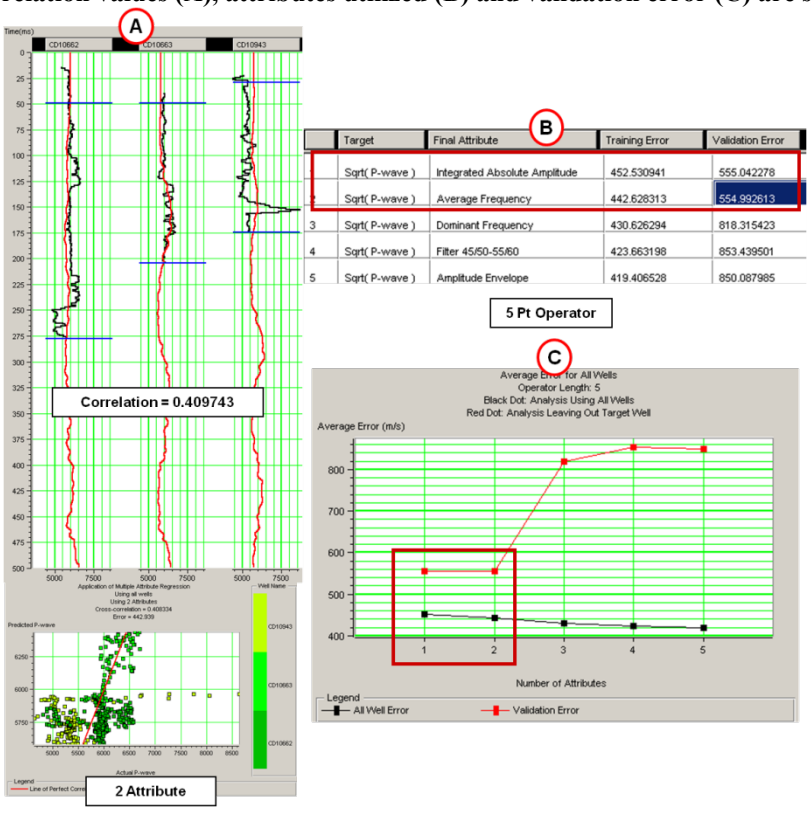

Figure 5-33. Far-offset multi-attribute analysis of P-wave prediction utilizing far-offset seismic. Correlation values (A), attributes utilized (B) and validation error (C) are shown.

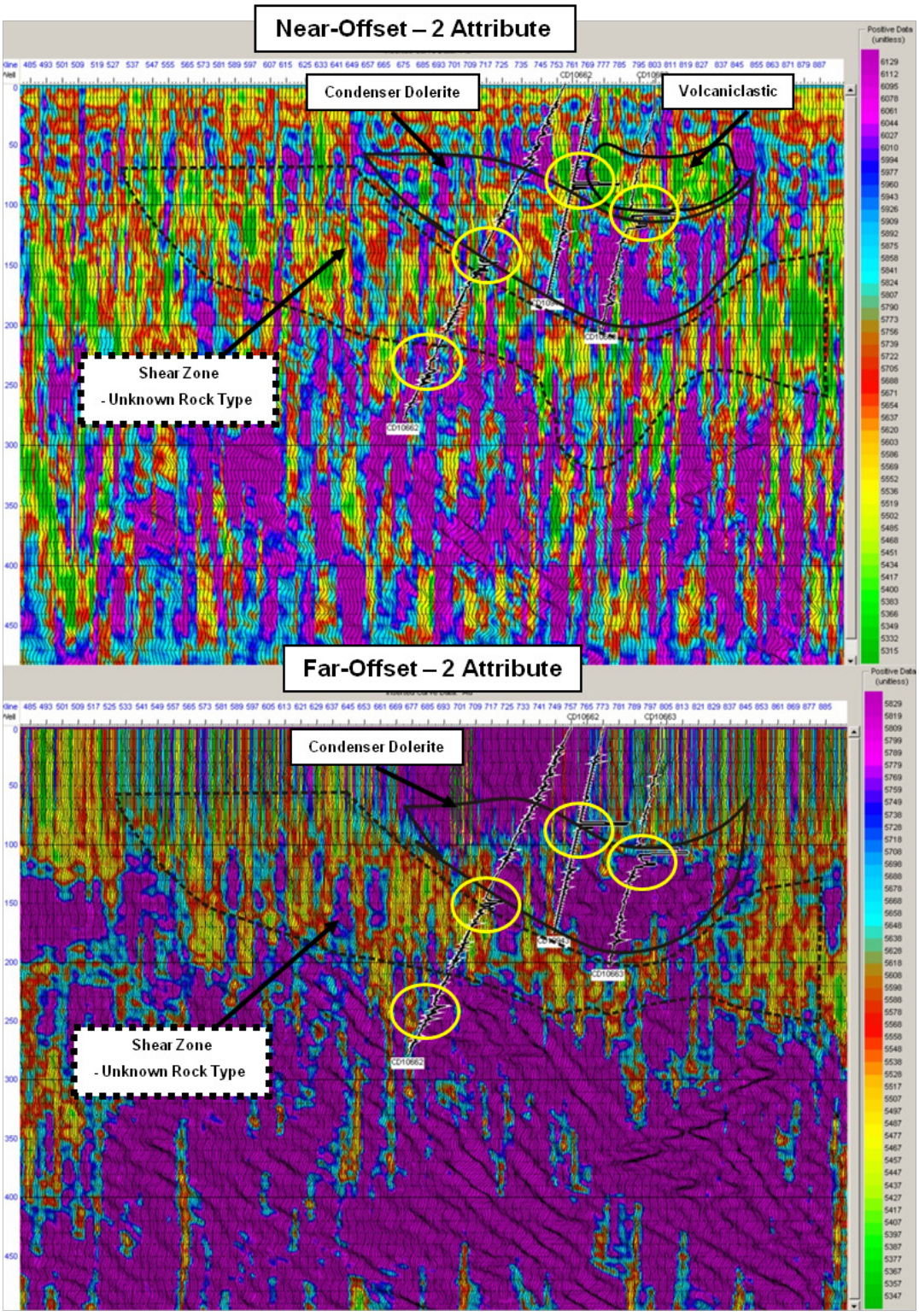

Figure 5-34. The P-wave prediction for near-offset (top) and far-offset (bottom) seismic images.

5.3.3 P-wave Prediction Including Inversion Results

To achieve better validation error in the P-wave multi-attribute prediction, top performing inversion results were included in the last set of compression wave analysis. Inclusion of inversion for attribute analysis is a common practice in hydrocarbon exploration to improve analysis results. However as pointed out by Barnes (2006), when reusing predicted results such as inversions for prediction on the same dataset, an increased correlation is bound to occur. Figure 5-35 illustrates the results of applying the neural network training to the seismic data. Indeed resulting P-wave velocity predictions are within the range of 5300 – 6200 m/s, which agree with core results and log data.

While the correlation differences between the inclusion (0.657821) and non-inclusion (0.64581) of acoustic impedance was small (Figure 5-30), the resulting P-wave prediction using acoustic impedance was far easier to interpret (Figure 5-35). The low velocity volcaniclastic above the Condenser dolerite has roughly the same dimensions as the inversions seen in Figure 4-31, Figure 4-32 and Figure 4-33. However, the major shear-zone on the flank of the St. Ives anticline is not as well defined. The lower basalt layers seen on CD10662 have also been predicted quite well.

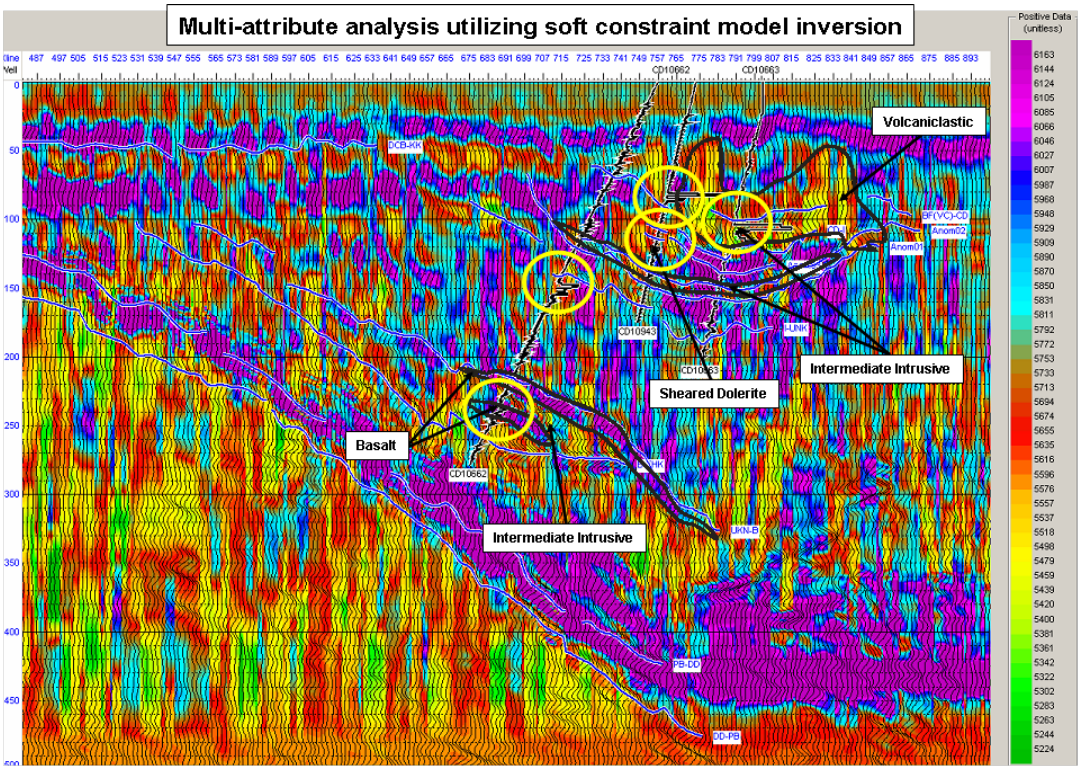

Figure 5-35. Multi-attribute prediction utilizing model inversion.

5.3.4 Gold-Content Prediction Using Multi Attribute Analysis

Hydrocarbon exploration uses attribute analysis to make porosity predictions for reservoirs properties. Mineralization at alteration plumes and at structural changes are analogous forms of porosity in hard rock environments. Gold assasy which is closely associated with magnetic susceptibility was used to find out if there was a seismic attribute or combination of attributes that will have some correlation with the gold content. Correlation results indicated only a 0.1956 correlation between 3 attributes and gold assessment. These low correlations results were used to produce a neural network to generate gold content predictions on the East Victory seismic image (Figure 5-36).

The "High" gold-content on Figure 5-36 was set to red and occurs where gold assessment has been predicted at 2000 ppb or greater. "Low" gold-content is white where analysis has determined gold assay to be less than 2000 ppb. Comparing the high gold-content zone predictions against impedance results (Figure 5-9, Figure 5-10, Figure 5-11 and Figure 5-20) reveals two possible areas of interest for targeted mining. These two zones coincide well with high gold content on borehole CD10663 and extensions of the intermediate intrusive near the Condesor dolerite. Two more generalized areas of high gold are also seen on CD10662. These results, however, are quite unstable. Subtle changing of the tolerance parameters was conducted repeatedly to achieve this "reasonable" statistical and visual gold prediction. A greater volume of borehole sonic logging is necessary for any further analysis to be complete. More importantly however, much higher resolution seismic acquisition is needed to resolve thin beds associated with gold zones. It is suggested that vertical seismic profiling may have the resolution needed for gold zone identification.

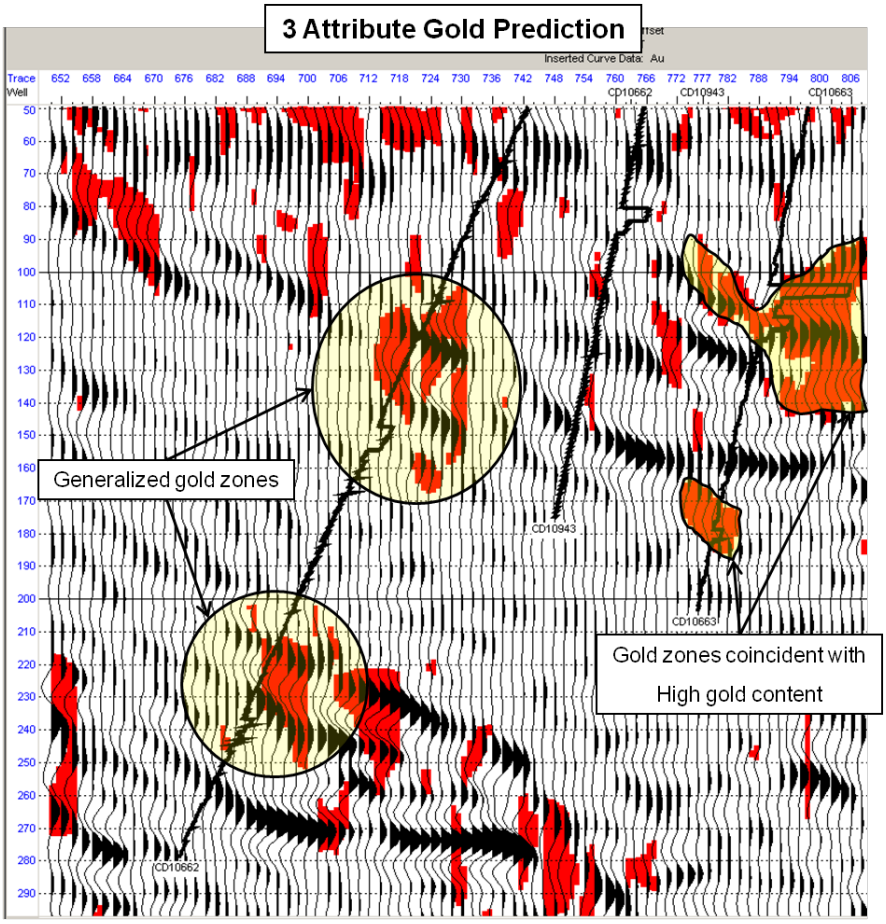

Figure 5-36. Multi-attribute gold prediction through the East Victory seismic line. Course gold zone predictions are indicated in yellow.

5.3.5 Attribute Analysis Summary

The results of seismic attribute analysis on the East Victory data sets have been encouraging overall. Basic lithology and structural predictions based on P-wave and log values revealed similar results to both acoustic and elastic inversions. Attribute assisted predictions imaged the high impedance / high velocity Condenser dolerite and lower impedance / lower velocity high gold content intermediate intrusive on both the full-stack and near-offset stack images. However, the multi-attribute predictions had lower final cross-correlation values, and took 45 minutes longer to generate than seismic impedance inversions. Given enough time and adjustments, volumetric predictions for gold content appeared accurate with attribute analysis, but the limited amount of borehole data and low-signal-to-noise ratio in the seismic data limited reliability of gold predictions. While good images were generated during attribute analysis, further research and core samples are needed before lithology and gold content predictions can be fully trusted.

6 Field Data Analysis: Intrepid Example

A second attempt to relate rock properties to seismic sonic logs was conducted in the same exploration area at the St. Ives gold camp in Western Australia. The Intrepid seismic line is crooked, short (4.63 km), and only two boreholes with sonic logs were available for calibration of seismic data. The geological model is incomplete and hence uncertain as is structural interpretation performed on reflection seismic data. Under these conditions, inversion and attribute analysis of recorded seismic image are far from trivial. Rigorous analysis is necessity to achieve viable conclusions from this data set.

To attempt an improved imaging, both post-stack migration and pre-stack depth migration were utilized on the Intrepid seismic line. Rigorous approach to seismic velocity analysis for proper placement of reflection energy is an important requirement of pre-stack migration techniques. This is, however, hard to achieve in hard rock environment due to complexity of the structures in 3D, fractured and unknown geology with low S/N. As an alternative a thorough examination of the borehole logs was conducted to ensure an accurate *a-prior* geological model could be constructed for velocity modelling. Consequently, acoustic, elastic inversion and multi-attribute analysis were utilized to evaluate lithological predictive ability.

Figure 6-1 shows the location of the Intrepid seismic line on the lake Lefroy. Due to the salt and mud cover on the salt lake, geological interpretations was only of a regional nature and not suitable for localized analysis. The acquisition parameters (e.g. shot spacing, receiver spacing, and vibroseis sweep) for the Intrepid line were the same as those for the East Victory line. Raw and pre-processed shots are shown in Figure 6-2. Reasonably high quality data, for hard rock environments, is recorded along this line.

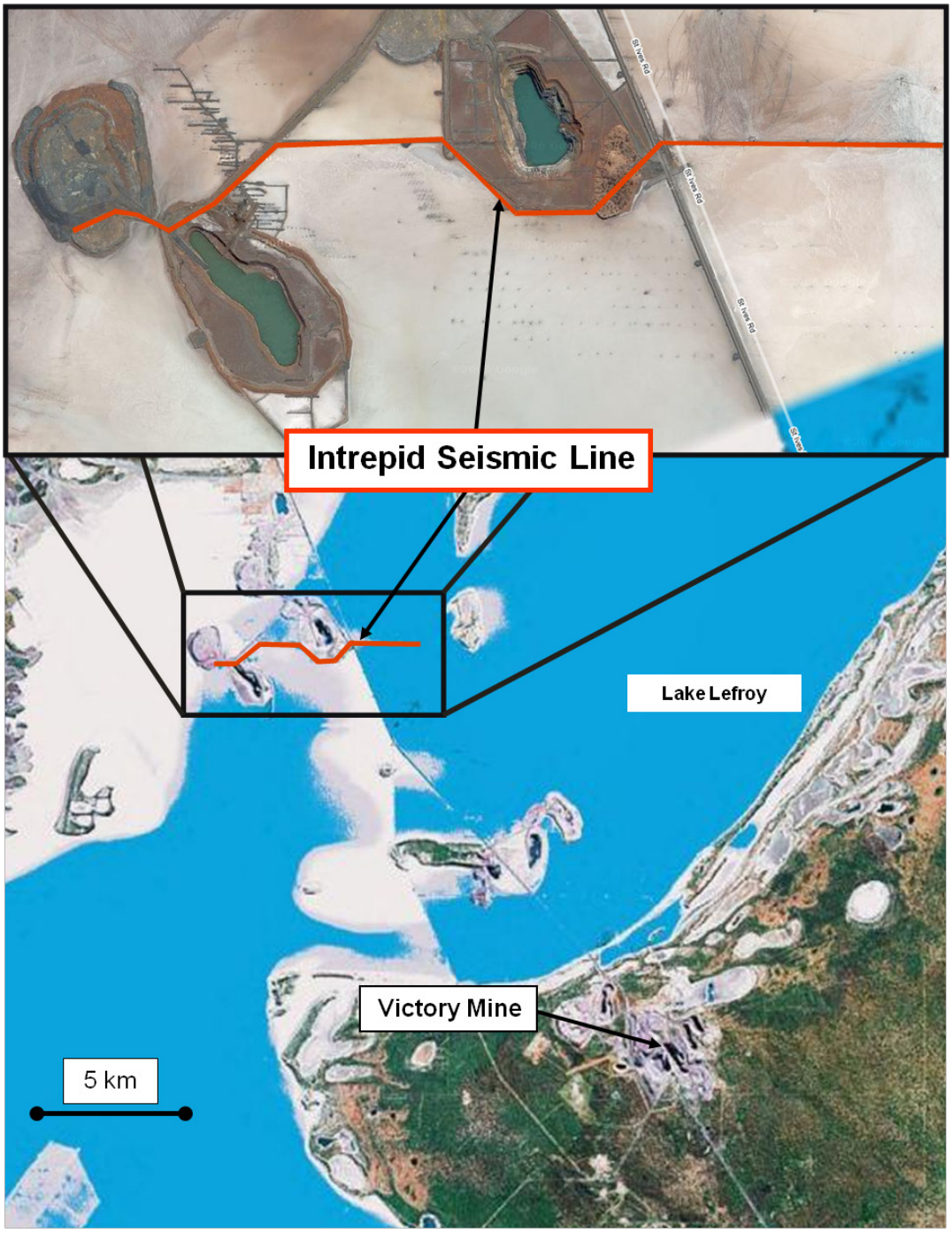

Figure 6-1. The Intrepid seismic line located at the St. Ives gold camp in Western Australia.

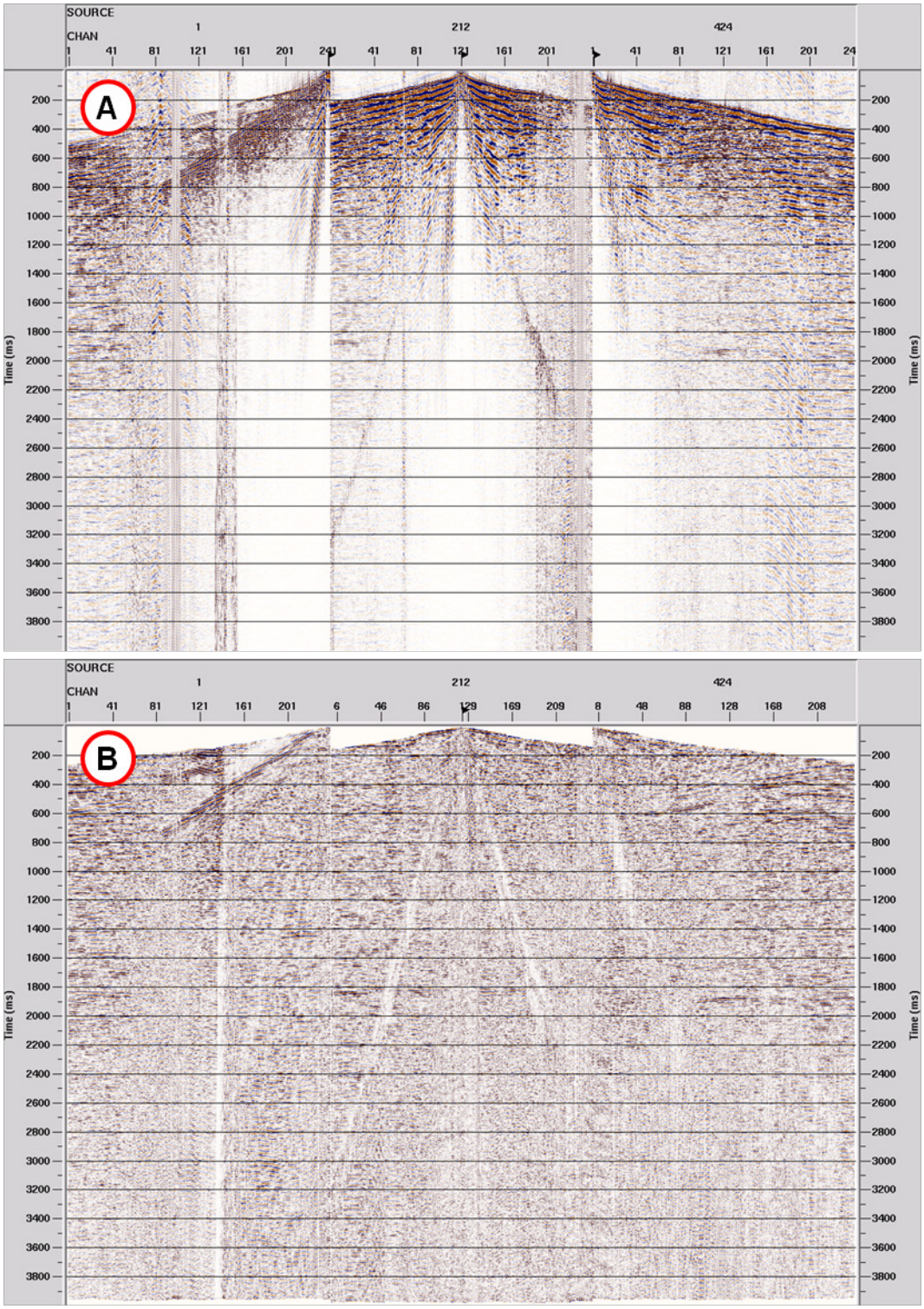

Figure 6-2. Raw (A) and Pre-processed (B) shot records from the beginning, middle and end of the Intrepid seismic survey respectively. Each shot is 2.4 kilometres long and 18 kilometres deep

6.1 Processing of the Intrepid Seismic Line

A sequence of pre-stack DMO and post-stack migration as well as a full pre-stack migration were carried on this data set. As a consequence of the limited amount of data available from the Intrepid line, extra care in data analysis was necessary. Post-stack migration was used in the initial phase of the processing. Multiple iterations of constant velocity stacks before and after DMO were completed for best estimates of the velocity field. This DMO-derived velocity was then utilized during the first round of processing of the Intrepid seismic data.

Pre-stack depth migration had been suggested as the most accurate seismic solution (Guo and Fagin, 2002) with the added benefit that the pre-stack Kirchhoff migration has superior shallow imaging capabilities compared to other techniques (Pasasa et al., 1997). An *a priori* velocity model preserves shallow structures while focusing complexity. The initial velocity model for PSDM was built on the *a priori* geological knowledge and log data. Discontinuities in the velocity model were eliminated by smoothing the model both in the vertical and horizontal directions across common image gathers. The final velocity model is shown in Figure 6-3 with the map view inset to show where the crooked nature of the seismic line.

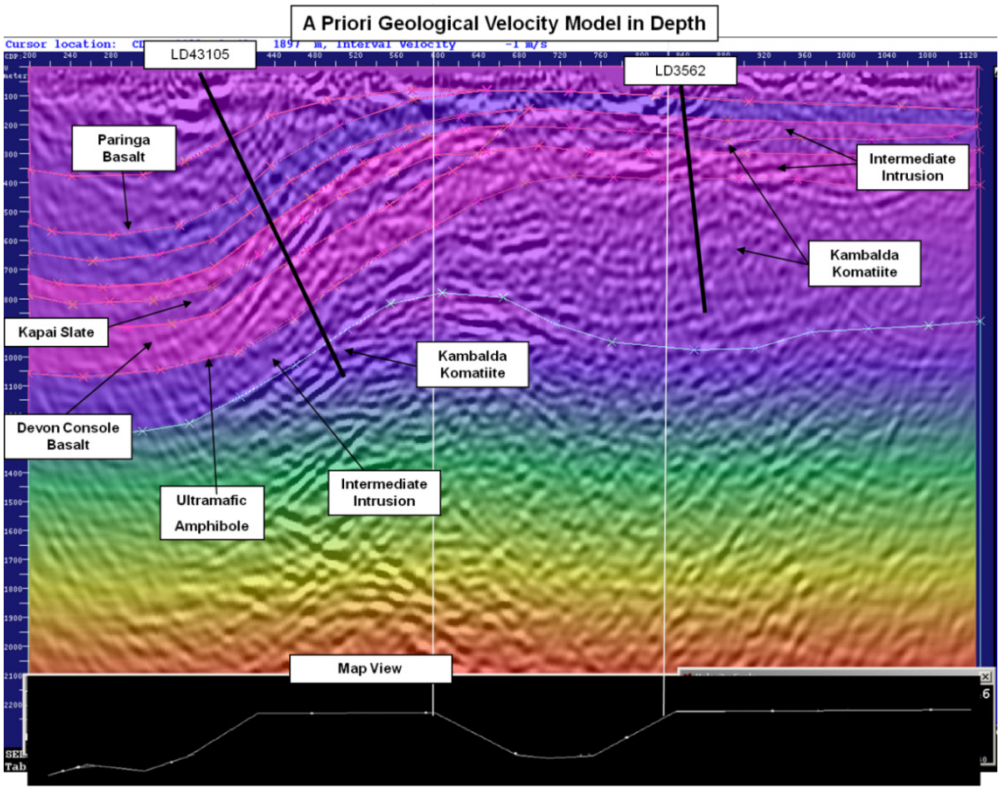

Figure 6-3. The *a priori* velocity model for the Intrepid seismic line, derived from log data and post-stack depth migration section.

6.1.1 Post-stack versus Pre-Stack Migration

Both the pre-stack and post-stack seismic images are shown in Figure 6-4. The highlighted areas on this figure show that PSDM had limited success in imaging geological complexity in this area. Compared to the post-stack image, quality was not maintained across the line. Application of DMO in the post-stack image has enhanced the steeps dips and overall improved image quality and thus was deemed as the most robust imaging method for the Intrepid seismic line. Figure 6-5 shows a geological interpretations on the post-stack image. Reflections of several thin beds, including the Kapai Slate, and an un-named intermediate formation, are masked or melded with reflections from the Devon console basalt and Paringa basalt formations. Thinner beds less than 20 metres are not interpreted on the seismic image due to resolution limitations.

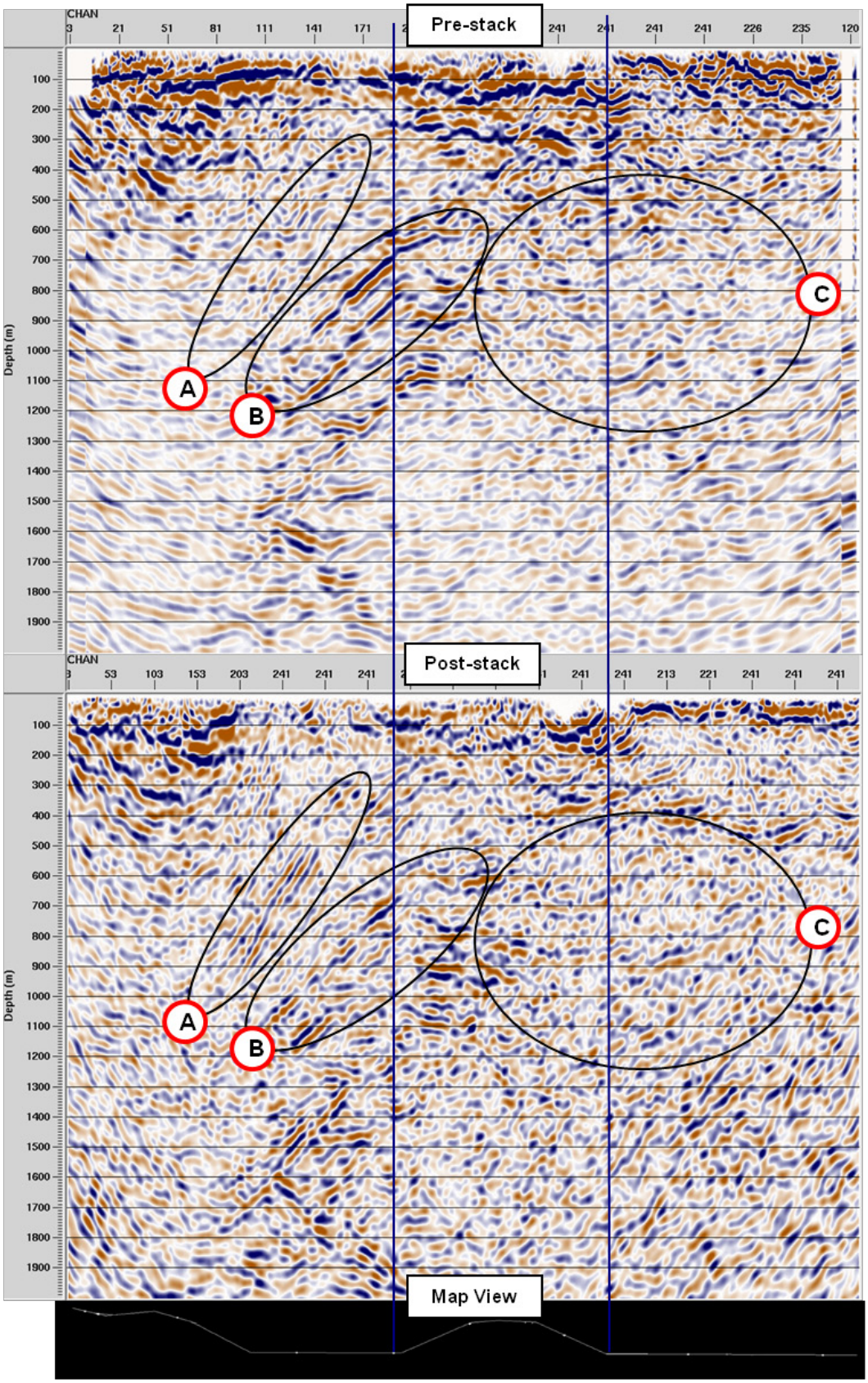

Figure 6-4. Pre-stack (top) and post-stack (bottom) migrations. Major differences between processing are indicated with (A) (B) and (C).

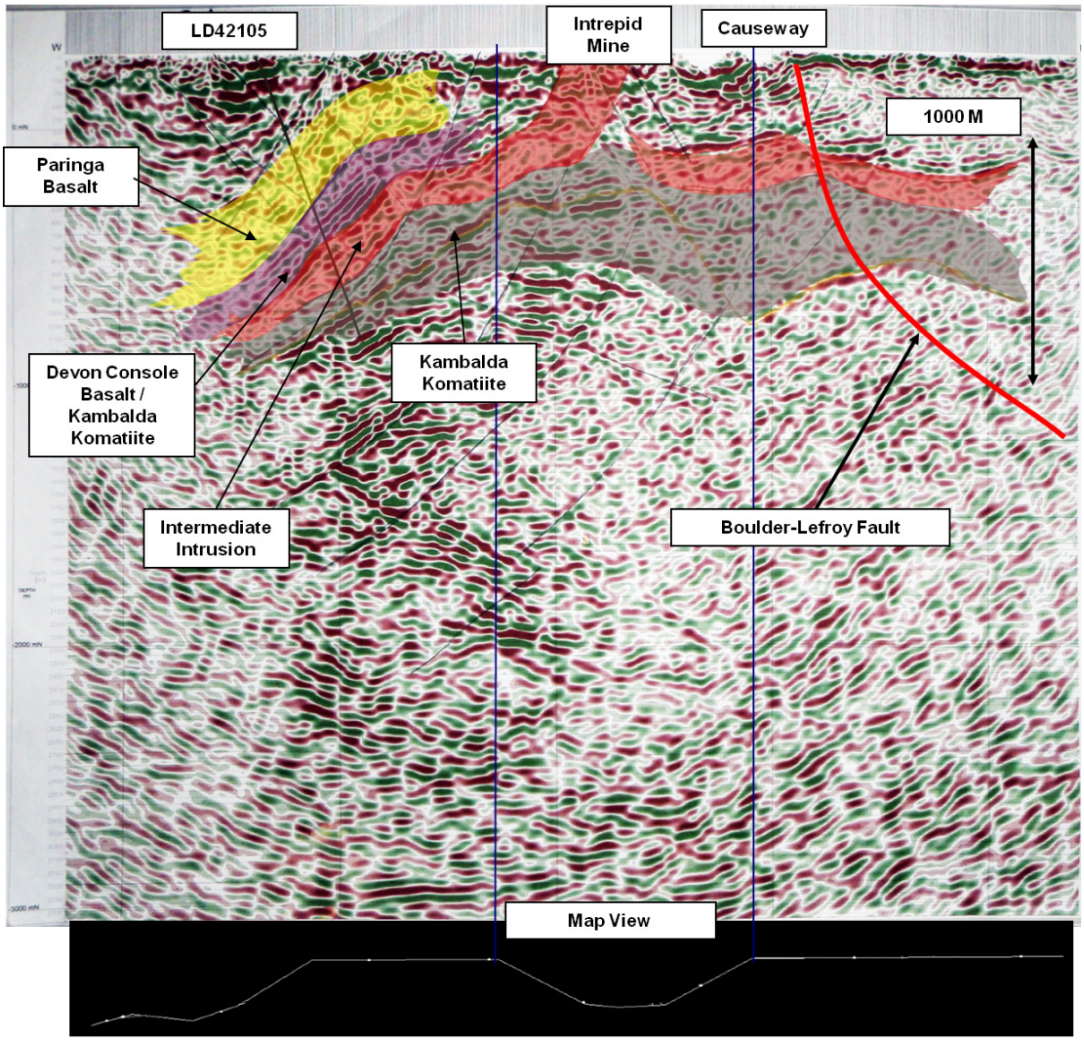

Figure 6-5. Geological interpretation of depth migrated Intrepid seismic line (Gold Fields Limited).

6.2 Statistical Sonic Log Evaluation

Two boreholes with full waveform sonic logs and interpretations were available for analysis on the Intrepid seismic line (Figure 6-6). Borehole LD42105 (**Error! Reference source not found.**) shows the complexity in differing rock type, structure type, and stratigraphy seen in the area.

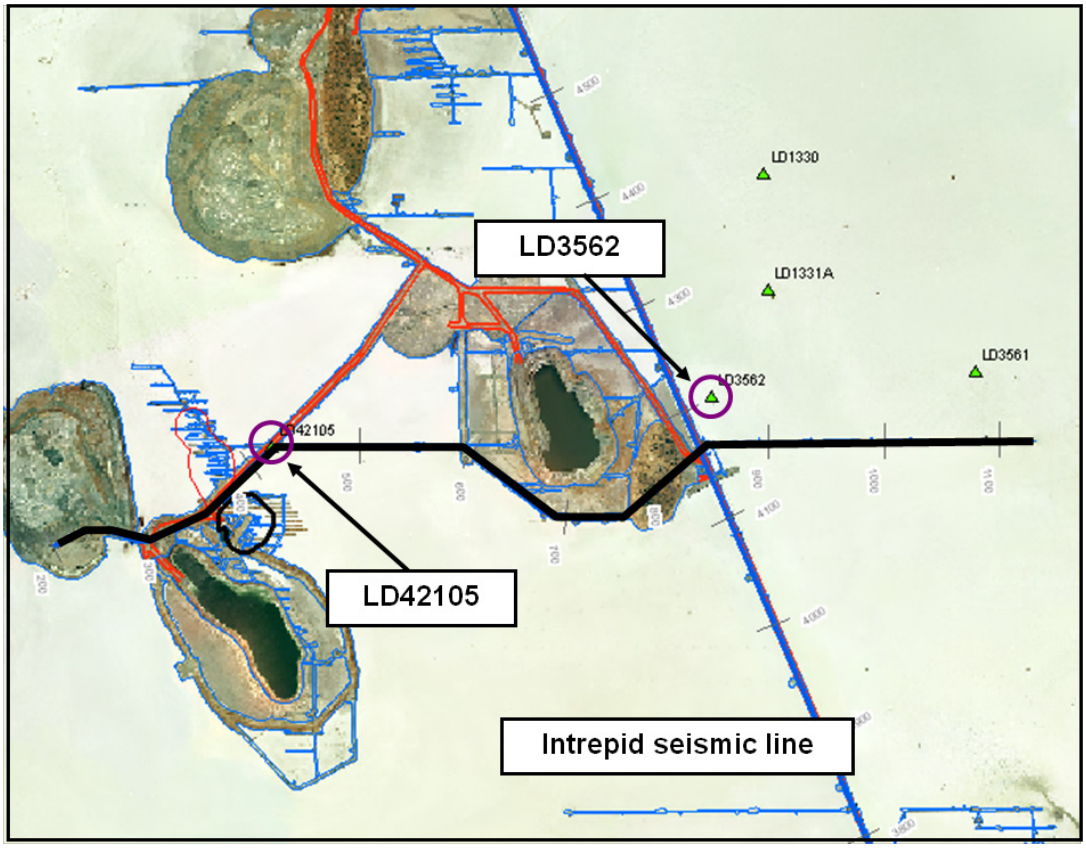

Figure 6-6. The borehole locations of the full waveform sonic (FWS) logs on and near the Intrepid seismic line.

6.2.1 Zero offset Synthetic Seismogram

A wavelet with dominant frequency of 50 Hz was extracted from the seismic data and convolved with the borehole reflectivity to investigate zero-offset synthetic responses. Results indicate synthetic seismic responses along each borehole were associated more with rock type changes and structural changes. These results were consistent with the previous study on the East Victory line.

6.2.2 Log Data Analysis

Cross-plots of log density versus log P-wave velocity were generated for LD42105 and LD3562 based on rock type, structure type and alteration type. Cross-plotting revealed that consistent statistically valid information was going to be extracted only from specific rock and structure types. Table 6-1 contains the cross-correlated and average values for density, P-wave and S-wave velocities for difference rock types from log data. Standard

deviation values were statistically more effective than cross-plotted correlation calculations for komatiite and ultramafic chlorite.

Rock	Structure	Density (g/cc)	P Wave Measured (m/s)	P Wave Predicted (m/s)	S Wave Measured (m/s)	S Wave Predicted (m/s)
Komatiite		2.78 (0.11)	5548.1	-	3241.6	-
Intermediate Intrusive	Sheared	2.72 (0.124)	5222	4357	3144	3420
Ultramafic Amphibole	Sheared	3.06 (0.066)	4973	5468	3057	2954
Ultramafic Chlorite		3.24 (0.1)	4657	-	2958	-
Basalt	Sheared	2.93 (0.065)	6428	6372	3744	3772

Table 6-1. Rock characterization from rock units on the Intrepid line.

6.2.2.1 Vp/Vs Ratio and Acoustic Impedance

Cross-plots of Vp/Vs versus acoustic impedance were generated for all rock types characterized on the Intrepid line. Results indicated that Vp/Vs ratios and acoustic impedance revealed a way to differentiate between “softer” rocks (intermediates, komatiite) and “harder” rocks (sheared basalt). The P-impedance and Vp/Vs ratio data for high gold content zones on borehole data are plotted in Figure 6-7 and Figure 6-8. Both of these figures show high gold content rock have specific separable Vp/Vs ratio and P-impedance from its host rock. P-impedance for high gold content on Figure 6-8 shows consistent stable results. While encouraging, the lack of overall sonic data required further statistical verification for reliable prediction results.

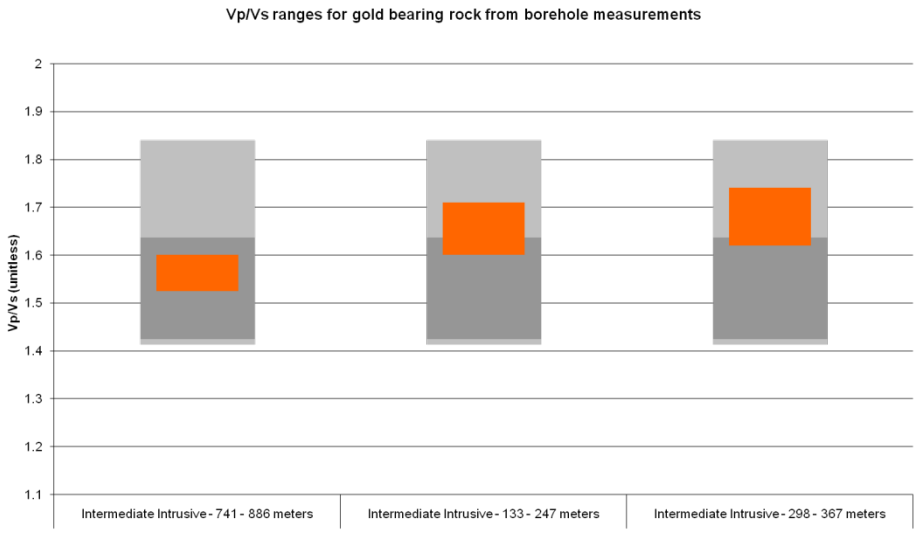

Figure 6-7. Vp/Vs ratio values for different gold-bearing rock. Light grey represents the highest and lowest Vp/Vs ratio found in the intermediate intrusive, dark grey represents the standard deviation Vp/Vs ratio orange represent the Vp/Vs ratio associated with gold-bearing rock.

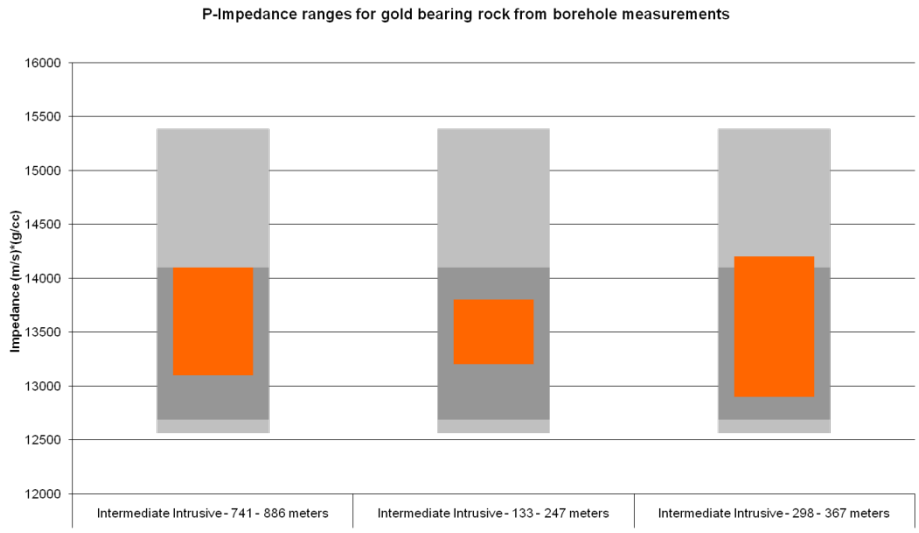

Figure 6-8. P-impedance values for gold-bearing rock. Light grey represents the highest and lowest values found in the intermediate intrusive, dark grey represents the standard deviation values, orange represents the impedances associated with gold-bearing rock.

6.2.3 Elastic Versus Acoustic Impedance

Near-offset and far-offset elastic impedance were calculated for each sonic log to investigate elastic impedance changes. Cross-plot of acoustic impedance versus offset dependant impedances were generated on both boreholes and complied rock data to observe correlations on the Intrepid seismic data. Both near-offset and far-offset calculations showed a marked separation between softer rocks (intermediate intrusive and

komatiite) and the harder sheared basalt. Measurements of near-offset and far-offset elastic impedance for high gold-bearing zones have been plotted in Figure 6-9. The near-offset cross-plot revealed weak impedance separations between the individual softer rocks such as intermediate intrusive and komatiite. Elastic impedances at high gold zones were shown to have consistent impedance values using both near-offset and far-offset elastic impedances.

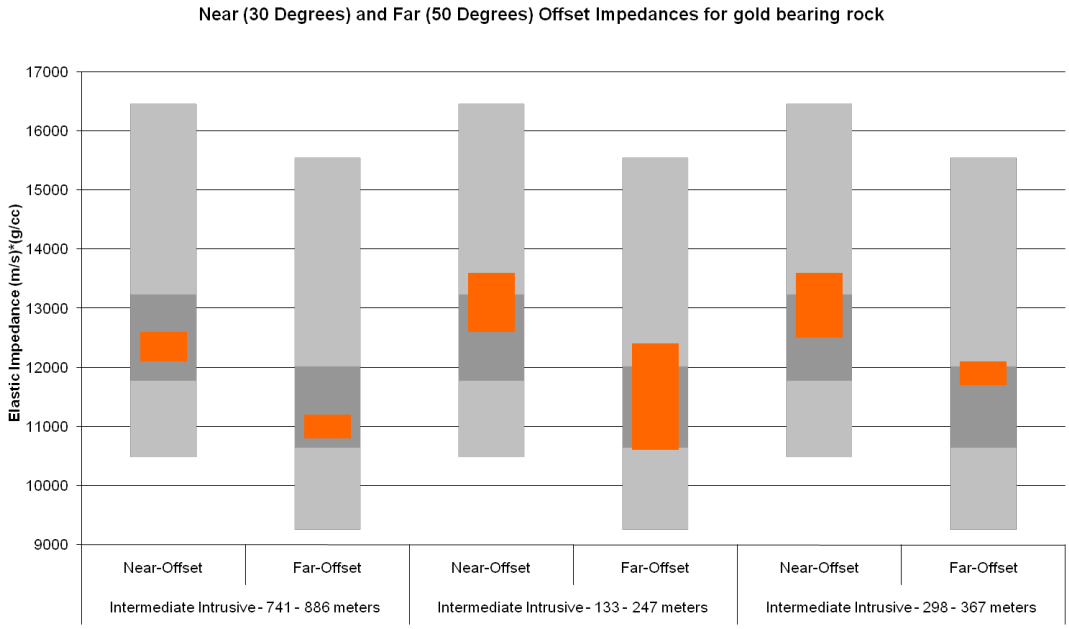

Figure 6-9. Near-offset and far-offset impedance measurements for gold-bearing zones on LD42105 and LD3562. Light grey represents the highest and lowest elastic impedances found in the intermediate intrusive, dark grey represents the standard deviation elastic impedances and orange represents the elastic impedances associated with gold-bearing rock.

6.2.4 Amplitude Versus Offset

Figure 6-10 illustrates four AVO analysis for typical rocks-in-contact from Intrepid borehole log data. Both P-P wave (red) and P-S wave (green) reflection amplitude are shown. Amplitude changes are weaker on near-offset (~20-30^{o}), but stronger on far-offset (~50-80^{o}) when approaching critical angles.

Synthetic seismic offset responses using offset ranges from 0 to 1000 metre were created on LD42105 (Figure 6-11) to generate offset records. The model for LD42105 (Figure 6-11) highlights a 100 metre gold-bearing intermediate intrusive below an ultramafic amphibole. The amplitude of reflections between these two layers increases with offset. This behaviour was also seen on East Victory logs at high gold content zones.

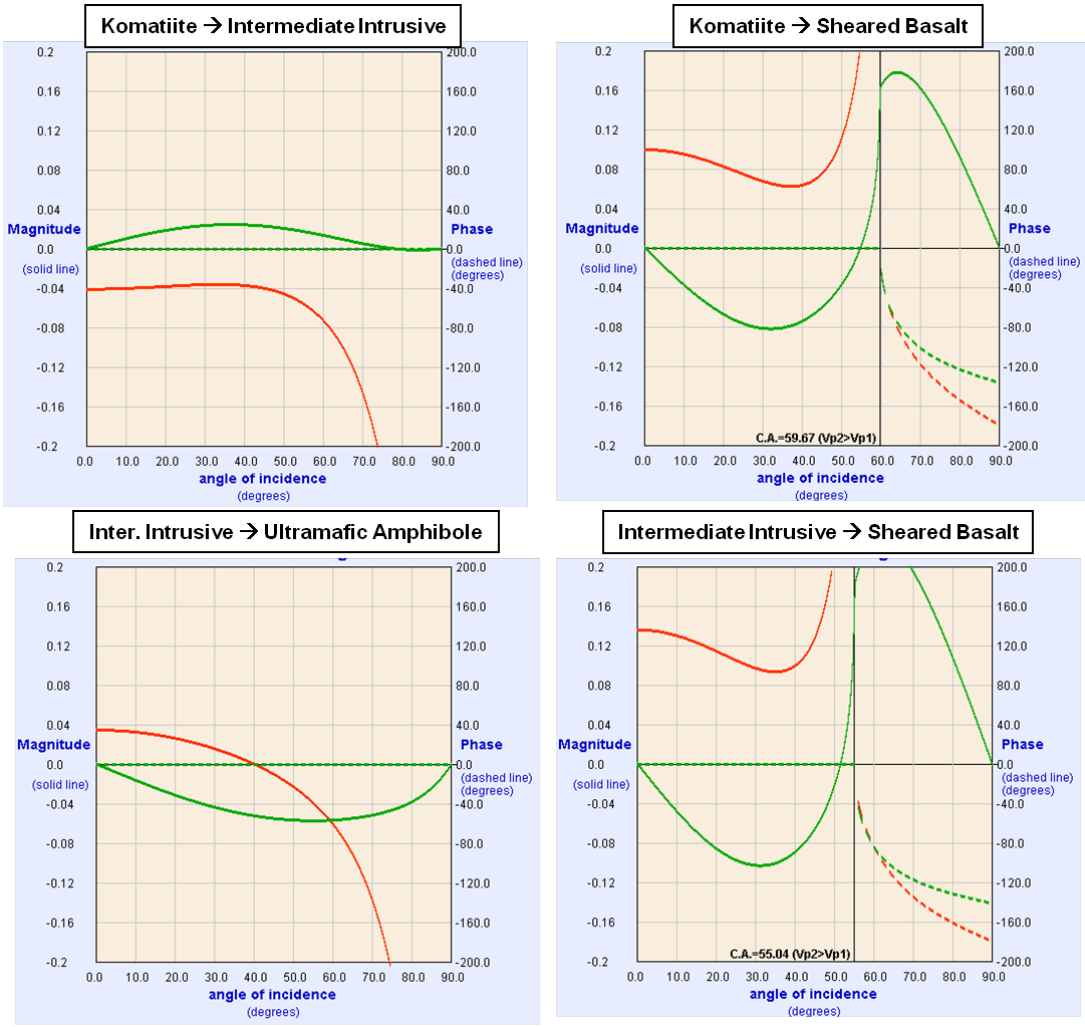

Figure 6-10. The amplitude versus angle of incidence (offset) of rock types found on the Intrepid boreholes. Red lines are reflectivity of P-P waves and green lines are reflectivity of P-S waves.

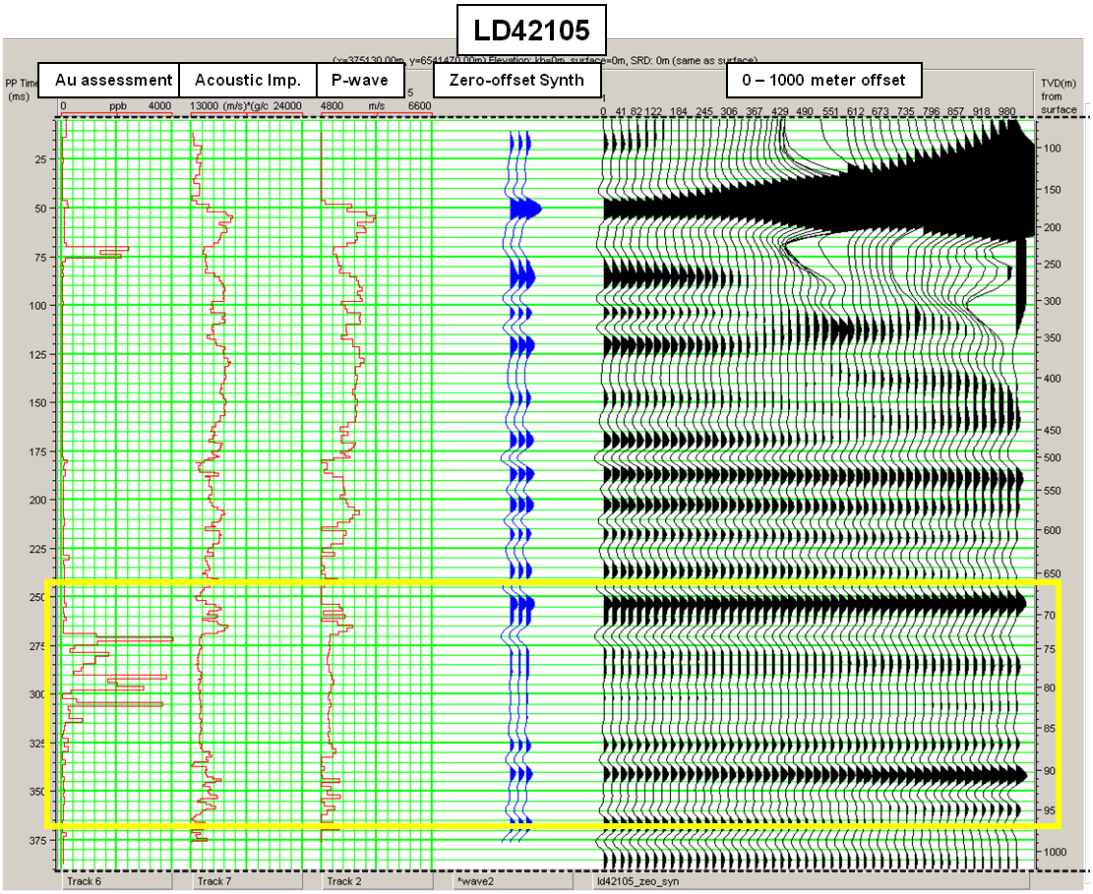

Figure 6-11. Zero to 1000 metre offset for borehole LD42105. The yellow box shows an area of interest with an ultramafic amphibole in contact with a gold-bearing intermediate intrusive.

6.2.5 Lambda-Mu-Rho

To maximize statistical analysis of the Intrepid data set, Lambda-Mu-Rho (LMR) calculations and cross-plots were conducted to observe further elastic properties within the log data. It was hoped that similar rock separation seen on the East Victory data set based on Lambda-Rho and Mu-Rho were possible. Figure 6-12 shows the Lambda-Rho versus Mu-Rho cross-plot for complied rock data from the Intrepid logs. Results indicate that the rock types of komatiite, ultramafic amphibole, and intermediate intrusive have similar Lambda-Rho and Mu-Rho values. Basalt remains reasonably separate from other rock types showing promise for rock identification ability. These cross plotted LMR values show similar rock separation results as those from the East Victory data sets.

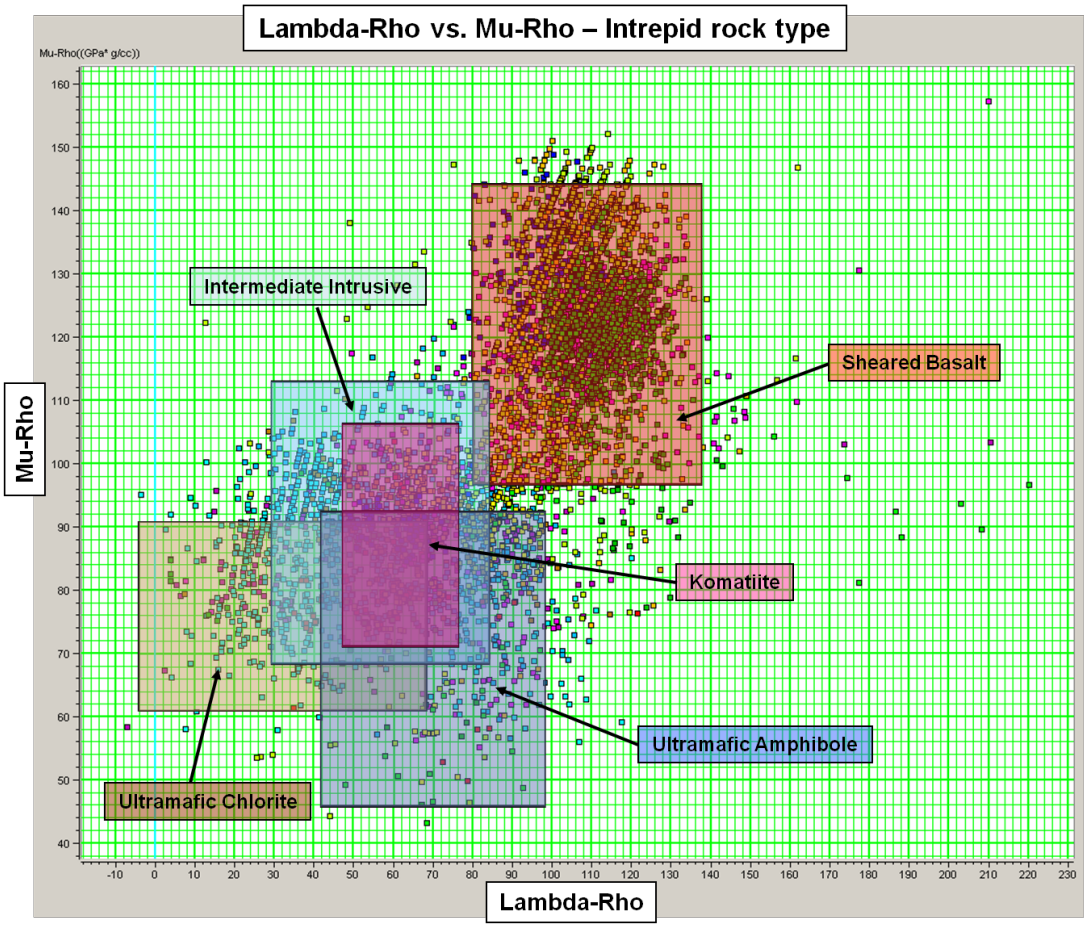

Figure 6-12. Lambda-Rho versus Mu-Rho cross-plot for all major rock types from the Intrepid line.

6.2.6 Rock Characterization Summary

Rock characterization on the Intrepid sonic log data confirmed that statistical separation between velocities, densities, acoustic impedance, and elastic impedance exist for different hard rock lithologies. Analysis indicated that softer rocks (e.g., intermediate intrusive, and komatiite) and harder rocks (e.g., sheared basalt) were easily distinguishable using log data. Log derived synthetic reflections resulted from rock type and structural changes. Similar to the East Victory logs, high gold content ore zones were again shown to have unique impedances and reflections. Calibration of the sonic and seismic data was necessary to correlate synthetic reflections with seismic data.

6.3 Acoustic Inversion

Steeply dipping reflections have been imaged using post-stack migration on the Intrepid seismic line. Calibration of the log derived synthetic seismograms and the seismic data for the Intrepid seismic line was conducted in the same way as the previous East Victory calibrations. With no time-depth data available from a check shot, careful sonic-seismic correlations were required.

Figure 6-13 shows the final statistical wavelet extracted from the post-stack migration. Borehole synthetic seismograms correlated with seismic image and the rock contacts picks are shown in Figure 6-14. Correlation values are shown adjacent to their respective borehole. Initial synthetic seismic correlations were low due to the limited number of reflections imaged on the seismic data at borehole locations. The map view of the seismic line has been inset on Figure 6-14 to illustrate where crooked parts of the seismic line may have affected reflection resolution. Seven contacts were identified on the post-stack image:

- top of the Paringa basalt (PB-01),
- bottom of the Paringa basalt (PB-Bot),
- intermediate intrusive through the Kambalda komatiite (KK(II)-In),
- location of Kapai slate (AA-Top),
- top of an intermediate intrusive on LD3562,
- top of a gold bearing intermediate intrusive (II(kk)-In),
- and the bottom of the Kambalda komatiite.

A geological interpretation is shown on Figure 6-15.

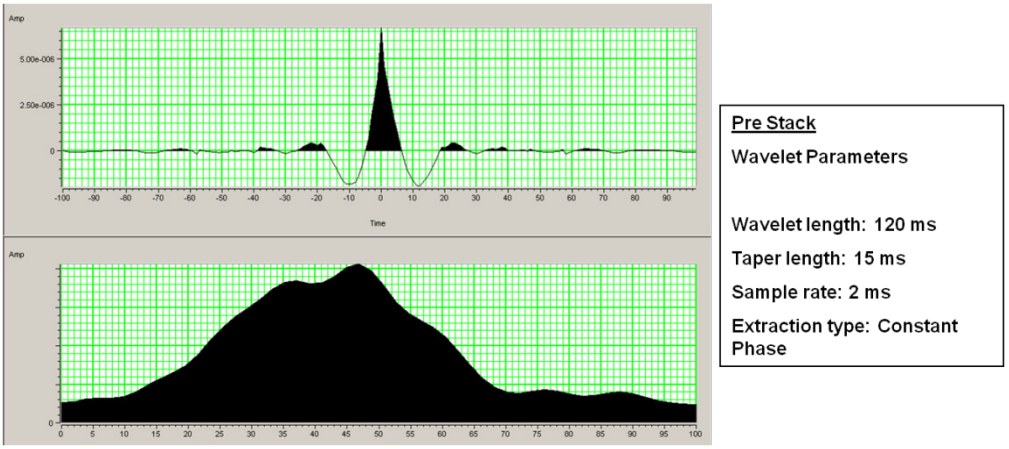

Figure 6-13. Statistical wavelet for sonic-seismic calibration.

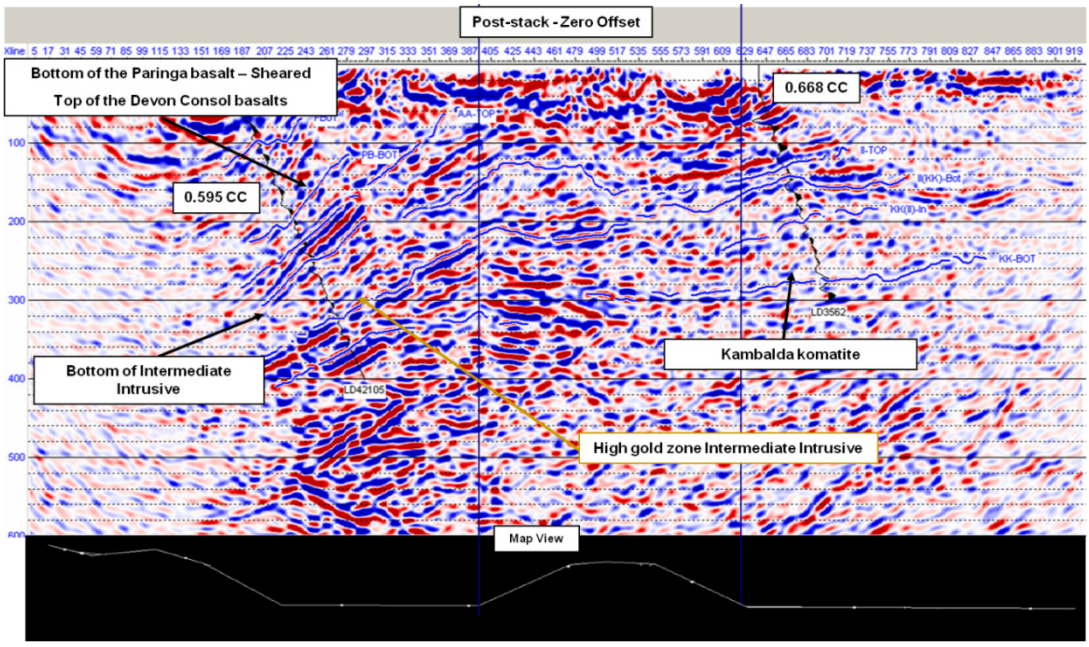

Figure 6-14. Post-stack migration of the Intrepid line with calibrated sonic logs and rock contact picks.

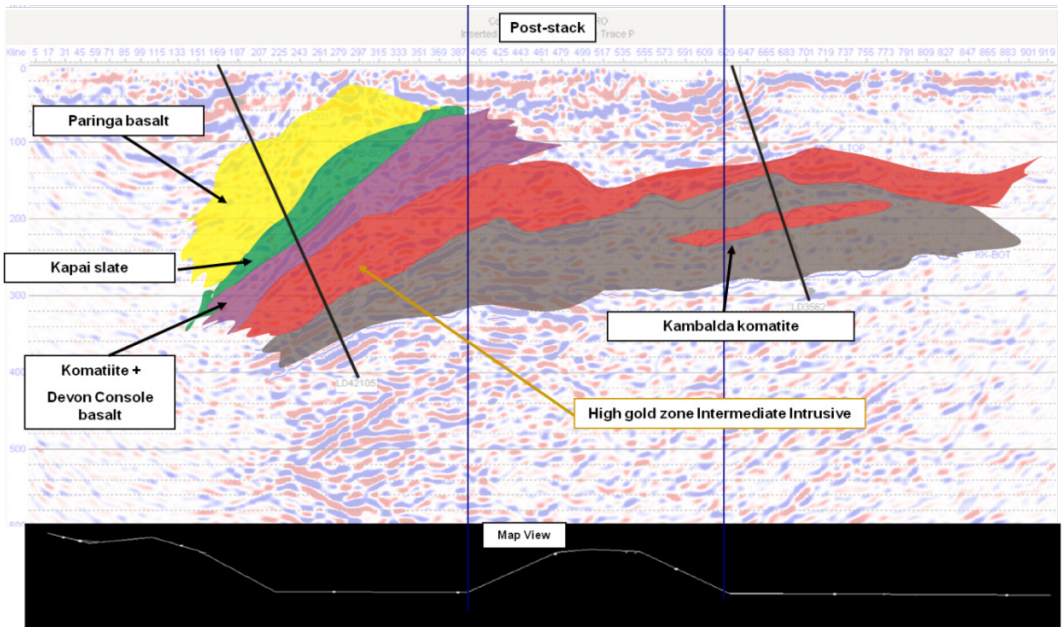

Figure 6-15. Geological interpretation of the reflections on the intrepid seismic line.

6.3.1 Results and Analysis of Acoustic Inversion

Figure 6-16 shows a log derived acoustic impedance model for a model based inversion scheme. (A), (B) and (C) on Figure 6-16 mark the zones where impedance model is just an extrapolation as geological information (horizons) are missing. Rock contact extensions in sections (B) and (C) were not possible to interpret even utilizing instantaneous phase for enhanced continuity. The following acoustic inversions were generated on each seismic image and model:

- Model Based
    - Hard Constraint
    - Soft Constraint
- Band Limited
- Coloured Inversion
- Linear Programming Sparse-Spike
- Maximum Likelihood Sparse-Spike.

With only two boreholes available, quality control of inversion using hidden sonic logs was impossible. Distance between the sonic logs and complexity of the rock environment was simply too large for accurate verification. Figure 6-17 displays the correlation and graphed results for error analysis of the inversions. Both model inversion and sparse spike inversions showed the highest correlations and are shown in Figure 6-18. The inversion results show a generalized distribution of impedances rather than specific separation of rock units and lithologies. Some rock units, such as the high impedance intermediate intrusive on LD3502 did have a good separation, other areas such as the high gold content unit on LD42105 are predicted as large low impedance zones.

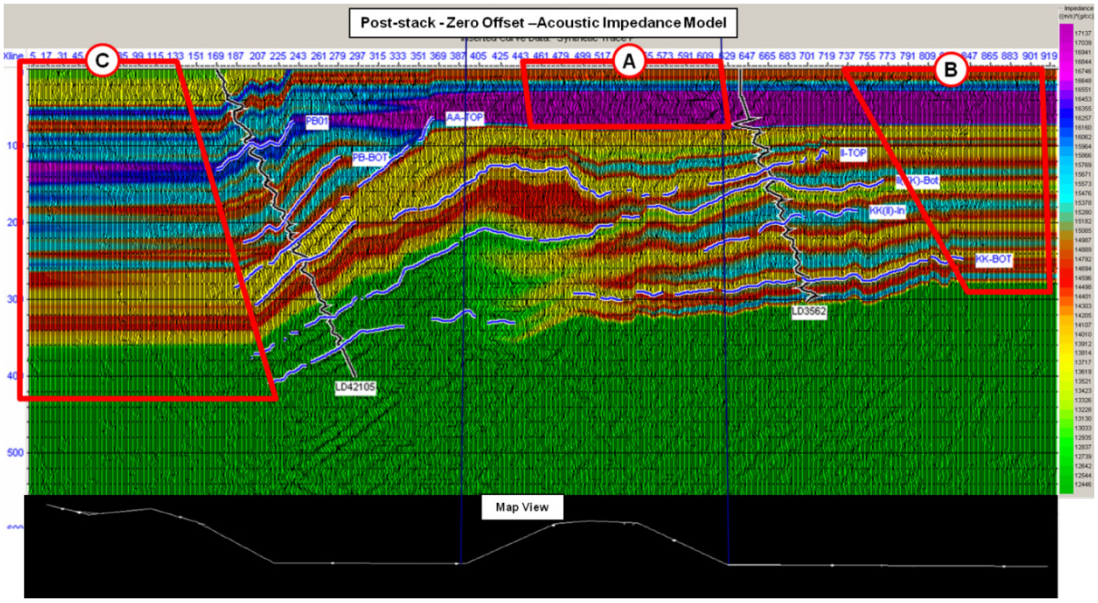

Figure 6-16. The Acoustic Impedance model the post-stacked migrated Intrepid seismic line.

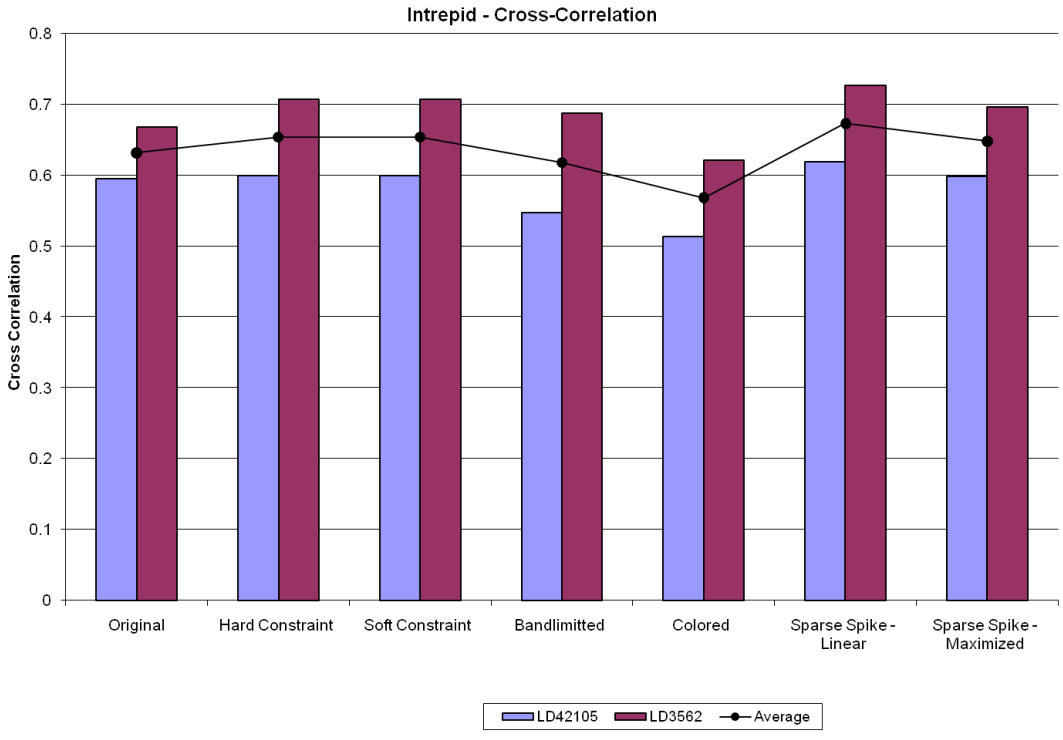

Figure 6-17. Cross correlation results for Intrepid acoustic inversion error analysis,

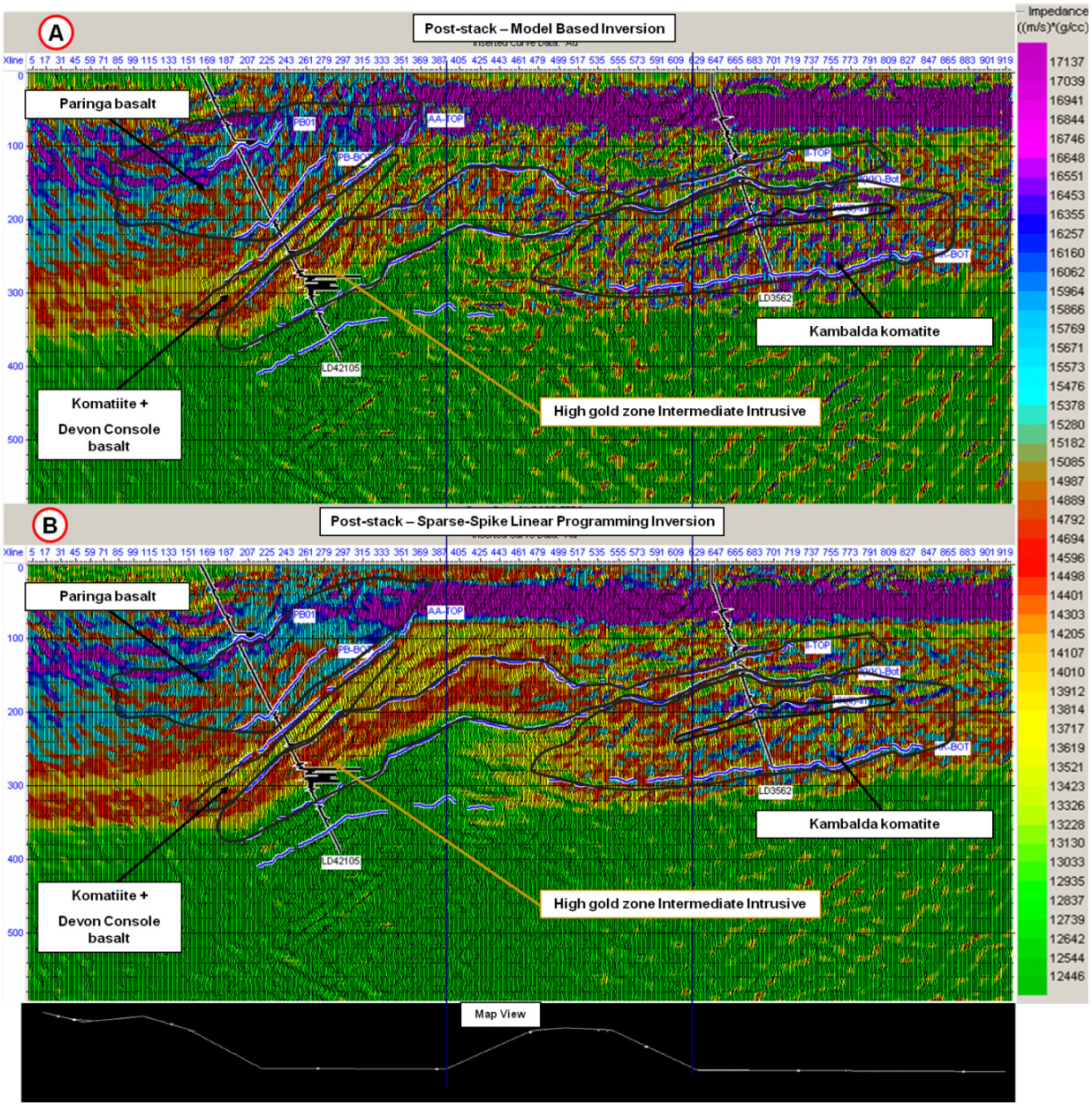

Figure 6-18. Model based (A) and Sparse-Spike acoustic inversions for the Intrepid seismic line.

Low correlations between sonic and seismic data as well as sparse reflections through the seismic image make acoustic inversions less reliable. The results reveal positive trends in the area for identifying larger rock units, but specific rock zoning is not obvious. An increase in the number of boreholes for calibration might reveal more predictive ability, but the crooked nature of the seismic line and low signal-to-noise ratio present serious obstacles for generation of valid inversions.

6.4 Elastic Inversion

To relate log elastic impedances to seismic images, the seismic image data was reprocessed to include near-offset and far-offset stacks. Near-offset ranges were 0 – 600 meters and far-offset ranges were 600 – 1200 meters. Both near-offset and far-offset migrated stacks are shown in Figure 6-19.

Figure 6-20 shows the difference between the near-offset and far-offset with full stack image. The near-offset reflections are thinner and have a superior shallow resolution. The far-offset reflections appear thicker, reveal no shallow reflections above 100-200 ms, but show more prominent deeper reflections. Dominant frequency was calculated at 50 Hz for the near-offset stacked image and 43 Hz for the far-offset stack image. This difference in frequency content is evident in the over-all loss of thin bed resolution on the far-offset seismic image (Figure 6-19). Further analysis on the far-offset image will be limited due to the lack of shallow reflections.

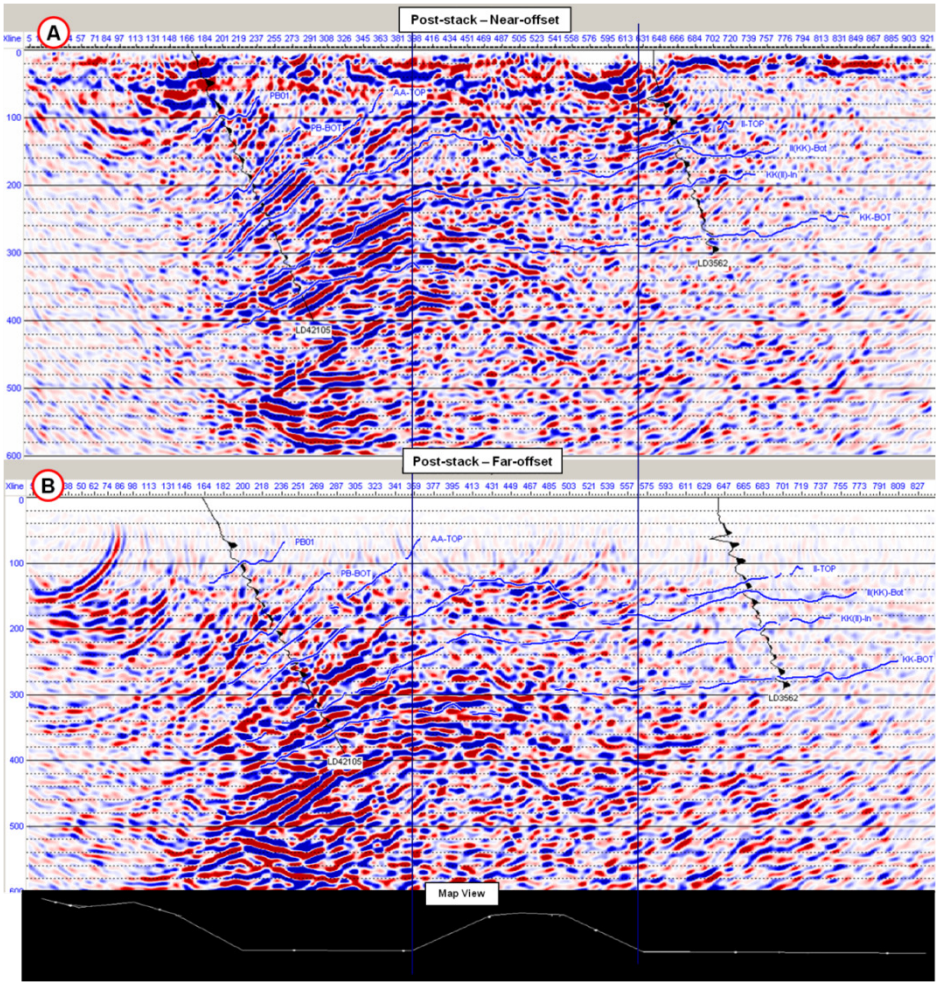

Figure 6-19. Near-offset (A) and far-offset (B) image of the post-stack Intrepid seismic line.

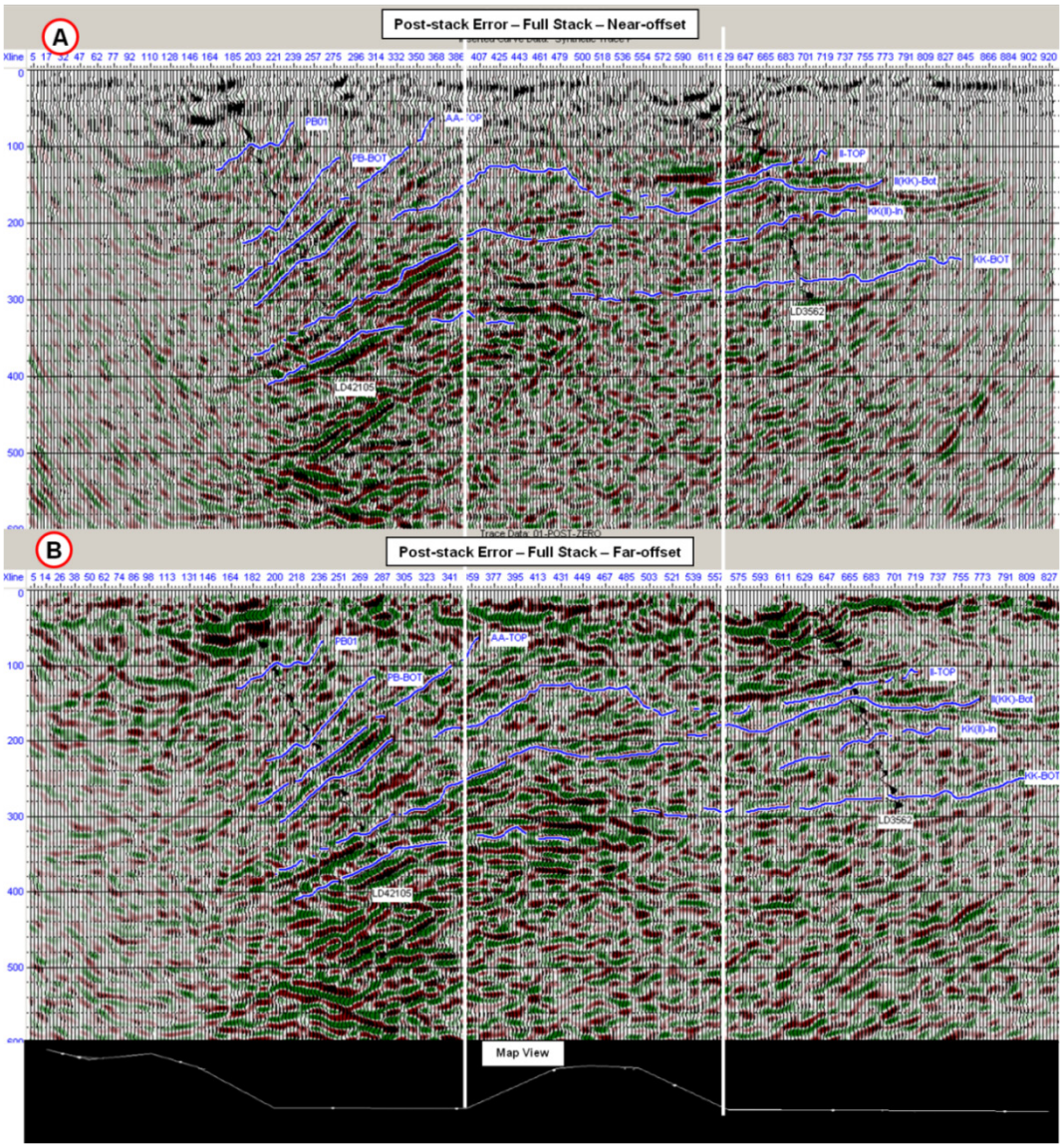

Figure 6-20. Difference between near-offset (A) and far-offset (B) image of the post-stack Intrepid seismic line.

6.4.1.1 Results and Analysis of Elastic Inversion

Only Model-based inversion and Sparse-Spike linear programming inversion were chosen for elastic impedance prediction because they were most reliable for acoustic impedance inversion. Figure 6-21 shows model-based and sparse spike inversion results plotted for near-offset migrated stack data. As was the case with acoustic inversions, the elastic inversions give a more generalized prediction appearance to rock zones. Error analysis of Figure 6-22 indicates both inversion results have low cross-correlation values with the seismic data.

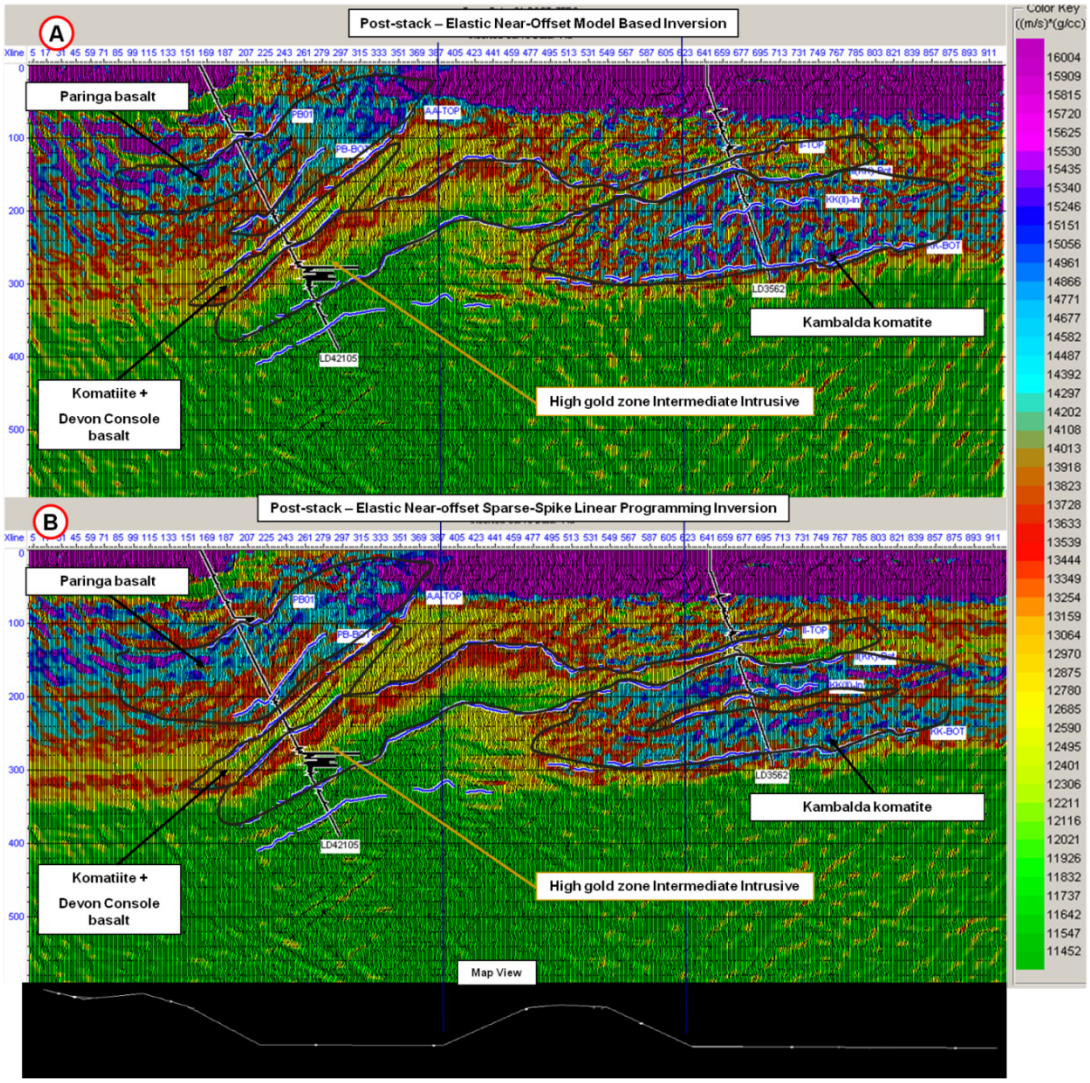

Figure 6-21. Model-based elastic inversion (A) and Sparse-Spike linear programming elastic inversion (B) for the post-stack Intrepid seismic line.

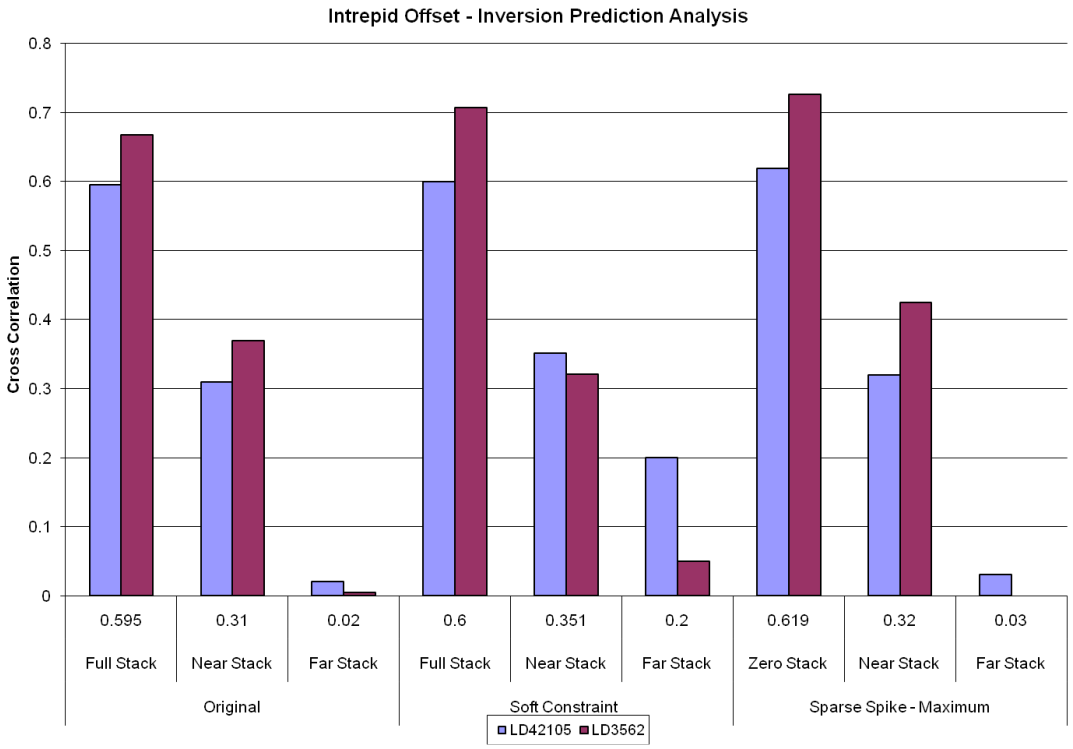

Figure 6-22. Cross correlation between elastic inversions and log data.

6.4.2 Simultaneous Use of Acoustic and Elastic Impedance

To increase predictive power both acoustic and elastic inversions were simultaneously cross-plotted based on rock characterization. Five zones were created on the cross-plots based on acoustic impedance values (Figure 6-8) and elastic impedance values (Figure 6-9) of gold-bearing ore. Zone separation results are shown in Figure 6-23. Harder and softer rock zones were easier to distinguish from each other. This shows that with a lack of log data, increased predictive ability is possible when integrating acoustic and elastic impedance.

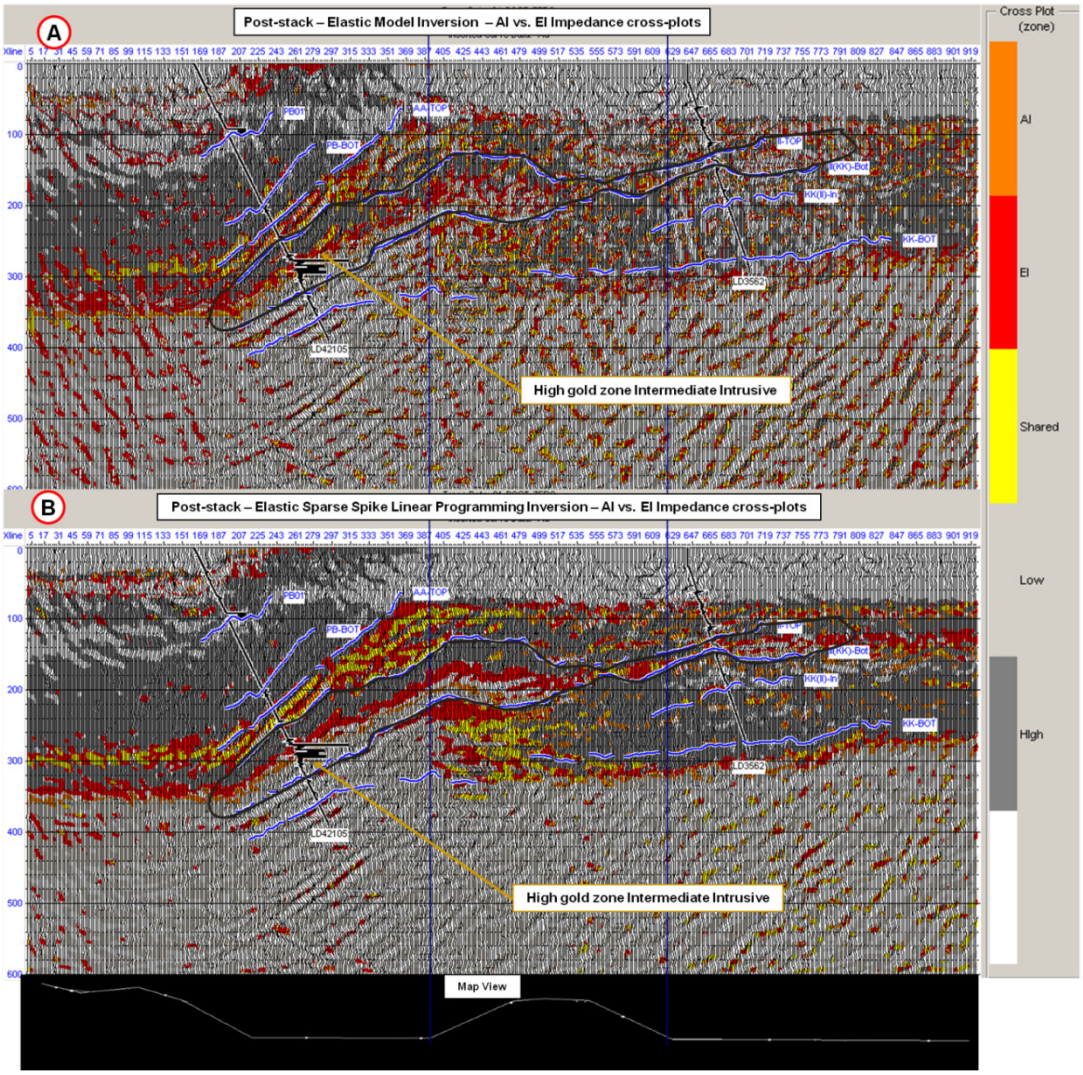

Figure 6-23. Common acoustic and elastic cross-plotted values for high gold content plotted for Model-based inversion (A) and Sparse-Spike inversion (B).

6.4.3 Lambda-Mu-Rho

Lambda-Mu-Rho (LMR) calculations on the Intrepid log data showed a good separation between softer and harder rocks. To capitalize on this discovery Lambda-Mu-Rho analysis was conducted on the Intrepid seismic image to further investigate elastic properties from sonic-seismic calibration. Figure 6-24 shows the results of Mu-Rho and Lambda-Rho predictions. Once again, harder and softer rock zones are reasonably separated. Cross-plotting LRM values were based on LMR values as seen on Figure 6-12. Results of applying cross-plotted areas to the image are shown on Figure 6-25. An increase in rock separation is observed, but consistent lithological separation or gold zone

predictions are not revealed. Overall, the LRM results appear promising but require far more data for reliable results.

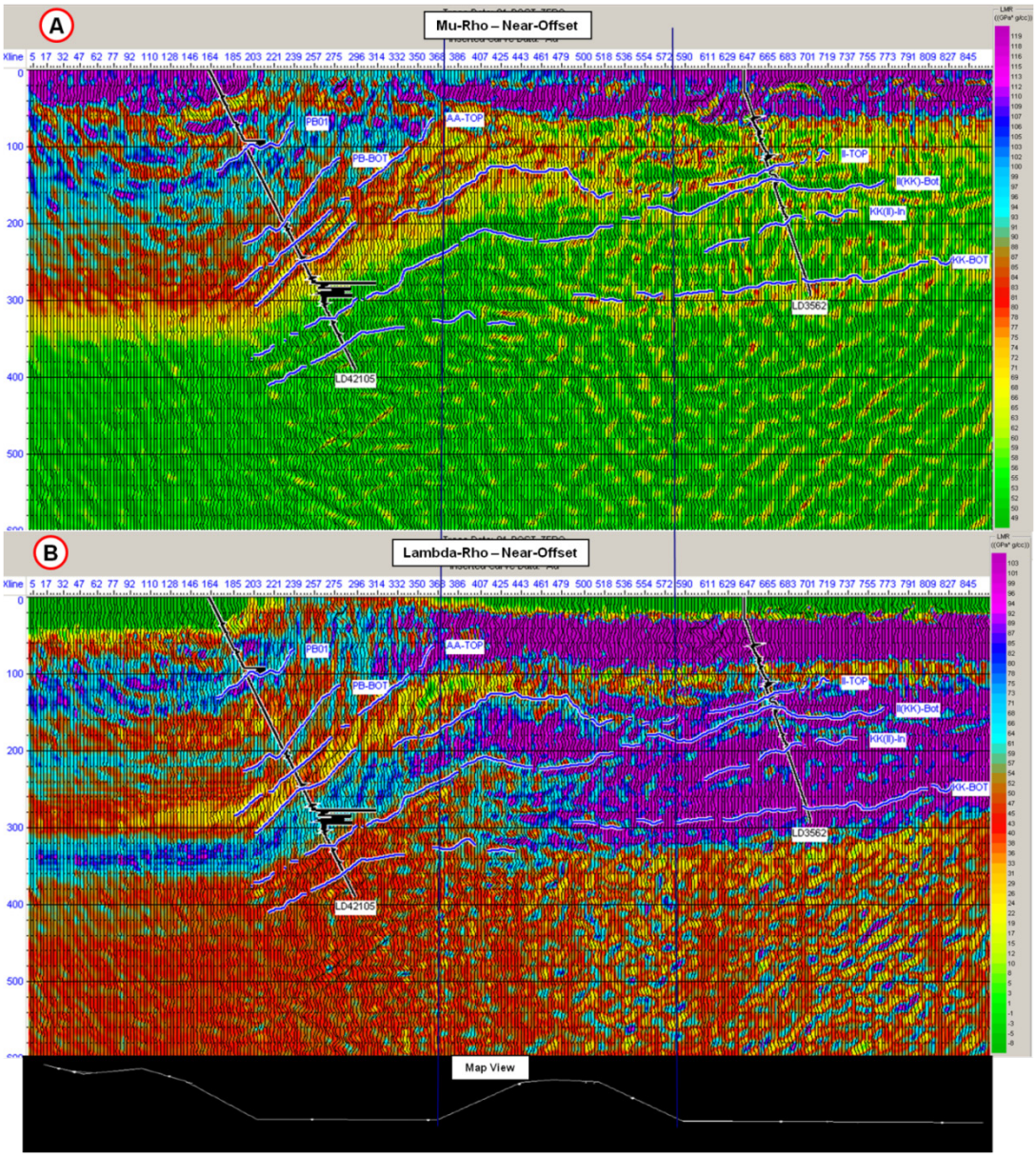

Figure 6-24. Mu-Rho (Top) and Lambda-Rho (bottom) predictions for the near-offset stacked Intrepid seismic line.

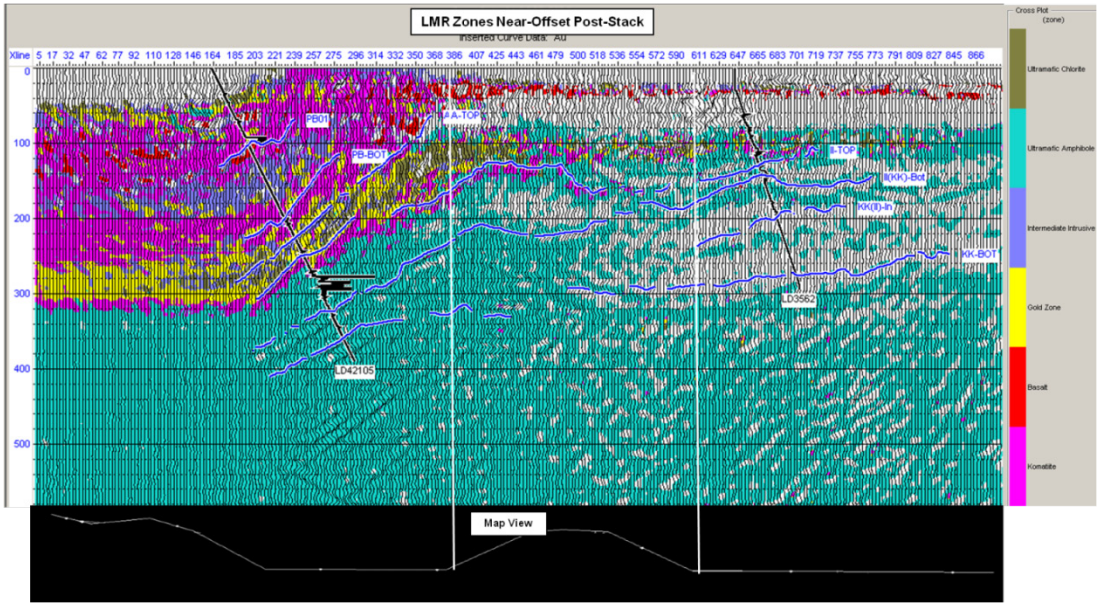

Figure 6-25. LMR cross-plotted zones applied to near-offset time converted PSDM for the Intrepid line.

6.4.4 Elastic Inversion Summary

Results for elastic inversion on the post-stack migrated Intrepid seismic line provided possible (not definitive) lithological prediction results. Sonic to seismic correlations were low but resulting inversions did provide support for ore zone separation based on harder and softer rock data. While these predictions are encouraging for target mining, the lack of borehole error analysis and low signal-to-noise ratio leaves the results unclear. Lambda-Mu-Rho predictions and cross plotting revealed possible rock separation results, but again require more borehole sonic logs for better calibration.

The most promising results came once again from the simultaneous use of acoustic and elastic inversions for ore zone predictions. Rock zones were more visible on seismic image using common impedances values as a basis for simultaneous cross-plotting.

6.5 Attribute Analysis

A final round of geostatistical analysis using waveform attributes was conducted on the Intrepid seismic line. The seismic attribute of instantaneous phase has already been used on the Intrepid seismic images to aid in rock-contact picking. Amplitude envelope and instantaneous frequency for the Intrepid seismic images are shown in Figure 6-26. The map

view of the Intrepid seismic line has been inset on Figure 6-26 to show effects of the crooked section of the seismic. Multi attribute analysis for impedance predictions were attempted to reveal more information than simple single attribute analysis did.

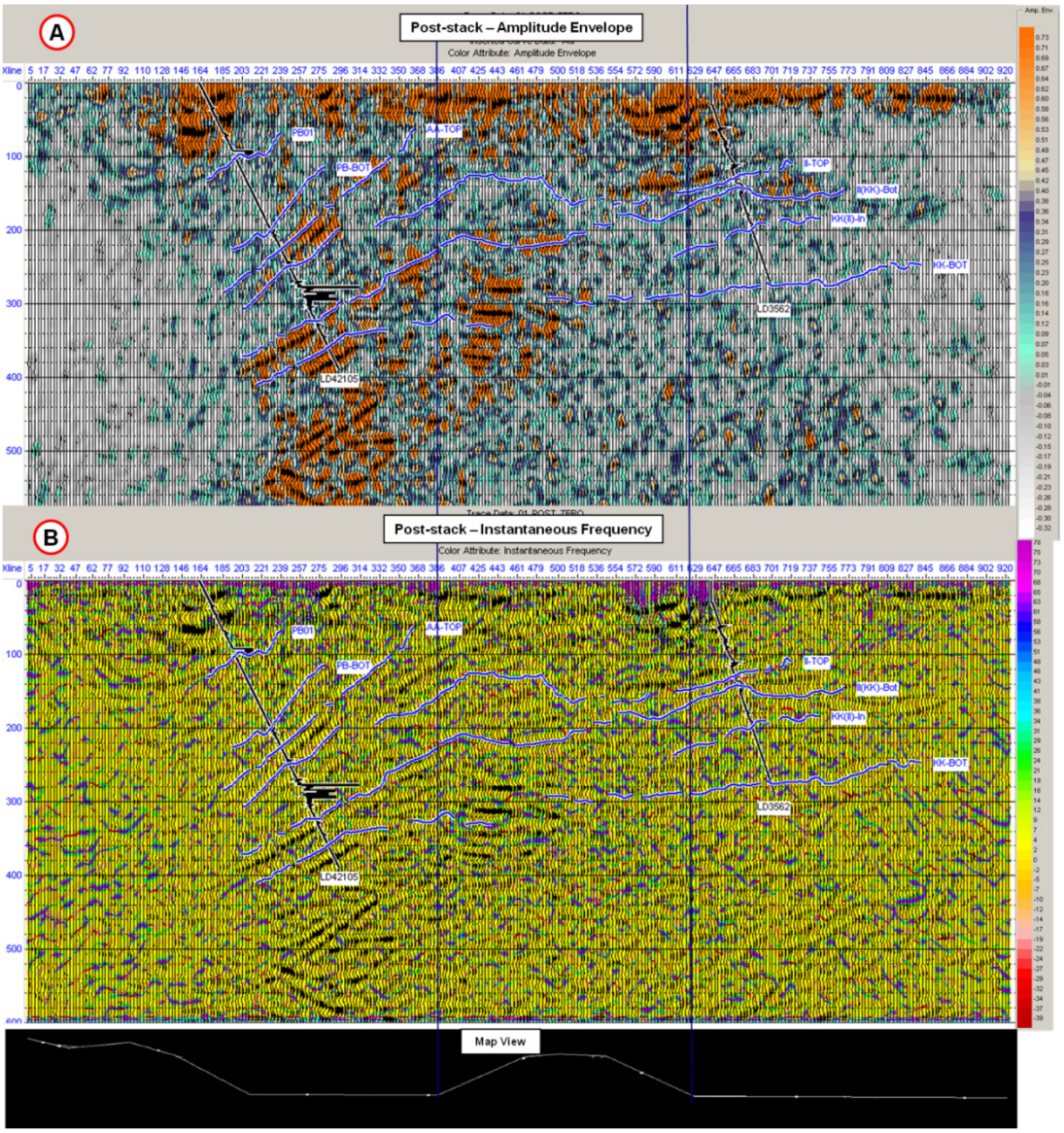

Figure 6-26. Amplitude envelope (A) and instantaneous frequency (B) for the post-stack Intrepid seismic line.

6.5.1 Impedance Predictions Using Attribute Analysis

Acoustic impedance predictions using attribute analyse were conducted to see how well their predictions compared against seismic inversions. Incremental operator lengths of 1 to 5 were chosen for step-wise regression to increase cross-correlation between log

impedance and attributes. Figure 6-27 displays the attributes used, and validation error attribute analysis prediction for acoustic impedance on the Intrepid seismic line. A neural network was trained and P-impedance prediction on the seismic image is shown on Figure 6-28. Overall, predictive alibility of results are inconclusive with simple low impedances predicted around known reflection on the seismic image.

Attribute analysis of elastic impedance was conducted on the near-offset image for elastic impedance inversion. Application of the neural network training throughout the seismic image is shown on Figure 6-29. The elastic impedance predictions appear fairly inconclusive once again for pinpointing lithology. The predicted lithology appears generally low impedance throughout the seismic image giving a smoothed appearance.

Neural network computations took an average of 70 minutes to generate these impedance predictions as compared to a few minutes for the acoustic and elastic impedance inversion. Poor results achieved most likely relate to low S/N ratio and the line crookedness.

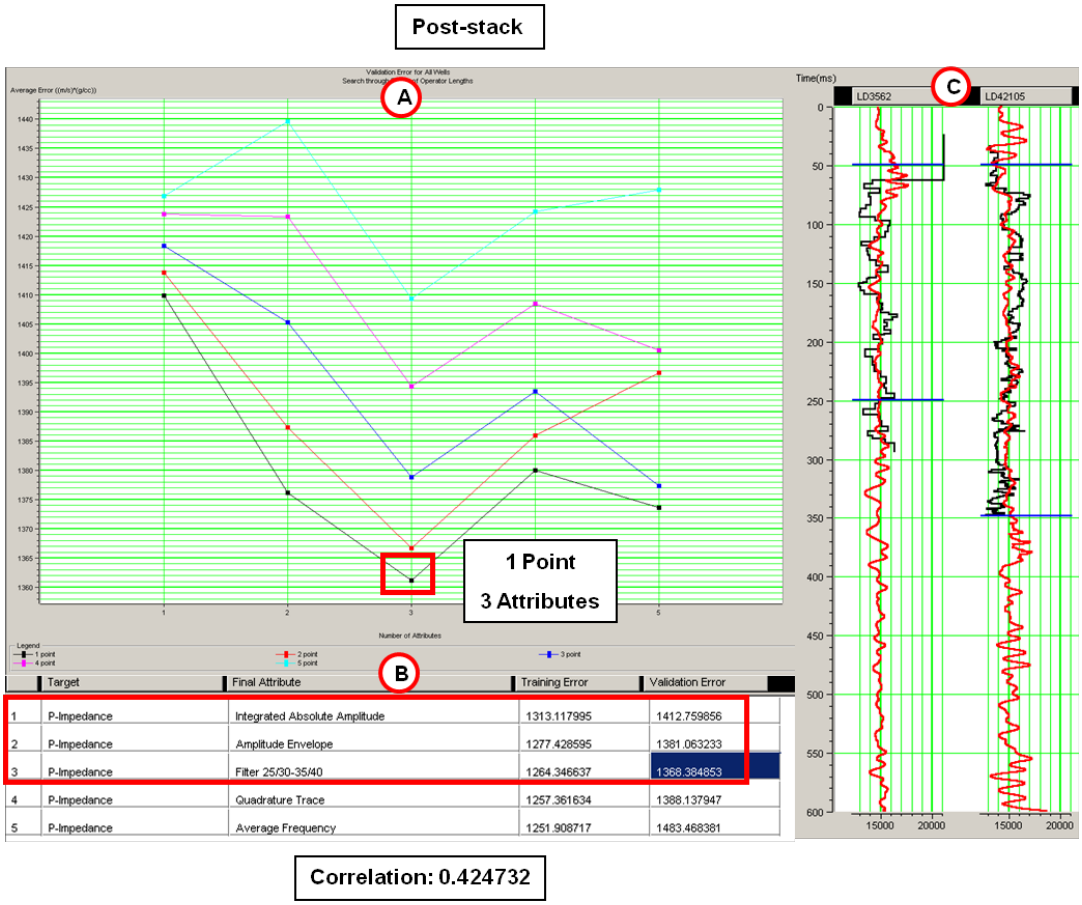

Figure 6-27. Results of multi-attribute analysis of acoustic impedance for the Intrepid seismic line. Validation error (A), attributes used (B) and prediction results along sonic (C) are shown.

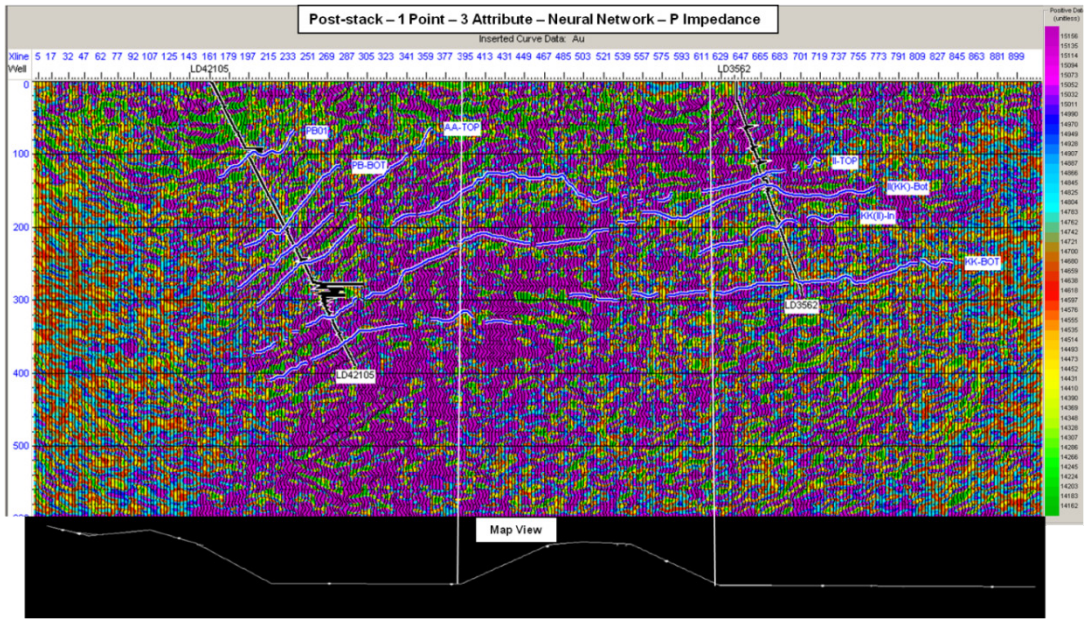

Figure 6-28. P-impedance predictions for attribute analysis on the Intrepid seismic line.

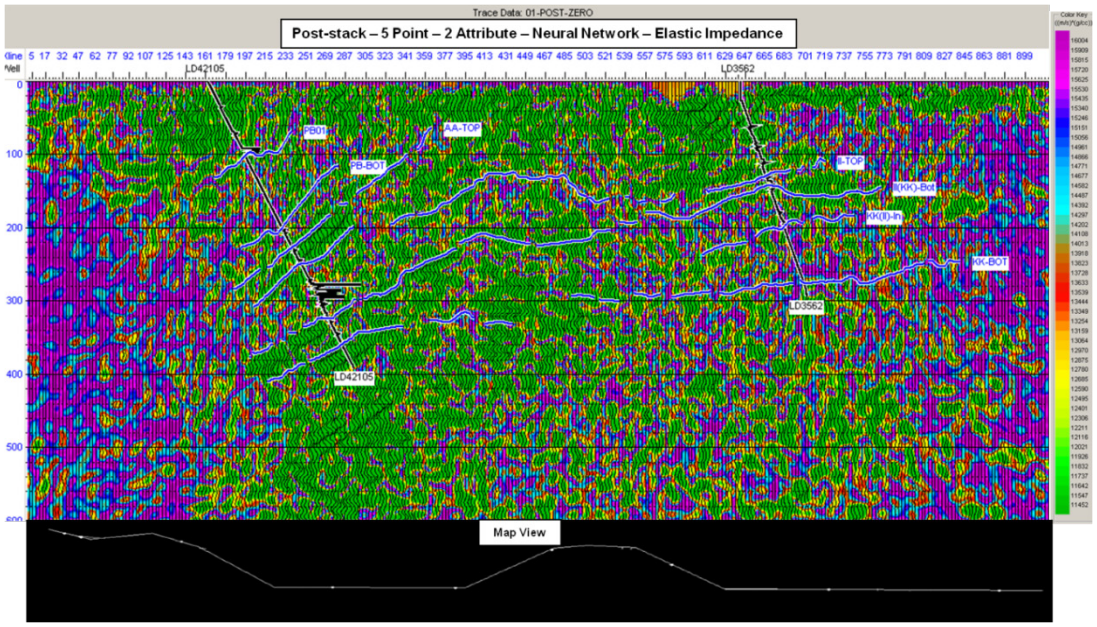

Figure 6-29. Elastic impedance predictions for attribute analysis on the Intrepid seismic line.

6.5.2 Combined Use of Acoustic Impedance, Elastic Impedance, and Attributes

With both acoustic and elastic impedance predictions being inconclusive from attribute analysis, it was hoped that simultaneously using both predictions would enhance their predictive ability. Cross-plots were created from attribute analysis predicted acoustic impedance and elastic impedance predictions around high gold content zones created based on rock characterization seen in Figure 6-8 and Figure 6-9. Cross-plotted results are shown on Figure 6-30. Dark grey indicates high impedance, light grey indicates low impedance, orange indicates acoustic impedance dominance, red indicates elastic impedance dominance, and yellow indicates where both acoustic and impedance dominate the image. Unlike simultaneous use of acoustic and elastic impedance inversions, the attribute analysis results are highly inconclusive. Complex attribute analysis for inversion testing appears ineffective without an increase in signal-to-noise ratio and more log data.

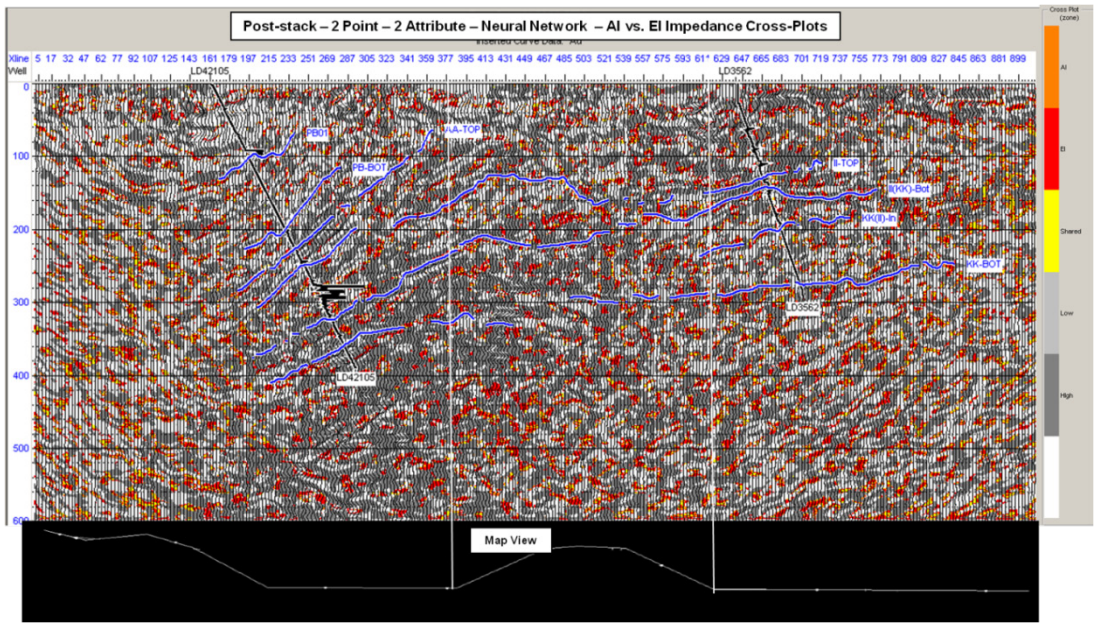

Figure 6-30. Simultaneous cross plotting acoustic and elastic impedance from attribute analysis on the Intrepid seismic line.

6.5.3 Gold-Content Predictions Using Attribute Analysis

Attribute analysis was tested one last time on the non-sonic log property of gold assessment. Two different attribute analysis processes were run: single attribute single

operator, and maximized number of attributes with maximized number of operators. Gold content predictions were made via neural networks and are shown on Figure 6-31. The correlation zones were limited to areas surrounding high gold-content on LD42105. Prediction areas are only valid below II-TOP (top of the Intermediate intrusive) and above KK-BOT (bottom of the Kambalda komatiite). "High" gold-content > 2000 ppb has been limited to red areas while "low" gold-content has been limited to blue areas. Both results are highly ambiguous. Single point, single attribute analysis predictions is erroneous. Multiple point multiple attribute show a possible distribution of gold content through the intermediate intrusive. Further attribute analysis was not possible without more borehole data for synthetic / seismic log calibration.

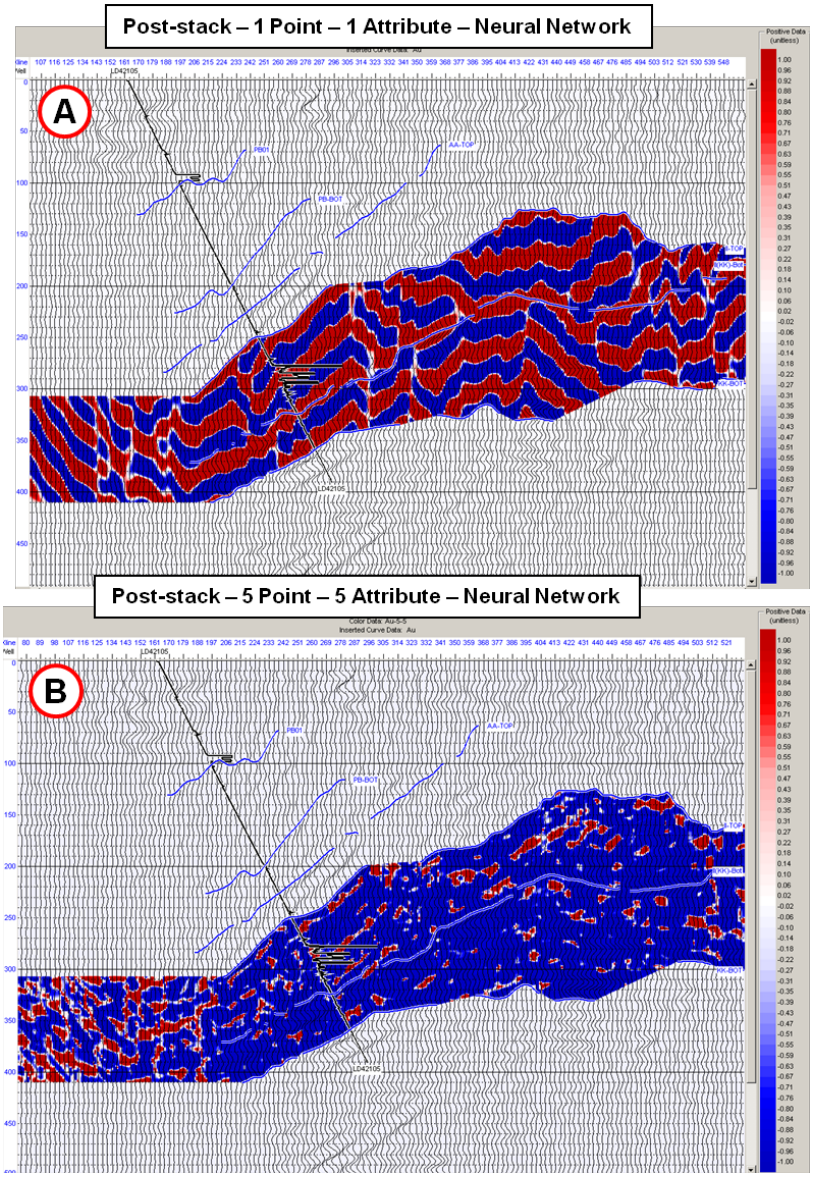

Figure 6-31. (A) single-attribute and (B) multi-attribute analysis for gold content of the post-stack seismic image.

6.5.4 Attribute Analysis Summary

The lack of borehole data for sonic calibrations and the crooked seismic line has hindered attribute analysis of the Intrepid seismic data. Gold content predictions were far less reliable than seismic inversions. More borehole and seismic data (3D most of all) are needed in this area for reliable prediction of gold content in rocks.

7 Conclusions, Discussions and Recommendations

"Every new beginning comes from some other beginning's end."

- **Attributed to Seneca the Younger (45 AD)**

7.1 On Seismic Imaging in Hard Rock Environments

Most of the shallow gold deposits in Western Australia Kambalda region have been discovered and/or mined out. New techniques to image deeper, more complex structures while facilitating lithological and mineralization prediction are required for future mineral exploration. Detailed processing and analysis of 2D seismic data along with the study of the relationship between the recorded wave-field and rock properties measured from borehole logs, core samples and open cut mining, provide a new means to reveal both shallow and deep mineral targets.

This study has shown that seismic imaging of both the East Victory and the Intrepid seismic lines were practical to reveal complex structures in hard rock environments. High-quality 2D images were produced for both seismic data sets revealing shear zones, faults, fractures, and thrusts. These images exposed structurally important information for mining particularly open-cut mining (100-200 metres). However, information concerning deep structural information (greater than 2000 metres) are essential to understand mesothermal fluid flow.

Hard rock seismic data processing is not trivial in general. Processing of both the East Victory and Intrepid seismic data proved no exception to this, and in fact proved to be a challenging task when processing is directed towards data preparation for inversion. Low signal-to-noise ratio, regolith signal distortions, and crooked seismic lines confounded imaging results on both data sets. Despite these challenges, analyses showed that acquiring good seismic imaging in hard rock environments is reducible to several key processes.

Effective seismic imaging requires high signal-to-noise ratios and in the case of 2D seismic the seismic line must be strictly and optimally oriented with respect to the main geological dip in the area. An improved signal-to-noise ratio can be achieved by increasing seismic source strength and/or by increasing nominal fold. The complex hard rock environment also requires very fine spatial sampling of the wavefield. Very large source-to-receiver separation is often required to capture energy reflected off steeply dipping structures, ever present in this environment. The last two factors call for a large number of active seismic channels which can prove difficult to deploy in active mine environments. Even if large numbers of channels are deployed, keeping the line direction straight and orthogonal to main geological dips would be significantly difficult.

Typically, very high levels of ambient noise in active mine sites along with the often poor source/receiver ground coupling due to mine site infrastructure presents difficulties for the application of seismic methods in hard rock environments. Finally in an all-out hard-rock environment, such as found in the Yilgarn craton, the contrasts in elastic properties of various rock units are often very small. While the application of seismic methods in hard-rock environments is very attractive, addressing the requirements and difficulties involved in the necessary inversion of seismic data and connection/correlation of acoustic impedance to underground lithology is not a trivial process.

The importance of acquiring straight, or near-as-possible straight, seismic lines can be observed when comparing the imaging results of the East Victory seismic line to the far more crooked Intrepid seismic line. Map views of the East Victory (Figure 4-1) and Intrepid seismic lines (Figure 6-1) illustrate the contrast of the acquisition geometry of the two data sets. Final seismic imaging on the East Victory seismic line (Figure 4-8) revealed excellent detail in both complex shallow and deep structure. Surface and mine interpretations confirmed locations of reflections on the East Victory seismic image including the Boulder-Lefroy fault, the Foster thrust, and the Condenser dolerite from as shallow as 100 metres to as deep as 5 kilometres. The Intrepid seismic image (Figure 6-5) also reveals structural information but the results are less reliable due to the misalignment of the seismic line with dominant geological trends. Reflection detail is imaged on the western section of the Intrepid seismic image, but significant reflection information is absent as seen on Figure 6-5. The Intrepid line is an example where the acquisition objectives had to be compromised by existing ground conditions.

The key processing step required for good seismic imaging in hard rock environments is elimination of travel-time delays caused by regolith heterogeneities. Regolith-caused travel-time distortions on both seismic lines were compensated for by "homogenizing" this layer through statics corrections as illustrated in Chapter 4.1 (Figure 4-4). Geological foreknowledge of the thickness of the regolith, as evidenced from bore-hole data, magnetic analyses, and gravity surveys (Chapter 3 Geological Setting of the St. Ives Gold Camp) are useful for verifying the statics correction solutions.

Hard rock environments are often considered as a "constant velocity medium", assuming that most of the rock velocities oscillate around 6000 m/s. This research showed that this is not the case and that the precision of images is highly dependent on accurate velocity modelling as used for both stacking and migration, particularly pre-stack depth migration. Because of high structural complexity in hard rock environments, inverse modelling or migration is a necessity to position reflections accurately in their true subsurface positions. However, due to intrinsically low S/N in hard-rock environments, an oil type approach of common image gather analysis for velocity model building, is difficult to implement. Instead, the most practical approach, in this instance, is to utilise *a priori* geological knowledge, log data and core sample measurements. If these data are unavailable then constant velocity stacks could be used to generate geologically-plausible velocity models. For the application of pre-stack imaging techniques utilizing post-stack depth migrated images for initial velocity model building is also useful. The importance of migration velocities in hard rock environments relates to potentially large horizontal displacement errors due to very fast velocities used. Related to that is the migration aperture which can produce overwhelming noise ("smiles") if significantly wrong velocities are used in migration. For the successful calibration of seismic images with sonic logs from hard-rock environments, an accurate migrated image proved vital to enable subsequent rock characterization.

7.2 Sonic Logging in Hard Rock Environments

The research conducted in this thesis shows that sonic logging is necessary for rock characterisation in hard rock environments. Rock type, structure type, alteration type, and even gold-content have been shown to exhibit statistically discernible characteristics based

solely on their sonic properties. Indeed, even with a restricted number of sonic logs, five in the case of the East Victory line, and two in the case of the Intrepid line, a strong base for lithology identification and gold prediction is developed. Hence, this type of information is shown to be under-utilized in mineral exploration in hard-rock environments.

The sonic logs from both the East Victory and Intrepid seismic lines were comprehensively analysed by re-sampling and separating of the data based on rock type, structure type, alteration type, and Au assay. This compiled data was subsequently used to produce a variety of cross-plots such as Log(ρ) versus log(Vp) (Figure 4-10), Vp/Vs ratio, acoustic impedance (Figure 4-11, and Figure 4-12), elastic impedance (Figure 4-15), and lambda-mu-rho (Figure 4-20, Figure 4-21, and Figure 6-12). The purpose of cross-plotting was to produce meaningful statistical results that could be used to derive empirical relationships between various seismic attributes and geology for these areas. Indeed, regression analysis consistently revealed that softer rocks (e.g., intermediate intrusive, mafic, and volcaniclastic), had sonic properties discernible from harder rocks (e.g., basalt, and dolerite). Classification changes within the sonic data further revealed that shear zones, within both basalts, and dolerites, had distinctive sonic properties. With high Au content being associated with softer intermediate intrusive, komatiites, and sheared dolerites, (Figure 4-13, Figure 4-14, Figure 4-16, Figure 6-7, Figure 6-8, and Figure 6-9), sonic logging can be seen as adding more precision to direct targeting of mineralised zones.

A library of synthetic reflection responses derived from each sonic log indicated that synthetic seismic reflections were mainly associated with structural changes (specifically shear zones), and then rock type (Table 4-6). The synthetic responses were of particular interest at high gold-content rock boundaries where harder rocks are often found in contact with softer rocks creating significant reflectivity differentiation (Figure 4-19 and Figure 6-11). Modelling of rock contacts further indicated that high gold-content soft rock zones would have distinctive amplitude versus offset (AVO) responses when in contact with harder rock zones (Figure 4-18 and Figure 6-10). Correlation of the synthetic seismograms and seismic data was necessary to assess whether sonic log synthetic-derived reflections were true representations of the earth under the seismic lines. Multiple iterations of synthetic-seismic reflection matching, sonic log stretching and wavelet extraction were required to calibrate both the East Victory (Figure 5-3) and Intrepid (Figure 6-14) seismic images to their respective borehole data sets. These calibrations provided proof those

reflections on the seismic images, especially high-amplitude reflections, correlated well with physical rock properties within the sonic data. However, the degree of correlation between the two data sets varied with signal-to-noise ratio, the crookedness of the line, and availability of borehole information. Nonetheless, for hard rock environments, successful seismic-to-sonic correlation was achieved which paved the way for lithological predictions through seismic inversion.

7.3 Volumetric Interpretation in Hard Rock environment

Two types of data representing two very different scales in rock property measurement were comprehensively studied in this research. The first data set was comprised of small-scale sonic log measurements which resolved rock properties on the centimetre scale. The second type of data was the seismic data, revealing valuable large-scale structural information on the 10's of meters along both the East Victory and Intrepid seismic lines. The scale differences between the two data sets were bridged through the calibration of synthetic seismograms generated from the sonic data with the structurally correct seismic images. These calibrations provided the final step to the investigation of the feasibility of rock characterization for mineral exploration using seismic data.

Since a limited amount of data was available to this research, multiple seismic inversions were executed to develop statistically relevant rock characterization results. Sonic log "hiding" was conducted by excluding boreholes from inversions, and subsequently revealing the borehole to the inversion, and cross-checking the results against the sonic data. Analyses indicated that Model-based (Figure 5-9, and Figure 6-21 (A)), Band-limited (Figure 5-10), and Sparse-Spike (Figure 5-11, and Figure 6-21 (B)) acoustic inversions resulted in the most accurate correlations for the East Victory and Intrepid seismic lines. Inversion results on the East Victory line showed good separation between harder rock zones, (the Condenser dolerite), and softer rock zones, (high gold-content intermediate intrusives). Lithological predictions on the Intrepid data set were not as successful due to the crooked nature of the seismic line and the limited amount of sonic logs available for that location.

To delve deeper into rock characterization, elastic inversion was tested using partial offset stacks for both the East Victory and Intrepid data sets. The angle-dependency of elastic inversions required both sets of seismic data to be re-processed to generate near-offset and far-offset stacks for migration. Reprocessing the two seismic images showed that near-offset stacks (Figure 5-12 (B), and Figure 6-19 (A)) produced better shallow images (under 1000 metres) and far-offset stacks (Figure 5-12 (C), and Figure 6-19 (B)) produced more accurate deeper images (over 3000 metres). Recalibrations of the seismic and sonic data were conducted on those stacks and subsequent elastic inversion was conducted. Regression analysis revealed that Model-Based (Figure 5-20, and Figure 6-21 (A)), Band-limited (Figure 5-21) and Sparse-Spike (Figure 6-21 (B)) elastic inversions were again the most accurate. Indeed, the Condenser dolerite and high gold-content intermediate intrusive rock zones were again identifiable on the East Victory seismic inversions. Elastic inversion results for the Intrepid line were again more "blurred" due to the reason previously discussed.

To enhance lithological prediction results, simultaneous investigation of respective Model-Based, Band-Limited, and Sparse-Spike acoustic and elastic inversions was conducted for both the East Victory and Intrepid lines. Cross-plots were generated for near-offset and far-offset and acoustic and elastic impedance from values extracted around gold-bearing zones on each set of data. Zones were created on the cross-plots based on acoustic impedance and elastic impedance data found from known gold zones on the East Victory (Figure 4-12, Figure 4-13, Figure 4-14 and Figure 4-16) and Intrepid (Figure 6-7, Figure 6-8, and Figure 6-9) sonic log analysis. Plotting of results revealed excellent differentiation between softer and harder rocks on the East Victory line (Figure 5-23). The harder Condenser dolerite once again stood out from softer intermediate rock formations. Simultaneous acoustic and elastic impedance investigations on the Intrepid line did delineate known rock contacts of high gold-content komatiite (Figure 6-23) and did show good separation between known rock formations, however, verification was difficult due to lack of data for cross-referencing.

Lambda-mu-rho (LMR) were also computed from both the East Victory and Intrepid seismic data. Cross-plotting each seismic line in respect to sonic data based on Lambda-Rho versus Mu-Rho (Figure 4-20 and Figure 6-12) revealed good separation between harder and softer rocks. With no S-wave seismic data available, near-offset stacked seismic data

was substituted on both seismic lines to conduct LRM calculations. The quasi-LMR results for the East Victory line (Figure 5-25) were once again superior to Intrepid line (Figure 6-25) with the Condenser dolerite being imaged well using cross-plot zoning (Figure 6-12).

A final study of rock characteristics incorporated a family of selected seismic attributes. By considering the relatively low S/N ratio, and to ensure stable results, the neural network computation was restricted to a limited number of seismic attributes which could have physical meaning in hard rock environments. These basic attributes include instantaneous frequency, amplitude envelope, and instantaneous phase. Neural networks were then used to predict both P-wave velocities and acoustic impedances.

The attribute analysis results on both East Victory and Intrepid seismic data showed low correlation with sonic and seismic data. Indeed results of both reflection imaging and statistical analysis on both the East Victory (Figure 5-31, Figure 5-34, and Figure 5-35), and the Intrepid lines (Figure 6-28, Figure 6-29, and Figure 6-30) did not reveal as clear predictions as either acoustic or elastic inversions. The Condenser dolerite and high gold-content intermediate intrusive on the East Victory seismic line were less distinguishable from each other on the attribute plots. To push multi-attribute analysis further, non-sonic predictions of gold-content were tested on both the East Victory (Figure 5-36) and Intrepid (Figure 6-31) data sets. A generous “tweaking” of the attribute parameters on the Au predictions produced interesting volumetric results on both data sets. Overall, due to lack of sonic data for further validation, all attribute analyses results can be accepted as merely the first step towards further research. Clearly, a greater quantity of sonic data is required before the actual value of hard rock attribute analysis can be fully evaluated.

7.4 Hard Rock Seismic Exploration

In general, a detailed processing and analysis of 2D seismic data and the study of the relationship between the recorded wave-field and rock properties measured from borehole logs, core samples, and open-cut mining, revealed that a significant degree of correlation between the two data sets is achievable. More specifically, the following can be stated:

- Seismic imaging in hard rock environments can be successful and can even produce sufficient signal-to-noise ratios required for detailed interpretation of such complex environments.
- Synthetic seismograms can be successfully calibrated to seismic data in hard rock environments, resulting in physical meaning in regards to the reflection information.
- Sonic logging revealed that softer and harder rocks, as well as sheared and un-sheared rock were distinguishable from each other based on sonic parameters. Subsequent numerical modeling and well-tying confirmed that indeed soft/hard rock separation is possible based on both general reflectivity patterns and also impedance contrasts.
- Comprehensive analysis of seismic and borehole data revealed that high gold-content rock had unique identifiable properties that differentiate it from surrounding host rock properties. This gives rise to direct detection of gold bearing formations from reflection seismic data!
- Acoustic inversions revealed that the most accurate impedance prediction results were achieved through Model-Based, Band-Limited, and Sparse-Spike inversion. Elastic inversions revealed impedance predictions but appeared more generalized in overall shape, with the most accurate being Model-Based inversion, and Band-Limited inversion.
- Simultaneous use of acoustic and elastic inversions produced more stable results and provided an improved separation of softer and harder rock zones. Similarly, Lambda-Mu-Rho inversions showed good separations between softer and harder rock zones.
- Attribute analysis produced interesting predictions of Au content, however results are ambiguous and further research-grounded truth is needed to verify its value.

The ultimate conclusion of this study is that rock characterization in hard rock environments is possible even with 2D seismic data. This further suggests that 3D seismic inversion could prove a powerful tool for mineral exploration!

7.5 Mineral Exploration in the Future

This study shows that the application of seismic methods for mineral exploration has very good potential. So "Where do we go from here?" The easy answer to this question is "Acquire more and better data". While a point of diminishing returns exists, as is the case with any type of survey, the more data available to the study, the more significant the correlation between data sets and the more trustworthy the earth-model generated. To further advance mineral exploration by seismic methods the following is necessary:

- Acquisition of more accurate and deeper borehole sonic logs,
- Acquisition of check shots (that is nowadays (VSP))
- Application of three-dimensional (3D) seismic reflection surveys.

Increasing the number, accuracy, and depth of borehole sonic logs is fundamental for reliable *in situ* sonic rock-property measures and subsequent sonic-seismic data calibration. This research showed that a restricted number of sonic logs allowed for reasonable lithological and mineralogical predictions to be generated for volumetric models of the earth. However, a greater number of sonic logs will make predictions far more statistically correct and increase the possibility for direct targeting of mineral resources from seismic data. Acquiring of at least one sonic log, drilled to a minimum of 1000 metres for every 1.5 kilometres of seismic survey is recommended for inversion of seismic data. However, for accurate time-to-depth relationship, necessary for high quality well-tie and thus borehole to seismic correlation, check-shot information is needed.

Check-shots are not readily achievable in hard rock environments due to borehole diameter being very narrow and hence not allowing for conventional VSP tools. Borehole stability is another issue that often prevents accurate measurements. Consequently new concepts and different tools are needed to enable routine application of borehole seismology in hard rock environments. The recent investigations of Greenwood et al., 2009, suggest that VSP methods can have an important role in mineral exploration.

Ultimately the future of mineral exploration rests on three-dimensional (3D) seismic acquisition. While the survey design and processing parameters are far more elaborate, the rewards of 3D acquisition include: superior complexity imaging for precise mineral-zone targeting, higher signal-to-noise ratio through larger folds, and superior

shallow and simultaneous deep-reflection imaging due to illumination of dips at all angles from variety of survey offsets and azimuths. Urosevic et al (2008) have documented this in recent years.

Clearly the exploration of mineral resources by seismic methods today looks much brighter than only several years ago!

References

Adam, E., Perron, G., Milkereit, B., Wu, J., Calvert, A.J., Salisbury, M., Verpaelst, P., and Dion, D.J., 2000, A review of high-resolution seismic profiling across the Sudbury, Selbaie, Noranda, and Matagami mining camps.: Canadian Journal of Earth Science, **37**, 503-516.

Adams, D., 1979, The Hitchhikers Guide to the Galaxy: Del Ray.

Aki, K., and Richards, P.G., 1980, Quantitative Seismology: Freeman and Co.

Al-Yahya, K., 1989, Velocity analysis by iterative profile migration: Geophysics, **54**, no. 6, 718-729.

Barnes, A.E., 2006, Redundant and useless seismic attributes: Geophysics, **72**, P33- P38.

Becquey, M., Lavergne, M., and William, C., 1979, Acoustic impedance logs computed form seismic traces: Geophysics, **9**, 1485-1501.

Box, R., and Lowrey, P., 2003, Reconciling sonic logs with check-shot surveys: Stretching synthetic seismograms: The Leading Edge, **June** 510-517.

Bradford, J.H., Liberty, L.M., Lyle, M.W., Clement, W.P., and Hess, S., 2006, Case study: Imaging complex structure in shallow seismic-reflection data using pre-stack depth migration: Geophysics, **71**, B175-B181.

Brown, A.R., 2000, Understanding seismic attributes: Geophysics, **66**, 47-48.

Bruhn, R.L., Parry, W. T., Yonkee, W. A., and Thompson, T., 1994, Fracturing and Hydrothermal Alteration in Normal Fault Zones: Geophysics, **142**, 609-644.

Buchholtz, H., 1972, A note on single distortion due to dynamic (NMO) corrections: Geophysical Prospection, **20**, 395-402.

Cambois, G., 1998, AVO attributes and noise: pitfalls of crossplotting: EAGE Abstract, 2-14.

Canales, L.L., 1984, Random noise reduction: 54th Annual Internat. Mtg., Soc. Expl. Geophys., **Expanded Abstracts**.

Cassidy, K.F., and Hagemann, S. G. , 2001, 'World Class' Achaean orogenic gold deposits eastern Yilgarn Craton: Diversity in timing, structural controls and mineralization styles: Geoscience Australia 2001, 382-384.

Castagna, J.P., and Backus, M.M., 1993, AVO analysis-tutorial and review, in Offset-dependent reflectivity - Theory and practice of AVO analysis: Soc. Expl. Geophys, 3-37.

Castagna, J.P., Batzle, M.L., and Eastwood, R.L., 1985, Relationships between compressional-wave and shear-wave velocities in clastic silicate rocks: Geophysics, **4**, 571-581.

Chabot, L., Henley, D.C., Brown, R.J., and Bancroft, J.C., 2002, Single-well seismic imaging using full waveform sonic data: An update: Presented at SEG Int'l Exposition and 72nd Annual Meeting

Chopra, S., and Marfur, K. J., 2005, Seismic attributes - A historical perspective: Geophysics, **70**, 3S0-28SO.

Connolly, P., 1999, Elastic impedance: The Leading Edge, **April**, 438-445.

Cox, M.J.G., 1999, Static corrections for seismic reflection surveys: Society of Exploration Geophysicists.

Cox, S.F., and Ruming, K., 2004, The St Ives mesothermal gold system, Western Australia – a case of golden aftershock: Journal of Structural Geology, **26**, 1109-1125.

Domenico, S.N., 1984, Rock lithology and porosity determination from shear and compressional wave velocity: Geophysics, **49**, 1188-1195.

Drummond, B.J., Goleby, B. R., Own, A. J., Yeates, A. N., Swager, C., Zhang, Y., and Jackson, J. K., 2000, Seismic reflection imaging of mineral systems: Three case histories: Geophysics, **65**, 1852- 1861.

Eastwood, J., 2002, The attribute explosion: The Leading Edge, **October**, 994.

Evans, B.J., 1997, A Handbook for Seismic Data Acquisition in Exploration: Society of Exploration Geophysics.

Faye, J.-P., and Jeannot, Jean-Paul., 1986, Prestack migration velocities from focusing depth analysis: Presented at 56th Annual International Meeting SEG

Gardner, G.H.F., Gardner, L.W., and Gregory, A.R., 1974, Formation velocity and density – The diagnostic basics for stratigraphic traps: Geophysics, **39**, 770-780.

Gassmann, F., 1951, Über die elastizität poröser medien: Vierteljahresschrift der Naturforschenden Gesellschaft in Zurich., **96**, 1-23.

Goodway, W., Chen, T. and Downton, J., 1997, Improved AVO fluid detection and lithology discrimination using Lame' petrophysical parameters: "λρ","μρ", & "λμ/ fluid stack", from P and S inversions: 68th Ann. Int. SEG Mtg, 183-186.

Greenhalgh, S.A., and Mason, I. M., 1997, Seismic imaging with application to mine layout and development, in Gubins, A., Ed., Geophysics and geochemistry at the millennium: Proc. Exploration 97 Fourth Decennial Internat. Conf. on Mineral Expl., 585–598.

Greenhalgh, S.A., Mason, Iain M., Sinadinovski, and Cvetan, 2000, In-mine seismic delineation of mineralization and rock structure: Geophysics, **65**, no. 6, 1908-1919.

Greenwood, A., M. Urosevic, and A. Kepic, 2009, Feasibility of the application of borehole seismology for hard rock exploration: Exploration Geophysics.

Groves, D.I., Barley, M. E., Barnicoat, A. C., Cassidy, K.F., Fare, R. J., Hagemann, S. G., Ho, S. E., Hronsky, J. M. A. Mikucki, E. J., Mueller, A. G., McNaughton, N. J., Perring, C. S., Ridley, J. R., and Vernecombe J. R., 1992, Sub-greenshist to granulite-hosted Archean lode-gold deposits of the Yilgarn Craton: A depositional continuum from deep-sourced hydrothermal fluids in crustal scale plumbing systems: Key centre for Strategic Mineral Deposits, Department of Geology, University of Western Australia, Publication, **22**, 325-337.

Guliyev, E., and Michelena, Reinaldo J., 2006, Application of multicomponent seismic for Vp-Vs ratio extraction: tight gas sandstones example, Rulison Field, Colorado: Presented at SEG Annual Meeting

Gulunay, N., 1986, Fx decon and complex wiener prediction filter: 56th Annual Internat. Mtg., Soc. Expl. Geophys., **Expanded Abstracts**.

Guo, N., and Fagin, S., 2002, Becoming effective velocity-model builders and depth imagers, Part 1 – The basics of prestack depth migration: The Leading Edge, **December**, 1205-1209.

Hale, D., 1995, DMO processing: Society of Exploration Geophysics.

Hammer, P.T.C., Clowes, R.M., and Ramachandran, K., 2004, Seismic reflection imaging of thin, kimberlite dykes and sills: exploration and deposit characterization of the Snap Lake dyke, Canada: Lithos, **76**, 259-367.

Hampson-Russell, 2007a, Guide to Emerge, p. PDF in the Hampson-Russell software package.

—, 2007b, Guide to Strata, p. PDF in the Hampson-Russell software package.

Hampson, D.P., Schuelke, James S., and Quirein, John A., 2001, Use of multiattribute transforms to predict log properties from seismic data: Geophysics, **66**, no. 1, 220-236.

Harrison, C.B., Urosevic, M., and Stolz, E., 2007, Processing, inversion and multi-attribute analysis of the Intrepid seismic line at the St. Ives gold camp, Western Australia: Presented at Society of Exploration Geophysicists Annual Meeting

Hart, B.S., 2002, Validating seismic attribute studies: Beyond statistics: The Leading Edge, **October**, 1016-1021.

Hatherly, P.J., Urosevic, M., Lambourne, A., and Evans, Brian.J., 1994, A simple approach to calculating refraction statics corrections: Geophysics, **59**, no. 1, 156-160.

Hearst, R.B., 1998, Reflections on Kimberlite: A Seismic Adventure: SEG Expanded Abstracts.

Hilterman, F., 1990, Is AVO the seismic signature of lithology? A case history of Ship Shoal-South Addition: The Leading Edge, **June**.

Ikwuakor, K.C., 2006, The Vp/Vs ratio after 40 years: Uses and abuses: Presented at SEG, New Orleans

Jackson, D.D., 1972, Interpretation of inaccurate, insufficient and inconsistent data: Gephys. J. Roy. Astr. Soc., **28**, 97-109.

Juhlin, C., and Palm, H., 2003, Experiences from Shallow Reflection Seismics over Granitic Rocks in Sweden *in* Geophysicists, S.o.E., eds., Hardrock Seismic Exploration, 93-109, Society of Exploration Geophysicsts.

Kallweit, R.S., and Wood, L.C., 1982, The limits of resolution of zero-phase wavelets: Geophysics, **47**, 1035-1046.

Lafond, C.F., and Levander, A.R., 1993, Migration moveout analysis and depth focusing: Geophysics, **58**, 91-100.

Landro, M., 2004, Vp-Vs ratio versus effective pressure and rock consolidation - a comparison between rock models and time-lapse AVO studies: Presented at SEG Int'l Exposition and 74th Annual Meeting

Larroque, M., Postel, J. J., Slabbert, M., and Duweke, W., 2002, How 3D seismic can help enhance mining: EAGE 64th Conference & Exhibition, Expanded abstract.

Latimer, R.B., and Van Reil, P., 2000, An interpreter's guide to understanding and working with seismic-derived acoustic impedance data: The Leading Edge, **March**, 242-249.

Levin, S.A., 1989, Surface-consistent deconvolution: Geophysics, **54**, no. 9, 1123-1133.

Libby, J., Groves, D.I., and Vearncombre J.R., 1991, The nature and tectonic significance of the crustal-scale Koolyanobbing Shear Zone, Yilgarn Craton, Western Australia: Australian Journal of Earth Science, **38**, 229-245.

Lindseth, R.O., 1979, Synthetic sonic logs – a process for stratigraphic interpretation: Geophysics, **44**, no. 1, 3-26.

Liner, C.L., 1999, Concepts of normal and dip moveout: Geophysics, **64**, 1637-1647.

Lines, R.L., and Newrick, R.T., 2004, Fundamentals of Geophysical Interpretation: Society of Exploration Geophysicists.

Machiavelli, N., 1512, The Prince.

Malehmir, A., and Bellefleur, G., 2009, 3D seismic reflection imaging of VHMS deposits: Insights from re-processing of the Halfmile Lake data, New Brunswick, Canada: Presented at Annual SEG meeting, workshop: "The state of the science in the use of seismic methods for mineral exploration". Extended abstract of 4 pages

Marfurt, K.J., 2006, Seismic attribute mapping of structure and Stratigraphy: 2006 Distinguished Instructor short course notes, SEG EAGE.

Meyers, J.B., Worral, L., Lane, R., and Bell, B., 2001, Exploring through cover - the integrated interpretation of high resolution aeromagnetic, AEM and ground gravity data from the Grants Patch area, Eastern Goldfields Province, Archaean Yilgarn Craton, part C: Combining geophysical methods for a holistic exploration model: Exploration Geophysics, **32**, 198-202.

Milkereit, B., Berrer, E.K., King, A.R., Watts, A.H., Robertrs, B., Adam, E., Eaton, D.W., Wu, J., and Salisbury M., 2000, Development of 3-D seismic exploration technology for deep nickel-copper deposits - A case history from the Sudbury basin, Canada: Geophysics, **65**, 1890-1899.

Nedimovic, M.R., and West, G.F., 2003a, Crooked-line 2D seismic reflection imaging in crystalline terrains: Part 1, data processing: Geophysics, **68**, 274-285.

—, 2003b, Crooked-line 2D seismic reflection imaging in crystalline terrains: Part 2, migration: Geophysics, **68**, 286-296.

Nelson, R.G., 1984, Seismic Reflection and Mineral Prospecting: Exploration Geophysics, 15, 229-250.

Neumayer, P., Walshe, J. L., Horn, L., Petersen, K., Deyell, C., Moran, K., Howe, D., Connors, K., Stolz, E., Morrison, R. S., and Hagemann, S.G., 2004, Hydrothermal alteration footprints and gold mineralization in the St Ives gold camp, Predictive mineral discovery: Presented at CRC Conference

Neves, F.A., Zahrani, M.S., and Bremkamp, S.W., 2004, Detection of potential fractures and small faults using seismic attributes: The Leading Edge, **September**, 903-906.

Pasasa, L., Wenzel, Friedemann., and Zhao, Ping., 1998, Prestack Kirchhoff depth migration of shallow seismic data: Geophysics, **63**, no. 4, 1241-1247.

Potter, C.C., and Stewart, R.R., 1998, Density prediction using Vp and Vs sonic logs: CREWES Research Report 1998, **10**.

Pretorius, C.C., Termick, W. F., and Irons, C., 1997, Applications of 3-D seismic to mine planning at Vaal Reefs Gold Mine, number 10 shaft, Republic of South Africa.

Roberts, B., Zaleski, E., Perron, G., Adam, E., Larry P., and Salisbury, M., 2003, Seismic exploration of the Manitouwadge Greenstone Belt, Ontario: A Case History, *in* Geophysicists, S.o.E., eds., Hardrock Seismic Exploration, 110-126, Society of Exploration Geophysicists.

Russell, B.H., 2006, Introduction to Seismic Inversion Methods, *in* SEG, ed., Course Notes Series, No. 2: Tulsa, OK, SEG.

Russell, B.H., Hampson, D., Schuelke, J., and Quirein, John., 1997, Multiattribute seismic analysis: The Leading Edge, **16**, no. 10, 1439-1443.

Rutherford, S.R., and Williams, R.H., 1989, Amplitude-versus-offset in gas sands: Geophysics, **54**, 680-688.

Salam, A., 1990, Unification of Fundamental Forces: Cambridge University Press.

Salisbury, M., and Snyder, M., 2004, Seismic methods in Mineral Exploration, http://gsc.nrcan.gc.ca/mindep/method/seismic/index_e.php., accessed July 5, 2008.

Salisbury, M.H., B. Milkereit, G. L. Ascough, R. Adair, D. Schmitt, and L. Matthews, 1997, Physical properties and seismic imaging of massive sulphides, *in* Canada, P.a.D.A.o., eds., Geophysics and Geochemistry at the Millennium, 383-390, GEO F/X Division of AG Infromation Systems Ltd.

Savic, M., VerWest, B., Masters, R., Sena A., and Gingrich, D., 2000, Elastic Impedance Inversion in Practice: Presented at SEG 2000

Shang, Z., MacDonald, J.A., and Gardner, G.H.F., 1990, True amplitude dip moveout through stacking of constant incident angle gathers: Presented at 60th Annual International Meeting

Sheriff, R.E., 2004, Encylopedic dictionary of exploration geophysics: Society of Exploration Geophysics.

Sheriff, R.E., and Geldart, L.P., 1995, Exploration seismology: SEG.

Stolz, E., Urosevic, M., and Connors, K., 2004, Reflection seismic surveys at St. Ives gold mine, WA: Presented at Geophysical Conference and Exhibition

Stolz, E.M.G., 2003, Direct detection of gold bearing structures at St Ives, WA - DHEM vs DHMMR: Exploration Geophysics, **34**, 131-136.

Stuart G. W., J., S. J., Polome, L. G. B. T., and Tucker, R. F. , 1999, Structural and stratigraphic analysis of 3D seismic attributes applied to mine planning: Target gold deposit, South Africa: Presented at SEG 1999

Stuart, G.W., Jolley, S.J., Polome, L.G.B.T., and Tucker, R.F., 2000, Application of 3D seismic attribute analysis to mine planning: Target gold deposit, South Africa: The Leading Edge, **July**, 736-742.

Taner, M.T., Koehler, F., and Sheriff R.E., 1979, Complex seismic trace analysis: Geophysics, **44**, no. 6, 1041-1063.

Tatham, R.H., 1982, Vp/Vs and lithology: Geophysics, **47**, 336-344.

Todorov, T., Hampson, D., and Russell, B., 1997, Sonic log predictions using seismic attributes: CREWES Research Report, **9**, 1-12.

Treitel, S., and Lines, L.R., 1982, Linear inverse theory and deconvolution: Geophysics, **47**, no. 8, 1153-1159.

—, 2001, Past, present, and future of geophysical inversion - A new millennium analysis: Geophysics, **66**, 21-24.

Urosevic, M., and Evans, B. J., 2000, Surface and borehole seismic methods to delineate kimberlite pipes in Australia: The Leading Edge, **July**, 756-758.

Urosevic, M., Evans, B.J., and Hatherly, P.J., 1992, The improvement in seismic resolution by Map and Trace attribute analysis: Exploration Geophysics, **23**, 387-392.

Urosevic, M., Stoltz, E., and Massey, S., 2005, Seismic Exploration for Gold in a Hard Rock Environment – Yilgarn Craton, Western Australia: Presented at EAGE 67th Meeting.

Urosevic, M., Kepic, A., Sheppard, S., & D. Johnson, 2008, Nickel exploration with 3D seismic - Lake Lefroy, Kambalda, WA, Presented at the 78th Annual SEG Conference, Las Vegas, 9-14 November 2008

Vearncombe, J.R., 1998, Shear zones, fault networks, and Archean gold: Geology, **26**, 855-858.

Walker, R., Wong, C., Malcotti, H., Perez, E., and Sierra, J., 2005, Seismic multi-attribute analysis for lithology discrimination in Ganso Filed, Oficina Formation, Venezuela: The Leading Edge, **November**, 1160-1165.

Wang, X., 1995, Random Noise Attenuation of Pre-stack seismic data by surface consistent prediction in frequency domain: CSEG Abstracts.

Wapenaar, C.P.A., 1996, Inversion versus migration: A new perspective to an old discussion: Geophysics, **61**, no. 3, 804-814.

Watson, I., and Lines, L., 2000, Seismic inversion at Pike's Peak, Saskatchewan: CREWES Research Report, **12**, 41-48.

Weinberg, R.F., Hodkiewicz, Paul F., and Groves, David I., 2004, What controls gold distribution in Archean terranes?: Geological Society of America, **32**, no. 7, 545-548.

White, R.E., and Hu, T., 1998, How accurate can a well tie be?: The Leading Edge, **August**, 1065-1071.

White, R.W., 1991, Properties of instantaneous seismic attributes: The Leading Edge, **July**, 26-32.

Whitford, M., 2004, Geophysical properties of the regolith near the Victory gold mine, Kambalda, Western Australia: Regolith, 398-399.

Whitford, M., Meyers, J., and Stolz, E., 2005, The SAM EQMMR response of the regolith at East Victory St Ives Gold Mine, Western Australia: Exploration Geophysics, **36**, 133-139.

Yilmaz, O., 2001, Seismic data analysis, Processing, inversion, and interpretation of seismic data: Society of Exploration Geophysicists.

Zoeppritz, K., 1919, Erdbebenwellen VIIIB, über Reflexion and Durchgang Seismischer Wellen durch Unstetigkeitsflachen: Gottinger Nachr, **1**, 66-84.

Appendix A

Aki-Richards equation which relates reflection amplitude to incidence angle (ϑ) as follows,

$$R(\theta) = A + B\sin^2\theta + C\sin^2\theta\tan^2\theta, \tag{A.1}$$

where

$$\mathrm{A}=\frac{1}{2}\left[\frac{\Delta V_P}{\overline{V}_P}+\frac{\Delta\rho}{\overline{\rho}}\right],$$
$$\mathrm{B}=\frac{1}{2}\frac{\Delta V_P}{\overline{V}_P}-4\left[\frac{V_S}{V_P}\right]^2\frac{\Delta V_S}{\overline{V}_S}-2\left[\frac{V_S}{V_P}\right]^2\frac{\Delta\rho}{\overline{\rho}},$$
$$C=\frac{1}{2}\frac{\Delta V_P}{\overline{V}_P}.$$

and

$$\overline{V}_P = (V_P(t_i)+V_P(t_{i-1}))/2,$$
$$\Delta V_P = V_P(t_i)-V_P(t_{i-1}),$$
$$\left[\frac{V_S}{V_P}\right]^2 = \left(\frac{V_S^2(t_i)}{V_P^2(t_i)}+\frac{V_S^2(t_{i-1})}{V_P^2(t_{i-1})}\right)/2.$$

The first term (A) is the *intercept*, the second term (B) is the *gradient* term, and the third term (C) is for the offset *curvature*. The *intercept* term is an approximation of the zero-offset reflection coefficient. The *gradient* has the biggest effect on amplitude change as a function of offset. The *curvature* has little amplitude variation with offset at small angles of incidence under 30^0.

In the zero-offset case:

$$R_0 = A = \frac{1}{2}\left[\frac{\Delta V_P}{V_P}+\frac{\Delta\rho}{\rho}\right]\approx\frac{1}{2}\frac{\Delta AI}{AI}, \tag{A.2}$$

where ΔV_P is the change in P-wave velocity between layers, ΔV_S is the change of S-wave velocity between layers, $\Delta\rho$ is the change in density between layers, AI is the acoustic impedance, ΔAI is the change acoustic impedance between layers, t_i is the travel time through layer i and t_{i-1} is travel time between layer $i-1$.

The equations can be redefined such that (Connolly, 1999):

$$R_\theta = \frac{f(t_i) - f(t_{i-1})}{f(t_i) + f(t_{i-1})},$$
$$R_\theta \approx \frac{1}{2}\frac{\Delta EI}{EI} \approx \frac{1}{2}\ln(EI), \tag{A.3}$$

where

$$EI(\theta) = V_P^{(1+\tan^2\theta)} V_S^{(-8K\sin^2\theta)} \rho^{(1-4K\sin^2\theta)}, \tag{A.4}$$

and

$$K = \frac{V_S^2}{V_P^2}, \tag{A.5}$$

where *EI* is the elastic impedance, and *ΔEI* is the change of elastic impedance between layers. Elastic impedance can be calculated from full waveform sonic logs using equation (A.4) and equation (A.5). Elastic impedance requires angle offset, shear seismic, or varying distance offset seismic data for matching.

References

Connolly, P., 1999, Elastic impedance: The Leading Edge, **April**, 438-445.

Appendix B

Seismic data can be considered as the convolution of a wavelet with reflectivity as can be seen in Figure B-1. In the one dimensional sense, the convolutional model appears as reflectivity r and wavelet w(t) convolved as follows.

$$s(t) = r * w(t) + n(t), \tag{B.1}$$

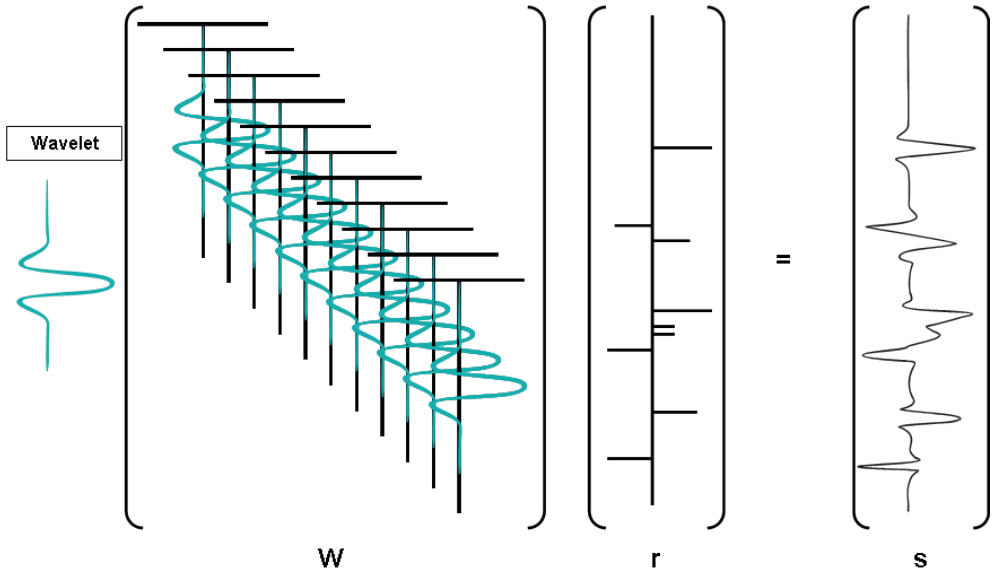

Figure B.1. Convolutional model for a wavelet (W) and reflectivity (r) resulting in a seismic signal (s) (after Bancroft, 2002).

where *n(t)* represents the additive noise. To simplify this function, additive noise is neglected. While this assumption is not correct, the resulting equations are less cumbersome. In the case of the Earth's response in equation (B.1), the reflectivity *r* is unknown. Equation (B.1) can also be expressed in a linear form in the frequency domain.

$$S(f) = R \bullet W(f) \tag{B.2}$$

Where *S(f)* is the Fourier transform of *s(t)*, *W(f)* is the Fourier transform of *w(t)*, and *f* is the frequency. The linear solution simplifies the reflectivity to:

$$R = \frac{S(f)}{W(f)}. \tag{B.3}$$

Equation (B.3) can be expressed in terms of a matrix equation becoming a linear process:

$$W_{[NxM]}r_{[M]} = S_{[N]}, \tag{B.4}$$

where $W_{[NxM]}$ is the wavelet matrix, $\boldsymbol{r}_{[M]}$ is the reflectivity matrix and $\boldsymbol{s}_{[N]}$ is the seismic matrix. The generalized inversion solution can be found in Bancroft (2002) and results in.

$$r_{[M]} \approx W_{[MxN]}S_{[N]}. \tag{B.5}$$

As the equation indicates, the solution is an estimation of the reflectivity of the Earth. The solution in the integral form as follows:

$$x(t) = \int k(t,\tau) f(\tau) d\tau, \tag{B.6}$$

where τ the temporal integration variable and *t* is the time. The function $k(t,\tau)$ is known as the mapping kernel which maps *f*(*t*) in to the x(*t*) observation. We are looking to identify the *f*(*t*) which requires the knowledge that the mapping kernel remains unchanged for the observation in time.

$$x(t) = \int k(\tau) f(t-\tau) d\tau. \tag{B.7}$$

The term *k*(*t*) is the seismic source wavelet, *f*(*t*) is the subsurface impulse response. In the case of seismic inversion, recovery of the impulse response is of most concern since there is at least some knowledge of the source wavelet *k*(*t*) (Treitel, 1982). In the case of seismic inversion the impulse response *f*(*t*) has to be expressed in a discrete estimation due to limited knowledge of the subsurface.

$$\hat{f}(t) = \sum_{\sigma} b_{t\sigma} x(\sigma) \quad t = 0,1,... \tag{B.8}$$

This term σ is a summation variable which ultimately controls the detail of the impulse response depending on the number of variables to be summed. In the generalized case, the number of variables, or length of the series (N+1) results in an impulse function **B** as follows,

$$B = \begin{bmatrix} b_{00} & b_{01} & \dots \\ \dots & \dots & \dots \\ b_{N0} & b_{N1} & \dots \end{bmatrix}.$$

Each row represents an impulse response function. The array **B** represents a discrete time-adaptive filter which reveals a model estimation when substituted into equation (B.6) and (B.8).

$$\hat{f}(t) = \sum_{\sigma} b_{t\sigma} \int k(\sigma,\tau) f(\tau) d\tau \,. \tag{B.9}$$

Assuming the summation and the integration are interchangeable leads to

$$\hat{f}(t) = \int \sum_{\sigma} b_{t\sigma} k(\sigma,\tau) f(\tau) d\tau = \int s(t,\tau) f(\tau) d\tau \,. \tag{B.10}$$

Simplifying leads to:

$$\hat{f}(t) = \int s(t,\tau) f(\tau) d\tau \,. \tag{B.11}$$

Which results in $\hat{f}(t)$ being an estimation of $f(t)$. The function $s(t,\tau)$ is called the scanning function which is responsible for the resolution that can be recovered from $f(t)$.

In the case that the wavelet *k*(*t*) is time shifted, it is assumed that all responses are discrete with a uniform time increment of $\Delta t = 1$. This results in using the discrete sequences x_t, k_t, f_t, $\hat{f}_t$ and s_r instead of the continuous time functions, *x*(*t*), *k*(*t*), *f*(*t*), $\hat{f}(t)$ and *s*(*t*) resulting in:

$$x_r = \sum_{\tau=0}^{m} k_\tau f_{t-\tau} \,, \tag{B.12}$$

where k_t is the discrete wavelet or mapping kernel (m+1)-length. Using (B.12) the model estimation can now be written as

$$\hat{f}_t = \sum_{\sigma} b_{t-\sigma} x_\sigma = \sum_{\sigma=0}^{n} b_\sigma x_{t-\sigma} \,, \tag{B.13}$$

where b_t is the time shift variant filter (n+1)-length. As before and substituting the observed time series results in:

$$\hat{f}_t = \sum_{\sigma} b_\sigma \sum_{\sigma=0}^{n} k_\tau f_{1-\tau-\sigma} \,.$$

Allowing $\tau + \sigma = \mu$

$$\hat{f}_t = \sum_{\mu} \left(\sum_{\tau} b_{\mu-\tau} k_\tau \right) f_{t-\mu} \,. \tag{B.14}$$

Where

$$s_\mu = \sum_{\tau} b_{\mu-\tau} k_\tau \,. \tag{B.15}$$

With results similar to equations (B.13)

$$\widehat{f}_t = \sum_{\mu} s_{\mu} f_{t-\mu} \,, \tag{B.16}$$

where s_t is defined as the discrete scanning function with limits

$$\begin{aligned} s_t &= 1, t = 0 \\ s_t &= 0, t \neq 0 \end{aligned}, \tag{B.17}$$

which shows from equation (B.15) that b_t is the inverse filter for the source wavelet k_t yielding $\widehat{f}_t = f_t$. This shows that the model can be recovered from the observation. A simplified prediction is presented by Treitel and Lines (1982) and results in:

$$b_t * x_t = b_1 * k_t * f_t = s_t * f_t = \widehat{f}_t \,. \tag{B.18}$$

These derivations have shown that the more information we can gather about the mapping kernel (source wavelet), the model term will still only give us estimation of what our observation (seismic) truly is.

References

Bancroft, J.C., 2002, A theoretical and visual description of the relationship between Kirchhoff migration and seismic inversion: SEG Extended Abstract.

Treitel, S., and Lines, L.R., 1982, Linear inverse theory and deconvolution: Geophysics, **47**, no. 8, 1153-1159.

Appendix C

The instantaneous seismic attributes describe the waveform shapes which were first calculated for seismic data by Taner et al. (1979). The trace defined as x(t) can be represented by a complex valued signal as follows.

$$x(t) = \mathrm{Re}(A(t)e^{i\phi(t)}) . \tag{C.1}$$

Equation (C.1) can be broken down into its attributes as follows

$x(t) =$ recorded seismic trace,

$A(t)e^{i\phi(t)} =$ complex trace or analytic signal,

$\mathrm{Im}(A(t)e^{i\phi(t)}) =$ quadrature trace,

$A(t) =$ amplitude envelope or instantaneous amplitude,

$\phi(t) =$ instantaneous phase,

and $\frac{1}{2}\pi\frac{d\phi(t)}{dt} =$ instantaneous frequency.

Since the trace is complex, the signal can be put into polar coordinates described by the composition of the seismic trace s(t) and its Hilbert transform, h(t), which is 90^0 phase shifted trace (Hampson-Russell, 2007).

$$C(t) = A(t)e^{i\phi(t)} = s(t) + ih(t) = A(t)\cos\phi(t) + iA(t)\sin\phi(t) . \tag{C.2}$$

With instantaneous attributes

$A(t) = \sqrt{s(t)^2 + h(t)^2}$ = amplitude envelope.

$\phi(t) = \tan^{-1}(\frac{h(t)}{s(t)})$ = instantaneous phase.

$\omega(t) = \frac{d\phi(t)}{dt}$ = instantaneous frequency.

$\cos\phi(t) =$ cosine instantaneous phase.

$A(t)\cos\phi(t) =$ amplitude weighted cos phase.

$A(t)\phi(t) =$ amplitude weighted phase.

$A(t)\omega(t) =$ amplitude weighted frequency.

Figure C.1 shows the comparison between several attributes and the equivalent seismic signal.

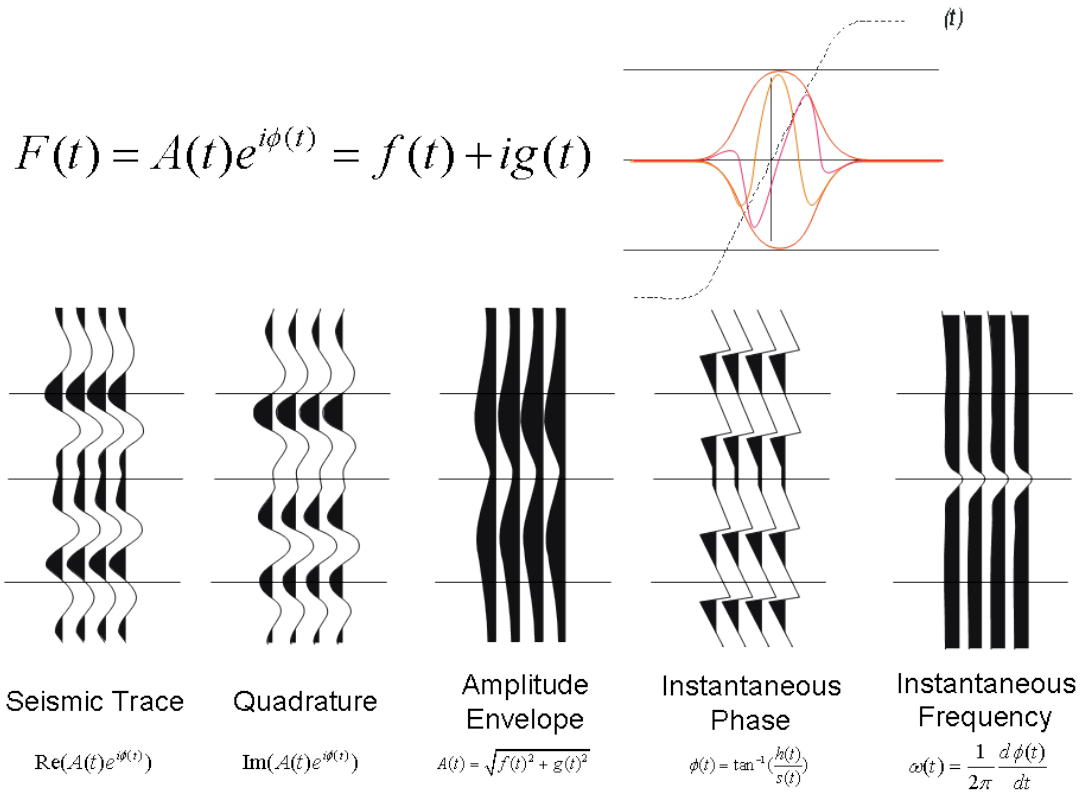

Figure C.1 Comparison of the instantaneous attribute with a seismic signal (after White, 1991).

Amplitude Envelope

Amplitude envelope, $A(t) = \sqrt{s(t)^2 + h(t)^2}$, emphasises the amplitude changes as seen on the seismic trace. It is sensitive to changes in the acoustic impedance and thus to lithology, porosity, hydrocarbon and thin-bed tuning (Chopra, 2005). Hard rock environment equivalents might be shear zone rock changes, possible alteration plumes, and structure changes. In general, any impedance contrast will be represented by amplitude envelope analysis.

Quadrature trace

The quadrature trace, $\mathrm{Im}(A(t)e^{i\phi(t)})$ is the product of the amplitude envelope and the sine of the instantaneous phase. Peaks and troughs on the quadrature trace correspond to zero crossings on the original data trace, consistent with the phase shift. As can be seen in Figure C.1 the quadrature trace is 90^0 phase shift from the seismic trace.

Instantaneous phase

Instantaneous phase $\phi(t) = \tan^{-1}(\frac{h(t)}{s(t)})$ shows sharp changes at ±180 degrees peaks and troughs of traces. The attribute emphasizes the continuity of events (Taner M. T., 1979) and tracking reflection continuity which aids in detection of unconformities, faults, and lateral changes in stratigraphy. Instantaneous phase is more ideal for imaging than statistical analysis because it tends to act like an extreme AGC where the wave shape is accentuated (Brown, 2000).

Instantaneous frequency

Seismic reflectors are quite often made up of several different reflections from events that are closely spaced and instantaneous frequency calculations can identify lithology on offsets. As shown on Figure C.1 instantaneous frequency, $\omega(t) = \frac{d\phi(t)}{dt}$ is useful in identifying thin beds and abnormal attenuation. The instantaneous frequency attribute itself is fairly steady and stable while the amplitude envelop is large, except at inflection points, associated with thin beds, where the response becomes unstable and dips below zero (White, 1991). In hydrocarbon exploration, the instantaneous frequency has been used to identify low frequency zones which correspond to potential sources of oil or gas. There are pitfalls in interpretation of these types of calculations due to low frequency zones also corresponding to brittle rock. Weighting is required due to phase and frequency being noisy and unstable attributes where variances in the attributes can become unbounded (White, 1991). However, weighting is not suggested unless there is prior knowledge of how attributes are affected by rock conditions. Abnormal signals statistically are usually geologically interesting.

Software dependant attributes

The attributes available through the Hampson-Russell software package include: *Windowed frequency* attributes, *filter slice* attributes, *derivative* (first and second), *integrated* attributes, *3D* attributes (not covered in this research) *AVO* attributes and *Model based* attributes. When a limited volume of seismic data and unknown attribute responses, attribute studies in hard rock environments allows for, at least, a preliminary usage of these other attributes.

The *windowed frequency* attributes are the Fourier transform of the seismic trace over a given sample window dependant on average or dominant frequency. *Filter slice* attributes calculates a band filter on different sets of frequencies. *Derivative* attributes are based on the first or second derivate of the amplitude envelope and indicate rates of change within the signal. *Integrated* attributes are based on the low frequency filtered integrated amplitude envelope.

References

Brown, A.R., 2000, Understanding seismic attributes: Geophysics **66**, 47-48.

Chopra, S., and Marfur, K. J., 2005, Seismic attributes - A historical perspective: Geophysics, **70**, 3S0-28SO.

Hampson-Russell, 2007, Guide to Emerge, p. PDF in the Hampson-Russell software package.

Taner M. T., K.F., and Sheriff R. E., , 1979, Complex seismic trace analysis: Geophysics **44**, no. 6, 1041-1063.

White, R.W., 1991, Properties of instantaneous seismic attributes: The Leading Edge, **July**, 26-32.